

Stacjonarne Studia Doktoranckie Genetyki
Molekularnej, Cytogenetyki i Biofizyki Medycznej

Karol Zbigniew Bukowski

NUMER ALBUMU: 5970

Aktywność przeciwnowotworowa nowych trójcyklicznych pochodnych układu pirazolo[4,3-*e*][1,5-*b*] [1,2,4]triazyny w komórkach linii nowotworowych człowieka

Praca doktorska

wykonana w Katedrze Biotechnologii
Molekularnej i Genetyki, Instytutu
Biologii Eksperymentalnej na
Wydziale Biologii i Ochrony
Środowiska UŁ

Promotor:

dr hab. Renata Kontek, prof. UŁ

Promotor pomocniczy:

dr Beata Marciniak

Anticancer activity of new tricyclic derivatives
of pyrazolo[4,3-*e*]tetrazolo[1,5-*b*][1,2,4]triazine
system in human cancer cell lines

Podziękowania

Serdeczne podziękowania składam moim promotorom
dr hab. Renacie Kontek oraz **dr Beacie Marciniak**
za poświęcony czas oraz cenne uwagi
i sugestie w trakcie realizacji badań naukowych, a także za
nieocenioną pomoc podczas realizacji niniejszej pracy doktorskiej.

Dziękuję serdecznie
Pracownikom i **Doktorantom**
Katedry Biotechnologii Molekularnej i Genetyki
za wielokrotnie okazaną pomoc, życzliwość, cenne wskazówki
oraz tworzenie wspaniałej atmosfery.

Szczególne podziękowania kieruję w stronę **Moich Bliskich**
za wsparcie, motywację, zrozumienie
oraz wiarę w moje możliwości

Spis treści

Współpraca naukowa	4
Źródło finansowania badań	5
Spis publikacji wchodzących w zakres rozprawy doktorskiej	6
Wprowadzenie	7
Cel pracy	10
Materiał i metody badawcze	12
Omówienie prac wchodzących w skład rozprawy doktorskiej	15
Wnioski	28
Literatura uzupełniająca	30
Streszczenie w języku polskim	33
Streszczenie w języku angielskim	35
Dorobek naukowy	37
Kopie publikacji wchodzących w zakres rozprawy doktorskiej	41
Oświadczenia współautorów publikacji	

Współpraca naukowa



**Uniwersytet
Przyrodniczo-
-Humanistyczny**
w Siedlcach

Katedra Chemii, Instytut Nauk Chemicznych,
Uniwersytet Przyrodniczo-Humanistyczny w
Siedlcach, przy współudziale **dr hab.
Mariusza Mojzycha, prof. UPH**



CHITKARA
UNIVERSITY
PUNJAB

Chitkara College of Pharmacy, Chitkara
University, Rajpura, Punjab, Indie, przy
współudziale **dr Somdutta Mujwara**

Źródło finansowania badań

Badania przeprowadzone w niniejszej pracy sfinansowano z subwencji Katedry Biotechnologii Molekularnej i Genetyki Uniwersytetu Łódzkiego oraz z dotacji dydaktycznej Stacjonarnych Studiów Doktoranckich Genetyki Molekularnej, Cytogenetyki i Biofizyki Medycznej Uniwersytetu Łódzkiego.

Spis publikacji wchodzących w zakres rozprawy doktorskiej

- I. **Bukowski, K.**; Kciuk, M.; Kontek, R. Mechanisms of Multidrug Resistance in Cancer Chemotherapy. *International Journal of Molecular Sciences* **2020**, *21*, 3233. <https://doi.org/10.3390/ijms21093233>.

Praca przeglądowa; IF: 5,923 (2020); Punkty MEiN: 140; **liczba cytowań: 494 (wg Scopus); 458 (wg Web of Science)**

- II. **Bukowski, K.**; Marciniak, B.; Kciuk, M.; Mojzych, M.; Kontek, R. Pyrazolo[4,3-e]tetrazolo[1,5-b][1,2,4]triazine Sulfonamides as Novel Potential Anticancer Agents: Cytotoxic and Genotoxic Activities In Vitro. *Molecules* **2022**, *27*, 3761. <https://doi.org/10.3390/molecules27123761>.

Praca doświadczalna; IF: 4,927 (2022); Punkty MEiN: 140

- III. **Bukowski, K.**; Marciniak, B.; Kciuk, M.; Mujwar, S.; Mojzych, M.; Kontek, R. Pyrazolo[4,3-e]tetrazolo[1,5-b][1,2,4]triazine Sulfonamides as Novel Potential Anticancer Agents: Apoptosis, Oxidative Stress, and Cell Cycle Analysis. *International Journal of Molecular Sciences* **2023**, *24*, 8504. <https://doi.org/10.3390/ijms24108504>.

Praca doświadczalna; IF: 6.208 (2023); Punkty MEiN: 140

Sumaryczna wartość IF publikacji wchodzących w zakres rozprawy doktorskiej wynosi 17,058 (420 punktów MEiN).

Bibliometria:

Całkowity IF = 44,562

Punktacja MEiN = 1100 pkt

Indeks Hirscha = 5 (wg Scopus oraz Web of Science)

Liczba cytowań (bez autocytowań) – 541 (wg SCOPUS); 506 (wg Web of Science)

Wprowadzenie

Choroby nowotworowe od lat stanowią jeden z głównych problemów zdrowia publicznego na świecie. 14 grudnia 2020 r. Międzynarodowa Agencja Badań nad Rakiem opublikowała zaktualizowane dane dotyczące globalnego obciążenia rakiem, wskazując, że w 2020 r. liczba nowych zachorowań na choroby nowotworowe wynosiła 19,3 miliona przypadków, zaś rak na całym świecie przyczynił się do 10 milionów zgonów. Najczęściej diagnozowanymi nowotworami na świecie był rak piersi u kobiet (2,26 mln przypadków), rak płuca (2,21 mln) oraz rak prostaty (1,41 mln), zaś najczęstszymi przyczynami zgonów z powodu nowotworów były nowotwory płuc (1,79 mln zgonów), wątroby (830 000) i żołądka (769 000). Rak piersi, szyjki macicy, płuc, tarczycy i jelita grubego to najczęstsze rodzaje raka u kobiet, podczas gdy rak prostaty, płuc, jelita grubego, wątroby i żołądka są najpowszechniejsze wśród mężczyzn. Do głównych czynników, które mogą przyczyniać się do zwiększonego ryzyka zachorowania na choroby nowotworowe są: palenie tytoniu, brak aktywności fizycznej, spożywanie alkoholu, niskie spożycie warzyw i owoców oraz wysoki wskaźnik masy ciała. Pomimo znacznego postępu w rozwoju różnych metod leczenia nowotworów, w tym chirurgii, radioterapii, terapii hormonalnej, terapii genowej i immunoterapii, chemioterapia pozostaje nadal głównym sposobem leczenia onkologicznego. Z tego powodu poszukiwanie nowych, skutecznych leków przeciwnowotworowych jest jednym z najszerzej badanych kierunków badań na świecie [1,2].

Wśród powszechnie stosowanych leków przeciwnowotworowych wyróżniamy związki heterocykliczne, takie jak 5-fluorouracyl, metotreksat, doksorubicyna, czy winblastyna. Heterocykliczne struktury rdzenia i/lub podstawników nadal stanowią podstawę projektowania i syntezy nowych biologicznie aktywnych cząsteczek. Leki antymetabolitowe o budowie chemicznej zbliżonej do zasad azotowych w DNA/RNA są uważane za jedną z głównych grup leków przeciwnowotworowych. Zakłócają one nie tylko kluczowe dla utrzymania wzrostu komórek szlaki biosyntezy DNA/RNA,

ale także przyczyniają się do powstawania pęknięć nici DNA. Włączanie analogów puryn/pirymidyn do DNA lub hamowanie aktywności niektórych enzymów, takich jak reduktaza rybonukleotydowa, reduktaza dihydrofolianowa, czy polimeraza DNA, może indukować uszkodzenia materiału genetycznego [3]. Liczne nukleozydy, które zawierają zamienione atomy węgla i azotu w swoich ugrupowaniach zasad, wykazały znaczny potencjał jako środki antymetabolitowe. Związki 6-aza, takie jak 6-azocytozyna i 6-azouracyl, są dobrze znanymi przykładami analogów zasad azotowych kwasów nukleinowych [4,5]. Do tej grupy związków należą również monocykliczne pochodne 1,2,4-triazyny. Rdzeń pirazolo[4,3-*e*]tetrazolo[4,5-*b*] [1,2,4]triazyny w połączeniu z ugrupowaniem sulfonamidowym, obecnym w wielu lekach stosowanych klinicznie, umożliwił zaprojektowanie nowych pochodnych o potencjalnie wyższej aktywności biologicznej. Znaczenie tej grupy farmakoforów wynika z ich różnych właściwości biologicznych, w tym przeciwnowotworowych, przeciwmalarycznych, przeciwpasożytniczych, przeciwbakteryjnych, przeciwtarczycowych, przeciwjaskrowych, przeciwzapalnych, hipoglikemizujących, hipotensyjnych czy moczopędnych [6–8].

W ten nurt badań wpisuje się tematyka prezentowanej rozprawy doktorskiej, w której podjęto się analizy właściwości przeciwnowotworowych nowych pochodnych pirazolo-triazyny: **MM129**, **MM130** i **MM131** [6,9–14]. Badania cytotoksyczności przeprowadzono na komórkach linii nowotworowych człowieka: raka szyjki macicy (HeLa), raka okrężnicy (HCT 116), raka prostaty (PC-3) oraz gruczolakoraka trzustki (BxPC-3). Uwzględniono również model komórek prawidłowych w postaci ludzkich fibroblastów napletka (linia Hs-27) oraz jednojądrzastych komórek krwi obwodowej człowieka (ang. *Peripheral Blood Mononuclear Cells*, PBMCs). Ze względu na uzyskaną w ww. badaniach niską cytotoksyczność związków **MM129**, **MM130** i **MM131** wobec komórek prawidłowych ($IC_{50} = 0,62\text{--}1,15 \mu\text{M}$), do dalszych badań zostały wykorzystane tylko komórki linii nowotworowych. Kolejne etapy zadań badawczych obejmowały ocenę stopnia genotoksyczności związków **MM129**, **MM130** i **MM131** oraz oznaczenie poziomu

działania prooksydacyjnego i proapoptotycznego badanych związków. Ponadto przeprowadzono analizę przebiegu cyklu komórkowego oraz jego poszczególnych faz po działaniu testowanych związków. Z kolei, wykonane badania *in silico*, pozwoliły na ocenę wiązania się badanych związków do kinaz zależnych od cyklin (ang. *cyclin-dependent kinases* CDKs) oraz sprawdzenie stabilności ww. kompleksów.

Cel pracy

Głównym celem badań przeprowadzonych w niniejszej pracy była ocena w warunkach *in vitro* profilu aktywności przeciwnowotworowej zsyntetyzowanych *de novo* pochodnych pirazolo[4,3-*e*]tetrazolo[1,5-*b*][1,2,4]triazyny: **MM129**, **MM130** i **MM131** oraz wytypowanie związku o najwyższej aktywności onkoterapeutycznej celem dalszej szczegółowej analizy w badaniach podstawowych, przedklinicznych i klinicznych.

Podstawą hipotezy badawczej i oczekiwanych rezultatów było założenie, że nowe pochodne układu pirazolo-triazyny będą:

1. Hamować proliferację komórek linii nowotworowych człowieka pochodzących z jednych z najczęściej występujących obecnie nowotworów: raka szyjki macicy, raka okrężnicy, raka prostaty oraz gruczolakoraka trzustki poprzez indukcję uszkodzeń DNA, zahamowanie replikacji i podziałów komórkowych.
2. Indukować śmierć komórek nowotworowych na drodze apoptozy jako najbardziej pożądanego sposobu ich eliminacji, z pominięciem niekorzystnego dla chorych procesu zapalnego jaki towarzyszy np. nekrozie.
3. Generować stres oksydacyjny w komórkach nowotworowych, którego udział w indukowaniu mechanizmów związanych z apoptozą i genotoksycznością należy do znaczących.

Szczegółowe badania, wykonane w warunkach *in vitro*, miały na celu:

1. Ocena stopnia cytotoksyczności analizowanych pochodnych wobec wytypowanych komórek linii nowotworowych człowieka, w tym analizę cytotoksyczności wobec komórek prawidłowych.

2. Określenie rodzaju uszkodzeń komórek eksponowanych na działanie badanych pochodnych układu pirazolo-triazyny (zmiany morfologii, uszkodzenia DNA, zmiany błony komórkowej, mitochondriów, chromatyny).
3. Ocenę przebiegu cyklu komórkowego i jego poszczególnych faz.
4. Poznanie mechanizmów molekularnych odpowiedzialnych za charakter działania badanych związków poprzez zastosowanie dokowania molekularnego i symulacji dynamiki molekularnej.

Zakładano, że uzyskane w badaniach wyniki stanowiąc będą solidny fundament dla dalszych, bardziej szczegółowych i wszechstronnych badań celem wykorzystania najbardziej efektywnych pochodnych pirazolo-triazyny, jako nowych, potencjalnych onkoterapeutyków.

Material i metody badawcze

Material badawczy

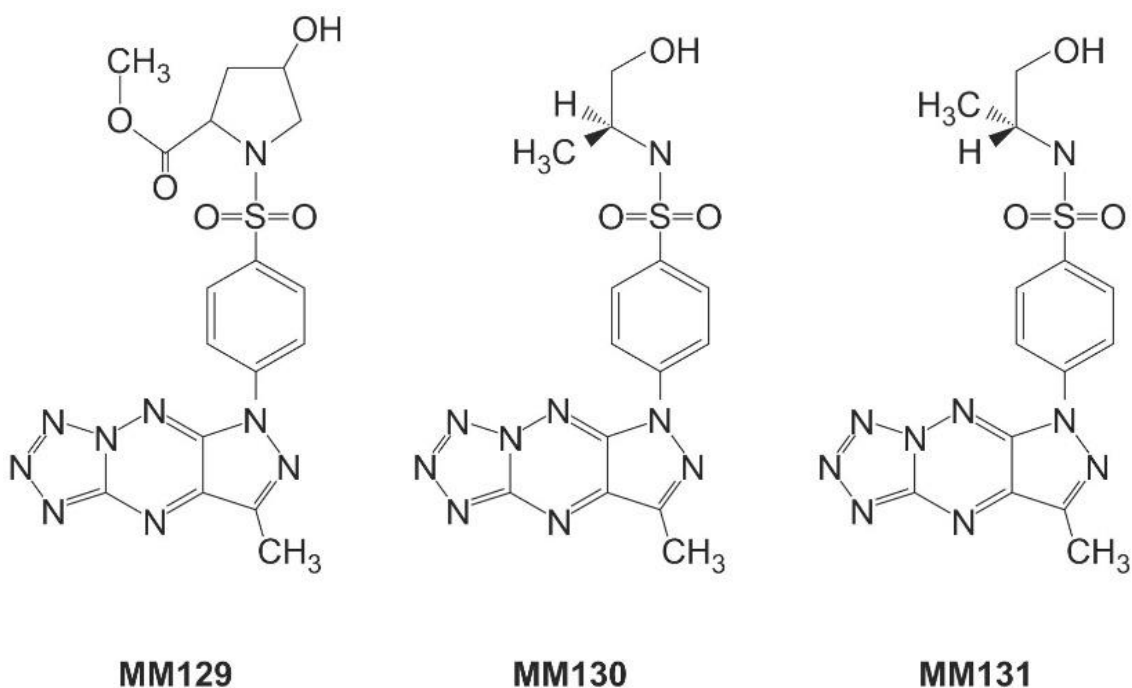
W przeprowadzonych badaniach wykorzystano cztery ludzkie, adherentne linie komórek nowotworowych: **HeLa** (komórki raka szyjki macicy; ATCC® CCL-2™), **HCT 116** (komórki raka okrężnicy; ATCC® CCL-247™), **PC-3** (komórki raka prostaty; ATCC® CCL-1435™) oraz **BxPC-3** (komórki gruczolaka trzustki; ATCC® CCL-1687™). Ocenę cytotoksyczności badanych związków poszerzono dodatkowo o serie z wykorzystaniem ludzkich komórek prawidłowych: **Hs27** (fibroblasty napletka; ATCC® CCL-1634™) oraz **PBMCs** (jednojądrzaste komórki krwi obwodowej).

Badane związki

- **MM129** – 4-hydroksy-1-[4-(7-metylo-5H-pirazolo[4,3-*e*]tetrazolo[1,5-*b*][1,2,4]triazyn-5-yl)fenylosulfonyl]pirolidyno-2-karboksylan metylu
- **MM130** – N-(S)-(1-hydroksy-propan-2-yl)-4-[7-metylo-5H-pirazolo[4,3-*e*]tetrazolo [1,5-*b*][1,2,4]-triazyn-5-yl)]benzenosulfonamid
- **MM131** – N-(R)-(1-hydroksy-propan-2-yl)-4-[7-metylo-5H-pirazolo[4,3-*e*]tetrazolo [1,5-*b*][1,2,4]-triazyn-5-yl)]benzenosulfonamid

Związki będące pochodnymi układu pirazolo-triazyny zostały zsyntetyzowane *de novo*, a następnie udostępnione do badań przez **dr hab. Mariusza Mojzycha**, prof. Uniwersytetu Przyrodniczo-Humanistycznego w Siedlcach (Zakład Chemii Organicznej). Szczegółowy opis syntezy chemicznej związku **MM130** znajduje się w publikacji II, zaś pochodnych **MM129** oraz **MM131** w wcześniejszych publikacjach współautorstwa **dr hab. Mariusza Mojzycha** [9,14]. Wzory chemiczne badanych związków zostały przedstawione na Rycinie 1.

We wszystkich przeprowadzonych testach, oprócz prób badanych, zastosowano kontrolę negatywną tj. zawiesinę komórkową, odpowiedniej linii nowotworowej wolną od testowanych związków.



Rycina 1. Wzory chemiczne badanych nowych trójcyklicznych pochodnych układu pirazolo[4,3-e]tetrazolo[4,5-b][1,2,4]triazyny. Rdzeń wszystkich związków stanowi tetrazol połączony z pierścieniem pirazolowo-triazynowym oraz ugrupowanie sulfonamidowe, do którego przyłączone jest ugrupowanie chemiczne charakterystyczne dla danego związku MM. Związek **MM129** zawiera jako dodatkową grupę chemiczną chlorowodorek estru metylowego cis-4-hydrokso-L-proliny, zaś związki **MM130** i **MM131**, będące odpowiednio izomerami S i R, jako resztę posiadają 2-amino-1-propanol.

Metody badawcze

- Analiza cytotoksyczności badanych związków przy użyciu testu MTT.
- Pomiar poziomu uszkodzeń DNA z wykorzystaniem metody kometowej w wersji alkalicznej.
- Oznaczanie poziomu uszkodzeń dwuniciowych DNA przy użyciu testu kometowego w wersji neutralnej.
- Immunocytochemiczne wykrywanie histonu γ -H2AX w celu weryfikacji właściwości genotoksycznych badanych związków.
- Określenie poziomu reaktywnych form tlenu za pomocą sondy fluorescencyjnej dioctanu 2',7'- dichlorodihydrofluoresceiny (H₂DCFDA).
- Analiza zmian apoptotycznych z wykorzystaniem podwójnego barwienia aneksyną V wyznakowaną izotiocyjanianem fluoresceiny (ang. *fluorescein*

isothiocyanate, FITC) i jodkiem propidyny przy zastosowaniu cytometrii przepływowej.

- Ocena zmian morfologicznych komórek metodą podwójnego barwienia z wykorzystaniem mieszaniny fluorochromów: oranżu akrydyny oraz bromku etydydy.
- Badanie zmian potencjału transbłonowego przy użyciu sondy fluorescencyjnej MitoTracker Red CMXRos.
- Analiza przebiegu cyklu komórkowego i jego poszczególnych faz z wykorzystaniem cytometrii przepływowej.
- Badania *in silico*, pozwalające na ocenę potencjału wiązania się badanych związków do enzymów CDK (dokowanie molekularne) oraz sprawdzenie stabilności ww. kompleksów (symulacja dynamiki molekularnej).

Omówienie prac wchodzących w skład rozprawy doktorskiej

Cykl publikacji wchodzących w skład niniejszej rozprawy doktorskiej otwiera publikacja przeglądowa pt. „*Multidrug resistance in Cancer Chemotherapy*”, w której został opisany podstawowy podział chemioterapeutyków ze względu na ich mechanizm działania (środki alkilujące, antymetabolity, inhibitory topoizomerazy, inhibitory wrzeciona mitotycznego oraz inne charakteryzujące się niejednorodnymi mechanizmami działania), a także szczegółowo omówiono molekularne podłoże mechanizmów związanych z lekoopornością (ang. *multidrug resistance* MDR) komórek nowotworowych. Dane statystyczne wskazują, że ponad 90% śmiertelności pacjentów z chorobą nowotworową przypisuje się lekooporności. MDR komórek nowotworowych podczas chemioterapii może być związany z różnymi mechanizmami, w tym zwiększonym wypływem leków, czynnikami genetycznymi (mutacje genów, amplifikacje i zmiany epigenetyczne), czynnikami wzrostu, zwiększoną zdolnością naprawy DNA i podwyższonym metabolizmem ksenobiotyków. Każdy z tych mechanizmów prowadzi do zmniejszenia skuteczności terapeutycznej podawanych leków, powodując trudności w leczeniu nowotworów.

Znajomość słabych punktów wspomnianych mechanizmów umożliwiła naukowcom opracowanie nowych strategii ukierunkowanych przeciwko komórkom nowotworowym o nabytej oporności wielolekowej. W omawianej publikacji przedstawiono nowe, potencjalne środki chemioterapeutyczne, z których znaczna część wykazała silną aktywność przeciwnowotworową, zarówno w badaniach *in vitro*, jak i *in vivo*. Ponadto dane literaturowe wykazały, że ich połączenie z obecnie stosowanymi onkoterapeutykami, wpływa na zwiększenie działania przeciwnowotworowego tych ostatnich leków. Potwierdza to obecny paradygmat, iż terapia skojarzona charakteryzuje się o wiele większą skutecznością, w porównaniu z zastosowaniem jakiegokolwiek pojedynczego leku. Jednakże, ze względu na skomplikowaną naturę mechanizmów związanych z opornością wielolekową, a także patrząc przez pryzmat niejednorodnego charakteru chorób nowotworowych

prawdopodobnie nigdy pojedynczy lek nie będzie wystarczająco uniwersalny i skuteczny w terapii każdego typu nowotworu. Fakt ten stanowi główny powód, dla którego w dalszym ciągu podejmowane są wysiłki w celu szczegółowego poznania mechanizmów związanych z lekoopornością komórek nowotworowych. Identyfikacja kolejnych słabych punktów, w komórkach nowotworowych z MDR, jest kluczowa dla projekcji onkoterapeutyków następnej generacji. Kształtujący się trend opracowywania substancji onkoterapeutycznych, nastawionych na cele molekularne, związane ze znoszeniem MDR w komórkach nowotworowych, może przyczynić się do podniesienia skuteczności obecnie stosowanych leków przeciwnowotworowych. Może to przynieść szczególnie istotne korzyści kliniczne w przypadku najbardziej opornych na leczenie nowotworów. W związku z tym synteza oraz badania podstawowe związane z badaniem aktywności biologicznej zsyntetyzowanych *de novo* związków, a w szczególności określenie ich potencjału przeciwnowotworowego, stanowi wciąż aktualne wyzwanie badawcze.

Część eksperymentalna prezentowanej rozprawy doktorskiej została opisana w dwóch publikacjach oryginalnych. W pierwszej z nich pt: "*Pyrazolo[4,3-e]tetrazolo[1,5-b][1,2,4]triazine Sulfonamides as Novel Potential Anticancer Agents: Cytotoxic and Genotoxic Activities In Vitro*" zostały przedstawione wyniki badań dotyczące oceny cyto- oraz genotoksyczności trzech pochodnych układu pirazolo[4,3-e]tetrazolo[1,5-b][1,2,4]triazyny: **MM129**, **MM130** i **MM131** wobec ludzkich komórek linii nowotworowych HeLa, HCT 116, PC-3 oraz BxPC-3. Dodatkowo analizę cytotoksyczności testowanych pochodnych pirazolo-triazyny uzupełniono o model ludzkich komórek prawidłowych tj. komórek Hs27 oraz PBMCs.

Opisane w publikacji wyniki testu MTT wskazały na silne właściwości przeciwnowotworowe badanych związków MM w stosunku do badanych typów komórek w bardzo niskim zakresie stężeń ($IC_{50} = 0,17-1,15 \mu M$) po 72 h inkubacji. Co ważne, odnotowano niższą wrażliwość na testowane pochodne pirazolo-triazyny komórek prawidłowych w porównaniu z komórkami badanych linii nowotworowych. Najbardziej efektywne cytotoksyczne działanie związków MM

odnotowano dla komórek linii nowotworowej BxPC-3, z kolei najmniej wrażliwe okazały się być komórki linii HeLa. Na uwagę zasługuje fakt, że efekt wywoływany w komórkach nowotworowych był od 1,2 do 4,9 razy silniejszy niż ich działanie na modelu z wykorzystaniem komórek prawidłowych (Tabela 1).

Tabela 1. Właściwości cytotoksyczne związków **MM129**, **MM130** i **MM131** wyrażone jako wartości IC₅₀ [μM] wraz z 95% przedziałami ufności (nawiasy).

Linia komórkowa	IC ₅₀	IC ₅₀	IC ₅₀
	MM129	MM130	MM131
PBMCs	1,11 (0,98–1,26)	0,77 (0,71–0,84)	0,62 (0,52–0,72)
Hs27	1,15 (0,95–1,37)	0,81 (0,64–0,99)	0,62 (0,43–0,82)
HeLa	0,9 (0,73–1,06)	0,59 (0,51–0,67)	0,41 (0,28–0,54)
HCT 116	0,6 (0,58–0,62)	0,44 (0,43–0,45)	0,39 (0,37–0,41)
PC-3	0,36 (0,32–0,4)	0,22 (0,18–0,28)	0,17 (0,16–0,17)
BxPC-3	0,26 (0,2–0,32)	0,17 (0,13–0,21)	0,13 (0,11–0,15)

Badane pochodne pirazolo-triazyny wykazały znacznie silniejszą cytotoksyczność w porównaniu do obecnie stosowanych onkoterapeutyków, takich jak 5-fluorouracyl (IC₅₀ – 96,1 μM dla komórek BxPC-3 i 3,2 μM dla komórek HCT 116), cisplatyna (IC₅₀ – 9 μM dla komórek PC-3 i HCT 116 oraz 12,3 μM dla komórek HeLa), oksaliplatyna (IC₅₀ – 72 μM dla komórek HCT 116 i 100 μM dla komórek PC-3), czy też irinotekan (IC₅₀ – 2,1 μM dla komórek PC-3 i 2,6 μM dla HCT 116) [15–19].

Na podstawie kryteriów przedstawionych przez American National Cancer Institute (USA) cytotoksyczność związku można zakwalifikować jako **wysoką** jeśli wyznaczona wartość IC₅₀ < 20 μg/mL, **umiarkowaną** kiedy IC₅₀ 21–200 μg/mL lub **słabą**, gdy IC₅₀ znajduje się między 201–500 μg/ml [20]. Ze względu na fakt, iż wyznaczone wartości IC₅₀ badanych pochodnych pirazolo-triazyny względem testowanych komórek były niższe niż 20 μg/mL, związki te można zaliczyć do grupy związków o wysokiej cytotoksyczności, przy czym najniższy potencjał cytotoksyczny odnotowano dla związku **MM129** zaś najwyższy dla **MM131**.

Zahamowanie proliferacji komórek spowodowane tworzeniem jedno- i dwuniciowych pęknięć DNA (odpowiednio ang. *single-strand break*, SSB i *double-strand break*, DSB) jest jednym z głównych efektów działania różnych leków przeciwnowotworowych. Tworzenie adduktów i/lub interakcja reaktywnych form tlenu z podwójną helisą DNA odgrywa bardzo ważną rolę w degradacji DNA [21,22]. Podwójne pęknięcia DNA, ze względu na ich niezwykłą trudność w naprawie, stanowią poważne zagrożenie dla komórki. Nienaprawione DSBs mogą prowadzić do śmierci komórki, z kolei naprawione nieprawidłowo mogą stać się potencjalnym czynnikiem dalszej progresji nowotworu [23]. Dlatego też, w dalszym etapie badań dokonano oceny genotoksyczności badanych pochodnych pirazolo-triazyny wykorzystując alkaliczną oraz neutralną wersję testu kometowego. Analiza poziomu jedno i dwuniciowych pęknięć DNA w komórkach nowotworowych została przeprowadzona po ich 24-godzinnej inkubacji z badanymi związkami. Badania wykazały, że związki MM indukowały istotny statystycznie ($p < 0,0001$) wzrost poziomu pęknięć jedno- i dwuniciowych DNA w komórkach wszystkich badanych linii nowotworowych w porównaniu z kontrolą negatywną, a także zaobserwowano dodatnią korelację między zastosowanym stężeniem, a poziomem uszkodzeń DNA (zależność dawka-efekt). Alkaliczna wersja testu kometowego wykazała, związek **MM131** charakteryzował się najsilniejszą aktywnością genotoksyczną wobec komórek PC-3 i HCT 116 (odpowiednio: 19,5%–40,3% i 8%–38,8% DNA w ogonie komety). Natomiast, komórki linii Hela charakteryzowały się najwyższą opornością na genotoksyczny potencjał testowanych związków (4,1%–8,1% DNA w ogonie komety dla wyższych zastosowanych stężeń badanych pochodnych pirazolo-triazyny). Dlatego też, do neutralnej wersji testu kometowego wykorzystano komórki HCT 116, PC-3 i BxPC-3. Najwyższy poziom pęknięć dwuniciowych DNA zaobserwowano w przypadku ekspozycji komórek HCT 116 na działanie badanych związków (Tabela 2).

Tabela 2. Wyniki alkalicznej i neutralnej wersji testu kometowego po 24-godzinnej inkubacji komórek linii nowotworowych z badanymi pochodnymi pirazolo-triazyny. Uszkodzenia DNA zostały przedstawione jako mediana zawartości procentowej DNA w ogonie komet wraz z zakresem międzykwartylowym (nawias).

Wersja alkaliczna	Linia komórkowa	Kontrola	MM129		MM130		MM131	
			IC ₅₀	2×IC ₅₀	IC ₅₀	2×IC ₅₀	IC ₅₀	2×IC ₅₀
alkaliczna	HeLa	1,1 (0,3-2,4)	4,8 * (2,7-9,8)	5,9 * (3,2-12,6)	2,8 * (1,5-7,6)	4,1 * (2,3-7,9)	3,4 * (1,6-7,4)	8,1 * (3,9-13,7)
	HCT 116	1,3 (0,5-2,1)	10,7 * (4,7-28,1)	24,9 * (12,4-46,3)	22,7 * (10,3-44)	25,6 * (14,1-41,3)	31,5 * (19,8-51,3)	38,8 * (25,3-57)
	PC-3	3,4 (2,2-4,8)	13,8 * (4-30,6)	21,8 * (10,4-38,2)	12,4 * (4,2-33,4)	19,8 * (9,6-34)	29,4 * (17,9-41)	40,3 * (28-53,2)
	BxPC-3	1,6 (0,5-2,6)	6,7 * (2,3-20,7)	20,7 * (10,5-27,4)	9,1 * (2,2-25)	15,8 * (4,5-29,9)	7,5 * (1,7-23,9)	17,4 * (2,5-27,7)
HeLa								
Wersja neutralna	HCT 116	2,9 (1,9-4)	19,4 * (13,3-29,2)	26,9 * (19,9-34,3)	21,2 * (14,9-31,7)	30,6 * (24,8-36,1)	15,8 * (11,7-23,1)	25,6 * (19,7-33,1)
	PC-3	1,3 (0,4-2,3)	2,4 * (1,1-3,8)	7,3 * (5,1-10,3)	1,5 * (0,4-3,1)	2,2 * (1,2-3,7)	2,3 * (1,3-3,6)	4,3 * (2,8-6,3)
	BxPC-3	2,5 (0,4-4,4)	8,7 * (6,1-13,9)	10 * (6,9-13,9)	7 * (4,7-12,2)	8,5 * (6,1-12,9)	9,6 * (6,8-13,4)	9,7 * (7,4-12,9)

* Różnice istotne statystycznie ($p < 0,0001$) w porównaniu z kontrolą negatywną.

■ Najwyższa aktywność genotoksyczna.

Celem potwierdzenia obecności DSBs, zastosowano immunocytochemiczne wykrywanie histonu γ -H2AX, które wykazało najsilniejszy potencjał genotoksyczny związku **MM131**.

Silniejsze właściwości cytotoksyczne i genotoksyczne **MM130** i **MM131** w porównaniu z **MM129** mogą wynikać z różnic w ugrupowaniu chemicznym pomiędzy tymi związkami. Związek **MM129** posiada w swojej strukturze chemicznej chlorowoderek estru metylowego cis-4-hydroksy-L-proliny, z kolei związki **MM130** i **MM131** stereoizomer 2-aminopropanolu, wśród których izomer R występujący w związku **MM131** wykazał silniejszy potencjał cytotoksyczny i genotoksyczny niż izomer S (**MM130**). Różnice w działaniu między stereoizomerami mogą wynikać z ich właściwości farmakokinetycznych, takich jak wchłanianie, biodostępność, dystrybucja i metabolizm, a także ich siły i aktywności farmakologicznej. Parametry te mogą wpływać na funkcjonalność danego związku, determinując jego właściwości biologiczne. Przykładem takiej zależności mogą być leki należące do selektywnych agonistów beta-2 będących racemiczną mieszaniną izomerów R- i S-. Co ciekawe, tylko izomer R ma działanie beta-2-agonistyczne, podczas gdy sam izomer S nie posiada tej aktywności, a co więcej, może sprzyjać stanom zapalnym. Przykładem może być lek Salbutamol, który jest dostępny w postaci pojedynczego preparatu izomerycznego R jako lewalbuterol. Inne związki mogą być w określonej izomerii niezwykle niebezpieczne (S-Thalidomid, S-Naproxen), czy też być nieaktywne biologicznie (R-ibuprofen) [24]. Powyższe dane wskazują, że zaobserwowane różnice w cytotoksyczności oraz w genotoksyczności pomiędzy izomerami **MM130** i **MM131** mogą wynikać z ich odmiennej struktury przestrzennej, co wydaje się potwierdzać zasadność badań izomerów danego związku chemicznego (jeśli w takich postaciach występuje).

Druga oryginalna publikacja pt: „*Pyrazolo[4,3-e]tetrazolo[1,5-b][1,2,4]triazine Sulfonamides as Novel Potential Anticancer Agents: Apoptosis, Oxidative Stress, and Cell Cycle Analysis*” dotyczy oceny zdolności do indukcji apoptozy, stresu oksydacyjnego

oraz zmian w przebiegu cyklu komórkowego oraz jego poszczególnych faz przez nowe pochodne pirazolo-triazyny (**MM129**, **MM130** i **MM131**).

Aktywność proapoptotyczną badanych pochodnych pirazolo-triazyny wykazano poprzez zaobserwowane obniżenie potencjału transbłonowego mitochondriów badanych komórek linii nowotworowych oraz eksternalizację fosfatydyloseryny na powierzchnię błony komórkowej. Zmiany morfologiczne komórek związane z procesem apoptozy potwierdzono wykorzystując mikroskopie fluorescencyjną i metodę podwójnego barwienia z użyciem oranżu akrydyny (ang. *acridine orange*, OA) i bromku etydyny (ang. *ethidium bromide*, EB). Analizując wyniki otrzymane z testu wiązania Aneksyny V z wykorzystaniem cytometru przepływowego stwierdzono, że pochodne pirazolo-triazyny indukowały apoptozę w komórkach linii HeLa i HCT 116 po 24 godzinach inkubacji z ww. związkami już przy stężeniu równym wyznaczonym wartościom IC_{50} . Dla komórek linii PC-3 i BxPC-3 zmiany te dla badanych pochodnych pirazolo-triazyny były odnotowane po zastosowaniu najwyższego stężenia $2 \times IC_{50}$. Spośród testowanych związków najwyższy potencjał proapoptotyczny wykazał związek **MM129**, który w stężeniu $\frac{1}{2} IC_{50}$ jako jedyny indukował apoptozę w komórkach HeLa po 24-godzinnym czasie ekspozycji. Ponadto był on również najbardziej skuteczny w stosunku do komórek linii PC-3, gdzie po 48 h inkubacji przy stężeniu IC_{50} zaobserwowano istotny statystycznie wzrost frakcji komórek apoptotycznych.

Obserwacja mikroskopowa (barwienie OA/BE) potwierdziła obecność zmian morfologicznych, charakterystycznych dla procesu apoptozy, do których należą: obkurczanie komórki przy jednoczesnym zachowaniu ciągłości błony komórkowej, gromadzenie się ziarnistości chromatyny, fragmentacja jądra komórkowego czy pofałdowanie błony komórkowej wraz z tworzeniem się na jej powierzchni ciałek apoptotycznych. Analogicznie do testu wiązania Aneksyny V największy wzrost liczby komórek apoptotycznych zaobserwowano po zastosowaniu najwyższego badanego stężenia ($2 \times IC_{50}$), gdzie odnotowano istotne statystycznie zmiany liczby komórek będących w fazie apoptozy, o czym świadczyły zmiany ich morfologii.

W przypadku komórek linii HeLa związek **MM129** indukował zwiększenie frakcji komórek apoptotycznych niemal dwukrotnie wyższe w porównaniu z pochodnymi **MM130** i **MM131** ($73,7 \pm 5,86\%$ komórek apoptotycznych dla **MM129** vs $38,67 \pm 4,73\%$ i $32,67 \pm 6,43\%$ dla **MM130** i **MM131**).

Dane literaturowe wskazują, iż spadek potencjału mitochondrialnego ($\Delta\Psi_m$) może stanowić o wczesnej inicjacji szlaku sygnalizacyjnego apoptozy, jak również być konsekwencją apoptozy, która jest indukowana poprzez otwarcie porów przejściowej przepuszczalności mitochondriów (ang. *permeability transition pore*, PTP) [25,26]. W związku z tym, w kolejnym etapie prezentowanej rozprawy doktorskiej oceniono wpływ pochodnych pirazolo-triazyny na zmiany w potencjale transbłonowym mitochondriów komórek nowotworowych. Podobnie jak w teście związanym z eksternalizacją fosfatydyloseryny, w przypadku komórek linii HeLa oraz HCT 116 istotne obniżenie $\Delta\Psi_m$ wskazujące na indukcję apoptozy zostało zaobserwowane po 24 godzinach ekspozycji ww. komórek na testowane pochodne pirazolo-triazyny w stężeniu $2 \times IC_{50}$. Zaburzenia w poziomie $\Delta\Psi_m$ odnotowano również dla komórek PC-3 i BxPC-3 po 48 godzinnym czasie inkubacji ze związkami MM w przypadku najwyższego zastosowanego stężenia. Z kolei, najwyższy spadek potencjału mitochondrialnego zaobserwowano w komórkach linii HeLa po ich 48-godzinnej ekspozycji na związek **MM129** ($67,53 \pm 7,94\%$ wartości kontrolnej). Spektrum badań dotyczących aktywności proapoptotycznej związków MM został przedstawiony w Tabeli 3.

Tabela 3. Porównanie potencjału proapoptycznego związków MM129, MM130 i MM131 po 24-godzinnej oraz 48-godzinnej inkubacji.

Metoda	Czas inkubacji	Linia komórkowa	Kontrola	MM129		MM130		MM131	
				IC ₅₀	2×IC ₅₀	IC ₅₀	2×IC ₅₀	IC ₅₀	2×IC ₅₀
Aneksyna V ¹	24 h	HeLa	6,7 ± 0,7	17,4 ± 1,7 *	73,5 ± 3,5 *	17,3 ± 2,6 *	55,6 ± 1,3 *	15,5 ± 1,4 *	26,1 ± 1,6 *
		HCT 116	6,9 ± 2,6	14,4 ± 2,7 *	18,6 ± 1,7 *	16,8 ± 6,3 *	20,7 ± 5,8 *	14,3 ± 3,3 *	14,8 ± 0,7 *
		PC-3	9 ± 2,8	9 ± 3,4	11,2 ± 2,5	5,9 ± 2,2	8,8 ± 3,5	6,2 ± 2,7	9,6 ± 3,4
	BxPC-3	13,8 ± 1,8	17,1 ± 1,2	19,2 ± 1,9	18,1 ± 3,2	19,2 ± 1,5	18,5 ± 1,3	20,1 ± 4,8	
	HeLa	7,1 ± 1,8	40 ± 0,82 *	89 ± 2,2 *	20,6 ± 1,7 *	76,5 ± 2,3 *	15,9 ± 0,7 *	52,2 ± 6,3 *	
	HCT 116	10,4 ± 2,3	61 ± 1,1 *	76,5 ± 1,9 *	57,3 ± 3 *	74,3 ± 0,3 *	50,2 ± 1 *	74,2 ± 0,8 *	
48 h	PC-3	6,7 ± 1,6	23,3 ± 9 *	32,8 ± 3,1 *	14,3 ± 0,8	23,7 ± 0,6 *	14,4 ± 1	17,4 ± 2 *	
	BxPC-3	12 ± 3,4	19,4 ± 3,3 *	38,4 ± 2,9 *	24,8 ± 4,4 *	34,1 ± 3,2 *	21,2 ± 1,9 *	34,1 ± 1,8 *	
	HeLa	85,5 ± 7,6	70,1 ± 7,4 *	87,6 ± 2,2	87,6 ± 2,2	74,3 ± 5,5 *	87,5 ± 0,9	76,9 ± 9 *	
24 h	HCT 116	83,6 ± 2,8 *	77,9 ± 6,6 *	88,6 ± 3,5	88,6 ± 3,5	81,8 ± 11,3 *	85,4 ± 1,8	75,5 ± 0,7 *	
	PC-3	91,7 ± 8,5	81,5 ± 7,1	91,2 ± 6,7	91,2 ± 6,7	87,8 ± 6,2	92,1 ± 1,4	89,3 ± 3,9	
	BxPC-3	90,5 ± 3,1	85,4 ± 4,3	87,3 ± 3,7	87,3 ± 3,7	84,7 ± 4	89,8 ± 7	85,8 ± 5,1	
MitoTracker Red ²	HeLa	86,5 ± 5,3	67,5 ± 7,9 *	88 ± 1,3	88 ± 1,3	77,8 ± 7,1 *	86,9 ± 6,9	75,5 ± 1,8 *	
	HCT 116	80,2 ± 7,9 *	78 ± 6,8 *	82,8 ± 5,2 *	82,8 ± 5,2 *	78,2 ± 5 *	85,3 ± 2,3	79,4 ± 7,3 *	
	PC-3	80,2 ± 10,8	70,1 ± 14,2 *	86,6 ± 2,1	86,6 ± 2,1	78 ± 9,2 *	83,2 ± 3,5	75,1 ± 10,1 *	
BxPC-3	84,5 ± 8,1	73,9 ± 7,8 *	87,4 ± 1,6	87,4 ± 1,6	76,8 ± 4,9 *	85,4 ± 8,7	74 ± 3,3 *		
Barwienie AO/EB ¹	HeLa	1,3 ± 0,6	32 ± 6,1 *	73,7 ± 5,9 *	23,3 ± 2,5 *	38,7 ± 4,7 *	13,3 ± 1,5 *	32,7 ± 6,4 *	
	HCT 116	2,3 ± 2,1	23,3 ± 5,5 *	27,7 ± 6,7 *	14,3 ± 4,5 *	31 ± 6,2 *	21 ± 7,2 *	28,7 ± 5,7 *	
	PC-3	6 ± 2	8,7 ± 1,5	13,3 ± 4,2 *	11,7 ± 1,5	18,3 ± 2,5 *	7 ± 3	16,3 ± 4 *	
	BxPC-3	3 ± 2	16,3 ± 3,5 *	26 ± 2 *	13 ± 2,6 *	23,7 ± 5,1 *	14,7 ± 2,3 *	27,7 ± 4,2 *	

¹ Liczba komórek apoptotycznych (%) wyrażona jako średnia ± SD.

² Zmiany w $\Delta\Psi_m$ wyrażone jako średnia ± SD względem kontroli (100%).

* Różnice istotne statystycznie ($p < 0,05$) w porównaniu z kontrolą negatywną.

■ Najwyższa aktywność proapoptotyczna.

Kolejnym etapem badań była ocena właściwości prooksydacyjnych nowych pochodnych pirazolo-triazyny z wykorzystaniem sondy fluorescencyjnej H₂DCFDA. Wszystkie testowane związki indukowały po 2 h inkubacji, zależny od stężenia, wzrost reaktywnych form tlenu (RFT) we wszystkich badanych typach komórek nowotworowych, co potwierdziło wysoką aktywność prooksydacyjną związków MM. Kumulacja RFT może prowadzić zarówno do inicjacji pęknięć nici DNA, jak i do uszkodzenia mitochondrialnego DNA prowadząc do jego degradacji [27]. Wysoka aktywność prooksydacyjna związków MM jest zgodna z wynikami uzyskanymi w publikacji *“Pyrazolo[4,3-*e*]tetrazolo[1,5-*b*][1,2,4]triazine Sulfonamides as Novel Potential Anticancer Agents: Cytotoxic and Genotoxic Activities In Vitro”*, w której badane związki wykazywały wysoką aktywność genotoksyczną wobec tych samych linii komórek nowotworowych. Podobnie jak w przypadku badań stopnia genotoksyczności pochodnych pirazolo-triazyny, najsilniejsze działanie prooksydacyjne wykazał związek **MM131**.

Niezwykle ważnym parametrem w aspekcie przeciwnowotworowego potencjału nowych związków jest analiza ich wpływu na przebieg cyklu komórkowego i jego faz. Przeprowadzone badania wykazały, że spośród badanych pochodnych pirazolo-triazyny tylko związek **MM129** w stężeniu IC₅₀ wywierał znaczący wpływ na przebieg cyklu komórkowego w komórkach linii HeLa, poprzez wzrost odsetka (%) komórek w fazie subG1, przy jednoczesnym spadku liczby komórek (%) w fazie G0/G1. W przypadku komórek HCT 116 zaobserwowano kumulację komórek w fazie S oraz zmniejszenie udziału komórek w fazie G2/M po potraktowaniu pochodnymi pirazolo-triazyny w stężeniu IC₅₀. Analiza przebiegu cyklu komórkowego w komórkach PC-3 wykazała, że wszystkie badane związki MM zwiększały liczbę komórek (%) w fazach G0/G1 i subG1 oraz powodowały spadek ich liczby w fazie S. W przypadku ekspozycji komórek BxPC-3 na badane pochodne pirazolo-triazyny w stężeniu IC₅₀, odnotowano wzrost liczby komórek w fazie G0/G1, przy jednoczesnym spadku liczby komórek w fazie G2/M. Wpływ testowanych

pochodnych pirazolo-triazyny na przebieg cyklu komórkowego i jego poszczególnych faz w komórkach badanych linii nowotworowych przedstawiono w Tabeli 4.

Tabela 4. Wpływ związków **MM129**, **MM130** i **MM131** w stężeniu IC₅₀ na przebieg cyklu komórkowego i jego poszczególnych faz w komórkach linii nowotworowych HeLa, HCT 116, PC-3 i BxPC-3 po ich 24-godzinnej inkubacji z badanymi pochodnymi pirazolo-triazyny. Statystycznie istotny ($p < 0,05$) wzrost (↑) lub spadek (↓) liczby komórek w danej fazie cyklu komórkowego w porównaniu z kontrolą negatywną.

Linia komórkowa	MM129	MM130	MM131
HeLa	↑ subG1; ↓ G0/G1	—	—
HCT 116	↑ S; ↓ G2/M	↑ S; ↓ G2/M	↑ S; ↓ G2/M; ↓ G0/G1
PC-3	↑ subG1; ↓ S;	↑ subG1; ↓ S; ↑ G0/G1	↑ subG1; ↓ S; ↑ G0/G1
BxPC-3	↑ G0/G1; ↓ G2/M	↑ G0/G1; ↓ G2/M	↑ G0/G1; ↓ G2/M

* Różnice istotne statystycznie ($p < 0,0001$) w porównaniu z kontrolą negatywną.

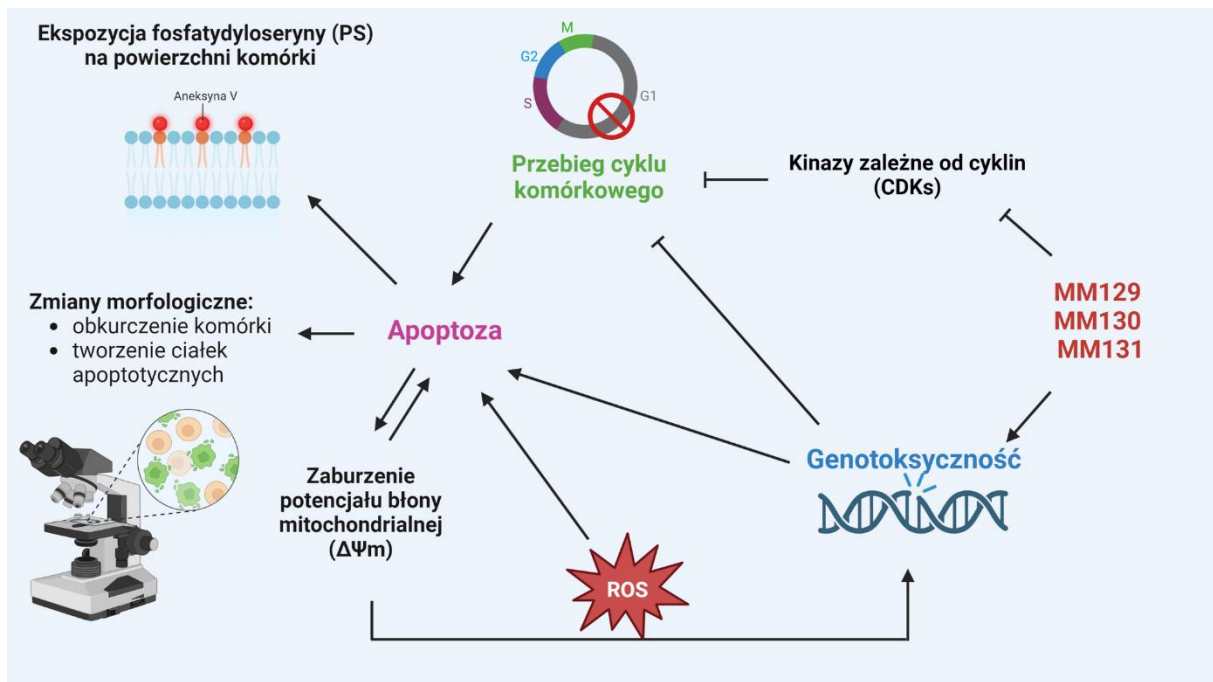
■ Najwyższy wzrost/spadek liczby komórek w danej fazie cyklu komórkowego.

Zaobserwowane, zróżnicowane działanie pochodnych pirazolo-triazyny wobec różnych typów komórek nowotworowych, potwierdzają dane literaturowe, w których wykazano, iż ten sam lek przeciwnowotworowy może działać odmiennie na różne linie komórek nowotworowych. Na przykład 5-fluorouracyl zwiększał akumulację komórek w fazie G0/G1 w komórkach raka żołądka AGS i w niektórych liniach komórkowych raka jelita grubego, takich jak HT-29 i DLD-1, podczas gdy w przypadku komórek raka jamy ustnej HSC-4 i komórek raka okrężnicy SW620 obserwowano zwiększoną liczbę komórek w fazie S [9,28,29].

W regulację cyklu komórkowego oraz w kontrolę transkrypcji, a także wzrost komórek i proliferację zaangażowane są kinazy zależne od cyklin (CDKs). Odgrywają one również kluczową rolę w patogenezie nowotworów [30]. W związku z tym, ostatnim etapem badań, były badania *in silico*, które obejmowały dokowanie molekularne pochodnych pirazolo-triazyny z enzymami CDK, a także symulacje dynamiki molekularnej dla związku o potencjalnie najwyższych zdolnościach do

tworzenia kompleksów z kinazami zależnymi od cyklin. Analiza dokowania molekularnego wskazała na wysoki potencjał badanych pochodnych pirazolo-triazyny do wiązania się z CDKs, a w szczególności związku **MM129**, który wykazywał najniższe wartości energii wiązania spośród badanych pochodnych pirazolo-triazyny, zwłaszcza dla CDK4 i CDK7. Wyniki symulacji dynamiki molekularnej potwierdziły wystarczającą stabilność kompleksów **MM129/CDKs**, głównie z CDK5 i CDK8. Interakcja badanych związków z CDKs może być jedną z potencjalnych przyczyn zaburzeń przebiegu cyklu komórkowego w komórkach nowotworowych inkubowanych z testowanymi pochodnymi pirazolo-triazyny.

Przedstawione w niniejszej pracy doktorskiej badania wykazały zróżnicowaną, zależną od linii komórkowej, aktywność cytotoksyczną, genotoksyczną, proooksydacyjną i proapoptotyczną nowych pochodnych układu pirazolo[4,3-*e*]tetrazolo[1,5-*b*][1,2,4]triazyny – **MM129**, **MM130** i **MM131** w badanym modelu komórkowym. W pierwszej publikacji eksperymentalnej wykazano dużą cytotoksyczność i genotoksyczność badanych związków, zaś w kolejnej, ich wysoki potencjał proooksydacyjny i proapoptotyczny wobec komórek HeLa, HCT 116, PC-3 i BxPC-3. Badane związki MM wpływały również na przebieg cyklu komórkowego, indukując zależne od linii komórkowej, zatrzymanie cyklu w fazie G0/G1 lub S. Powyższe zmiany sugerują, że zmiany w przebiegu poszczególnych faz cyklu komórkowego oraz wzrost liczby komórek w fazie apoptozy mogą wynikać z silnej genotoksyczności badanych pochodnych pirazolo-triazyny. Ponadto, badania *in silico* wskazują na zdolność badanych pochodnych pirazolo-triazyny do hamowania CDK, przez co mogą wpływać na przebieg cyklu komórkowego. Dodatkowo, silne właściwości proooksydacyjne związków MM mogą zwiększać ich właściwości genotoksyczne i proapoptotyczne (Rycina 2).



Rycina 2. Potencjalny mechanizm działania MM129, MM130 i MM131 w oparciu o przeprowadzone badania *in vitro* i *in silico*.

Wnioski

Wyniki badań przeprowadzonych w celu realizacji postawionych w pracy doktorskiej zadań badawczych, pozwalają na sformułowanie następujących wniosków:

- Nowe, trójpierścieniowe pochodne układu pirazolo[4,3-*e*]tetrazolo[1,5-*b*] [1,2,4]triazyny wykazały wyższą cytotoksyczność w stosunku do komórek linii nowotworowych: raka szyjki macicy (HeLa), raka okrężnicy (HCT 116), raka prostaty (PC-3) oraz gruczolakoraka trzustki (BxPC-3) w porównaniu z komórkami prawidłowymi: jednojądrzastymi komórkami krwi obwodowej (PBMCs) i fibroblastami napletka (Hs27).
- Badane pochodne pirazolo-triazyny (**MM129**, **MM130** i **MM131**) charakteryzowały się wysokim potencjałem genotoksycznym, proooksydacyjnym i proapoptotycznym względem badanego modelu komórkowego.
- Komórki linii nowotworowej HCT 116 były najbardziej wrażliwe na indukcję podwójnych pęknięć DNA przez badane związki MM.
- Najwyższe działanie proapoptotyczne zaobserwowano w komórkach linii nowotworowej HeLa i HCT 116.
- Analiza zmian w przebiegu cyklu komórkowego wskazała na akumulację komórek linii BxPC-3 i PC-3 w fazie G₀/G₁, zaś komórek linii HCT 116, w fazie S. Ponadto w przypadku komórek PC-3 oraz HeLa zaobserwowano wzrost fazy subG₁, co potwierdza proapoptotyczny charakter związków MM.
- Dokowanie molekularne i symulacja dynamiki molekularnej wykazała zdolność badanych pochodnych pirazolo-triazyny do hamowania CDKs, przez co mogą wpływać na przebieg cyklu komórkowego.
- Związek **MM131** wykazywał najsilniejsze właściwości cytotoksyczne, genotoksyczne oraz proooksydacyjne, natomiast **MM129** powodował największą kumulację komórek linii HeLa i PC-3 w fazie subG₁ potwierdzając tym samym

efektywne działanie proapoptotyczne oraz charakteryzował się najwyższym potencjałem do tworzenia kompleksów z enzymami CDK.

- Wszystkie badane związki MM będące pochodnymi pirazolo-triazyny wykazały silny potencjał onkoterapeutyczny względem badanych komórek linii nowotworowych, w układzie *in vitro*.

Literatura uzupełniająca

1. Ferlay, J.; Colombet, M.; Soerjomataram, I.; Parkin, D.M.; Piñeros, M.; Znaor, A.; Bray, F. Cancer Statistics for the Year 2020: An Overview. *Int. J. Cancer* **2021**, *149*, 778–789, doi:10.1002/ijc.33588.
2. Bukowski, K.; Kciuk, M.; Kontek, R. Mechanisms of Multidrug Resistance in Cancer Chemotherapy. *IJMS* **2020**, *21*, 3233, doi:10.3390/ijms21093233.
3. Nussbaumer, S.; Bonnabry, P.; Veuthey, J.-L.; Fleury-Souverain, S. Analysis of Anticancer Drugs: A Review. *Talanta* **2011**, *85*, 2265–2289, doi:10.1016/j.talanta.2011.08.034.
4. Chen, X.-Y.; Yin, Y.; Xi, J.; Yuan, Y.; Li, Y.; Li, Q.; Wang, R.-X.; Yao, Z.-J.; Tang, G.-L. 11-Aza-Artemisinin Derivatives Exhibit Anticancer Activities by Targeting the Fatty Acid Binding Protein 6 (FABP6): 11-Aza-Artemisinin Derivatives Exhibit Anticancer Activities by Targeting the Fatty Acid Binding Protein 6 (FABP6) †. *Chin. J. Chem.* **2018**, *36*, 1197–1201, doi:10.1002/cjoc.201800361.
5. Makhmudiyarova, N.N.; Ishmukhametova, I.R.; Dzhemileva, L.U.; Dzhemilev, U.M. (3-(1H-Indol-3-Yl)-2-(7,8,12,13-Tetraoxa-10-Azaspiro[5.7]Tridecan-10-Yl)Propanoic Acid) with Cytotoxic Activity. *Molbank* **2023**, *2023*, M1572, doi:10.3390/M1572.
6. Gornowicz, A.; Szymanowska, A.; Mojzych, M.; Bielawski, K.; Bielawska, A. The Effect of Novel 7-Methyl-5-Phenyl-Pyrazolo[4,3-e]Tetrazolo[4,5-b][1,2,4]Triazine Sulfonamide Derivatives on Apoptosis and Autophagy in DLD-1 and HT-29 Colon Cancer Cells. *IJMS* **2020**, *21*, 5221, doi:10.3390/ijms21155221.
7. Kumar, R.; Sirohi, T.S.; Singh, H.; Yadav, R.; Roy, R.K.; Chaudhary, A.; Pandeya, S.N. 1,2,4-Triazine Analogs as Novel Class of Therapeutic Agents. *MRMC* **2014**, *14*, 168–207, doi:10.2174/1389557514666140131111837.
8. Supuran, C. Special Issue: Sulfonamides. *Molecules* **2017**, *22*, 1642, doi:10.3390/molecules22101642.
9. Gornowicz, A.; Szymanowska, A.; Mojzych, M.; Czarnomysy, R.; Bielawski, K.; Bielawska, A. The Anticancer Action of a Novel 1,2,4-Triazine Sulfonamide Derivative in Colon Cancer Cells. *Molecules* **2021**, *26*, 2045, doi:10.3390/molecules26072045.
10. Kciuk, M.; Mujwar, S.; Szymanowska, A.; Marciniak, B.; Bukowski, K.; Mojzych, M.; Kontek, R. Preparation of Novel Pyrazolo[4,3-e]Tetrazolo[1,5-b][1,2,4]Triazine

- Sulfonamides and Their Experimental and Computational Biological Studies. *IJMS* **2022**, *23*, 5892, doi:10.3390/ijms23115892.
11. Kciuk, M.; Mujwar, S.; Marciniak, B.; Gielecińska, A.; Bukowski, K.; Mojzych, M.; Kontek, R. Genotoxicity of Novel Pyrazolo[4,3-e]Tetrazolo[1,5-b][1,2,4]Triazine Sulfonamides in Normal and Cancer Cells In Vitro. *IJMS* **2023**, *24*, 4053, doi:10.3390/ijms24044053.
 12. Hermanowicz, J.M.; Kalaska, B.; Pawlak, K.; Sieklucka, B.; Miklosz, J.; Mojzych, M.; Pawlak, D. Preclinical Toxicity and Safety of MM-129—First-in-Class BTK/PD-L1 Inhibitor as a Potential Candidate against Colon Cancer. *Pharmaceutics* **2021**, *13*, 1222, doi:10.3390/pharmaceutics13081222.
 13. Hermanowicz, J.M.; Pawlak, K.; Sieklucka, B.; Czarnomysy, R.; Kwiatkowska, I.; Kazberuk, A.; Surazynski, A.; Mojzych, M.; Pawlak, D. MM-129 as a Novel Inhibitor Targeting PI3K/AKT/MTOR and PD-L1 in Colorectal Cancer. *Cancers* **2021**, *13*, 3203, doi:10.3390/cancers13133203.
 14. Hermanowicz, J.M.; Szymanowska, A.; Sieklucka, B.; Czarnomysy, R.; Pawlak, K.; Bielawska, A.; Bielawski, K.; Kalafut, J.; Przybyszewska, A.; Surazynski, A.; et al. Exploration of Novel Heterofused 1,2,4-Triazine Derivative in Colorectal Cancer. *Journal of Enzyme Inhibition and Medicinal Chemistry* **2021**, *36*, 535–548, doi:10.1080/14756366.2021.1879803.
 15. Huanwen, W.; Zhiyong, L.; Xiaohua, S.; Xinyu, R.; Kai, W.; Tonghua, L. Intrinsic Chemoresistance to Gemcitabine Is Associated with Constitutive and Laminin-Induced Phosphorylation of FAK in Pancreatic Cancer Cell Lines. *Mol Cancer* **2009**, *8*, 125, doi:10.1186/1476-4598-8-125.
 16. Ikehata, M.; Ogawa, M.; Yamada, Y.; Tanaka, S.; Ueda, K.; Iwakawa, S. Different Effects of Epigenetic Modifiers on the Cytotoxicity Induced by 5-Fluorouracil, Irinotecan or Oxaliplatin in Colon Cancer Cells. *Biological & Pharmaceutical Bulletin* **2014**, *37*, 67–73, doi:10.1248/bpb.b13-00574.
 17. Becit, M.; Aydın Dilsiz, S.; Başaran, N. Interaction of Curcumin on Cisplatin Cytotoxicity in HeLa and HepG2 Carcinoma Cells. *IJP* **2020**, *50*, doi:10.26650/IstanbulJPharm.2020.0039.
 18. Barbanente, A.; Iacobazzi, R.M.; Azzariti, A.; Hoeschele, J.D.; Denora, N.; Papadia, P.; Pacifico, C.; Natile, G.; Margiotta, N. New Oxaliplatin-Pyrophosphato Analogs with Improved In Vitro Cytotoxicity. *Molecules* **2021**, *26*, 3417, doi:10.3390/molecules26113417.

19. Aras, B.; Yerlikaya, A. Bortezomib and Etoposide Combinations Exert Synergistic Effects on the Human Prostate Cancer Cell Line PC-3. *Oncology Letters* **2016**, *11*, 3179–3184, doi:10.3892/ol.2016.4340.
20. Canga, I.; Vita, P.; Oliveira, A.I.; Castro, M.Á.; Pinho, C. In Vitro Cytotoxic Activity of African Plants: A Review. *Molecules* **2022**, *27*, 4989, doi:10.3390/molecules27154989.
21. Stornetta, A.; Zimmermann, M.; Cimino, G.D.; Henderson, P.T.; Sturla, S.J. DNA Adducts from Anticancer Drugs as Candidate Predictive Markers for Precision Medicine. *Chem. Res. Toxicol.* **2017**, *30*, 388–409, doi:10.1021/acs.chemrestox.6b00380.
22. Reuvers, T.G.A.; Kanaar, R.; Nonnekens, J. DNA Damage-Inducing Anticancer Therapies: From Global to Precision Damage. *Cancers* **2020**, *12*, 2098, doi:10.3390/cancers12082098.
23. Alhmoud, J.F.; Woolley, J.F.; Al Moustafa, A.-E.; Malki, M.I. DNA Damage/Repair Management in Cancers. *Cancers* **2020**, *12*, 1050, doi:10.3390/cancers12041050.
24. Chhabra, N.; Aseri, M.L.; Padmanabhan, D. A Review of Drug Isomerism and Its Significance. *Int J Appl Basic Med Res* **2013**, *3*, 16–18, doi:10.4103/2229-516X.112233.
25. Ly, J.D.; Grubb, D.R.; Lawen, A. The Mitochondrial Membrane Potential ($\Delta\psi(m)$) in Apoptosis; an Update. *APOPTOSIS* **2003**, *8*, 115–128, doi:10.1023/A:1022945107762.
26. Wacquier, B.; Combettes, L.; Dupont, G. Dual Dynamics of Mitochondrial Permeability Transition Pore Opening. *Sci Rep* **2020**, *10*, 3924, doi:10.1038/s41598-020-60177-1.
27. Moon, J.; Kitty, I.; Renata, K.; Qin, S.; Zhao, F.; Kim, W. DNA Damage and Its Role in Cancer Therapeutics. *IJMS* **2023**, *24*, 4741, doi:10.3390/ijms24054741.
28. Gao, K.; Liang, Q.; Zhao, Z.-H.; Li, Y.-F.; Wang, S.-F. Synergistic Anticancer Properties of Docosahexaenoic Acid and 5-Fluorouracil through Interference with Energy Metabolism and Cell Cycle Arrest in Human Gastric Cancer Cell Line AGS Cells. *WJG* **2016**, *22*, 2971, doi:10.3748/wjg.v22.i10.2971.
29. Villalpando-Rodriguez, G.E.; Gibson, S.B. Reactive Oxygen Species (ROS) Regulates Different Types of Cell Death by Acting as a Rheostat. *Oxidative Medicine and Cellular Longevity* **2021**, *2021*, 1–17, doi:10.1155/2021/9912436.
30. Thoma, O.-M.; Neurath, M.F.; Waldner, M.J. Cyclin-Dependent Kinase Inhibitors and Their Therapeutic Potential in Colorectal Cancer Treatment. *Front. Pharmacol.* **2021**, *12*, 757120, doi:10.3389/fphar.2021.757120.

Streszczenie w języku polskim

Choroby nowotworowe są jednym z głównych problemów zdrowia publicznego na świecie. Pomimo znacznego rozwoju innowacyjnych metod leczenia nowotworów, chemioterapia w dalszym ciągu stanowi główną strategię w onkoterapiach. W związku z tym, poszukiwanie nowych, bardziej skutecznych leków przeciwnowotworowych jest wciąż wiodącym i stale rozwijającym się kierunkiem badań na świecie. W ten nurt badań wpisuje się tematyka niniejszej rozprawy doktorskiej, w której zostały przeprowadzone badania aktywności biologicznej zsyntetyzowanych *de novo* pochodnych pirazolo[4,3-*e*]tetrazolo[1,5-*b*][1,2,4]triazyny o potencjalnych właściwościach przeciwnowotworowych: **MM129**, **MM130** i **MM131**.

Badania obejmowały analizę cyto- oraz genotoksyczności, a także ocenę aktywności prooksydacyjnej i proapoptotycznej badanych pochodnych pirazolo-triazyny względem ludzkich komórek linii nowotworowych HeLa (rak szyjki macicy), HCT 116 (rak okrężnicy), PC-3 (rak prostaty) oraz BxPC-3 (gruczolakorak trzustki). Ponadto zbadano wpływ testowanych związków na przebieg cyklu komórkowego i jego poszczególnych faz oraz przeprowadzono badania komputerowe (*in silico*), które pozwoliły na ocenę oddziaływań badanych związków z kinazami zależnymi od cyklin (CDKs). W celu określenia selektywności testowanych związków wobec komórek nowotworowych, badania cytotoxyczności zostały uzupełnione o model ludzkich komórek prawidłowych, który obejmował komórki Hs27 (ludzkie fibroblasty napletka) oraz PBMCs (jednojądrzaste komórki krwi obwodowej człowieka).

Przeprowadzone badania wykazały, że pochodne pirazolo-triazyny są silnie cytotoxyczne w stosunku do badanych komórek w bardzo niskim zakresie stężeń ($IC_{50} = 0,17\text{--}1,15 \mu\text{M}$) po 72 h ekspozycji komórek na działanie związków **MM129**, **MM130** i **MM131**. Testowane pochodne pirazolo-triazyny charakteryzowały się wyższą cytotoxycznością w stosunku do komórek nowotworowych w porównaniu z komórkami prawidłowymi – PBMCs i Hs27. Wykazano, iż związki **MM129**, **MM130** i **MM131** posiadają wysoką aktywność genotoksyczną, prooksydacyjną

i proapoptotyczną wobec badanego modelu komórkowego. Komórki linii nowotworowej HCT 116 wykazały najwyższą wrażliwość na działanie genotoksyczne i proapoptotyczne badanych pochodnych. Efektywne działanie proapoptotyczne badanych związków zaobserwowano również w komórkach linii HeLa. Ocena przebiegu cyklu komórkowego oraz jego poszczególnych faz wykazała wzrost liczby komórek HCT 116 w fazie S, a w przypadku komórek linii BxPC-3 i PC-3 wzrost frakcji G0/G1. Dodatkowo w odniesieniu do komórek linii HeLa i PC-3 nastąpił wzrost ich liczby w fazie subG1. Wyniki badań *in silico* sugerują, iż zdolność testowanych pochodnych pirazolo-triazyny może wynikać z ich potencjału do hamowania CDKs.

Spośród badanych związków, **MM129** charakteryzował się najwyższym potencjałem do tworzenia kompleksów z enzymami CDK oraz indukował najwyższy wzrost liczby komórek PC-3 i HeLa w fazie subG1, zaś związek **MM131** posiadał najsilniejszą aktywność cytotoksyczną, genotoksyczną oraz proooksydacyjną we wszystkich testowanych komórkach. Przeprowadzone badania stanowią istotny wkład w wiedzę dotyczącą właściwości biologicznych nowych pochodnych układu pirazolo[4,3-*e*]tetrazolo[4,5-*b*][1,2,4]triazyny i ich syntez chemicznych. Pozwolą także na efektywne zaplanowanie kolejnych eksperymentów dotyczących dalszej szczegółowej analizy ich aktywności zarówno, w badaniach podstawowych, jak i przedklinicznych i klinicznych.

Streszczenie w języku angielskim

Cancer is one of the primary public health problems worldwide. Despite the significant development of cancer treatment methods, the use of chemotherapeutical agents is still the dominant strategy. Therefore, searching for new and more effective antineoplastic agents is a leading and constantly developing research direction. The subject of this doctoral dissertation was to assess the anticancer activity of de novo synthesized pyrazolo[4,3-*e*]tetrazolo[1,5-*b*][1,2,4]triazine sulfonamide derivatives (**MM129**, **MM130**, and **MM131**).

The studies included the analysis of cyto- and genotoxicity, as well as the examination of the pro-oxidative and pro-apoptotic activity of the tested pyrazole-triazine derivatives against human cancer cells of HeLa (cervical cancer), HCT 116 (colorectal carcinoma), PC-3 (prostate cancer), and BxPC-3 (pancreatic adenocarcinoma) cell lines. In addition, the effect of the tested compounds on the cell cycle distribution was examined, and computational (*in silico*) studies were conducted, which allowed us to test the interaction of the tested compounds with cyclin-dependent kinases (CDKs). Cancer cell-directed cytotoxicity studies were supplemented with the use of normal human cells: Hs27 (human foreskin cells) and PBMCs (peripheral blood mononuclear cells) to determine the selectivity of tested compounds for malignant cells.

Our results demonstrated that pyrazole-triazine derivatives are highly cytotoxic towards the tested cells in very low concentrations ($IC_{50} = 0.17\text{--}1.15\ \mu\text{M}$) following 72 h exposure of cells to **MM129**, **MM130**, and **MM131** compounds. The tested pyrazole-triazine derivatives were more cytotoxic against cancer cells compared to normal PBMCs and Hs27 cells. It was shown that **MM129**, **MM130**, and **MM131** possess high genotoxic, prooxidative, and proapoptotic activity toward investigated types of cancer cells. The highest sensitivity to the genotoxic and proapoptotic effects of the tested derivatives was noticed in HCT 116 cancer cells. Similarly, the high proapoptotic activity of the tested compounds was also observed in HeLa cells. The assessment of

the cell cycle distribution showed an increase in the number of HCT 116 cells in the S phase, while in the case of BxPC-3 and PC-3 cells, an accumulation in the G0/G1 fraction was observed. Moreover, an increase in the number of cells in the subG1 phase was detected in HeLa and PC-3 cells. The results of *in silico* studies suggest that the activity of the tested pyrazole-triazine derivatives may result from their potential inhibitory activity toward CDK enzymes.

Among investigated pyrazole-triazine derivatives, **MM129** exhibited the strongest predicted binding efficacy with CDK enzymes and induced the highest increase of cells in the subG1 phase in PC-3 and HeLa cell lines. In contrast, **MM131** showed the highest cytotoxic, genotoxic, and prooxidative potential in all investigated cell lines. The research provides a significant contribution to the knowledge on the biological properties of new derivatives of the pyrazolo[4,3-*e*]tetrazolo[4,5-*b*][1,2,4]triazine system and their chemical synthesis. The acquired findings will facilitate the efficient design of subsequent experiments using the *in vivo* models.

Dorobek naukowy

Publikacje wchodzące w zakres rozprawy doktorskiej:

1. **Bukowski, K.**; Kciuk, M.; Kontek, R. Mechanisms of Multidrug Resistance in Cancer Chemotherapy. *International Journal of Molecular Sciences* **2020**, *21*, 3233. <https://doi.org/10.3390/ijms21093233> (MEiN = 140 pkt, IF = 5,923).
2. **Bukowski K.**, Marciniak, B.; Kciuk, M.; Mojzych, M.; Kontek, R. Pyrazolo[4,3-e]tetrazolo[1,5-b][1,2,4]triazine Sulfonamides as Novel Potential Anticancer Agents: Cytotoxic and Genotoxic Activities In Vitro. *Molecules* **2022**, *27*, 3761. <https://doi.org/10.3390/molecules27123761>. (MEiN = 140 pkt, IF = 4,927).
3. **Bukowski K.**, Marciniak, B.; Kciuk, M.; Mujwar, S.; Mojzych, M.; Kontek, R. Pyrazolo[4,3-e]tetrazolo[1,5-b][1,2,4]triazine Sulfonamides as Novel Potential Anticancer Agents: Apoptosis, Oxidative Stress, and Cell Cycle Analysis. *International Journal of Molecular Sciences* **2023**, *24*, 8504. <https://doi.org/10.3390/ijms24108504> (MEiN = 140 pkt, IF = 6,208).

Pozostałe publikacje z listy JCR:

4. **Bukowski, K.**; Woźniak, K. Polymorphism of Genes Encoding Proteins of DNA Repair vs. Occupational and Environmental Exposure to Lead, Arsenic and Pesticides. *Medycyna Pracy* **2017**. <https://doi.org/10.13075/mp.5893.00595> (MEiN = 40 pkt, IF = 0,76).
5. Mokra, K.; **Bukowski, K.**; Woźniak, K. Effects of Tris(1-Chloro-2-Propyl)Phosphate and Tris(2-Chloroethyl)Phosphate on Cell Viability and Morphological Changes in Peripheral Blood Mononuclear Cells (in vitro Study). *Human and Experimental Toxicology* **2018**, *37*, 1336–1345, <https://doi.org/10.1177/0960327118783529> (MEiN = 70 pkt, IF = 2,903).
6. **Bukowski, K.**; Wysokinski, D.; Mokra, K.; Wozniak, K. DNA Damage and Methylation Induced by Organophosphate Flame Retardants: Tris(2-Chloroethyl) Phosphate and Tris(1-Chloro-2-Propyl) Phosphate in Human Peripheral Blood

- Mononuclear Cells. *Human and Experimental Toxicology* **2019**, 38, 724–733, <https://doi.org/10.1177/0960327119839174> (MEiN = 70 pkt, IF = 2,903).
7. Kciuk, M.; **Bukowski, K.**; Marciniak, B.; Kontek, R. Advances in DNA Repair—Emerging Players in the Arena of Eukaryotic DNA Repair. *International Journal of Molecular Sciences* **2020**, 21, 3934. <https://doi.org/10.3390/ijms21113934> (MEiN = 140 pkt, IF = 5,924).
 8. Malinowski, Z.; Fornal, E.; Sumara, A.; Kontek, R.; **Bukowski, K.**; Pasternak, B.; Sroczyński, D.; Kusz, J.; Małecka, M.; Nowak, M. Amino- and Polyaminophthalazin-1(2 H)-Ones: Synthesis, Coordination Properties, and Biological Activity. *Beilstein J. Org. Chem.* **2021**, 17, 558–568, <https://doi.org/10.3762/bjoc.17.50> (MEiN = 70 pkt, IF = 2,883)
 9. Kciuk, M.; Mujwar, S.; Szymanowska, A.; Marciniak, B.; **Bukowski, K.**; Mojzych, M.; Kontek, R. Preparation of Novel Pyrazolo[4,3-e]tetrazolo[1,5-b][1,2,4]triazine Sulfonamides and Their Experimental and Computational Biological Studies. *International Journal of Molecular Sciences* **2022**, 23, 5892. <https://doi.org/10.3390/ijms23115892> (MEiN = 140 pkt, IF = 5,924).
 10. Kciuk, M.; Mujwar, S.; Marciniak, B.; Gielecińska, A.; **Bukowski, K.**; Mojzych, M.; Kontek, R. Genotoxicity of Novel Pyrazolo[4,3-e]tetrazolo[1,5-b][1,2,4]triazine Sulfonamides in Normal and Cancer Cells In Vitro. *International Journal of Molecular Sciences* **2023**, 24, 4053. <https://doi.org/10.3390/ijms24044053> (MEiN = 140 pkt, IF = 6,208).

Rozdziały w monografiach pokonferencyjnych:

1. **Bukowski K**; Rola polimorfizmu genów naprawy DNA w narażeniu na związki obecne w dymie tytoniowym i ich związek z indukcją nowotworów; Zdrowie i choroba w ujęciu socjomedycznym; 97 – 106; ISBN: 978-83-65374-25-7; Exante Wydawnictwo Naukowe (MEiN = 5 pkt)

2. **Bukowski K**; Fosforoorganiczne związki opóźniające palenie i ich przenikanie do organizmu człowieka; Zagadnienia aktualnie poruszane przez młodych naukowców 12; 185 – 191; ISBN: 978-83-63058-81-4; CreativeTime (MEiN = 5 pkt)
3. **Bukowski K**; Właściwości biologiczne kapsaicyny; Zagadnienia aktualnie poruszane przez młodych naukowców 14; 99– 104; ISBN: 978-83-63058-87-6; CreativeTime (MEiN = 5 pkt)
4. **Bukowski K**; Wpływ ekstraktów z *Rhodiola rosea* L. na układ nerwowy człowieka – właściwości adaptogenne, przeciwdepresyjne i obniżające „wypalenie zawodowe” w monografii; Nauki medyczne i nauki o zdrowiu – Część V; 16– 22; eISBN: 978-83-66392-21-2; CreativeTime (MEiN = 5 pkt)

Sumaryczny IF = 44,562 (1110 pkt MEiN)

Doniesienia zjazdowe:

1. **Bukowski K.**, Woźniak K.; Organiczne związki fosforowe zmniejszające palność jako alternatywa dla polibromowanych eterów difenylowych; VI Konferencja Biologii Molekularnej; Łódź, 6-8.04.2017; str 60
2. **Bukowski K.**, Mokra K., Woźniak K.; Analiza żywotności i zmian morfologicznych jednojądrzastych komórek krwi obwodowej człowieka inkubowanych z organicznymi hydrofilowymi związkami fosforowymi tris(1-chloro-2-propylo) i tris(2-chloroetylo) fosforanem; Nowe Wyzwania dla Polskiej Nauki, Edycja II; Kraków, 9.12.2017; str 77
3. **Bukowski K**, Wysokiński D, Woźniak K.; Analiza genotoksyczności oraz działania epigenetycznego związków fosforowych zmniejszających palność: tris(2-chloropropylo) i tris (2-chloroetylo) fosforanu w jednojądrzastych komórkach krwi obwodowej człowieka; BiOpen, IV Ogólnopolska Konferencja Doktorantów Nauk o Życiu; Łódź, 24-25.05.2018; str 118
4. **Bukowski K.**, Woźniak K.; Wpływ związków fosforoorganicznych zmniejszających palność na poziom metylacji i uszkodzeń DNA w komórkach człowieka; IX Sesja Magistrantów i Doktorantów Łódzkiego Środowiska

Chemików; Łódź, 21.06.2018; str. 16; plakat został nagrodzony podwójnym wyróżnieniem (najlepszy plakat prezentujący wyniki pracy magisterskiej) – wyróżnienie Dziekana Wydziału Biologii i Ochrony Środowiska Uniwersytetu Łódzkiego oraz Oddziału Łódzkiego Towarzystwa Chemicznego

5. **Bukowski K.**, Materska M., Marciniak B.; Ocena cytotoksyczności ekstraktów z owoców papryki słodkiej i ostrej; Nowe Wyzwania Dla Polskiej Nauki, Edycja IV; Warszawa, 2.12.18; str. 79.
6. **Bukowski K.**, Kontek R, Bernat Z, Mojzych M, Marciniak B.; Evaluation of cytotoxicity of de novo synthesized tricyclic derivatives of the pyrazolo [4,3-e] [1,2,4] triazine; 5th International Conference of Cell Biology; str. 86
7. **Bukowski K.**, Kciuk M, Barylak K, Kontek R, Mojzych M.; Ocena cytotoksyczności syntetyzowanych de novo trójcyklicznych pochodnych układu pirazolo[4,3-e][1,2,4]triazyny; IV Studencka Konferencja Biologii Medycznej Biofuzje; str. 43
8. **Bukowski K.**, Nowak M, Malinowski Z, Kontek R; Ocena cytotoksyczności zsyntetyzowanych de novo pochodnych ftalazynonu; V Ogólnopolska Konferencja Doktorantów Nauk o Życiu Bioopen; str. 86
9. **Bukowski K.**, Mojzych M.; Ocena genotoksycznych właściwości zsyntetyzowanych de novo pochodnych pyrazolo[4,3 E][1,2,4] triazyny in vitro; VI Ogólnopolska Konferencja Doktorantów Nauk o Życiu Bioopen; str. 36

Kopie publikacji wchodzących w zakres rozprawy doktorskiej



Review

Mechanisms of Multidrug Resistance in Cancer Chemotherapy

Karol Bukowski *, Mateusz Kciuk and Renata Kontek

Department of Molecular Biotechnology and Genetics, Faculty of Biology and Environmental Protection, University of Lodz, 12/16 Banacha St., 90-237 Lodz, Poland; mateusz.kciuk@unilodz.eu (M.K.); renata.kontek@biol.uni.lodz.pl (R.K.)

* Correspondence: karol.bukowski@unilodz.eu

Received: 9 April 2020; Accepted: 30 April 2020; Published: 2 May 2020



Abstract: Cancer is one of the main causes of death worldwide. Despite the significant development of methods of cancer healing during the past decades, chemotherapy still remains the main method for cancer treatment. Depending on the mechanism of action, commonly used chemotherapeutic agents can be divided into several classes (antimetabolites, alkylating agents, mitotic spindle inhibitors, topoisomerase inhibitors, and others). Multidrug resistance (MDR) is responsible for over 90% of deaths in cancer patients receiving traditional chemotherapeutics or novel targeted drugs. The mechanisms of MDR include elevated metabolism of xenobiotics, enhanced efflux of drugs, growth factors, increased DNA repair capacity, and genetic factors (gene mutations, amplifications, and epigenetic alterations). Rapidly increasing numbers of biomedical studies are focused on designing chemotherapeutics that are able to evade or reverse MDR. The aim of this review is not only to demonstrate the latest data on the mechanisms of cellular resistance to anticancer agents currently used in clinical treatment but also to present the mechanisms of action of novel potential antitumor drugs which have been designed to overcome these resistance mechanisms. Better understanding of the mechanisms of MDR and targets of novel chemotherapy agents should provide guidance for future research concerning new effective strategies in cancer treatment.

Keywords: cancer; multidrug resistance; chemotherapeutics; inhibitors; P-glycoprotein; drug metabolism; growth factors; DNA repair; epigenetic alterations; microRNA

1. Introduction

Cancer is responsible for about 1 in 6 deaths worldwide. It is the second leading cause of death globally, with 8.7 million deaths in 2015 [1]. Factors that are associated with elevated risk of cancer are tobacco use (22% of cancer deaths), lack of physical activity, alcohol use, low vegetable and fruit intake, and high body mass index. These factors are thought to be responsible for approximately one third of cancer deaths. Breast, cervical, lung, thyroid, and colorectal cancers are the most common types of cancer in women, while prostate, lung, colorectal, liver, and stomach cancer are the most common among men [2]. Despite the fact that there are several different methods of cancer treatments, including radiation therapy, surgery, immunotherapy, endocrine therapy, and gene therapy, chemotherapy still remains the most common method of cancer healing. In this paper, we have presented the latest data on the mechanisms of cellular resistance to chemotherapy and chemotherapeutics currently used in clinical treatment as well as on the mechanisms of action of novel potential anticancer agents which have been designed to overcome these resistance mechanisms.

2. Types of Chemotherapeutics

Chemotherapeutics can be divided into two classes depending on/regarding their origin. They can either be plant-derived (extracted from plants) [3,4] or of synthetic origin [5,6]. Depending on the mechanism of action, they can be divided into alkylating agents, antimetabolites, topoisomerase inhibitors, mitotic spindle inhibitors, and others (Figure 1) [7–9].

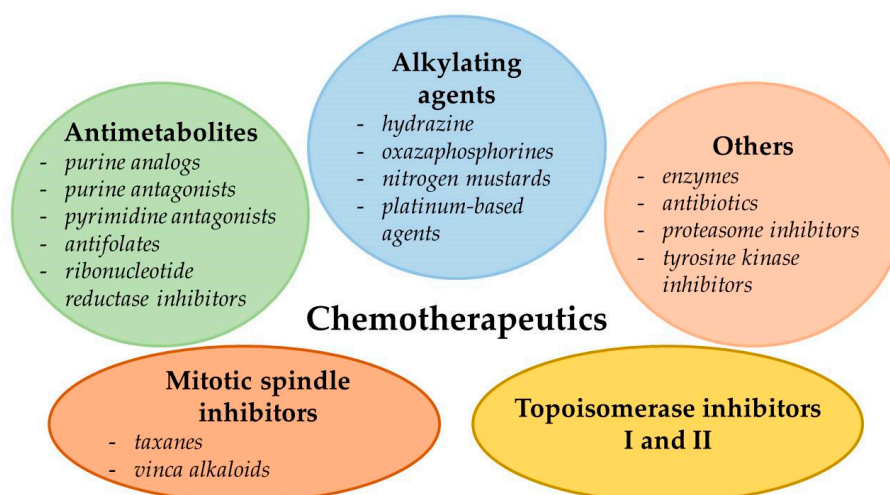


Figure 1. Classification of commonly used chemotherapeutics depending on their mechanism of action [7–9].

Alkylating agents include the oxazaphosphorines (cyclophosphamide and ifosfamide); nitrogen mustards (busulfan, chlorambucil, and melphalan); hydrazine (temozolomide); platinum-based agents (cisplatin, carboplatin, and oxaliplatin) [7]; and novel, still under investigation OFF-ON-type alkylating agents such as vinyl-quinazolinone (VQ) [10]. Chemotherapeutics belonging to this class of molecules create either inter or intra-strand cross links or transfer alkyl groups to the guanine residues of DNA, which results in mispair formation in DNA bases and prevents strand separation during DNA synthesis [7,8].

Antimetabolites can be divided into several groups: pyrimidine antagonists (cytarabine, 5-fluorouracil (5-FU), gemcitabine, and capecitabine), purine antagonists (fludarabine), purine analogs (6-mercaptopurine, azathioprine, and cladribine), antifolates (methotrexate, pemetrexed, and pralatrexate), and ribonucleotide reductase inhibitors (hydroxyurea). These anticancer drugs interfere with essential biosynthetic pathways, disturb the DNA/RNA synthesis, or cause the formation of DNA strand breaks through inhibition of particular enzymes (dihydrofolate reductase, ribonucleotide reductase, and DNA polymerase) or incorporation of false structural analogues of pyrimidine/purine into DNA [5,7,8].

Topoisomerase I inhibitors (irinotecan and topotecan) and topoisomerase II inhibitors (etoposide; teniposide; and anthracyclines, e.g., idarubicin, daunorubicin, and doxorubicin (DOX)) inhibit topoisomerases activities involved in replication of DNA and cause DNA strand breaks [7,8,11,12].

Mitotic spindle inhibitors such as taxanes (docetaxel and paclitaxel) and vinca alkaloids (vincristine (VCR) and vinblastine) modify the function/formation of spindle microtubules by inhibition of nuclear division (mitotic arrest in metaphase), leading to cell death [7,8]. Recently, Peng et al. [6] demonstrated that one of the newly synthesized N-carbonyl acridines inhibited tubulin polymerization, presenting high antiproliferative activity against human mammary gland/breast cancer cells MB-468 (half-maximum inhibitory concentration—IC₅₀—value comparable to colchicine and paclitaxel).

Other chemotherapeutic agents, including some enzymes (L-asparaginase), proteasome inhibitors (bortezomib), tyrosine kinase inhibitors (imatinib and erlotinib), and antibiotics (bleomycin, actinomycin D, and anthracyclines), are characterized by non-homogenous mechanisms of action.

While L-asparaginase cleaves the amino acid L-asparagine essential for normal cell metabolism, bortezomib drives the cell to apoptotic death by inhibition of apoptotic protein degradation. Imatinib and erlotinib inhibit tyrosine kinases activities involved in multiple intracellular pathways associated with receptor-mediated growth signaling, leading to cellular dysfunction and subsequent cell death. Bleomycin, an antibiotic, induces formation of free radicals that cause DNA damage and the cell cycle arrest in G2 phase. Another anticancer agent, actinomycin D, intercalates into DNA and interferes in DNA transcription. Anthracyclines exhibit anti-proliferatory effects in the abovementioned processes and inhibit topoisomerase II activity [7].

3. The Problem of Drug Resistance in Cancer Chemotherapy

Statistical data shows that over 90% mortality of cancer patients is attributed to drug resistance. MDR of cancer cells during chemotherapy can be associated with a variety of mechanisms, including enhanced efflux of drugs, genetic factors (gene mutations, amplifications, and epigenetic alterations), growth factors, increased DNA repair capacity, and elevated metabolism of xenobiotics (Figure 2). Each of these mechanisms leads to reduction of the therapeutic efficacy of administered drugs, causing more difficulty in tumor treatment [9,13–16].

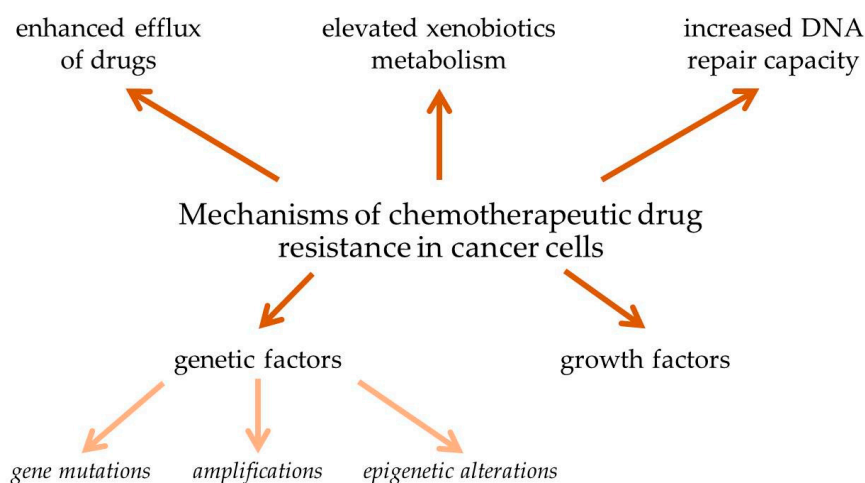


Figure 2. Mechanisms of chemotherapeutic drug resistance in cancer cells [9,13–16].

3.1. Enhanced Efflux of Drugs

ATP-binding cassette (ABC) proteins such as P-glycoprotein (P-gp)/ATP-binding cassette subfamily B member 1 (ABCB1) or Breast Cancer Resistance Protein (BCRP) present in the cell membrane are responsible for regulation of distribution, absorption, and excretion of a variety of chemical compounds. Because these proteins protect cells from death caused by high intracellular drug concentration, they can also interfere with drug administration, decreasing its bioavailability, intracellular concentration, and its transition of the blood–brain barrier (BBB). P-gp, highly expressed on the endothelial cell surface contributes to reduced chemotherapeutic drug penetration to the specific sites, especially in case of brain tumor treatment where anticancer agents are generally incapable of passing through the BBB. The size of the tumor also plays a crucial role in drug penetration. Because of the poor blood supply in large tumors, chemotherapeutic agents are usually less efficient in large tumors due to the poor blood supply compared to smaller ones with nearly unlimited access of oxygen and nutrient supply. The P-gp protects the brain from potentially damaging compounds but, at the same time, restricts access of therapeutic agents responsible for higher complexity of the therapy. In most cases, the only way to overcome the barrier is to increase the concentration of the drug, which often leads to systemic toxicity. This is the reason why elevated efflux of the drug has been considered to be one of the key mechanisms of cancer cell resistance against chemotherapeutics [9,14,15,17].

P-gp and BCRP can eliminate from cancer cells a wide variety of structurally and functionally unrelated anticancer agents, including epipodophyllotoxins, anthracyclines, vinca alkaloids, bisantrene, colchicine, taxanes, imatinib, saquinavir, camptothecins, thiopurines, actinomycin D, methotrexate, and mitoxantrone to the extracellular space, reducing intracellular drug accumulation [14,15,18–20]. Among a variety of chemotherapeutics, significant correlation between increased expression of P-gp in cancer cells and their enhanced resistance to paclitaxel, etoposide, olaparib, DOX, and vinblastine has been found [15,21–24]. Overexpression of P-gp has been observed in about 50% of all human cancers. While, in some tumor types such as lung, liver, kidney, rectum, and colon, increased P-gp expression has been observed before chemotherapy treatment, in others, including hematological malignancies such as acute lymphoblastic leukemia and acute myeloid leukemia, overexpression of P-gp has been noticed after anticancer agents exposure [15,20]. Overexpression of P-gp and BCRP has been associated with poor clinical response and MDR in patients with multiple myeloma, acute lymphocytic leukaemia, chronic lymphocytic leukaemia, acute myelogenous leukaemia, and metastatic breast cancer [18]. Additionally, it has been reported that P-gp plays a role in cancer cells MDR not only by participating in the efflux of intracellular chemotherapeutic agents but also by inhibiting tumor necrosis factor-related apoptosis-inducing ligand TRAIL-mediated and caspase-related pathways of apoptosis [19,25,26].

Although P-gp inhibitors show a high efficacy in vitro and in vivo studies, none of them have been approved by the U.S. Food and Drug Administration (FDA) for clinical use in cancer treatment [18,27]. However, Nanayakkara et al. [27] presented some new P-gp inhibitors, which potentially may be promising drugs in cancer chemotherapy. Despite the fact that they have still not entered clinical trials, researchers using computational approach found several compounds that were able to inhibit the P-gp activity and confirmed their anticancer properties against MDR cancer cell lines. Furthermore, Nanayakkara et al. [27] tested coadministration of chemotherapeutics with the investigated compounds against two-dimensional MDR prostate and ovarian cancer cells and three-dimensional prostate cancer microtumor spheroids. The results showed a significant decrease in cell motility and cell survival and viability. Additionally, the researchers demonstrated that all of the tested P-gp inhibitors did not exhibit toxic potential and were not P-gp transport substrates. Moreover, tested compounds increased not only cellular retention of anticancer agents but also the amount of reporter compounds being P-gp transport substrates.

Another example of new potential P-gp inhibitors are naturally occurring potassium ionophores such as salinomycin. Guberović et al. [28] demonstrated that some of the investigated crown ethers revealed to be significantly more efficient in sensitising MDR cells to adriamycin and paclitaxel compared to a well-known P-gp inhibitor verapamil.

Furthermore, the results obtained by Liu et al. [29] showed that combining administration of ascorbic acid with DOX could increase the sensitivity of human MDR breast cancer (MCF-7/MDR) cells to DOX in vitro and in vivo. As those researchers showed, ascorbate improved responsiveness of the cells to DOX through promoting the cellular accumulation of the drug associated with induction of reactive oxygen species-dependent ATP depletion.

Moreover, the compound that potentially could find its application in chemotherapy treatment is tometodione M (TTM), a novel natural syncarpic acid-conjugated monoterpene. In the study of Zhou et al. [30], the drug increased intracellular rhodamine 123 and DOX accumulation in human MDR leukemia cells (K562/MDR) and MCF-7/MDR cells by decreasing P-gp-related drug efflux. TTM reduced expression of both P-gp protein and mRNA via inhibition of p38 mitogen-activated protein kinase (MAPK) signaling, leading to MDR reversion in cancer cells. Additionally, TTM not only enhanced the cytotoxicity of docetaxel in K562/MDR and MCF-7/MDR cells but also triggered apoptosis and decreased colony formation in docetaxel-treated cells [30].

In addition, the results of Yuan et al. [31] demonstrated that cinobufagin, a substance isolated from the posterior auricular glands and skin of the Asiatic toad (*Bufo gargarizans*), affected modulation of P-gp activity in human P-gp-overexpressing colorectal carcinoma cells, including Caco-2/ADR, HCT116/L, and LoVo/ADR, which could potentially find it useful in combination with chemotherapeutic agents in

colon cancer treatment. Data showed that cinobufagin significantly enhanced intracellular accumulation of rhodamine 123 and DOX and exhibited apoptotic properties in MDR cells. Moreover, cinobufagin remarkably influenced P-gp overexpressing in LoVo/ADR cells by increasing their sensitivity to DOX belonging to P-gp substrate drugs. Despite the fact that further investigations on the mechanisms of action of cinobufagin showed no changes in the expression of P-gp, a significant effect of cinobufagin on noncompetitive inhibition of P-gp ATPase activity was observed [31].

Furthermore, the chemical substance which could be potentially used in cancer chemotherapy is iso-pencillixanthone A (iso-PXA), which naturally occurs in the fungus *Penicillium oxalicum*. Chen et al. [32] found that iso-PXA could increase the intracellular concentration of (VCR) in the human cervical cancer cell line HeLa/VCR by P-gp ATPase stimulation and reduction in P-gp expression. As those researchers showed, iso-PXA effectively induced the intrinsic pathway of apoptosis by poly (ADP-ribose) polymerase (PARP), caspase-3, and caspase-9 activation. Moreover, iso-PXA initiated apoptotic events by degradation of induced myeloid leukemia cell differentiation protein (Mcl-1), accumulation of F-box and WD repeat domain-containing 7 protein (FBW7), and increase of the Bax/Bcl-2 ratio.

Chen et al. [33] investigated the association between the activities of natural flavonoids, including (–)-catechin, (–)-gallocatechin, luteolin, taxifolin, and human P-gp activity. The researchers found that taxifolin in a concentration-dependent manner significantly decreased ABCB1 expression and inhibited the P-gp function through DOX efflux and uncompetitive inhibition of rhodamine 123.

Quinidine is a well-known, FDA-approved drug used clinically for the treatment of pseudobulbar effect, arrhythmia, and malaria. However, side effects of the drug associated with myocardium condition, including factors such as torsade de pointes and long QT syndrome (LQTS), complicate its clinical usage as a P-gp inhibitor. The results of Snyder et al. [34] showed potential application of polymer-drug conjugates such as methoxypolyethylene glycol (mPEG) glycine-quinidine conjugate in reversing MDR through P-gp inhibition. The investigated conjugate not only inhibited the function of P-gp comparable to quinidine but also significantly mitigated distribution of quinidine into the mouse myocardium, resulting in reduced off-target pharmacologic effects.

Sitratatinib, a novel promising receptor tyrosine kinase inhibitor, which presently is on clinical trials, has been shown to be correlated with reversing MDR of P-gp and BCRP-overexpressing cancer cells. The investigated compound inhibited the drug efflux function of P-gp and BCRP in a concentration-dependent manner without altering the protein expression of P-gp and BCRP in MDR cancer cells. As Wu et al. [18] suggested, despite the fact that sitratatinib at submicromolar concentrations reversed MDR mediated by P-gp and BCRP, further clinical trials are required.

Furthermore, the effect of novel P-gp inhibitors, polyethylene glycol-modified titanium dioxide nanoparticles (TiO₂ PEG NPs), on cisplatin cytotoxicity against P-gp overexpressing HepG2 cells was examined. This study showed that increased cisplatin cytotoxicity was associated with downregulation of the expression of P-gp in HepG2 cells by TiO₂ PEG NPs [35].

3.2. Genetic Factors

3.2.1. Gene Mutations

Gene mutations, which are commonly observed in tumor cells are considered one of the main causes of the failure of chemotherapy treatment. As Duesberg et al. [36,37] concluded, the best explanation of MDR development in cancer cells is their aneuploidy nature. Researchers have suggested that frequently losing chromosomes or their reassortments during mitosis are responsible for losing drug-sensitive genes or for changes in biochemical pathways, which both seems to be crucial in chemotherapeutic drug resistance. In addition, normal cells, which rarely gain or lose a chromosome, usually stays sensitive to drugs, which makes the treatment even more complex.

Mutations of the *TP53* gene, frequently observed in tumor cells, are one of the best-known biomarkers of the tumorigenesis. As Mantovani et al. [38] described, forty years of studies have

demonstrated the irreplaceable role of the *TP53* gene in protecting an organism against neoplastic transformation and tumor progression. The *TP53* tumor suppressor is responsible for genome stability and cellular homeostasis by coordinating multiple processes and effector pathways, including regulation of the cell cycle and inducing apoptosis or G1 arrest in the case of any genotoxic stress caused during replication. Losing the tumor-suppressive activities by missense mutations in the *TP53* gene, which are especially widespread in human cancers, reverses the protective role of the *TP53* pathway by initiating chemoresistance, invasion, and metastasis. In a normal case, anticancer drugs, which induce DNA damage, cause cell death by *TP53* activity. In contrast, loss of the *TP53* activity in cancer cells allows continued replication no matter the type/level of DNA damage, which makes them resistant to genotoxic drugs (Figure 3) [38].

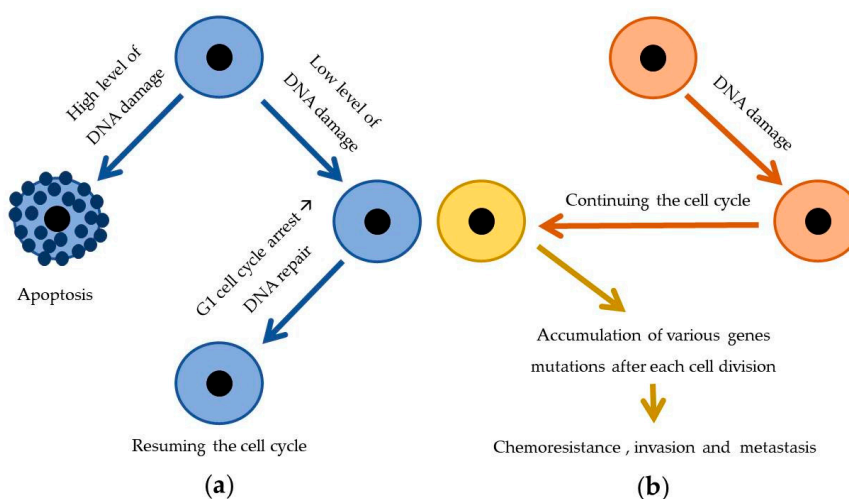


Figure 3. Differences in *TP53* gene expression level between normal (a) and cancer cells (b) and consequences thereof: (a) accurate level of expression of *TP53* gene and (b) decreased level of expression of *TP53* gene [38].

Furthermore, function of the chimeric *BCR-ABL* gene seems to be key for initiation and maintenance of tumorigenicity, especially in chronic myeloid leukemia (CML). The oncogenic gene product increases frequency of cell division, blocks DNA repair, and inhibits apoptosis. *BCR-ABL* tyrosine-kinase inhibitors, such as imatinib, commonly used as the first-line drug for patients with CML, prevent ATP binding to the *BCR-ABL* kinase receptor, therefore inducing apoptosis in cancerous cells [39,40]. Data shows that mutations of the *BCR-ABL* gene associated with the drug-binding region commonly result in imatinib resistance during the CML treatment [39]. Additionally, in some clinical studies, scientists have observed significant correlation between reactivation of the *BCR-ABL* gene and remission of CML disease [41].

Topoisomerase II-targeted agents, such as etoposide, are frequently used in order to inhibit the replication process by stopping the activity of this enzyme. Unfortunately, gene mutations of topoisomerase alter its nuclear localization, which results in the tumor cells' resistance to the use of drug. In addition, these drugs are not specific toward cancer cells, interacting with the entire genome, which significantly limits their safe usage in cancer management [11].

The aim of cytotoxic drugs is to disable components of cells, for which the functions are key for its survival. Because of the commonly observed gene mutations in tumor cells, they are able to make some alterations in response in target molecules, which make them resistant to the specific drug. The product of the mutated gene still retains its activity, but because of some changes in its stereochemical structure, it is not able to bind to the drug anymore. A well-known example of this mechanism of resistance is antiestrogen therapy of breast cancer. Patients, who initially show proper response to tamoxifen treatment, often at some point become insensitive to an endocrine manipulation. The state of complete

unresponsiveness results from the gradual loss of estrogen receptors in mutated cells. Probably, an estrogen is no longer needed for growth and functioning of survived tumor cells [42,43].

3.2.2. Amplifications

The main role of many chemotherapeutics, such as methotrexate, is inhibition of key enzymes, e.g., dihydrofolate reductase engaged in controlling cell proliferation. Because of the possibility of gene amplification, which appears in 10% of the cancers, mainly in leukemias, cancer cells can overcome this inhibition by enhancing transcription of the gene, which encodes the enzyme. This process is associated with selective synthesis of a specific region of the chromosome, which provides multiple copies of the same gene. These amplified sequences are identified with homogeneously staining regions or double minute chromosomes. Each of those gene are transcribed in order to increase the mRNA level, which after that is used in the translation process to produce more enzymes. Because the drug concentration is limited, at some point, it is not able to inhibit the increased amount of enzyme [9,44].

Zhang et al. [45], using the clinically annotated genomic database, The Cancer Genome Atlas (TCGA), analyzed the transcriptomics, genomics, and clinical data of a variety of cancer samples, especially breast cancer (1082 samples). As the result, significant associations between amplification of the glycosylphosphatidylinositol-linked cell surface glycoprotein (*CD24*) gene and mutations in the *TP53* gene, cancer proliferation, and metastasis were observed. As the researchers suggested, a copy number variation of *CD24* could serve as a simple potential prognostic marker for identifying populations of interest for cancer treatment and risk subtype.

Other data present that factors such as gene rearrangements/amplification or anticancer drugs (e.g., rifampicin) could significantly increase the expression of *ABCB1* gene, leading to elevation of P-gp activity. Data from one rifampicin therapy showed that the drug increased the intestinal P-gp level 3.5-fold and decreased the oral bioavailability of another used drug (digoxin) by 30% during the whole treatment [46,47].

Genovese et al. [48] observed that even application of a single dose of chemotherapeutics, such as DOX and paclitaxel targeting cancer cells lines or hematological malignancies and various solid tumors in vivo, led to amplification of chromosome region 7q21 containing gene *ABCB1*, subsequently resulting in overexpression of P-gp and other resistance-related proteins. As the researchers pointed out, additional factors such as epigenetic modifications and single nucleotide polymorphisms (SNPs) increased expression of *ABCB1* as well. The results of a variety of studies have demonstrated that not only paclitaxel and DOX but also other anticancer agents, including anthracyclines and taxenes, caused overexpression and/or amplification of genes surrounding the *ABCB1* locus.

The upregulation of oncogene human epidermal growth factor receptor-2 (*HER2*) expression occurs in approximately 20% of breast cancers. Amplification of *HER2* leads to transcriptional modifications associated with a variety of genes and pathways in breast cancer cells. *HER2* abnormal breast cancers are correlated with increased chemotherapy resistance and general worse prognosis. Anti-*HER2* agents, such as lapatinib, trastuzumab, margetuximab, pertuzumab, and trastuzumab, have been used in *HER2* abnormal breast cancers patients for many years. Unfortunately, administration of the inhibitor of *HER2* signaling to *HER2*+ breast cancer patients often results in loss of initial drug sensitivity and development of resistance to used agent. The promising novel strategy of *HER2* abnormal breast cancers' clinical treatment assumes alternate combinatory agents, including cyclin-dependent kinase (CDK) 4/6 inhibitors, endocrine therapy, cholesterol pathway inhibitors, or receptor tyrosine kinase (RTK) inhibitors [49].

3.2.3. Epigenetic Alterations

The latest data strongly emphasizes the significant role of epigenetic alterations in cancer cells in anticancer drug resistance. Silencing tumor suppressor genes by their DNA hypermethylation or enhancing the expression of oncogenes by their DNA hypomethylation could be the potential factors involved in cancer development. During tumorigenesis, the epigenome goes through multiple

alterations, including genome-wide loss of DNA methylation, regional hypermethylation (especially in CpG promoter islands of tumor suppressor genes), global changes in histone modification marks, and alterations in the miRNAs expression (Figure 4) [50–52].

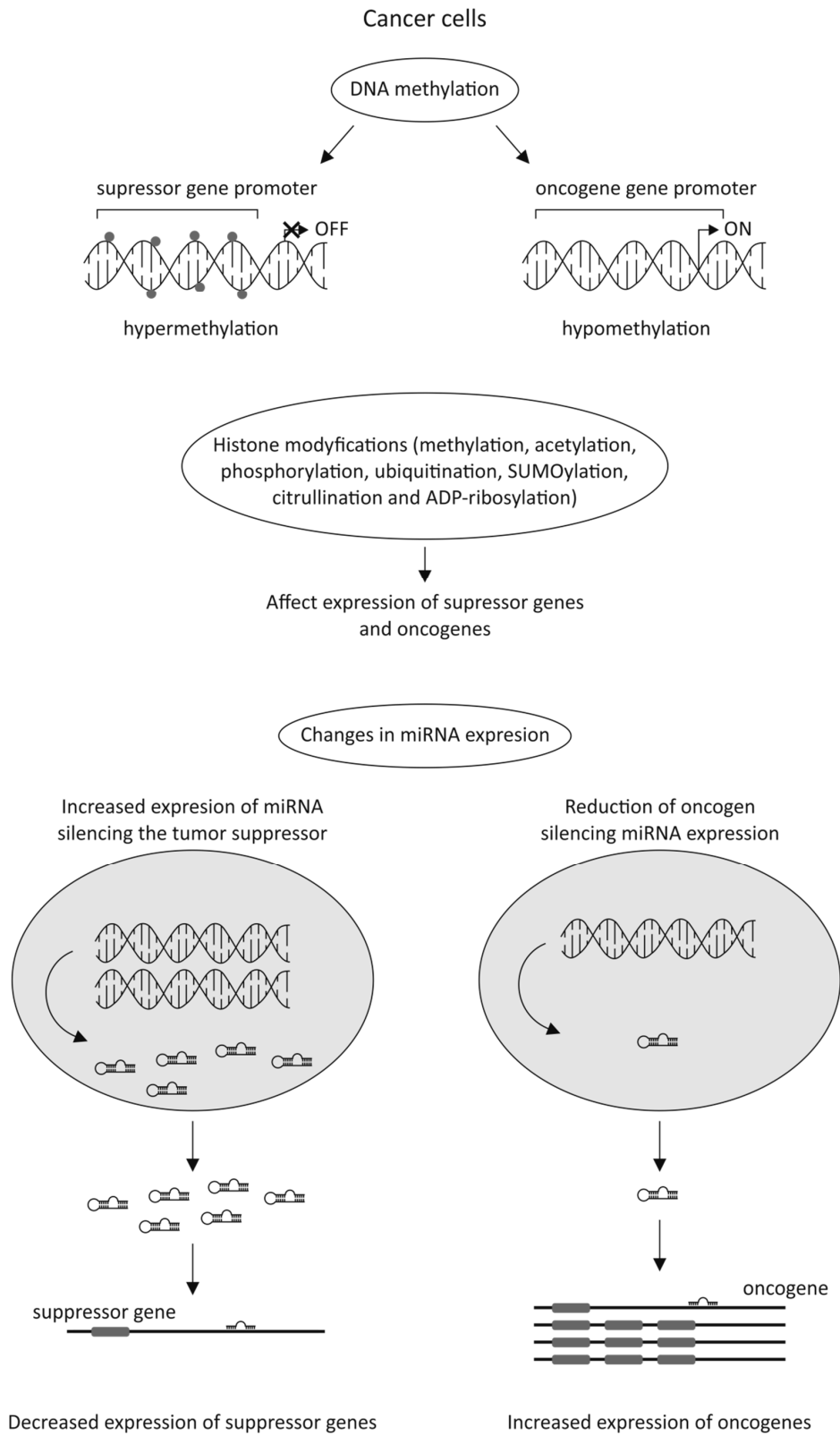


Figure 4. Cancer cell gene regulation by epigenetic alterations [50–52].

Currently, only two classes of epigenetic drugs have been approved by the FDA, i.e., DNA methylation inhibitors (iDNMT), including 5-azacitidine [53] and 5-aza-2'-deoxycytidine (decitabine; DAC) [54], as well as histone deacetylase inhibitors (iHDACs), such as Vorinostat, Belinostat, Romidepsin, and Panobinostat [55].

Demethylation of the *ABC1* gene in the cancer cell lines leads to decreased accumulation of the anticancer agent inside the cancer cells and results in acquisition of the MDR phenotype. Furthermore, the epigenetic alterations can affect the DNA repair system. For example, hypermethylation or mutation of the human MutL homolog 1 (*hMLH1*) gene, for which the product is involved in the mismatch repair system, can result in colorectal cancer development. Data has shown that the combination of conventional chemotherapeutics and epigenetic drugs such as DAC can be an effective solution in the treatment of cancerous cells and resisted tumors. Despite the fact that DAC does not affect directly the tumor growth, it inhibits DNA methylation which sensitizes the tumor to other chemotherapeutics, including carboplatin, cisplatin, and 5-FU [44].

Development of colorectal cancer is commonly associated with a variety of epigenetic alterations, such as histone modifications, DNA methylation, noncoding RNAs, and chromatin remodeling. While DNA methylation in genes *MDF1*, *SSTR2*, *CMTM3*, *TGFB2*, and *NDRG4* is a potential marker for the detection of colorectal cancer in the early stages of its development, hypermethylation in gene *CLDN11* is associated with metastasis and poor prospect of patient survival with colorectal cancer. Furthermore, silencing of tumor suppressor candidate 3 (*TUSC3*) mRNA expression by promoter methylation induces signaling of epidermal growth factor receptor (EGFR), which leads to colorectal cancer cells protection from apoptosis [56]. As Patnaik and Anupriya [56] suggested, development of DNA methyltransferase inhibitors and drugs targeting histone deacetylases could be a potential novel anticancer strategy. The latest data has demonstrated that CUDC-101 and CUDC-907, new synthesized histone deacetylase/kinase inhibitors, showed therapeutic potential as anticancer agents [57,58].

Despite the fact that microRNAs (miRNAs) have only 19–25 nucleotides and are unable to code any proteins, they affect regulation of gene expression by posttranscriptional modifications. Epigenetic changes associated with miRNAs frequently play an important role in the development of chemoresistance of various types of cancer. In recent years, many studies have shown that miRNAs affect the sensitivity of tumor cells against anticancer agents by influencing drug-resistance-related genes or genes related to cell proliferation, cell cycle, and apoptosis [59]. As Mansoori et al. [44] suggested, miRNAs could serve as a biomarker for prognosis of the effectiveness of chemotherapy treatment. The list of selected miRNAs involved in tumor transformation is presented in Table 1.

Table 1. Exemplary miRNAs that play an important role in cancer resistance.

Cancer Type	miRNA	Chemotherapy Agent	Reference
prostate cancer	microRNA-34a	paclitaxel	[60]
	microRNA-217, microRNA-181b-5p	docetaxel, cabazitaxel	[61]
pancreatic cancer	microRNA-320a micro-146	5-FU	[62]
	microRNA-205, microRNA-7	gemcitabine	[63]
colorectal cancer	microRNA-519c	5-FU	[64]
	microRNAs-384	oxaliplatin	[65]
	microRNA-96	5-FU	[66]
cervical cancer	microRNA-499a	paclitaxel	[67]
	microRNA -125a	paclitaxel	[68]
	microRNA-224	paclitaxel	[69]
breast cancer	microRNA-27b-3p	tamoxifen	[70]
	microRNA-21	trastuzumab	[71]
	microRNA-134	DOX	[72]
ovarian cancer	miR-23b	paclitaxel	[73]
	microRNA-125b	paclitaxel	[74]
	microRNAs-449	DOX	[75]
gastric cancer	microRNA-508-5p	VCR, adriamycin, cisplatin, 5-FU	[76]
	microRNA-103/107	DOX	[77]
	microRNA-495-3p	adriamycin, cisplatin, 5-FU, VCR	[78]

3.3. Growth Factors

Experimental and clinical data have shown significant associations between inflammation and cancer development and progression. The results of accumulated experimental and clinical data have revealed that acute inflammation promotes tumor eradication while chronic immune response leads to tumor growth and invasion. Increased autocrine production of the growth factors, including interleukin (IL)-1, IL-4, IL-6, and IL-8, has been observed in MDR cancer cells, compared to drug-sensitive tumor cells [79–82].

It has been widely reported that IL-6 can affect various biological processes such as metabolism, differentiation, cell growth, and death by increasing *ABCB1* gene expression and the CCAAT enhancer-binding protein family activation [81]. Furthermore, Ham et al. [82] provided convincing evidence for correlation between the activity of IL-6 in cancer-associated fibroblasts occurring in the tumor stroma and MDR of gastric cancer cells. The results of the researchers showed that IL-6 was a chromatin assembly factor-1 (CAF)-specific secretory protein, which conferred gastric cancer cell chemoresistance by paracrine signaling. Moreover, they observed that application of tocilizumab, an anti-IL-6 receptor monoclonal antibody, reversed the CAF-mediated inhibition of apoptosis in both in vitro and in vivo experimental models. This data demonstrated the potential therapeutic use of IL-6 inhibitors in order to increase the responsiveness to anticancer agents in gastric cancer cells.

The results of Wang et al. [80] indicated strong association between overexpression of IL-8 in tumor tissue, serum, ovarian cyst fluid, and ascites from ovarian cancer patients and poor sensitivity for a variety of anticancer agents used during their chemotherapy. As the researchers observed, MDR in ovarian cancer cells caused by increased expression of IL-8 was associated not only with activation of Ras/MEK/ERK and PI3K/Akt signaling and overexpression of MDR-related genes, including *ABCB1* and apoptosis inhibitory proteins (XIAP, Bcl-xL, and Bcl-2) but also with decreased proteolytic activation of

caspase-3. This is the reason why modulation of the IL-8 signaling pathway or IL-8 expression may be a potential strategy of MDR ovarian cancer treatment.

Cancer chemoresistance can be elevated not only by intracellular factors but also by increased level of extracellular fibroblast growth factors present in the media of metastatic and solid tumors. Data has shown that drugs with different mechanisms of action, including 5-FU, DOX, and paclitaxel, were ineffective against tumors with elevated levels of these extracellular factors. In order to prove the importance of fibroblast growth factors in development of cancer chemoresistance, Song et al. [83] applied suramin (a well-known inhibitor of these factors), which effectively reversed the 10-fold increased resistance observed in combination of intracellular and extracellular factors.

Glioblastoma, the most lethal brain cancer among adults, is a tumor characterized by marked genetic heterogeneity. However, changes in activation of receptor tyrosine kinase signaling are among the most common molecular modifications in glioblastoma. Data from a variety of studies has suggested significant association between signaling through fibroblast growth factor (FGF) receptors and glioblastoma progression. For that reason, blocking this signaling pathway by currently trialed small-molecule inhibitors of FGF receptors may be a potential strategy in glioblastoma treatment [84].

The aim of the study of Suzuki et al. [85] was to determine how extracellular FGFs affect the biology of small cell lung cancer (SCLC) cells and non-small cell lung cancer (NSCLC) cells. The results of the researchers showed significant associations between the activity of examined FGFs, i.e., FG2, FGF9, and FGF10, and proliferation, apoptosis, and treatment sensitivity of SCLC and NSCLC cells in vitro in a cell-specific manner.

Many data has shown that increased activity of protein kinase C [86] and extracellular matrix (ECM) [87] in breast tumor cells are associated with their chemotherapy resistance. It has been proven that ECM plays the key role in breast cancer progression, invasion, and metastasis. As Jena and Janjanam [87] suggested, remodeling of ECM is the major factor responsible for promoting cancer invasion and metastasis, especially matrix metalloproteinases (MMPs), including MMP-2, -9, -11, and -14, which degrade the matrix proteins. It was reported that β -D mannuronic acid could be a potential anticancer agent by inhibition of MMP-2 and -9. However, other factors such as ECM integrin b1-, b5-, and b6-; Hic-5 and ECM1 proteins; and enzymes, including heparanase, procollagen lysyl hydroxylase-2, LOXL2, and LOXL4 have also been shown to play a role in the regulation of breast cancer development and progression. Furthermore, stromal cells, including adipocytes, cancer-associated fibroblasts, and tumor-associated macrophages (TAMs) have been shown to be associated with tumor progression via a variety of processes (e.g., creating a vessel network which supports the nourishment of the tumor mass and secretion of vascular endothelial growth factor A (VEGF-A) by TAMs leading to tumor invasion) [87].

3.4. Increased DNA Repair Capacity

Another possibility of becoming tumor cells resistant to a variety of anticancer drugs is their ability to repair DNA damage. DNA repair endonuclease XPF and DNA excision repair protein ERCC1 involved in the nucleotide excision repair (NER) pathway are essential for the efficient repair of DNA damage induced by crosslinking and platinum-based agents [88]. A significant correlation between overexpression of both the XPF and ERCC-1 proteins and the development of cisplatin resistance in cancer cells was shown [89]. Low target specificity of a variety of anticancer drugs developed so far is the reason of their failure in chemotherapy treatment. However, successful use of PARP inhibitors against breast cancer (*BRCA*)-deficient tumors showed a new perspective on developing novel potential inhibitors of DNA repair proteins [90].

Novel compounds, i.e., E-X PPI2 and E-X AS7 have been identified as ERCC1-XPF inhibitors. Enhanced melanoma cell sensitivity to cisplatin, inhibition of NER activity, and decreased level of ERCC1-XPF heterodimers in ovarian cancer cells were observed after E-X PPI2 or E-X AS7 usage [91]. Additionally, one of the investigated catechol-based inhibitors of ERCC1-XPF (13 compound) displayed high activity in NER and selectivity against deoxyribonuclease I and Flap structure-specific

endonuclease 1 (FEN-1), which resulted in enhanced cisplatin activity in A375 melanoma cells [92]. Gentile et al. [88], using a multistep computational approach, found potential modification sites of F06, an inhibitor of the ERCC1-XPF. Among investigated analogs of F06, increased IC₅₀ value (0.49 μM) for the inhibition of ERCC1-XPF activity was observed in a case of B5 compound. These results require further testing and optimization; however, methods based on the computational approach described by the researchers can be used to develop novel potential ERCC1-XPF inhibitors.

Repair and tolerance of Pt-DNA lesions depend not only on NER but also on efficiency of homologous recombination (HR) pathway. Data has demonstrated that replication protein A (RPA) can be a new promising target in chemotherapy treatment. RPA, as a single-strand DNA (ssDNA)-binding protein, not only is involved in DNA recombination and replication but also plays key functions in DNA-damage response (DDR), HR, and NER DNA repair pathways [93–95]. In some studies, the activity of novel derivatives of RPA inhibitors against in vitro and in vivo models of NSCLC and epithelial ovarian cancer (EOC) has been examined. One of the investigated compounds, the TDRL-551, showed anticancer activity both as a single agent and in combination with Pt in an NSCLC in vivo model. In addition, synergy of TDRL-551 with platinum in both xenograft and tissue culture models of EOC was observed [93]. Furthermore, anticancer properties of one of the previously identified RPA inhibitors, SMI MCI13E, was investigated using both ovarian and lung cancer cell lines. In this study, decreasing RPA DNA-binding activity and disruption's RPA role in the cell cycle regulation was noted. Addition of SMI MCI13E to cisplatin enhanced its anticancer properties. The results have shown that RPA small molecule inhibitors can be applied as a single chemotherapeutic or may be used in combination with current anticancer agents to enhance their efficacy [94]. Moreover, new analogues of a previously reported RPA inhibitor, TDRL-551, were designed in order to enhance physicochemical properties and anticancer activity. Compounds 43, 44, 45, and 46 were identified as chemical substances with increased solubility, low micromolar RPA inhibitory activity, and enhanced cellular uptake, holding promise for further investigation of novel chemotherapeutics [95].

Opposite to other DNA repair pathways, decreased activity of the DNA mismatch repair (MMR) pathway is associated with enhanced damage tolerance that leads to increased mutagenicity and chemoresistance. Hypermethylation of the *hMLH1* gene promoter, causing a decreased expression of the MLH1 protein involved in the MMR pathway has been found in many cancers. In vitro studies have demonstrated that 5-fluoro-2-deoxycytidine and the cytidine analog, decitabine, can reverse this hypermethylation and increase cell sensitivity to cisplatin via restoring MMR functionality [96,97].

Ataxia telangiectasia and Rad3-related protein ATR kinase plays an essential role in the regulation of the DDR pathway. Its inhibition has been shown to be associated with enhanced sensitivity of some cancer cells in vitro to DNA-damaging agents, including platinum-based compounds. However, data about successful application of ATR inhibitors in vivo is limited. Hall et al. [98] examined VX-970 anticancer properties in both in vitro and in vivo lung cancer models. The researchers observed enhanced sensitivity of most of the investigated lung cancer cell lines in vitro to a variety of DNA-damaging drugs after VX-970 usage. In vivo, in primary lung xenografts derived from patients, VX-970 inhibited ATR activity in tumors and significantly increased the efficacy of cisplatin. The combination of cisplatin and VX-970 resulted in tumor regression in a model sensitive to cisplatin and complete inhibition of tumor growth in three cisplatin-resistance models [98]. The substance AZD6738 is another ATR kinase inhibitor which induces senescence and cell death in NSCLC cells. AZD6738 increases cytotoxicity of gemcitabine and cisplatin in NSCLC cell lines and enhances cisplatin anticancer properties in ATM-deficient NSCLC cells. ATR kinase inhibition caused by daily administration of AZD6738 for 14 days was well tolerated in mice and increased the therapeutic properties of cisplatin in xenograft models. The synergy of AZD6738 and cisplatin showed strong anticancer properties against ATM-deficient lung cancer xenografts [99].

Due to interrupted HR repair in *BRCA1*-deficient breast cancer cells, DNA double-strand breaks (DSBs) in these cells can be repaired only by the nonhomologous end joining (NHEJ) pathway. This is the reason why inhibition of DNA-dependent protein kinases (DNA-PKcs) involved in DDR and

NHEJ pathways could be a new promising target in *BRCA1*-deficient breast cancer treatment [100,101]. Albarakati et al. [100] observed a synergy between cisplatin and two highly selective DNA-PKcs inhibitors, NU7026 and NU7441, in *BRCA1*-deficient breast cancer cell lines.

Sustained regressions in patient-derived xenograft models after treatment with AZD7648, the highly selective DNA-PK inhibitor and efficient sensitizer of DOX, and radiotherapy (radiation-induced DNA damage) was observed. In addition, combination of AZD7648 with olaparib, a well-known PARP inhibitor, resulted in cell growth inhibition, apoptosis, and enhanced genomic instability in ATM-deficient cells model. Furthermore, AZD7648 elevated olaparib efficacy in both patient-derived xenograft and xenograft models contributing to sustained tumor regression [101].

RAD51 is a protein involved in HR pathway responsible for DNA DSB repair. It binds to ssDNA and assists in HR repair by exchanging DNA strand breaks. Enhanced HR and overexpression of RAD51 have been found in multiple myeloma cells. Furthermore, high RAD51 expression in vivo has been shown to be correlated with chemoresistance and poor patient survival. The compound B02 interrupted binding RAD51 to ssDNA, inhibiting HR pathway, which resulted in enhanced cancer sensitivity to a variety of DNA damaging agents, such as DOX. In contrast, the combination of DOX and B02 had no impact on normal human CD19+ B cells from peripheral blood [102].

In a case of DNA-damaging chemotherapy treatment, the process of mutagenic translesion synthesis (TLS) was significantly associated with development of MDR in cancer cells. Wojtaszek et al. [103] demonstrated the highly specific small-molecule inhibitor JH-RE-06 that interrupted recruitment of mutagenic POL ζ involved in TLS activity. Coadministration of JH-RE with cisplatin increased cisplatin-induced cytotoxicity both in cultured mouse and human cell lines. Previous research also revealed association between disturbing POL ζ and enhanced efficiency of DNA-lesion chemotherapy [104].

The TLS pathway is responsible for repair of inter-strand DNA cross-links (ICLs). This process is regulated by Lys-164-mono-ubiquitinated proliferating cell nuclear antigen (PCNA). Inoue et al. [105] observed that T2 amino alcohol (T2AA) inhibited TLS repair and increased DNA DSBs by interrupting the function of Lys-164-mono-ubiquitinated PCNA. Blocking the interaction between genes involved in the DNA repair, *REV1* and mono-ubiquitinated PCNA, resulted in inhibition of ICL repair and enhanced cisplatin cytotoxicity.

Mutation of TLS DNA polymerase Rev1 in cancer cells modified their TLS activity, increasing proliferating cells survival by enhancing tolerance to DNA damage occurring during replication. Sail et al. (2017) showed that two new synthesized compounds—4 and 5—inhibited mutagenic Rev1/Pol ζ -dependent TLS in cells, sensitizing human fibrosarcoma HT1080 cells to cisplatin. Additional experiments confirmed specificity of the investigated compounds, making them first inhibitors of TLS that target C-terminal domain of Rev1 (Rev1-CT) [106].

It has been reported that DNA DSBs in a DICER- and DROSHA-dependent manner generate DNA damage response RNAs (DDRNs), responsible not only for the DDR management but also for guiding DNA repair. As Gioia et al. [107] observed, enoxacin, a compound being a DICER activity booster, increased the DDR signaling and DNA repair in cells exposed to ionizing radiations. Stimulation of DDRNs production by enoxacin at dysfunctional telomeres and at chromosomal DSBs promoted accumulation of TP53 at damaged sites and, in consequence, caused suppression of homologous recombination, leading to DNA repair towards more accurate and faster nonhomologous end-joining. Unfortunately, augmented DNA repair elevated by the enoxacin not only increased the survival of normal cells but also affected cancer cells treated with anticancer agents, which might potentially result in acquisition of MDR phenotype by these cells.

3.5. Elevated Metabolism of Xenobiotics

As known, carrier molecules and enzymes responsible for drug metabolism play role in cancer cells chemotherapy resistance. Several studies have suggested that exposure to anticancer drugs may lead to induction and expression of gene products that protect the cell. Drug metabolizing enzymes

are an integral part of phase I and phase II metabolism that helps in the detoxification of endogenous and exogenous substrates (xenobiotics).

Isoforms of cytochrome (CYP) such CYP1A6, CYP1A2, CYP1B1, CYP2C9, CYP2B6, CYP2C19, CYP3A4/5, and CYP2D6 are essential for phase I of drug metabolism and detoxification. Overexpression of CYP1B1 has been observed in various cancer cell types that modify the biotransformation of chemotherapeutics, such as mitoxantrone, flutamide, docetaxel, and paclitaxel [108]. Furthermore, increased expression of CYP2A6 enzyme, which is involved in metabolism of anticancer agents, including ifosfamide, cyclophosphamide, aflatoxin, and fluorouracil, has been reported in breast tumor tissues. In addition, highly upregulated expression of CP4Z1, CYP1B1, and CYP2A7 in cancer cells was associated with their enhanced resistance to a variety of chemotherapeutics [109].

Altered expression of enzymes involved in phase II of drug metabolism, including glutathione-S-transferases (GSTs), gamma-glutamyl transferases (γ GTs), uridine diphospho-glucuronosyltransferases (UGTs), thiopurine methyltransferases (TPMTs), and dihydropyrimidine dehydrogenases (DPDs) in cancer cells may enhance their MDR [108,110]. The ability to inhibit the UGT activity, mainly UGT1A1, by kinase inhibitors, including sorafenib, regorafenib, pazopanib, and lapatinib, has been observed. However, in contrast to pazopanib and lapatinib activities, inhibition of UGT1A1 by sorafenib and regorafenib has been shown to be correlated with hyperbilirubinemia in patients [111]. Furthermore, novel UGT1A4 inhibitors that selectively increased sensitivity of cancer cells to chemotherapeutic agents demonstrated a new potential strategy in overcoming cancer MDR [112].

In order to overcome MDR in cancer cells with elevated GST and γ GT expression, γ GT-activated arsenic-based prodrugs, including darinaparsin and 4-(N-(S-glutathionylacetyl)amino)phenylarsonous acid (GSAO), as well as GST-activated agents such as nitrogen mustard have been employed [110,113]. Additionally, natural flavonoids derivatives, such as phloretin, phloridzin, baicalein, and baicalin (with micromolar concentrations), were shown to be associated with inhibition of GST activity [114]. Other novel inhibitors of GST enzymes and chalcone derivatives, including 4-methoxychalcone, 4,4'-difluorochalcone, 2'-hydroxy-4-methoxychalcone, 4'-hydroxychalcone, and 4-fluorochalcone, were also reported [115].

As FeiFei et al. [116] found, there was a significant correlation between losing an F-box only protein 8 (FBX8), a key component of the SKP1-CUL1-F-box (SCF) E3 ubiquitin ligases, and acceleration of colon tumorigenesis. FBXB, through the ubiquitination process, led to degradation of GSTP1, resulting in suppression of colorectal cancer progression.

Glutathione (GSH) functions are associated with maintaining cellular redox homeostasis. GSH detoxifies xenobiotics as well as enhances MDR in cancer cells. In contrast to normal cells, cancer cells show a higher reactive oxygen species (ROS) production. Due to vicious proliferation and enhanced metabolism in cancer cells, these cells developed an enhanced antioxidant defense system to manage the elevated oxidant state. As many data suggested, alterations in GSH level have been correlated with multiple pathways of programmed cell death in cancer cells [117–119]. Tumor tissues derived from lung, liver, colon, and breast cancers show overexpression of GSH compared to normal tissues. The enhanced detoxifying ability of GSH in cancer cells has been shown to be associated with decreased activity of chemotherapeutic agents [117,119,120].

The impairment of the GSH antioxidant defense system could sensitize cancer cells to currently used chemotherapeutics. It was suggested that the moderate decline in the GSH level would be an effective strategy to increase the sensitivity of cancer cells to chemotherapies [121]. The ways to deplete the cellular GSH level include the following: reduction of GSH precursor availability [122,123], inhibition of the GSH synthesis process [124], increase of GSSG levels [125], direct conjugation with GSH [110], and promotion of cellular GSH efflux [126].

4. Discussion

In this paper, molecular mechanisms of MDR in cancer cells have been widely described. Moreover, based on data of recent studies and discovery in the field of molecular biology, the most prospective antineoplastic agents have been presented. Highly specific molecular targets of each individual anticancer drug seemingly indicate that mutual features of these substances cannot be found. However, surprisingly, the mechanisms of action of all described (potential) chemotherapeutics are based on their inhibitory properties. Furthermore, those substances may be divided into some groups depending on their interactions with particular enzymes or other proteins involved in individual mechanisms of MDR.

The main group of these antineoplastic agents are those which interact with molecular components necessary for proper functioning of DNA repair mechanisms pathways. This includes ERCC1-XPF inhibitors (E-X PPI2, E-X AS7, compound 13, and compound B5), RPA inhibitors (TDRL-551, SMI MCI13E, and TDRL-55 derivatives), ATR kinase inhibitors (VX-970 and AZD6738), DNA-PKcs inhibitors (NU7026, NU7441, and AZD7648), HR inhibitors (B02 compound), and TLS inhibitors (JH-RE-06, T2AA, and compounds 4 and 5) [88,91–95,98–106]. Other substances, such as taxifolin, sitravatinib, cinobufagin, crown ethers, ascorbic acid, TTM, so-PXA, mPEG glycine-quinidine conjugate, and TiO₂ PEG NPs that have been designed to block efflux of drugs outside the cancer cells are known as P-gp inhibitors [18,28–35]. Another group involves drugs that are capable of increasing metabolism of xenobiotics in tumor cells. This includes inhibitors of GST (flavonoids and chalcone derivatives) directly involved in phase II of drug metabolism [114,115]. Furthermore, growth factor inhibitors such as IL-6 inhibitors (tocilizumab) and MMP-2/-9 inhibitors (β -D mannuronic acid) have been designed to affect tumor progression, invasion, and metastasis by inhibition of chronic immune response and prevention of remodeling ECM [82,87]. The last group of novel anticancer agents like CUDC-101 and CUDC-907 are histone deacetylase/kinase inhibitors that alter expression of specific genes, for which products are involved in different mechanisms of chemotherapy resistance in cancer cells [57,58].

Currently, only Sitravatinib and CUDC-101 are on the stage of clinical trials [18,57]. The majority of previously described novel potential chemotherapeutic agents are recently discovered or synthesized. For that reason, these compounds achieved only *in vitro* and *in vivo* successful results so far, and further investigations are required. However, new trends for searching for antineoplastic agents are well visible. In spite of researchers still focused on general anticancer properties of designed drugs such as their cytotoxic or genotoxic activity, more and more studies are being conducted in order to recognize specific molecular activity of these substances that would allow to develop the strategies for overcoming MDR in tumor cells. Particularly, understanding complex mechanisms responsible for MDR in cancer cells may be a key factor in designing novel strategies of cancer treatment in future. This may include a combination of multiple specific inhibitors that together will be able to change expression of key genes associated with cancer development, to inhibit efflux of drugs outside the cell, to prolong the presence of the active form of drugs inside the cell, and to increase tumor cell sensibility to DNA damage. Due to those reasons, we can speculate that future tumor treatment strategies will be based on combination therapies that will include the use of different types of drugs that target specific weak points of particular mechanisms of MDR.

5. Conclusions

The development of MDR is a complex process associated with enhanced efflux of drugs, elevated metabolism of xenobiotics, increased DNA repair capacity, growth and genetic factors, or any combination of these mechanisms. Knowledge of weak points of these mechanisms enabled scientists to develop new strategies against MDR cancer cells. Among novel potential anticancer agents presented in this paper, a remarkable part of these compounds demonstrated a strong anticancer activity in single application in both *in vitro* and *in vivo* studies. However, data has shown that their combination with other drugs significantly increased efficiency of cancer treatment. This confirms the current paradigm that combination therapy is considerably more efficient compared to any one drug on its own.

Due to complicated nature of the mechanisms of MDR and heterogeneity of tumor diseases, probably, there will never be an individual drug which will find its use in every type of cancer treatment. This is the reason why further efforts to investigate the mechanisms of cancer drug resistance, especially identifying their currently unknown vulnerabilities, seems to be crucial in designing novel potential chemotherapeutics. Identifying new drugs that will be able to reverse MDR in cancer cells will increase the efficiency of commonly used chemotherapeutic agents, especially on the last stages of cancer development, and will give us an opportunity to treat currently incurable tumors.

Author Contributions: Conceptualization, K.B. and R.K.; collected literature K.B. and M.K.; wrote the manuscript K.B.; supervised project and proofread the paper K.B., M.K. and R.K. All authors have read and agreed to the published version of the manuscript.

Funding: This research received no external funding.

Conflicts of Interest: The authors declare no conflict of interest.

Abbreviations

ABC	ATP-binding cassette
ATR	Ataxia telangiectasia and Rad3-related protein
5-FU	5-Fluorouracil
BCRP	Human breast cancer resistance protein
BBB	Blood–brain barrier
BRCA	Breast cancer gene
CAF	Chromatin assembly factor-1
CD24	Glycosylphosphatidylinositol-linked cell surface glycoprotein gene
CDK 4/6	Cyclin-dependent kinase 4/6
CML	Chronic myeloid leukemia
CYP	Cytochrome
DDR	DNA-damage response
DDRNAS	DNA damage response RNAs
decitabine; DAC	5-Aza-2'-deoxycytidine
DNA-PKc	DNA-dependent protein kinase
DOX	Doxorubicin
DPDs	Dihydropyrimidine dehydrogenases
DSB	Double-strand break
ECM	Extracellular matrix
EOC	Epithelial ovarian cancer
FBW7	F-box and WD repeat domain-containing 7 protein
FBX8	F-box only protein 8
FDA	U.S. Food and Drug Administration
FEN-1	Flap structure-specific endonuclease 1
FGF	Fibroblast growth factor
GSAO	4-(N-(S-glutathionylacetyl)amino)phenylarsonous acid
GSH	Glutathione
GSTs	Glutathione-S-transferases
HER2	Human epidermal growth factor receptor-2 gene
hMLH1	Human MutL homolog 1 gene
HR	Homologous recombination
IC50	Half-maximum inhibitory concentration
ICLs	Interstrand DNA cross-links
iDNMT	DNA methylation inhibitor
iHDAC	Histone deacetylase inhibitor
iso-PXA	Iso-pencillixanthone A
LQTS	Long QT syndrome
MAPK	Mitogen-activated protein kinase
Mcl-1	Induced myeloid leukemia cell differentiation protein

MDR	Multidrug resistance
MMP	Matrix metalloproteinase
MMR	Mismatch repair
mPEG	Methoxypolyethylene glycol
NER	Nucleotide excision repair
NHEJ	Nonhomologous end joining pathway
NSCLC	Non-small cell lung cancer
PARP	Poly (ADP-ribose) polymerase protein
PCNA	Lys-164-mono-ubiquitinated proliferating cell nuclear antigen
P-gp; ABCB1	P-glycoprotein; ATP-binding cassette subfamily B member 1
ROS	Reactive oxygen species
RPA	Replication protein A
RTK	Receptor tyrosine kinase
SCF	SKP1-CUL1-F-box
SCLC	Small cell lung cancer
SNP	Single nucleotide polymorphism
ssDNA	Single-strand DNA
T2AA	T2 amino alcohol
TAM	Tumor-associated macrophage
TCGA	The Cancer Genome Atlas
TiO ₂ PEG NP	Polyethylene glycol-modified titanium dioxide nanoparticle
TLS	Translesion synthesis
TPMTs	Thiopurine methyltransferases
TRAIL	Tumor necrosis factor-related apoptosis-inducing ligand
TTM	Tometodione M
UGTs	Uridine diphospho-glucuronosyltransferases
VCR	Vincristine
VEGF-A	Vascular endothelial growth factor A
γGTs	Gamma-glutamyl transferases

References

- Global Burden of Disease Cancer Collaboration; Fitzmaurice, C.; Allen, C.; Barber, R.M.; Barregard, L.; Bhutta, Z.A.; Brenner, H.; Dicker, D.J.; Chimed-Orchir, O.; Dandona, R.; et al. Global, regional, and national cancer incidence, mortality, years of life lost, years lived with disability, and disability-adjusted life-years for 32 cancer groups, 1990 to 2015: A systematic analysis for the global burden of disease study. *JAMA Oncol.* **2017**, *3*, 524–548. [PubMed]
- WHO. Available online: <https://www.who.int/news-room/fact-sheets/detail/cancer> (accessed on 12 September 2018).
- Kikuchi, H.; Yuan, B.; Hu, X.; Okazaki, M. Chemopreventive and anticancer activity of flavonoids and its possibility for clinical use by combining with conventional chemotherapeutic agents. *Am. J. Cancer Res.* **2019**, *9*, 1517–1535.
- Lichota, A.; Gwozdziński, K. Anticancer Activity of Natural Compounds from Plant and Marine Environment. *Int. J. Mol. Sci.* **2018**, *19*, 11. [CrossRef] [PubMed]
- Marchi, E.; O'Connor, O.A. Safety and efficacy of pralatrexate in the treatment of patients with relapsed or refractory peripheral T-cell lymphoma. *Ther. Adv. Hematol.* **2012**, *3*, 227–235. [CrossRef]
- Peng, X.; Li, L.; Ren, Y.; Xue, H.; Liu, H.; Wen, S.; Chen, J. Synthesis of N-Carbonyl Acridanes as Highly Potent Inhibitors of Tubulin Polymerization via One-Pot Copper-Catalyzed Dual Arylation of Nitriles with Cyclic Diphenyl Iodoniums. *Adv. Synth. Catal.* **2020**, 1–7. [CrossRef]
- Le, T.; Bhushan, V.; Sochat, M.; Chavda, Y. *First Aid for the USMLE Step 1*, 1st ed.; McGraw-Hill Education: New York, NY, USA, 2017; pp. 416–419.
- Nussbaumer, S.; Bonnabry, P.; Veuthey, J.L.; Fleury-Souverain, S. Analysis of anticancer drugs: A review. *Talanta* **2011**, *85*, 2265–2289. [CrossRef]

9. Luqmani, Y.A. Mechanisms of drug resistance in cancer chemotherapy. *Med. Princ. Pract.* **2005**, *14*, 35–48. [[CrossRef](#)]
10. Onizuka, K.; Hazemi, M.E.; Sato, N.; Tsuji, G.; Ishikawa, S.; Ozawa, M.; Tanno, K.; Yamada, K.; Nagatsugi, F. Reactive OFF-ON type alkylating agents for higher-ordered structures of nucleic acids. *Nucleic Acids Res.* **2019**, *47*, 6578–6589. [[CrossRef](#)]
11. Infante Lara, L.; Fenner, S.; Ratcliffe, S.; Isidro-Llobet, A.; Hann, M.; Bax, B.; Osheroff, N. Coupling the core of the anticancer drug etoposide to an oligonucleotide induces topoisomerase II-mediated cleavage at specific DNA sequences. *Nucleic Acids Res.* **2018**, *46*, 2218–2233.
12. Bax, B.D.; Murshudov, G.; Maxwell, A.; Germe, T. DNA Topoisomerase Inhibitors: Trapping a DNA-Cleaving Machine in Motion. *J. Mol. Biol.* **2019**, *431*, 3427–3449. [[CrossRef](#)]
13. Wu, Q.; Yang, Z.; Nie, Y.; Shi, Y.; Fan, D. Multi-drug resistance in cancer chemotherapeutics: Mechanisms and lab approaches. *Cancer Lett.* **2014**, *347*, 159–166. [[CrossRef](#)] [[PubMed](#)]
14. Wang, J.; Seebacher, N.; Shi, H.; Kan, Q.; Duan, Z. Novel strategies to prevent the development of multidrug resistance (MDR) in cancer. *Oncotarget* **2017**, *8*, 84559–84571. [[CrossRef](#)] [[PubMed](#)]
15. Wang, X.; Zhang, H.; Chen, X. Drug resistance and combating drug resistance in cancer. *Cancer Drug Resist.* **2019**, *2*, 141–160. [[CrossRef](#)]
16. Dallavalle, S.; Dobričić, V.; Lazzarato, L.; Gazzano, E.; Machuqueiro, M.; Pajeva, I.; Tsakovska, I.; Zidar, N.; Fruttero, R. Improvement of conventional anti-cancer drugs as new tools against multidrug resistant tumors. *Drug Resist. Updat.* **2020**, *50*, 100682. [[CrossRef](#)]
17. Mesci, S.; Marakli, S.; Yazgan, B.; Yildirim, T. The effect of ATP-binding cassette (ABC) transporters in human cancers. *Int. J. Sci. Lett.* **2019**, *1*, 1–14.
18. Wu, C.P.; Hsiao, S.H.; Huang, Y.H.; Hung, L.C.; Yu, Y.J.; Chang, Y.T.; Hung, T.H.; Wu, Y.S. Sitravatinib Sensitizes ABCB1- and ABCG2-Overexpressing Multidrug-Resistant Cancer Cells to Chemotherapeutic Drugs. *Cancers* **2020**, *12*, 195. [[CrossRef](#)]
19. Zu, Y.; Yang, Z.; Tang, S.; Han, Y.; Ma, J. Effects of P-glycoprotein and its inhibitors on apoptosis in K562 cells. *Molecules* **2014**, *19*, 13061–13075. [[CrossRef](#)]
20. Karvar, S. The role of ABC transporters in anticancer drug transport. *Turk. J. Biol.* **2014**, *38*, 800–805. [[CrossRef](#)]
21. Lagas, J.S.; Fan, L.; Wagenaar, E.; Vlaming, M.L.; van Tellingen, O.; Beijnen, J.H.; Schinkel, A.H. P-glycoprotein (P-gp/Abcb1), Abcc2, and Abcc3 determine the pharmacokinetics of etoposide. *Clin. Cancer Res.* **2010**, *16*, 130–140. [[CrossRef](#)]
22. Lal, S.; Wong, Z.W.; Sandanaraj, E.; Xiang, X.; Ang, P.C.; Lee, E.J.; Chowbay, B. Influence of ABCB1 and ABCG2 polymorphisms on doxorubicin disposition in Asian breast cancer patients. *Cancer Sci.* **2008**, *99*, 816–823. [[CrossRef](#)]
23. Satake, K.; Tsukamoto, M.; Mitani, Y.; Regasini, L.O.; da Silva Bolzani, V.; Efferth, T.; Nakagawa, H. Human ABCB1 confers cells resistance to cytotoxic guanidine alkaloids from *Pterogyne nitens*. *Biomed. Mater. Eng.* **2015**, *25*, 249–256. [[CrossRef](#)] [[PubMed](#)]
24. Vaidyanathan, A.; Sawers, L.; Gannon, A.L.; Chakravarty, P.; Scott, A.L.; Bray, S.E.; Ferguson, M.J.; Smith, G. ABCB1 (MDR1) induction defines a common resistance mechanism in paclitaxel- and olaparib-resistant ovarian cancer cells. *Br. J. Cancer* **2016**, *115*, 431–441. [[CrossRef](#)]
25. Souza, P.S.; Madigan, J.P.; Gillet, J.P.; Kapoor, K.; Ambudkar, S.V.; Maia, R.C.; Gottesman, M.M.; Fung, K.L. Expression of the multidrug transporter P-glycoprotein is inversely related to that of apoptosis-associated endogenous TRAIL. *Exp. Cell Res.* **2015**, *336*, 318–328. [[CrossRef](#)] [[PubMed](#)]
26. Galski, H.; Oved-Gelber, T.; Simanovsky, M.; Lazarovici, P.; Gottesman, M.M.; Nagler, A. P-glycoprotein-dependent resistance of cancer cells toward the extrinsic TRAIL apoptosis signaling pathway. *Biochem Pharmacol.* **2013**, *86*, 584–596. [[CrossRef](#)] [[PubMed](#)]
27. Nanayakkara, A.K.; Follit, C.A.; Chen, G.; Williams, N.S.; Vogel, P.D.; Wise, J.G. Targeted inhibitors of P-glycoprotein increase chemotherapeutic-induced mortality of multidrug resistant tumor cells. *Sci. Rep.* **2018**, *8*, 967. [[CrossRef](#)] [[PubMed](#)]
28. Guberović, I.; Marjanović, M.; Mioč, M.; Ester, K.; Martin-Kleiner, I.; Šumanovac Ramljak, T.; Mlinarić-Majerski, K.; Kralj, M. Crown ethers reverse P-glycoprotein-mediated multidrug resistance in cancer cells. *Sci. Rep.* **2018**, *8*, 14467. [[CrossRef](#)] [[PubMed](#)]

29. Liu, Y.; Zhang, L.; Ma, Z.; Tian, L.; Liu, Y.; Liu, Y.; Chen, Q.; Li, Y.; Ma, E. Ascorbate promotes the cellular accumulation of doxorubicin and reverses the multidrug resistance in breast cancer cells by inducing ROS-dependent ATP depletion. *Free Radic. Res.* **2019**, *53*, 758–767. [[CrossRef](#)] [[PubMed](#)]
30. Zhou, X.W.; Xia, Y.Z.; Zhang, Y.L.; Luo, J.G.; Han, C.; Zhang, H.; Zhang, C.; Yang, C.; Kong, L.Y. Tomentodione M sensitizes multidrug resistant cancer cells by decreasing P-glycoprotein via inhibition of p38 MAPK signaling. *Oncotarget* **2017**, *8*, 101965–101983. [[CrossRef](#)]
31. Yuan, Z.; Shi, X.; Qiu, Y.; Jia, T.; Yuan, X.; Zou, Y.; Liu, C.; Yu, H.; Yuan, Y.; He, X.; et al. Reversal of P-gp-mediated multidrug resistance in colon cancer by cinobufagin. *Oncol. Rep.* **2017**, *37*, 1815–1825. [[CrossRef](#)]
32. Chen, L.; Xin, L.; Cheng, M.; Wang, S.; Zheng, Q.; Liu, Q. Iso-pencillixanthone A from a marine-derived fungus reverses multidrug resistance in cervical cancer cells through down-regulating P-gp and re-activating apoptosis. *RSC Adv.* **2018**, *8*, 41192–41206. [[CrossRef](#)]
33. Chen, H.J.; Chung, Y.L.; Li, C.Y.; Chang, Y.T.; Wang, C.C.N.; Lee, H.Y.; Lin, H.Y.; Hung, C.C. Taxifolin Resensitizes Multidrug Resistance Cancer Cells via Uncompetitive Inhibition of P-Glycoprotein Function. *Molecules* **2018**, *23*, 3055. [[CrossRef](#)] [[PubMed](#)]
34. Snyder, S.; Murundi, S.; Crawford, L.; Putnam, D. Enabling P-glycoprotein inhibition in multidrug resistant cancer through the reverse targeting of a quinidine-PEG conjugate. *J. Controlled Release.* **2020**, *317*, 291–299. [[CrossRef](#)] [[PubMed](#)]
35. Salama, B.; El-Sherbini, E.S.; El-Sayed, G.; El-Adl, M.; Kanehira, K.; Taniguchi, A. The Effects of TiO₂ Nanoparticles on Cisplatin Cytotoxicity in Cancer Cell Lines. *Int. J. Mol. Sci.* **2020**, *21*, 605. [[CrossRef](#)] [[PubMed](#)]
36. Duesberg, P.; Stindl, R.; Hehlmann, R. Explaining the high mutation rates of cancer cells to drug and multidrug resistance by chromosome re-assortments that are catalyzed by aneuploidy. *Proc. Natl. Acad. Sci. USA* **2000**, *97*, 14295–14300. [[CrossRef](#)]
37. Duesberg, P.; Stindl, R.; Hehlmann, R. Origin of multidrug resistance in cells with and without multidrug resistance genes: Chromosome re-assortments catalyzed by aneuploidy. *Proc. Natl. Acad. Sci. USA* **2001**, *98*, 11283–11288. [[CrossRef](#)]
38. Mantovani, F.; Collavin, L.; Del Sal, G. Mutant p53 as a guardian of the cancer cell. *Cell Death Differ.* **2019**, *26*, 199–212. [[CrossRef](#)]
39. Chandrasekhar, C.; Kumar, P.S.; Venkata, P.; Sarma, G.K. Novel mutations in the kinase domain of BCR-ABL gene causing imatinib resistance in chronic myeloid leukemia patients. *Sci. Rep.* **2019**, *9*, 2412. [[CrossRef](#)]
40. Greenfield, G.; McMullan, R.; Robson, N.; McGimpsey, J.; Catherwood, M.; McMullin, M.F. Response to Imatinib therapy is inferior for e13a2 BCR-ABL1 transcript type in comparison to e14a2 transcript type in chronic myeloid leukaemia. *BMC Hematol.* **2019**, *19*, 7. [[CrossRef](#)]
41. Shih, Y.T.; Cortes, J.E.; Kantarjian, H.M. Treatment value of second-generation BCR-ABL1 tyrosine kinase inhibitors compared with imatinib to achieve treatment-free remission in patients with chronic myeloid leukaemia: A modelling study. *Lancet Haematol.* **2019**, *6*, 398–408. [[CrossRef](#)]
42. Campos, S.M. Aromatase inhibitors for breast cancer in postmenopausal women. *Oncologist* **2004**, *9*, 126–136. [[CrossRef](#)]
43. Katzenellenbogen, J.A.; Mayne, C.G.; Katzenellenbogen, B.S.; Greene, G.L.; Chandarlapaty, S. Structural Underpinnings of Estrogen Receptor Mutations in Endocrine Therapy Resistance. *Nat. Rev. Cancer.* **2018**, *18*, 377–388. [[CrossRef](#)] [[PubMed](#)]
44. Mansoori, B.; Mohammadi, A.; Davudian, S.; Shirjang, S.; Baradaran, B. The Different Mechanisms of Cancer Drug Resistance: A Brief Review. *Adv. Pharm. Bull.* **2017**, *7*, 339–348. [[CrossRef](#)] [[PubMed](#)]
45. Zhang, P.; Zheng, P.; Liu, Y. Amplification of the CD24 Gene Is an Independent Predictor for Poor Prognosis of Breast Cancer. *Front. Genet.* **2019**, *10*, 560. [[CrossRef](#)] [[PubMed](#)]
46. Fromm, M.F.; Kauffmann, H.M.; Fritz, P.; Burk, O.; Kroemer, H.K.; Warzok, R.W.; Eichelbaum, M.; Siegmund, W.; Schrenk, D. The effect of rifampin treatment on intestinal expression of human MRP transporters. *Am. J. Pathol.* **2000**, *157*, 1575–1580. [[CrossRef](#)]
47. Greiner, B.; Eichelbaum, M.; Fritz, P.; Kreichgauer, H.P.; von Richter, O.; Zundler, J.; Kroemer, H.K. The role of intestinal P-glycoprotein in the interaction of digoxin and rifampin. *J. Clin. Invest.* **1999**, *104*, 147–153. [[CrossRef](#)]

48. Genovese, I.; Ilarib, A.; Assarafc, Y.G.; Fazid, F. Not only P-glycoprotein: Amplification of the ABCB1-containing chromosome region 7q21 confers multidrug resistance upon cancer cells by coordinated overexpression of an assortment of resistance-related proteins. *Drug Resist. Updat.* **2017**, *32*, 23–46. [[CrossRef](#)]
49. Wahdan-Alaswad, R.; Liu, B.; Thor, A.D. Targeted lapatinib anti-HER2/ErbB2 therapy resistance in breast cancer: Opportunities to overcome a difficult problem. *Cancer Drug Resist.* **2020**, *3*, 1–20. [[CrossRef](#)]
50. Zhao, Z.; Shilatifard, A. Epigenetic modifications of histones in cancer. *Genome Biol.* **2019**, *20*, 245. [[CrossRef](#)]
51. Kanwal, R.; Gupta, S. Epigenetic modifications in cancer. *Clin. Genet.* **2012**, *81*, 303–311. [[CrossRef](#)]
52. Mohammad, H.P.; Barbash, O.; Creasy, C.L. Targeting epigenetic modifications in cancer therapy: Erasing the roadmap to cancer. *Nat. Med.* **2019**, *25*, 403–418. [[CrossRef](#)]
53. Kaminskas, E.; Farrell, A.T.; Wang, Y.C.; Sridhara, R.; Pazdur, R. FDA drug approval summary: Azacitidine (5-azacytidine, Vidaza) for injectable suspension. *Oncologist* **2005**, *10*, 176–182. [[CrossRef](#)] [[PubMed](#)]
54. He, P.F.; Zhou, J.D.; Yao, D.M.; Ma, J.C.; Wen, X.M.; Zhang, Z.H.; Lian, X.Y.; Xu, Z.J.; Qian, J.; Lin, J. Efficacy and safety of decitabine in treatment of elderly patients with acute myeloid leukemia: A systematic review and meta-analysis. *Oncotarget* **2017**, *8*, 41498–41507. [[CrossRef](#)] [[PubMed](#)]
55. Goey, A.K.L.; Sissung, T.M.; Peer, C.J.; Figg, W.D. Pharmacogenomics and histone deacetylase inhibitors. *Pharmacogenomics* **2016**, *17*, 1807–1815. [[CrossRef](#)] [[PubMed](#)]
56. Patnaik, S.; Anupriya. Drugs Targeting Epigenetic Modifications and Plausible Therapeutic Strategies Against Colorectal Cancer. *Front. Genet.* **2019**, *10*, 588. [[CrossRef](#)] [[PubMed](#)]
57. Shimizu, T.; LoRusso, P.M.; Papadopoulos, K.P.; Patnaik, A.; Beeram, M.; Smith, L.S.; Rasco, D.W.; Mays, T.A.; Chambers, G.; Ma, A.; et al. Phase I first-in-human study of CUDC-101, a multitargeted inhibitor of HDACs, EGFR, and HER2 in patients with advanced solid tumors. *Clin. Cancer Res.* **2014**, *20*, 5032–5040. [[CrossRef](#)] [[PubMed](#)]
58. Okabe, S.; Tanaka, Y.; Moriyama, M.; Gotoh, A. Effect of dual inhibition of histone deacetylase and phosphatidylinositol-3 kinase in Philadelphia chromosome-positive leukemia cells. *Cancer Chemother. Pharmacol.* **2020**, *85*, 401–412. [[CrossRef](#)]
59. Si, W.; Shen, J.; Zheng, H.; Fan, W. The role and mechanisms of action of microRNAs in cancer drug resistance. *J. Clin. Epigenet.* **2019**, *11*, 25. [[CrossRef](#)]
60. Liu, X.; Luo, X.; Wu, Y.; Xia, D.; Chen, W.; Fang, Z.; Deng, J.; Hao, Y.; Yang, X.; Zhang, T.; et al. MicroRNA-34a Attenuates Paclitaxel Resistance in Prostate Cancer Cells via Direct Suppression of JAG1/Notch1 Axis. *Cell Physiol. Biochem.* **2018**, *50*, 261–276. [[CrossRef](#)]
61. Lin, H.M.; Nikolic, I.; Yang, J.; Castillo, L.; Deng, N.; Chan, C.L.; Yeung, N.K.; Dodson, E.; Elsworth, B.; Spielman, C.; et al. MicroRNAs as potential therapeutics to enhance chemosensitivity in advanced prostate cancer. *Sci. Rep.* **2018**, *8*, 7820.
62. Wang, W.; Zhao, L.; Wei, X.; Wang, L.; Liu, S.; Yang, Y.; Wang, F.; Sun, G.; Zhang, J.; Ma, Y. MicroRNA-320a promotes 5-FU resistance in human pancreatic cancer cells. *Sci. Rep.* **2016**, *6*, 27641. [[CrossRef](#)]
63. Singh, S.; Chitkara, D.; Kumar, V.; Behrman, S.W.; Mahato, R.I. miRNA profiling in pancreatic cancer and restoration of chemosensitivity. *Cancer Lett.* **2013**, *334*, 211–220. [[CrossRef](#)] [[PubMed](#)]
64. To, K.K.; Leung, W.W.; Ng, S.S. Exploiting a novel miR-519c-HuR-ABCG2 regulatory pathway to overcome chemoresistance in colorectal cancer. *Exp. Cell Res.* **2015**, *338*, 222–231. [[CrossRef](#)] [[PubMed](#)]
65. Evert, J.; Pathak, S.; Sun, X.F.; Zhang, H. A Study on Effect of Oxaliplatin in MicroRNA Expression in Human Colon Cancer. *J. Cancer* **2018**, *9*, 2046–2053. [[CrossRef](#)] [[PubMed](#)]
66. Kim, S.A.; Kim, I.; Yoon, S.K.; Lee, E.K.; Kuh, H.J. Indirect modulation of sensitivity to 5-fluorouracil by microRNA-96 in human colorectal cancer cells. *Arch. Pharm. Res.* **2015**, *38*, 239–248. [[CrossRef](#)] [[PubMed](#)]
67. Chen, Y.; Song, Y.; Mi, Y.; Jin, H.; Cao, J.; Li, H.; Han, L.; Huang, L.; Zhang, X.; Ren, S.; et al. MicroRNA-499a promotes the progression and chemoresistance of cervical cancer cells by targeting SOX6. *Apoptosis* **2020**, *25* (Suppl. 3–4), 205–216. [[CrossRef](#)]
68. Fan, Z.; Cui, H.; Yu, H.; Ji, Q.; Kang, L.; Han, B.; Wang, J.; Dong, Q.; Li, Y.; Yan, Z.; et al. MiR-125a promotes paclitaxel sensitivity in cervical cancer through altering STAT3 expression. *Oncogenesis* **2016**, *5*, e197. [[CrossRef](#)]
69. Lin, F.; Wang, P.; Shen, Y.; Xie, X. Upregulation of microRNA-224 sensitizes human cervical cells SiHa to paclitaxel. *Eur. J. Gynaecol. Oncol.* **2015**, *36*, 432–436.

70. Zhu, J.; Zou, Z.; Nie, P.; Kou, X.; Wu, B.; Wang, S.; Song, Z.; He, J. Downregulation of microRNA-27b-3p enhances tamoxifen resistance in breast cancer by increasing NR5A2 and CREB1 expression. *Cell Death Dis.* **2016**, *7*, e2454. [[CrossRef](#)]
71. De Mattos-Arruda, L.; Bottai, G.; Nuciforo, P.G.; Di Tommaso, L.; Giovannetti, E.; Peg, V. MicroRNA-21 links epithelial-to-mesenchymal transition and inflammatory signals to confer resistance to neoadjuvant trastuzumab and chemotherapy in HER2-positive breast cancer patients. *Oncotarget* **2015**, *6*, 37269–37280. [[CrossRef](#)]
72. Lu, L.; Ju, F.; Zhao, H.; Ma, X. MicroRNA-134 modulates resistance to doxorubicin in human breast cancer cells by downregulating ABCC1. *Biotechnol. Lett.* **2015**, *37*, 2387–2394. [[CrossRef](#)]
73. Yan, J.; Jiang, J.Y.; Meng, X.N.; Xiu, Y.L.; Zong, Z.H. MiR-23b targets cyclin G1 and suppresses ovarian cancer tumorigenesis and progression. *J. Exp. Clin. Cancer Res.* **2016**, *35*, 31. [[CrossRef](#)] [[PubMed](#)]
74. Ying, X.; Wei, K.; Lin, Z.; Cui, Y.; Ding, J.; Chen, Y.; Xu, B. MicroRNA-125b Suppresses Ovarian Cancer Progression via Suppression of the Epithelial-Mesenchymal Transition Pathway by Targeting the SET Protein. *Cell Physiol. Biochem.* **2016**, *39*, 501–510. [[CrossRef](#)] [[PubMed](#)]
75. Tormo, E.; Ballester, S.; Artigues, A.A.; Burgués, O.; Alonso, E.; Bermejo, B.; Menéndez, S.; Zazo, S.; Madoz-Gúrpide, J.; Rovira, A.; et al. The miRNA-449 family mediates doxorubicin resistance in triplenegative breast cancer by regulating cell cycle factors. *Sci. Rep.* **2019**, *9*, 5316. [[CrossRef](#)] [[PubMed](#)]
76. Shang, Y.; Zhang, Z.; Liu, Z.; Feng, B.; Ren, G.; Li, K.; Zhou, L.; Sun, Y.; Li, M.; Zhou, J.; et al. miR-508-5p regulates multidrug resistance of gastric cancer by targeting ABCB1 and ZNRD1. *Oncogene* **2014**, *33*, 3267–3276. [[CrossRef](#)]
77. Wang, Z.; Wang, N.; Liu, P.; Chen, Q.; Situ, H.; Xie, T.; Zhang, J.; Peng, C.; Lin, Y.; Chen, J. MicroRNA-25 regulates chemoresistance-associated autophagy in breast cancer cells, a process modulated by the natural autophagy inducer isoliquiritigenin. *Oncotarget* **2014**, *5*, 7013–7026. [[CrossRef](#)]
78. Chen, S.; Wu, J.; Jiao, K.; Wu, Q.; Ma, J.; Chen, D.; Kang, J.; Zhao, G.; Shi, Y.; Fan, D.; et al. MicroRNA-495-3p inhibits multidrug resistance by modulating autophagy through GRP78/mTOR axis in gastric cancer. *Cell Death Dis.* **2018**, *9*, 1070. [[CrossRef](#)]
79. Setrerrahmane, S.; Xu, H. Tumor-related interleukins: Old validated targets for new anti-cancer drug development. *Mol. Cancer* **2017**, *16*, 153. [[CrossRef](#)]
80. Wang, Y.; Qu, Y.; Niu, X.L.; Sun, W.J.; Zhang, X.L.; Li, L.Z. Autocrine production of interleukin-8 confers cisplatin and paclitaxel resistance in ovarian cancer cells. *Cytokine* **2011**, *56*, 365–375. [[CrossRef](#)]
81. Conze, D.; Weiss, L.; Regen, P.S.; Bhushan, A.; Weaver, D.; Johnson, P.; Rincon, M. Autocrine production of interleukin 6 causes multidrug resistance in breast cancer cells. *Cancer Res.* **2001**, *61*, 8851–8858.
82. Ham, I.H.; Oh, H.J.; Jin, H.; Bae, C.A.; Jeon, S.M.; Choi, K.; Yongon, S.; Han, S.U.; Brekken, R.A.; Lee, D.; et al. Targeting interleukin-6 as a strategy to overcome stroma-induced resistance to chemotherapy in gastric cancer. *Mol. Cancer* **2019**, *18*, 68. [[CrossRef](#)]
83. Song, S.; Wientjes, M.G.; Gan, Y.; Au, J.L. Fibro-blast growth factors: An epigenetic mechanism of broad-spectrum resistance to anticancer drugs. *Proc. Natl. Acad. Sci. USA* **2000**, *97*, 8658–8663. [[CrossRef](#)] [[PubMed](#)]
84. Jimenez-Pascual, A.; Siebzehnrubl, F.A. Fibroblast Growth Factor Receptor Functions in Glioblastoma. *Cells* **2019**, *8*, 715. [[CrossRef](#)] [[PubMed](#)]
85. Suzuki, T.; Yasuda, H.; Funaiishi, K.; Arai, D.; Ishioka, K.; Ohgino, K.; Tani, T.; Hamamoto, J.; Ohashi, A.; Naoki, K.; et al. Multiple roles of extracellular fibroblast growth factors in lung cancer cells. *Int. J. Oncol.* **2014**, *46*, 423–429. [[CrossRef](#)] [[PubMed](#)]
86. Singh, R.K.; Kumar, S.; Gautam, P.K.; Tomar, M.S.; Verma, P.K.; Singh, S.P.; Kumar, S.; Acharya, A. Protein kinase C- α and the regulation of diverse cell responses. *BioMol. Concepts* **2017**, *8*, 143–153. [[CrossRef](#)]
87. Jena, M.K.; Janjanam, J. Role of extracellular matrix in breast cancer development: A brief update. *F1000Research* **2018**, *7*, 274. [[CrossRef](#)]
88. Gentile, F.; Elmenoufy, A.H.; Ciniero, G.; Jay, D.; Karimi-Busheri, F.; Barakat, K.H.; Weinfeld, M.; West, F.G.; Tuszynski, J.A. Computer-Aided Drug Design of Small Molecule Inhibitors of the ERCC1-XPF Protein-Protein Interaction. *Chem. Biol. Drug Des.* **2019**, *95*, 460–471. [[CrossRef](#)]

89. Rosell, R.; Taron, M.; Ariza, A.; Barnadas, A.; Mate, J.L.; Reguart, N.; Margel, M.; Felip, E.; Mendez, P.; Garcia-Campelo, R. Molecular predictors of re-sponse to chemotherapy in lung cancer. *Semin. Oncol.* **2004**, *31*, 20–27. [[CrossRef](#)]
90. Rocha, C.R.R.; Silva, M.M.; Quinet, A.; Cabral-Neto, J.B.; Menck, C.F.M. DNA repair pathways and cisplatin resistance: An intimate relationship. *Clinics* **2018**, *73*, e478s. [[CrossRef](#)]
91. McNeil, E.M.; Astell, K.R.; Ritchie, A.M.; Shave, S.; Houston, D.R.; Bakrania, P.; Jones, H.M.; Khurana, P.; Wallace, C.; Chapman, T.; et al. Inhibition of the ERCC1-XPF structure-specific endonuclease to overcome cancer chemoresistance. *DNA Repair (Amst)*. **2015**, *31*, 19–28. [[CrossRef](#)]
92. Chapman, T.M.; Gillen, K.J.; Wallace, C.; Lee, M.T.; Bakrania, P.; Khurana, P.; Coombs, P.J.; Stennett, L.; Fox, S.; Bureau, E.A.; et al. Catechols and 3-hydroxypyridones as inhibitors of the DNA repair complex ERCC1-XPF. *Bioorg. Med. Chem. Lett.* **2015**, *25*, 4097–4103. [[CrossRef](#)]
93. Mishra, A.K.; Dormi, S.S.; Turchi, A.M.; Woods, D.S.; Turchi, J.J. Chemical inhibitor targeting the replication protein A-DNA interaction increases the efficacy of Pt-based chemotherapy in lung and ovarian cancer. *Biochem. Pharmacol.* **2015**, *93*, 25–33. [[CrossRef](#)] [[PubMed](#)]
94. Neher, T.M.; Bodenmiller, D.; Fitch, R.W.; Jalal, S.I.; Turchi, J.J. Novel irreversible small molecule inhibitors of replication protein A display single-agent activity and synergize with cisplatin. *Mol. Cancer Ther.* **2011**, *10*, 1796–1806. [[CrossRef](#)] [[PubMed](#)]
95. Navnath, S.; Gavande, N.S.; VanderVere-Carozza, P.S.; Pawelczak, K.S.; Vernon, T.L.; Jordan, M.R.; Turchi, J.J. Structure-Guided Optimization of Replication Protein A (RPA)–DNA Interaction Inhibitors. *ACS Med. Chem. Lett.* **2020**. [[CrossRef](#)]
96. Kelley, M.R.; Logsdon, D.; Fishel, M.L. Targeting DNA repair pathways for cancer treatment: What’s new? *Future Oncol.* **2014**, *10*, 1215–1237. [[CrossRef](#)] [[PubMed](#)]
97. Helleday, T.; Petermann, E.; Lundin, C.; Hodgson, B.; Sharma, R.A. DNA repair pathways as targets for cancer therapy. *Nat. Rev. Cancer.* **2008**, *8*, 193–204. [[CrossRef](#)]
98. Hall, A.B.; Newsome, D.; Wang, Y.; Boucher, D.M.; Eustace, B.; Gu, Y.; Hare, B.; Johnson, M.A.; Milton, S.; Murphy, C.E.; et al. Potentiation of tumor responses to DNA damaging therapy by the selective ATR inhibitor VX-970. *Oncotarget* **2014**, *5*, 5674–5685. [[CrossRef](#)]
99. Vendetti, F.P.; Lau, A.; Schamus, S.; Conrads, T.P.; O’Connor, M.J.; Bakkenist, C.J. The orally active and bioavailable ATR kinase inhibitor AZD6738 potentiates the anti-tumor effects of cisplatin to resolve ATM-deficient nonsmall cell lung cancer in vivo. *Oncotarget* **2015**, *6*, 44289–44305. [[CrossRef](#)]
100. Albarakati, N.; Abdel-Fatah, T.M.; Doherty, R.; Russell, R.; Agarwal, D.; Moseley, P.; Perry, C.; Arora, A.; Alsubhi, N.; Seedhouse, C.; et al. Targeting BRCA1-BER deficient breast cancer by ATM or DNA-PKcs blockade either alone or in combination with cisplatin for personalized therapy. *Mol. Oncol.* **2015**, *9*, 204–217. [[CrossRef](#)]
101. Fok, J.H.L.; Ramos-Montoya, A.; Vazquez-Chantada, M.; Wijnhoven, P.W.G.; Follia, V.; James, N.; Farrington, P.M.; Karmokar, A.; Willis, S.E.; Cairns, J.; et al. AZD7648 is a potent and selective DNA-PK inhibitor that enhances radiation, chemotherapy and olaparib activity. *Nat. Commun.* **2019**, *10*, 5065. [[CrossRef](#)]
102. Alagpulins, D.A.; Ayyadevara, S.; Shmookler Reis, R.J. A Small-Molecule Inhibitor of RAD51 Reduces Homologous Recombination and Sensitizes Multiple Myeloma Cells to Doxorubicin. *Front. Oncol.* **2014**, *4*, 289. [[CrossRef](#)]
103. Wojtaszek, J.L.; Chatterjee, N.; Najeeb, J.; Ramos, A.; Lee, M.; Bian, K.; Xue, J.Y.; Fenton, B.A.; Park, H.; Li, D.; et al. A Small Molecule Targeting Mutagenic Translesion Synthesis Improves Chemotherapy. *Cell* **2019**, *178*, 152–159.e11. [[CrossRef](#)] [[PubMed](#)]
104. Yamanaka, K.; Chatterjee, N.; Hemann, M.T.; Walker, G.C. Inhibition of mutagenic translesion synthesis: A possible strategy for improving chemotherapy? *PLoS Genet.* **2017**, *13*, e1006842. [[CrossRef](#)] [[PubMed](#)]
105. Inoue, A.; Kikuchi, S.; Hishiki, A.; Shao, Y.; Heath, R.; Evison, B.J.; Actis, M.; Canman, C.E.; Hashimoto, H.; Fujii, N. A small molecule inhibitor of monoubiquitinated Proliferating Cell Nuclear Antigen (PCNA) inhibits repair of interstrand DNA cross-link, enhances DNA double strand break, and sensitizes cancer cells to cisplatin. *J. Biol. Chem.* **2014**, *289*, 7109–7120. [[CrossRef](#)] [[PubMed](#)]
106. Sail, V.; Rizzo, A.A.; Chatterjee, N.; Dash, R.C.; Ozen, Z.; Walker, G.C.; Korzhnev, D.M.; Hadden, M.K. Identification of Small Molecule Translesion Synthesis Inhibitors That Target the Rev1-CT/RIR Protein-Protein Interaction. *ACS Chem. Biol.* **2017**, *12*, 1903–1912. [[CrossRef](#)] [[PubMed](#)]

107. Gioia, U.; Francia, S.; Cabrini, M.; Brambillasca, S.; Michelini, F.; Jones-Weinert, C.W.; d'Adda di Fagagna, F. Pharmacological boost of DNA damage response and repair by enhanced biogenesis of DNA damage response RNAs. *Sci. Rep.* **2019**, *239*, 6460. [[CrossRef](#)] [[PubMed](#)]
108. Pathania, S.; Bhatia, R.; Baldi, A.; Singh, R.; Rawala, R.K. Drug metabolizing enzymes and their inhibitors' role in cancer resistance. *Biomed. Pharmacother.* **2018**, *105*, 53–65. [[CrossRef](#)] [[PubMed](#)]
109. Li, Y.; Steppi, A.; Zhou, Y.; Mao, F.; Miller, P.C.; He, M.M.; Zhao, K.; Sun, Q.; Zhang, J. Tumoral expression of drug and xenobiotic metabolizing enzymes in breast cancer patients of different ethnicities with implications to personalized medicine. *Sci. Rep.* **2017**, *7*, 4747. [[CrossRef](#)]
110. Ramsay, E.E.; Dilda, P.J. Glutathione S-conjugates as prodrugs to target drug-resistant tumors. *Front. Pharmacol.* **2014**, *5*, 181. [[CrossRef](#)]
111. Miners, J.O.; Chau, N.; Rowland, A.; Burns, K.; McKinnon, R.A.; Mackenzie, P.I.; Tucker, G.T.; Knights, K.M.; Kichenadasse, G. Inhibition of human UDP-glucuronosyltransferase enzymes by lapatinib, pazopanib, regorafenib and sorafenib: Implications for hyperbilirubinemia. *Biochem. Pharmacol.* **2017**, *129*, 85–95. [[CrossRef](#)]
112. Osborne, M.J.; de Oliveira, L.C.; Volpon, L.; Zahreddine, A.A.; Borden, K.L.B. Overcoming drug resistance through the development of selective inhibitors of UDP-glucuronosyltransferase enzymes. *J. Mol. Biol.* **2019**, *431*, 258–272. [[CrossRef](#)]
113. Wu, J.; Henderson, C.; Feun, L.; Van Veldhuizen, P.; Gold, P.; Zheng, H.; Ryan, T.; Blaszkowsky, L.S.; Chen, H.; Costa, M.; et al. Phase II study of darinaparsin in patients with advanced hepatocellular carcinoma. *Invest. New Drugs* **2010**, *28*, 670–676. [[CrossRef](#)] [[PubMed](#)]
114. Aksoy, M.; Küfrevioğlu, I. Inhibition of human erythrocyte glutathione S-transferase by some flavonoid derivatives. *Toxin Rev.* **2017**, *36*, 1–7. [[CrossRef](#)]
115. Özaslan, M.S.; Demir, Y.; Aslan, H.E.; Beydemir, Ş.; Küfrevioğlu, Ö.İ. Evaluation of chalcones as inhibitors of glutathione S-transferase. *J. Biochem. Mol. Toxicol.* **2018**, *32*, e22047. [[CrossRef](#)] [[PubMed](#)]
116. Wang, F.F.; Xu, H.H.; Yan, Y.R.; Wu, P.X.; Wu, J.H.; Zhu, X.H.; Li, J.Y.; Sun, J.B.; Zhou, K.; Ren, X.L.; et al. FBX8 degrades GSTP1 through ubiquitination to suppress colorectal cancer progression. *Cell Death Dis.* **2019**, *10*, 1–12.
117. Lv, H.; Zhen, C.; Liu, J.; Yang, P.; Hu, L.; Shang, P. Unraveling the Potential Role of Glutathione in Multiple Forms of Cell Death in Cancer Therapy. *Oxidative Medicine and Cellular Longevity* **2019**, *3150145*, 1–16. [[CrossRef](#)]
118. Nunes, S.C.; Serpa, J. Glutathione in Ovarian Cancer: A Double-Edged Sword. *Int. J. Mol. Sci.* **2018**, *19*, 1882. [[CrossRef](#)]
119. Bansal, A.; Simon, M. Glutathione metabolism in cancer progression and treatment resistance. *J. Cell Biol.* **2018**, *217*, 2291. [[CrossRef](#)]
120. Desideri, E.; Ciccarone, F.; Ciriolo, M.R. Targeting Glutathione Metabolism: Partner in Crime in Anticancer Therapy. *Nutrients* **2019**, *11*, 1926. [[CrossRef](#)]
121. Ogiwara, H.; Takahashi, K.; Sasaki, M.; Kuroda, T.; Yoshida, H.; Watanabe, R.; Maruyama, A.; Makinoshima, H.; Chiwaki, F.; Sasaki, H.; et al. Targeting the Vulnerability of Glutathione Metabolism in ARID1A-Deficient Cancers. *Cancer Cell* **2019**, *35*, 177–190.e8. [[CrossRef](#)]
122. Lee, Y.S.; Lee, D.H.; Jeong, S.Y.; Park, S.H.; Oh, S.C.; Park, Y.S.; Yu, J.; Choudry, H.A.; Bartlett, D.L.; Lee, Y.J. Ferroptosis-inducing agents enhance TRAIL-induced apoptosis through upregulation of death receptor 5. *J. Cell. Biochem.* **2019**, *120*, 928–939. [[CrossRef](#)]
123. Pan, X.; Lin, Z.; Jiang, D.; Yu, Y.; Yang, D.; Zhou, H.; Zhan, D.; Liu, S.; Peng, G.; Chen, Z.; et al. Erastin decreases radioresistance of NSCLC cells partially by inducing GPX4-mediated ferroptosis. *Oncol. Lett.* **2019**, *17*, 3001–3008. [[CrossRef](#)] [[PubMed](#)]
124. Villablanca, J.G.; Volchenboum, S.L.; Cho, H.; Kang, M.H.; Cohn, S.L.; Anderson, C.P.; Marachelian, A.; Groshen, S.; Tsao-Wei, D.; Matthay, K.K.; et al. A Phase I New Approaches to Neuroblastoma Therapy Study of Buthionine Sulfoximine and Melphalan With Autologous Stem Cells for Recurrent/Refractory High-Risk Neuroblastoma. *Pediatr. Blood Cancer* **2016**, *63*, 1349–1356. [[CrossRef](#)] [[PubMed](#)]

125. Catanzaro, D.; Gaude, E.; Orso, G.; Giordano, C.; Guzzo, G.; Rasola, A.; Ragazzi, E.; Caparrotta, L.; Frezza, C.; Montopoli, M. Inhibition of glucose-6-phosphate dehydrogenase sensitizes cisplatin-resistant cells to death. *Oncotarget* **2015**, *6*, 30102–30114. [[CrossRef](#)] [[PubMed](#)]
126. Elgendy, M.; Cirò, M.; Hosseini, A.; Weiszmann, J.; Mazzarella, L.; Ferrari, E.; Cazzoli, R.; Curigliano, G.; DeCensi, A.; Bonanni, B.; et al. Combination of Hypoglycemia and Metformin Impairs Tumor Metabolic Plasticity and Growth by Modulating the PP2A-GSK3-MCL-1 Axis. *Cancer Cell* **2019**, *35*, 798–815. [[CrossRef](#)]



© 2020 by the authors. Licensee MDPI, Basel, Switzerland. This article is an open access article distributed under the terms and conditions of the Creative Commons Attribution (CC BY) license (<http://creativecommons.org/licenses/by/4.0/>).

Article

Pyrazolo[4,3-*e*]tetrazolo[1,5-*b*][1,2,4]triazine Sulfonamides as Novel Potential Anticancer Agents: Cytotoxic and Genotoxic Activities In Vitro

Karol Bukowski ^{1,*}, Beata Marciniak ¹, Mateusz Kciuk ^{1,2}, Mariusz Mojzych ³ and Renata Kontek ¹

¹ Department of Molecular Biotechnology and Genetics, Faculty of Biology and Environmental Protection, University of Lodz, 12/16 Banacha St., 90-237 Lodz, Poland; beata.marciniak@biol.uni.lodz.pl (B.M.); mateusz.kciuk@edu.uni.lodz.pl (M.K.); renata.kontek@biol.uni.lodz.pl (R.K.)

² Doctoral School of Exact and Natural Sciences, University of Lodz, 12/16 Banacha St., 90-237 Lodz, Poland

³ Department of Chemistry, Siedlce University of Natural Sciences and Humanities, 3 Maja 54, 08-110 Siedlce, Poland; mariusz.mojzych@uph.edu.pl

* Correspondence: karol.bukowski@edu.uni.lodz.pl

Abstract: In this paper, we present for the first time the evaluation of cytotoxicity and genotoxicity of de novo synthesized pyrazolo[4,3-*e*]tetrazolo[1,5-*b*][1,2,4]triazine sulfonamides **MM129**, **MM130**, and **MM131** in human tumor cell lines: HeLa, HCT 116, PC-3, and BxPC-3. Cytotoxic and genotoxic properties of the tested compounds were estimated using the MTT assay, comet assay (alkaline and neutral version), and γ -H2AX immuno-staining. Examined sulfonamides exhibited strong anticancer properties towards tested cells in a very low concentration range ($IC_{50} = 0.17$ – $1.15 \mu M$) after 72 h exposure time. The results of the alkaline and neutral version of the comet assay following 24 h incubation of the cells with tested compounds demonstrated the capability of heterocycles to induce significant DNA damage in exposed cells. HCT 116 cells were the most sensitive to the genotoxic activity of novel tricyclic pyrazolo[4,3-*e*]tetrazolo[1,5-*b*][1,2,4]triazine sulfonamides in the neutral version of the comet assay. Immunocytochemical detection of γ -H2AX showed an increase in DNA DSBs level in the HCT 116 cell line, after 24 h incubation with all tested compounds, confirming the results obtained in the neutral comet assay. Among all investigated compounds, **MM131** showed the strongest cytotoxic and genotoxic activity toward all tested cell types. In conclusion, our results suggest that **MM129**, **MM130**, and **MM131** exhibit high cytotoxic and genotoxic potential in vitro, especially towards the colorectal cancer cell line HCT 116. However, further investigations and analyses are required for their future implementation in the field of medicine.

Keywords: pyrazolo[4,3-*e*]tetrazolo[1,5-*b*][1,2,4]triazine; sulfonamides; anticancer agents; cancer cells; PBMCs; cytotoxicity; genotoxicity; MTT; comet assay; γ -H2AX



Citation: Bukowski, K.; Marciniak, B.; Kciuk, M.; Mojzych, M.; Kontek, R. Pyrazolo[4,3-*e*]tetrazolo[1,5-*b*][1,2,4]triazine Sulfonamides as Novel Potential Anticancer Agents: Cytotoxic and Genotoxic Activities In Vitro. *Molecules* **2022**, *27*, 3761. <https://doi.org/10.3390/molecules27123761>

Academic Editor: Jóhannes Reynisson

Received: 26 April 2022

Accepted: 7 June 2022

Published: 11 June 2022

Publisher's Note: MDPI stays neutral with regard to jurisdictional claims in published maps and institutional affiliations.



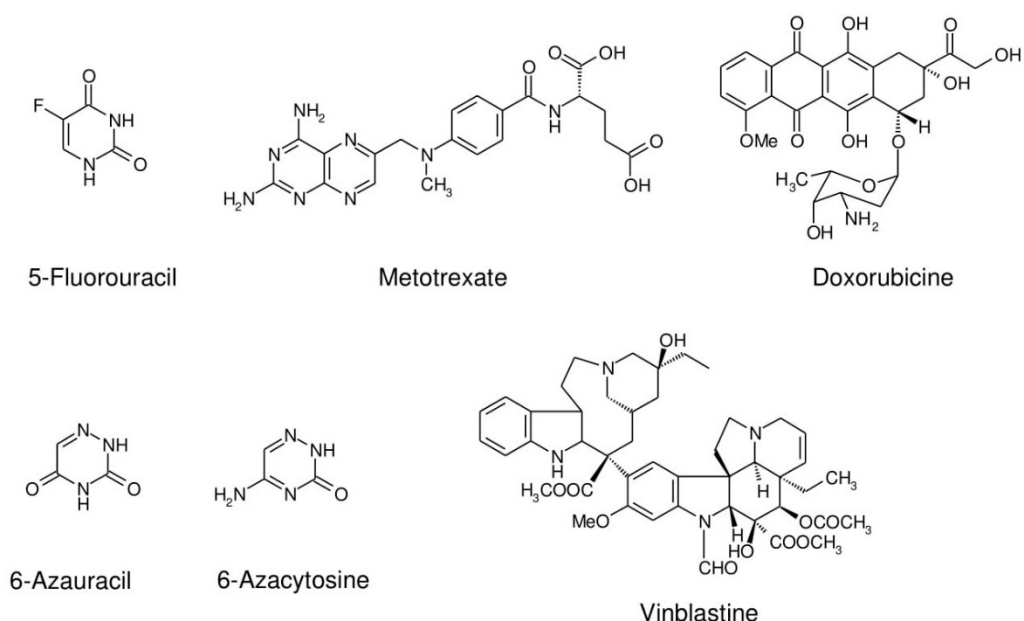
Copyright: © 2022 by the authors. Licensee MDPI, Basel, Switzerland. This article is an open access article distributed under the terms and conditions of the Creative Commons Attribution (CC BY) license (<https://creativecommons.org/licenses/by/4.0/>).

1. Introduction

According to recent data, in 2020 nearly 10 million people died due to cancer, which is now the leading cause of death worldwide. Lack of physical activity and high body mass index, as well as tobacco and alcohol use, are the main factors associated with an elevated risk of cancer. They are considered to be the reason for approximately one-third of cancer deaths. Breast, lung, colon and rectum, prostate, skin (non-melanoma), stomach, and cervical cancers are the most common types of malignancies [1,2]. Despite the remarkable progress in the development of different methods for the treatment of cancer, including surgery, radiation therapy, endocrine therapy, gene therapy, and immunotherapy, chemotherapy remains the first line of cancer treatment. This is the reason why searching for novel effective antineoplastic agents is one of the most broadly investigated topics worldwide [3–8].

Several commonly used anticancer drugs in medicine are heterocyclic compounds, such as 5-fluorouracil, methotrexate, doxorubicin, vinblastine, etc. (Scheme 1). However,

heterocyclic core and/or substituent structures are still the base for the design and synthesis of new biologically active molecules. Antimetabolite drugs with a chemical structure similar to nitrogenous bases in DNA/RNA are considered as one of the main groups of antineoplastic agents. These anticancer drugs not only disturb DNA/RNA biosynthetic pathways that are key for maintaining cell growth, but are also responsible for the formation of DNA strand breaks. The incorporation of purine/pyrimidine analogs into DNA or inhibition of the activity of some enzymes, such as ribonucleotide reductase, dihydrofolate reductase, and DNA polymerase may generate strand breaks [9,10]. Numerous nucleosides that contain interchanged carbon and nitrogen atoms in their base moieties have presented significant potential as antimetabolite agents. 6-Aza compounds, such as 6-azacytosine and 6-azauracil, are well-known examples of the nucleic acids components analogs [11,12]. The group of aza-compounds also includes monocyclic 1,2,4-triazine derivatives. These monocyclic 1,2,4-triazine-based compounds display various biological activities, including anticancer, antimicrobial, antifungal, anti-inflammatory, antimalarial, and antiviral properties [13,14]. Due to the fact that 1,2,4-triazines fused with five-membered heterocycles are considered as bioisosteric with a purine core, these compounds have attracted considerable attention in the field of medical chemistry. The group of isosteric purine analogs also includes derivatives of the little-known pyrazolo[4,3-*e*][1,2,4]triazine ring system [15]. They exhibit various biological properties, including antibacterial and anticancer activities [16–18]. It has been revealed that some synthetic pyrazolo[4,3-*e*][1,2,4]triazine sulfonamides display inhibitory activity towards urease [19], tyrosinase [15,16], carbonic anhydrase (CA) [20,21], and protein kinases (Bcr-Abl and CDK2) [22].



Scheme 1. Anticancer drugs used in medicine.

There are 538 protein kinases encoded by the human genome [23,24]. Amplifications or mutations of the cyclin-dependent kinases (CDKs), the main group of cell cycle regulatory proteins, are commonly observed in malignant cells [25]. The ability to inhibit the kinase-signaling pathways has particular importance due to the possibility of more personalized tumor treatment with decreased risk of cytotoxicity in normal cells [26]. A fusion gene *BCR-ABL*, which is frequently found in patients with chronic myeloid leukemia (CML), is responsible for enhanced resistance to apoptosis and increased proliferation of myeloid cells, as well as their adhesion properties [27–31]. Interestingly, blocking only a single ATP-binding site of the particular protein kinase prevents phosphorylation in *BCR-ABL*-expressing cells, resulting in their apoptosis or growth inhibition [29]. Among many carbonic anhydrase (CA) isoforms, there are two whose overexpression is correlated with

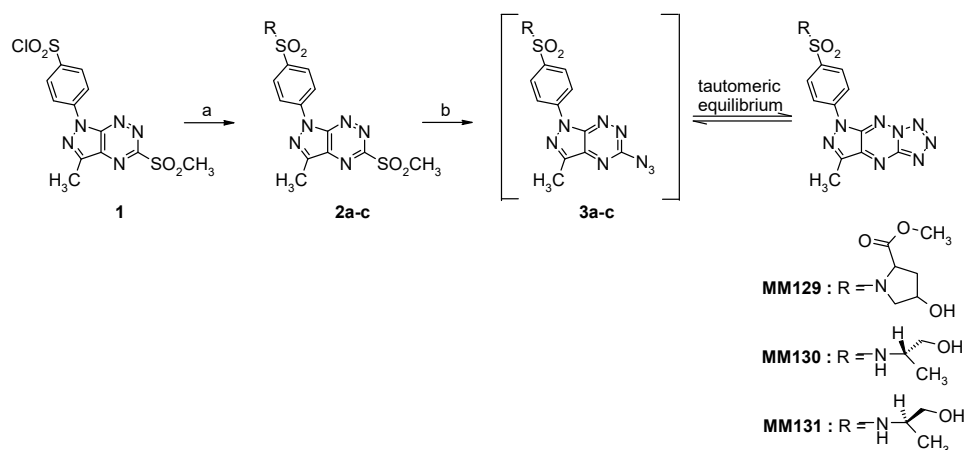
tumor development and progression—hCA IX and hCA XII. Results of Mojzych et al. [20,21] have shown that two of investigated pyrazolo[4,3-*e*][1,2,4]triazine derivatives significantly inhibited cancer-associated isoenzymes hCA IX and XII, and were ineffective toward non-tumor isoenzymes hCA I and II.

Furthermore, some of our previously synthesized pyrazolo[4,3-*e*][1,2,4]triazine derivatives with a tetrazole or triazole ring exhibited strong antineoplastic properties toward several cancer cell lines [32] (colorectal adenocarcinoma (Colo205)—IC₅₀ 4–91 μM; breast cancer (MCF-7)—IC₅₀ 50–90 μM; prostate cancer (PC-3)—IC₅₀ 25–98 μM; non-small-cell lung cancer (H460) IC₅₀ 25–86 μM). These results encouraged us to design a novel group of tricyclic derivatives, i.e., pyrazolo[4,3-*e*]tetrazolo[1,5-*b*][1,2,4]triazine with sulfonamidophenyl substituent. Sulfonamide moiety is a functional group present in various drugs, including antineoplastic agents. Moreover, aryl/heteroaryl compounds can disturb microtubule synthesis and stop the cell cycle in the G1 phase, as well as block tumor angiogenesis [33]. Bearing in mind the above literature reports, in this paper, we present the cytotoxicity and genotoxicity of the three sulfonamide derivatives of the new pyrazolo[4,3-*e*]tetrazolo[1,5-*b*][1,2,4]triazine ring system in vitro: **MM129**, **MM130**, and **MM131**. Importantly, anticancer properties of tested compounds against prostate cancer (PC-3), cervical cancer (HeLa), colorectal carcinoma (HCT 116), and pancreatic adenocarcinoma (BxPC-3) have not been examined so far.

2. Results

2.1. Synthesis of Novel 1,2,4-Triazine Derivatives

The target tricyclic sulfonamides (**MM129**, **MM130**, and **MM131**) were obtained according to our general multi-step procedure described in the literature (Scheme 2) [34]. Briefly, the corresponding chlorosulfone derivative **1**, achieved in multi-step synthesis, is the pivotal starting material for the synthesis of tricyclic sulfonamides [34,35]. The general character of the developed method synthesis enables the functionalization of the heterocyclic core by replacing the chlorine atom in the chlorosulfone group with any amine derivative.



Scheme 2. Reagents and conditions: (a) (*R*)- or (*S*)-2-aminopropanol or *cis*-4-hydroxy-L-proline methyl ester hydrochloride, MeCN, rt, overnight; (b) NaN₃, EtOH, reflux, 18 h.

The reaction of **1** with the appropriate amine derivatives yields suitable sulfonamides **2a-c** with a good leaving group (-SO₂CH₃) that undergoes nucleophilic displacement upon reaction with sodium azide and leads in the first step to the formation of intermediates **3a-c** that, under reaction conditions, can undergo intramolecular cyclization to afford final tricyclic sulfonamide derivatives **MM129**, **MM130** and **MM131** [34]. All intermediates and final derivatives were characterized using the ¹H- and ¹³C-NMR, and HRMS methods together with elemental analysis. The obtained spectroscopic data for **1**, **2a**, **2c**, **MM129**,

and **MM131** were consistent with the literature and fully confirmed the structure of these compounds (Supplementary Materials Figures S1–S19).

2.2. Cytotoxicity—MTT Assay

The results obtained from the MTT assay (72 h incubation period) show that new tricyclic derivatives of the pyrazolo[4,3-*e*][1,2,4]triazine are more cytotoxic toward tested cancer cell lines in comparison to human peripheral blood mononuclear cells (PBMCs) and the fibroblast Hs27 (human foreskin) (Figure 1; examined compounds have shown 1.2–4.9-times higher cytotoxicity in cancer cell lines compared to the normal cells). Among tested pyrazolo[4,3-*e*]tetrazolo[1,5-*b*][1,2,4]triazine sulfonamides **MM129** exhibited the lowest cytotoxic activity, while **MM131** presented the highest one. The reduction in cell viability corresponded with the increasing concentration of examined compounds. The sensitivity of the cells from the lowest to the highest is presented as follows: Hs27, PBMCs, HeLa, HCT 116, PC-3, and BxPC-3 (Figure 1).

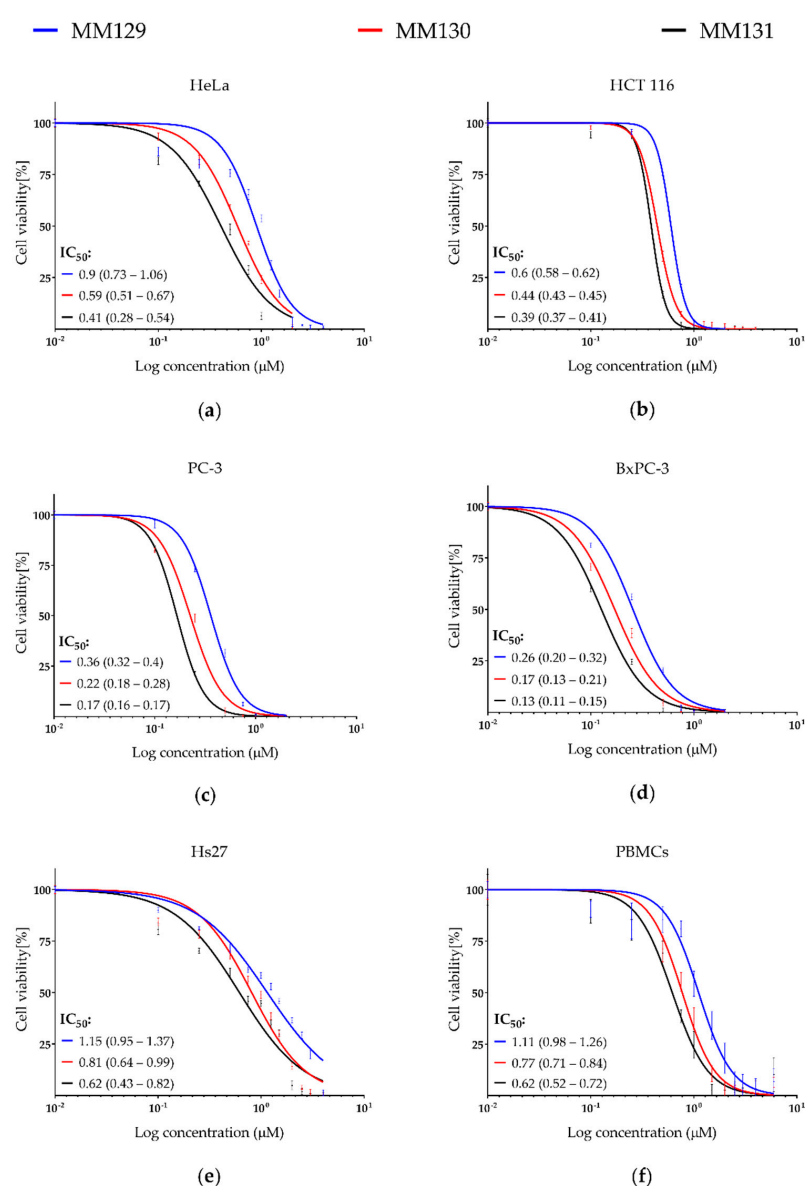


Figure 1. Evaluation of cell viability (%) of cancer cell lines: (a) HeLa; (b) HCT 116; (c) PC-3; (d) BxPC-3 and normal cells: (e) Hs27 and (f) PBMCs treated with **MM129**, **MM130**, and **MM131**. The survival curves \pm SEM were presented for each tested compound. IC₅₀ values and 95% confidence intervals (parentheses) are given in μ M.

2.3. Genotoxicity

2.3.1. Comet Assay

Alkaline Version (pH > 13)

The genotoxic potential of examined derivatives was assessed only in cancer cells. Figure 2 represents the level of DNA damage (SSBs, DSBs, alkali labile sites) induced by **MM129**, **MM130**, **MM131**, and bleomycin following 24 h incubation of the cells and measured as a percentage of DNA in comet tail. The results show that each of the examined pyrazolo[4,3-*e*]tetrazolo[1,5-*b*][1,2,4]triazine sulfonamides significantly ($p < 0.0001$) induced DNA damage, even at their lowest concentrations ($0.5 \times \text{IC}_{50}$), compared to untreated cells, in all cancer cell lines in a concentration–response manner.

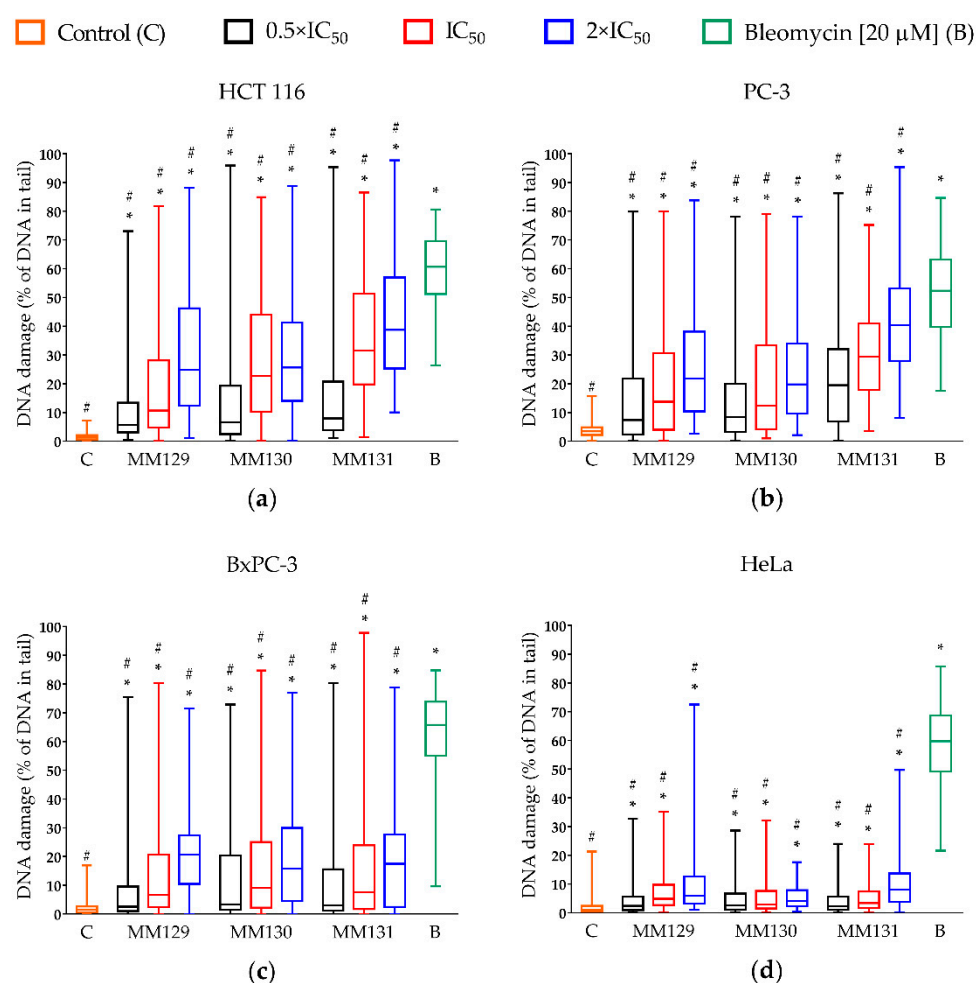


Figure 2. Evaluation of DNA damage (SSBs, DSBs, and alkali-labile sites) in human cancer cell lines: (a) HCT 116; (b) PC-3; (c) BxPC-3; (d) HeLa treated with **MM129**, **MM130**, and **MM131** in the concentrations of 0.5, 1, and $2 \times \text{IC}_{50}$ for 24 h using the alkaline version of the comet assay. The applied concentrations of investigated compounds were at least 10 times lower than the concentration of bleomycin (positive control) used in the experiment. DNA damage was shown as a median of the percentage of DNA in comet tail with interquartile range and minimal and maximal values. Significant differences ($p < 0.0001$) compared with negative (*) and positive (#) control.

Differences in response of the cells to genotoxic activity of investigated compounds were noticed. From all tested compounds, **MM131** exhibited the strongest genotoxic activity against PC-3 and HCT 116 cells (19.5–40.3% and 8–38.8% of DNA in comet tail, respectively). The moderate effect of investigated compounds with no significant differences ($p > 0.05$) between their genotoxic activity was observed in the BxPC-3 and the HeLa

cell line (2.5–20.7% and 2.3–8.1% of DNA in comet tail, respectively). Figure 3 demonstrates the representative photos of comets from this experiment.

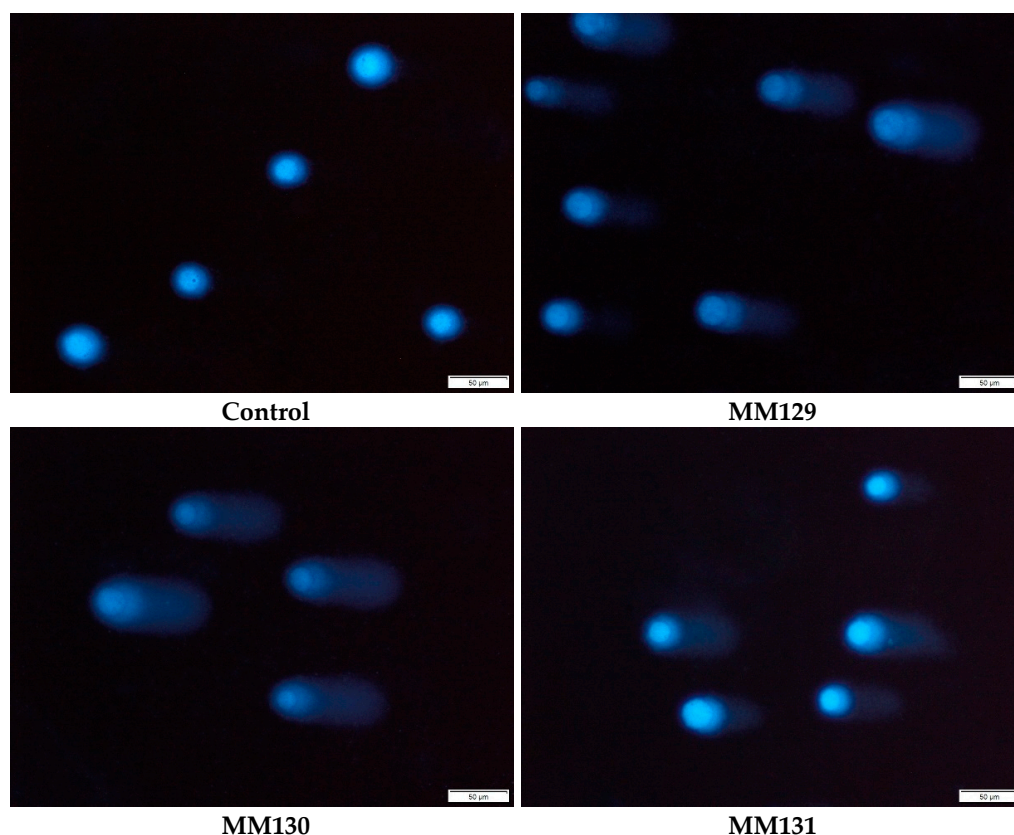


Figure 3. Exemplary images of the comets obtained in the alkaline version of the comet assay after incubation of PC-3 cells with MM129, MM130, and MM131 in the concentrations equal to their $2 \times IC_{50}$ values. The scale bar is 50 μ m.

Neutral Version (pH 9.0)

Table 1 shows the comparison of DNA damage level in both versions of the comet assay measured as a percentage of DNA in the comet tail, after 24 h incubation with tested compounds. Among the investigated cells, HCT 116 showed the highest level of DSBs induced by examined pyrazolo[4,3-*e*]tetrazolo[1,5-*b*][1,2,4]triazine sulfonamides (15.8–30.6% of DNA in the tail), while DNA damage levels in BxPC-3 and PC-3 cell lines were in the range of 7.1–10% and 1.5–7.4% of DNA in the comet tail, respectively.

The HeLa cell line was omitted in the neutral comet assay, due to its low response to the examined compounds in comparison to other cell lines in the alkaline version of the comet assay. The compounds that presented the strongest genotoxic activity in the HCT 116 and PC-3 cell lines were MM130 and MM129, respectively. There was no significant difference ($p > 0.05$) between the genotoxicity of tested sulfonamides in BxPC-3 cells (Table 1). Figure 4 demonstrates the representative photos of comets from this experiment.

Table 1. Comparison of the results of the alkaline and the neutral comet assay. DNA damage was shown as a median of the percentage of DNA in comet tail with an interquartile range (parentheses). Significant differences ($p < 0.0001$) compared with control (*).

Cancer Cell Line	Compound	Alkaline Version	Neutral Version
HCT 116	Control	1.3 (0.5–2.1)	2.9 (1.9–4)
	MM129 IC ₅₀	10.7 * (4.7–28.1)	19.4 * (13.3–29.2)
	MM129 2 × IC ₅₀	24.9 * (12.4–46.3)	26.9 * (19.9–34.3)
	MM130 IC ₅₀	22.7 * (10.3–44)	21.2 * (14.9–31.7)
	MM130 2 × IC ₅₀	25.6 * (14.1–41.3)	30.6 * (24.8–36.1)
	MM131 IC ₅₀	31.5 * (19.8–51.3)	15.8 * (11.7–23.1)
	MM131 2 × IC ₅₀	38.8 * (25.3–57)	25.6 * (19.7–33.1)
PC-3	Control	3.4 (2.2–4.8)	1.3 * (0.4–2.3)
	MM129 IC ₅₀	13.8 * (4–30.6)	2.4 * (1.1–3.8)
	MM129 2 × IC ₅₀	21.8 * (10.4–38.2)	7.3 * (5.1–10.3)
	MM130 IC ₅₀	12.4 * (4.2–33.4)	1.5 * (0.4–3.1)
	MM130 2 × IC ₅₀	19.8 * (9.6–34)	2.2 * (1.2–3.7)
	MM131 IC ₅₀	29.4 * (17.9–41)	2.3 * (1.3–3.6)
	MM131 2 × IC ₅₀	40.3 * (28–53.2)	4.3 * (2.8–6.3)
BxPC-3	Control	1.6 * (0.5–2.6)	2.5 * (0.4–4.4)
	MM129 IC ₅₀	6.7 * (2.3–20.7)	8.7 * (6.1–13.9)
	MM129 2 × IC ₅₀	20.7 * (10.5–27.4)	10 * (6.9–13.9)
	MM130 IC ₅₀	9.1 * (2.2–25)	7 * (4.7–12.2)
	MM130 2 × IC ₅₀	15.8 * (4.5–29.9)	8.5 * (6.1–12.9)
	MM131 IC ₅₀	7.5 * (1.7–23.9)	9.6 * (6.8–13.4)
	MM131 2 × IC ₅₀	17.4 * (2.5–27.7)	9.7 * (7.4–12.9)

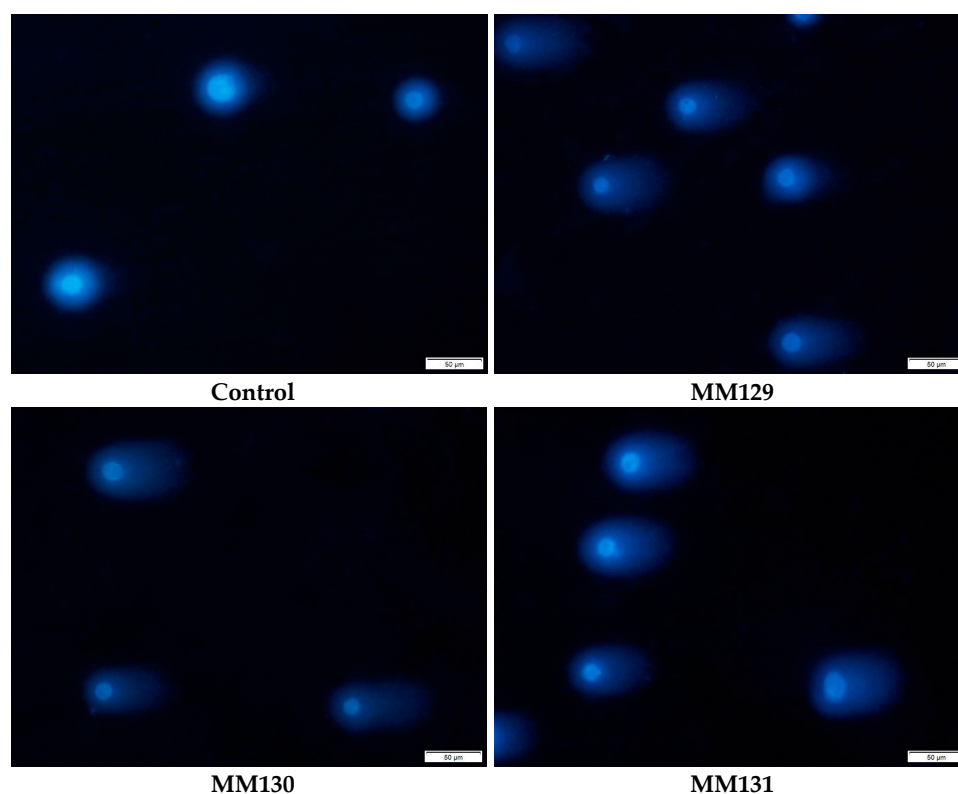


Figure 4. Representative images of comets acquired in the neutral version of the comet assay after incubation of HCT 116 cells with MM129, MM130, and MM131 in the concentrations equal to their 2 × IC₅₀ values. The scale bar is 50 μm.

2.3.2. Immunocytochemical Detection of γ -H2AX

The γ -H2AX staining was employed to confirm the genotoxic properties of examined compounds presented in the neutral comet assay. The HCT 116 cell line was the most sensitive to the DSBs induction (Table 1) and was therefore selected for this analysis. Incubation of HCT 116 cells for 24 h with examined compounds caused an increase in the levels of DNA damage, measured as a median of the number of γ -H2AX foci per nucleus in these cells. Significant differences ($p < 0.0001$) between compound-treated and control cells were noticed. The concentration–response relationship was observed for each examined compound. From all investigated derivatives of pyrazolo[4,3-*e*]tetrazolo[1,5-*b*][1,2,4]triazine, **MM131** exhibited the strongest genotoxic potential (median of the number of γ -H2AX foci per nucleus for the highest concentration used in the study was 15) (Figure 5). Figure 6 demonstrates the representative pictures of γ -H2AX foci in HCT 116 cells from this experiment.

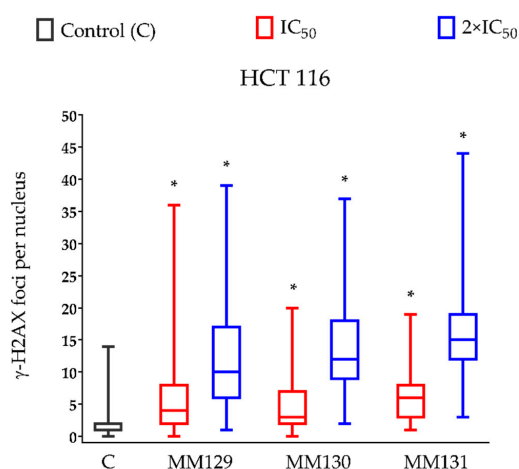


Figure 5. The presence of the γ -H2AX foci of DSBs per nucleus in HCT 116 cells treated with **MM129**, **MM130**, and **MM131** for 24 h. The data are shown as a median of the number of γ -H2AX foci with interquartile range and minimal and maximal values. Significant differences ($p < 0.0001$) compared with negative control (*).

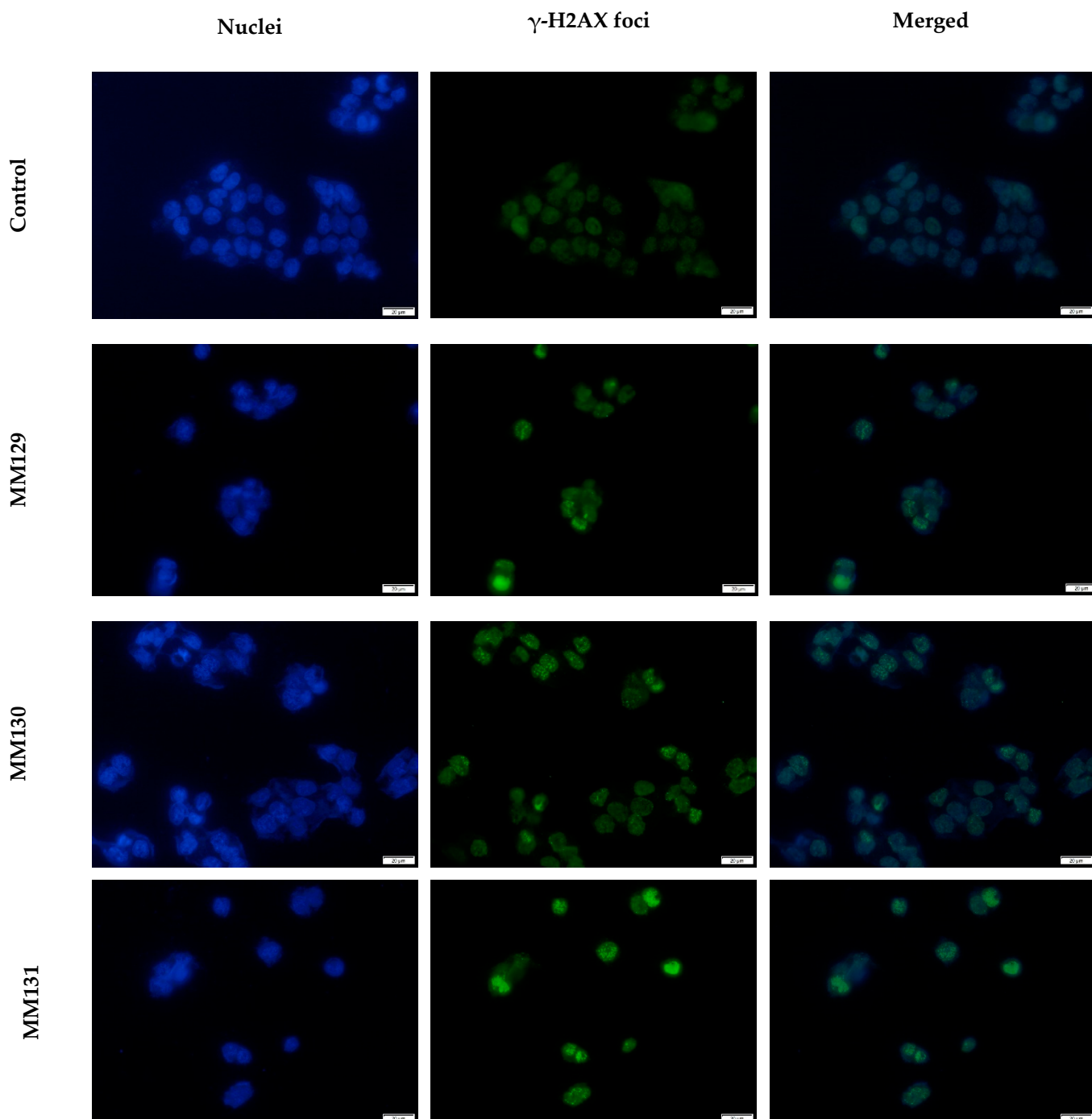


Figure 6. Exemplary images of γ -H2AX foci in HCT 116 cells after 24 h treatment with MM compounds in the concentrations equal to their $2 \times \text{IC}_{50}$ values; nuclear DNA stained with DAPI (blue); γ -H2AX foci (green). The scale bar is 20 μm .

3. Discussion

Antineoplastic properties of several MM compounds, including MM124, MM137 [34], MM129 [35,36], and MM131 [37] with promising results have been examined so far. The mechanistic study showed that down-regulation of PD-L1 (programmed death-ligand 1) expression, which plays a fundamental role in the immunological self-tolerance, was correlated with the use of MM129. Moreover, data indicate that MM129 can inhibit intracellular molecules associated with cell cycle arrest and tumorigenesis promotion, such as CDK2, mTOR, or AKT [36]. In the present study, we showed for the first time cytotoxic and

genotoxic potential of **MM129**, **MM130**, and **MM131** towards HCT 116, HeLa, PC-3, and BxPC-3 cancer cell lines.

Data obtained by Gornowicz et al. [34] demonstrated high cytotoxicity of **MM124** and **MM137** against colorectal cancer (CRC) cell lines HT-29 and DLD-1 (IC_{50} values in the range of 0.16–1.54 μ M). In addition, the results presented by Hermanowicz et al. [35] and Gornowicz et al. [37] have shown cytotoxic activity of **MM129** and **MM131** towards the same CRC cell lines (IC_{50} values in the range of 3.1–3.9 μ M). Importantly, in all cases, obtained IC_{50} values were much lower than those for the reference drugs 5-fluorouracil and/or roscovitine (RSC) [34,35,37]. Our results of the MTT assay confirmed cytotoxic activity of previously mentioned triazine derivatives **MM129** and **MM131** towards another CRC cell line (HCT 116), as well as other cancer cell lines, including HeLa, PC-3, and BxPC-3, in a similar concentration range (Figure 1; IC_{50} = 0.13–0.9 μ M). In this research, the cytotoxicity of **MM130** was demonstrated for the first time. **MM130** presented moderate cytotoxic potential in comparison to other MM compounds in all studied cancer cell lines. Despite the high cytotoxic potential of the tested compounds towards the CRC cell line HCT 116 (IC_{50} in the range of 0.39–0.6 μ M), the tested derivatives of pyrazolo[4,3-*e*]tetrazolo[1,5-*b*][1,2,4]triazine showed even more profound cytotoxic activity against PC-3 and BxPC-3 cell lines (IC_{50} in the range of 0.17–0.36 μ M and 0.13–0.26 μ M, respectively). Importantly, the higher resistance of normal PBMCs and Hs27 cells compared to the cancer cell lines toward the tested tricyclic triazine derivatives (Figure 1; cancer/normal cells IC_{50} ratio showed that MM compounds were 1.2–4.9-times more cytotoxic in cancer cell lines compared to normal cells) was observed (Figure 1).

Based on the criteria demonstrated by National Cancer Institute (NCI), the cytotoxicity of a compound can be classified as high, moderate, and weak (IC_{50} < 20 μ g/mL, 21–200 μ g/mL, or in the range of 201–500 μ g/mL, respectively). All investigated sulfonamides are classified as compounds with high cytotoxicity [38]. In addition, the examined MM compounds exhibit significantly stronger cytotoxicity in comparison to various currently used chemotherapeutics, such as 5-fluorouracil (IC_{50} –96.1 μ M for BxPC-3 and 3.2 μ M for HCT 116 [39,40]), cisplatin (IC_{50} –9 μ M for PC-3 and HCT 116 and 12.3 μ M for HeLa [41,42]), oxaliplatin (IC_{50} –72 μ M for HCT 116 and 100 μ M for PC-3 [42]), or irinotecan (IC_{50} –2.1 μ M for PC-3 and 2.6 μ M for HCT 116) [40,43]. The limitation of doses of antineoplastic agents seems to be crucial for the reduction in side effects that occur during chemotherapy treatment. Further investigations of the anticancer properties of **MM129**, **MM130**, and **MM131** are required; however, their high cytotoxicity indicates the potential implementation of these compounds in the field of cancer treatment.

Inhibition of cell proliferation caused by DNA SSBs and DSBs formation is one of the main mechanisms of the action of various antineoplastic drugs. The creation of adducts and/or interactions of free radicals with the double helix of DNA plays a fundamental role in DNA degradation. DNA DSBs, due to their extreme difficulty to repair, are the most serious threat to the cell. Unrepaired DSBs may promote cell death, while misrepaired ones can be a potential factor for further neoplastic progression [44–46]. DNA DSBs induced through factors such as chemotherapeutic agents or ionizing radiation result in phosphorylation of H2AX on its residue serine 139 via kinases, such as ataxia telangiectasia mutated (ATM), DNA-dependent, and ATM-RAD-3-related protein kinase [47–52]. The phosphorylation of H2AX leads to recruitment of MRN (hRAD50/hMRE11/NBS1) and mediator of the DNA damage checkpoint (MDC1) repair complex, which enhances the ATM activation, and subsequently results in phosphorylation even more of H2AX histone proteins surrounding the DSB sites. MDC1 works as a platform for other DDR components that enhance the conveyed signal and activate DNA repair pathways through nonhomologous end-joining or homologous recombination via recruitment of 53BP1 or BRCA1 proteins, respectively. The studies have shown that the number of DNA DSBs in cells directly correlates with the number of γ -H2AX foci, which are considered as a well-known marker for DSBs [53].

The high genotoxicity of investigated compounds towards HCT 116 cells, especially the high level of DNA DSBs measured via the neutral comet assay (Table 1) and by the

immunocytochemical detection of γ -H2AX (Figure 5), is worth noting. Despite strong genotoxic properties of **MM129**, two other MM compounds, **MM130** and **MM131**, exhibited similar or even higher genotoxic potential toward HCT 116 cells, measured in the alkaline, as well as in the neutral version of the comet assay (Table 1). Moreover, the median number of γ -H2AX foci in HCT 116 cells after 24 h incubation with **MM130** and **MM131** was higher when compared to **MM129** (Figure 5). The results of the alkaline version of the comet assay strongly indicate higher genotoxicity of **MM131** when compared to **MM130** at the concentrations equal to their $2 \times IC_{50}$ values (Figure 2; 38.8% vs. 25.6% of the DNA in the tail, respectively). Differences between the genotoxic activity of **MM130** and **MM131** in the neutral comet assay and γ -H2AX staining are slightly more subtle. Immunocytochemical detection of γ -H2AX showed the strongest genotoxic potential of **MM131** (Figure 5; median of 12 vs. 15 foci per nucleus for **MM130** and **MM131** at their highest concentrations used, respectively). However, the results of the neutral comet assay revealed stronger genotoxicity of **MM130**, when compared to **MM131** for both IC_{50} and $2 \times IC_{50}$ values (Table 1).

The results obtained from the alkaline version of the comet assay demonstrated high genotoxic potential of tested compounds not only towards HCT 116 cells, but also against PC-3 and BxPC-3 cell lines (Figure 2). Surprisingly, HeLa was much more resistant to genotoxic activity of the investigated tricycle triazine derivatives (Figure 2; 4.1–8.1% of the DNA in the comet tail for higher concentrations of tested compounds). To find an explanation of this dissimilarity, further investigation of **MM129**, **MM130**, and **MM131** against the HeLa cell line is required. Interestingly, **MM131** exhibited the strongest genotoxic activity among tested derivatives of pyrazolo[4,3-*e*]tetrazolo[1,5-*b*][1,2,4]triazine on the PC-3 cells (Figure 2; 19.5–40.3% of the DNA in the comet tail for **MM131** vs. 7.4–21.8% of the DNA in the comet tail for **MM129** and **MM130**). There were no significant differences ($p > 0.05$) observed between **MM129** and **MM130** genotoxicity for the PC-3 cell line. Furthermore, similar genotoxicity, with no significant difference within examined MM compounds ($p > 0.05$), was noticed in the case of the BxPC-3 and HeLa cell lines (Figure 2). The only cell line that demonstrated comparable DNA damage in both versions of the comet assay was HCT 116, suggesting that DSBs are the major DNA damage induced in these cells (Table 1; 38.8% vs. 30.6% of DNA in the comet tail for the higher used concentrations). Nevertheless, even if the level of the DSBs determined in the BxPC-3 and PC-3 cells after the MM compounds' treatment was relatively low, unrepaired SSBs can lead to DSB formation and initiate cell death through the apoptosis.

High antineoplastic properties of **MM129** were confirmed not only by an in vitro model but also via an in vivo model. During the two weeks of **MM129** treatment, a significant reduction in tumor mass and volume in the mouse model of xenotransplantation (mice challenged with HT-29 and DLD-1 cancer cells) was observed [54]. Furthermore, in the previous study of Hermanowicz et al. [31], the inhibition of tumor development in the zebrafish embryo xenograft model was correlated with **MM129** activity. Our results on another CRC cell line are in agreement with these data. In the present paper, the HCT 116 cell line was the most sensitive to DNA DSBs formation induced by **MM129** among tested cancer cells (Table 1). Immunocytochemical detection of γ -H2AX confirmed the results obtained in the neutral comet assay, showing the highly genotoxic potential of **MM129** against HCT 116 cells (Figure 5). We speculate that the efficiency of anticancer activity of **MM129** against colon cancer in Cby.Cg-Foxn1nu/cmdb mice, as well as in the zebrafish embryo xenograft model, may be correlated with strong genotoxic activity of **MM129**.

Higher cytotoxic and genotoxic properties of **MM130** and **MM131** vs. **MM129** are due to differences in one moiety between those compounds—*cis*-4-hydroxy-L-proline methyl ester hydrochloride present in **MM129** vs. 2-aminopropanol presents as stereoisomers in the other two compounds. However, to find a proper molecular explanation for these differences in anticancer activity between the remaining two compounds, molecular target identification and in silico studies of examined substances are required. Nevertheless, despite the same moiety in **MM130** and **MM131**, in our study **MM131** inhibited stronger cy-

tototoxic and genotoxic potential than **MM130** (Figures 1, 2 and 5). Data show that differences between stereoisomers are associated with their pharmacokinetic properties, such as their absorption, bioavailability, distribution, and metabolism, as well as their pharmacological potency and activity. Because of these differences, some of them can be useful in some fields of medicine, while the others may be extremely dangerous (*S*-Thalidomide, *S*-Naproxen) or biologically inactive (*R*-ibuprofen) [55]. We suggest that the differences in cytotoxicity, as well as in genotoxicity of **MM130** and **MM131** (Table 1 and Figures 1, 2 and 6) may result from their stereoisomerism. To confirm our speculations, further investigations of the biological activities, as well as the pharmacokinetic and pharmacodynamics properties of both compounds, are required.

4. Materials and Methods

4.1. Synthesis

4.1.1. General

Melting points were determined on a Mel-Temp apparatus and were uncorrected. ^1H - and ^{13}C -NMR spectra were recorded on a Varian spectrometer (400 MHz for ^1H and 100 MHz for ^{13}C). The chemical shift values were expressed in ppm (part per million) with tetramethylsilane (TMS) as an internal reference. The relative integrals of peak areas agreed with those expected for the assigned structures. The molecular weight of the final compounds was assessed by electrospray ionization mass spectrometry (ESI/MS) on Agilent Technologies 6538 UHD Accurate Mass Q-TOF LC/MS. Elemental analyses were within $\pm 0.4\%$ of the calculated values. For the preparation and spectroscopic data of the compounds **2a**, **2c**, **MM129**, and **MM131**, see the literature [34,35].

4.1.2. Preparation of *N*-(*S*)-(1-hydroxy-propan-2-yl)-4-(3-methyl-5-methylsulfonyl-1H-pyrazolo[4,3-*e*][1,2,4]triazin-1-yl)benzenesulfonamide (**2b**)

Chlorosulfonyl derivative **1** [34] (194 mg, 0.5 mmol) was dissolved in anhydrous acetonitrile (10 mL) and (*S*)-2-aminopropanol (131 mg, 1.75 mmol) was added and stirred overnight at room temperature. Then, the reaction mixture was concentrated in vacuo to afford the crude product **2b**. The residue was purified on silica gel using a mixture of CH_2Cl_2 :EtOH (25:1) as eluent to give the final sulfonamide as a yellow solid.

Yield 96%. Melting point: 215–220 °C; ^1H -NMR (methanol) δ : 1.03 (d, 3H, $J = 6.4$ Hz), 2.85 (s, 3H), 3.33–3.38 (m, 2H), 3.43–3.50 (m, 1H), 3.57 (s, 3H), 4.57 (bs, 1H, NH), 8.13 (d, 2H, $J = 8.8$ Hz), 8.65 (d, 2H, $J = 8.8$ Hz); ^{13}C -NMR (methanol) δ : 11.12, 17.98, 41.04, 52.55, 66.90, 121.36, 129.62, 139.31, 141.45, 147.73, 149.90, 162.88, 210.13. HRMS (ESI, m/z) Calcd for $\text{C}_{15}\text{H}_{19}\text{N}_6\text{O}_5\text{S}_2$ [$M + \text{H}$] 427.1322. Found [$M + \text{H}$] 427.1320. Anal. Calcd for $\text{C}_{15}\text{H}_{18}\text{N}_6\text{O}_5\text{S}_2$: C, 42.25; H, 4.25; N, 19.71. Found: C, 42.50; H, 4.47; N, 19.54.

4.1.3. Synthesis of *N*-(*S*)-(1-hydroxy-propan-2-yl)-4-[7-methyl-5H-pyrazolo[4,3-*e*]tetrazolo[1,5-*b*][1,2,4]-triazin-5-yl]benzenesulfonamide (**MM130**)

To a solution of compound **2b** (140 mg, 0.33 mmol) in anhydrous ethanol (25 mL), sodium azide (21 mg, 0.33 mmole) was added. The reaction mixture was refluxed until the substrate disappeared (control TLC). Then, the solvent was evaporated, and the crude product was purified using column chromatography and CH_2Cl_2 : MeOH (50:1) mixture as eluent to give the final sulfonamide as a yellow solid.

Yield 91%. Melting point: 197–202 °C; ^1H -NMR (methanol) δ : 1.01 (d, 3H, $J = 6.4$ Hz), 2.85 (s, 3H), 3.30–3.36 (m, 2H), 3.43–3.48 (q, 1H, $J = 5.6$ Hz), 4.58 (bs, 1H, NH), 8.10 (d, 2H, $J = 8.8$ Hz), 8.45 (d, 2H, $J = 8.8$ Hz); ^{13}C -NMR (methanol) δ : 11.18, 17.96, 52.51, 66.87, 120.21, 129.66, 140.65, 141.93, 143.32, 148.29, 148.85, 149.32. HRMS (ESI, m/z) Calcd for $\text{C}_{14}\text{H}_{16}\text{N}_9\text{O}_3\text{S}$ [$M + \text{H}$] 390.13220. Found [$M + \text{H}$] 390.13210. Anal. Calcd for $\text{C}_{14}\text{H}_{15}\text{N}_9\text{O}_3\text{S}$: C, 43.18; H, 3.88; N, 32.37. Found: C, 43.40; H, 4.02; N, 32.15.

4.2. Chemicals

Trypsin/EDTA and media used for cell culture (DMEM, DMEM-F12, IMDM, and RPMI 1640), as well as gradient cell separation medium used for PBMCs isolation (Lymphosep), were supplied by Biowest (Nuaille, France). Normal-melting-point (NMP) agarose, low-melting-point (LMP) agarose, Triton X-100, 3-(4,5-dimethylthiazol-2-yl)-2,3-diphenyltetrazolium bromide (MTT), dimethyl sulfoxide (DMSO), 4,6-diamidino-2-phenylindole (DAPI), penicillin–streptomycin solution stabilized, fetal bovine serum (FBS), phytohaemagglutinin (PHA), phosphate-buffered saline (PBS), and *N,N*-Dimethylformamide (DMF) were purchased from Sigma-Aldrich (St Louis, MO, USA). Microplates, as well as 96-well and 12-well plates, were supplied by Thermo Fisher Scientific (Waltham, MA, USA). Other chemicals used in the experiments: fluoromount-G (Invitrogen, Carlsbad, CA, USA); bleomycin (TCI); SDS (ROTH); paraformaldehyde (Polysciences, Inc; 400 Valley Rd, Warrington, PA 18976, USA); goat serum (Abcam, Cambridge, UK); the primary antibody, anti-gamma-H2AX (phospho-Ser139) (Abcam, Cambridge, UK); the secondary Goat anti-Mouse IgG Cross-adsorbed antibody, Alexa Fluor 488 p (Invitrogen, Carlsbad, CA, USA).

4.3. Cell Culture

All tested adherent human cell lines, including Hs27, PC-3, HeLa, HCT 116, and BxPC-3, were provided by American Type Culture Collection (ATCC[®], Rockville, Manassas, VA, USA). PC-3 and HeLa cells were cultivated in DMEM-F12 and IMDM media, respectively, while RPMI 1640 medium was used for HCT 116 and BxPC-3 cells. DMEM was used for the Hs27 cell line. All media were supplemented with 10% (*v/v*) FBS and 1% (*v/v*) penicillin–streptomycin solution. Each of the adherent human tumor cell lines was maintained in a humidified incubator at 37 °C in a 5% CO₂ atmosphere and was regularly scanned for mycoplasma contamination. In order to maintain the proper amount of culture cells, subculture was performed by their routine passaging at 90% confluence three times a week using 0.025% trypsin/EDTA. Furthermore, to provide the cells with stable growth conditions, the culture medium was changed every 48 h.

Human PBMCs were isolated from the leucocyte buffy coat obtained from the blood of healthy and nonsmoking volunteers (aged 18–65). Leukocyte buffy coats were collected from Blood Bank in Lodz, Poland. The use of the leukocyte buffy coat in the investigation of the effect of novel tricyclic pyrazolo[4,3-*e*][1,2,4]triazine derivatives on human PBMCs was approved by the Bioethics Committee for Scientific Investigation, University of Lodz (agreement no. 8/KBBN-UL/I//2019). Isolation of PBMCs was performed by density gradient of Lymphosep (25 min, 1400 rpm, RT). PBMCs were cultured in RPMI-1640 medium, supplemented with 1% (*v/v*) penicillin–streptomycin solution, 1.5% PHA and 10% (*v/v*) FBS.

Each experiment on adherent human cell lines or human PBMCs was conducted on cells from three independent passages or cells obtained from the blood of three independent leukocyte buffy coats, respectively.

4.4. Cytotoxicity—MTT Assay

In order to characterize the effect of tested compounds on cell viability, the MTT test was used [56]. MTT microplate assay enables evaluation of cell viability via measuring cell metabolic activity represented as an ability to incorporate and reduce yellow tetrazolium salt to the violet-blue formazan compounds via the activity of mitochondrial succinate dehydrogenase enzyme. The number of metabolically active cells positively correlates with the amount of reduced tetrazolium salt. The absorbance of formazan solution obtained after solubilizing formazan crystals in an organic solvent, e.g., DMSO, can be measured spectrophotometrically at 570 nm [57].

The suspension of $8\text{--}10 \times 10^3$ (adherent cells) and 8×10^4 (PBMCs) cells in 200 μL and 100 μL medium, respectively, was transferred to each well of 96-well microplate. Plates were incubated for 24 h in controlled conditions (5% CO₂; 37 °C) to ensure cell growth.

Subsequently, the medium was replaced, and the cells were exposed to tested compounds in a wide range of concentrations (0.1–6 μM). Before investigated compounds were diluted in a culture medium, they had been diluted in DMSO in the final concentration of <0.5% *v/v*, which were not toxic to the cells [58,59]. The experimental design included blanks (wells without cells) as well as non-treated control cells. Following the 72 h incubation period, a volume of 20 μL of fresh tetrazolium salt solution (5 mg/mL in PBS) was added per well. In the case of adherent cancer cells, after 3 h of incubation (conditions as previously), the solutions were replaced by 100 μL of DMSO to dissolve formazan complexes. In contrast, the solutions in plates containing PBMCs were not removed and a 100 μL mixture of 50% DMF and 20% SDS was added to each well for the next 24 h. Absorbance was measured via spectrophotometer (microplate reader Power Wave XS BioTek Instruments, Inc., Winooski, VT, USA) at 570 nm. To determine the IC_{50} values (concentration of tested inhibitor, which decreases the cell metabolic rate by 50%, expressed as the reduction in absorbance level in treated cells in comparison to untreated cells by half) of studied compounds, the concentration–response analysis was conducted in a GraphPad Prism 8.0 software system (GraphPad Prism Software Inc., San Diego, CA, USA).

4.5. Genotoxicity

4.5.1. Comet Assay

The alkaline version (pH > 13), as well as the neutral version (pH 9.0) of the comet assay, was performed on cancer cell lines according to the procedures described by Singh et al. [60] with modifications [61,62]. 12-well plates were seeded at a density of $1.2\text{--}1.5 \times 10^5$ cells per well. Subsequently, the cells were cultured for 24 h in controlled conditions (5% CO_2 ; 37 $^\circ\text{C}$), and then were exposed to investigated compounds in different concentrations (0.5 IC_{50} , IC_{50} , and $2 \times \text{IC}_{50}$ values obtained in MTT assay). In addition, negative and positive controls (cells treated only with DMSO at <0.5% and with bleomycin at 20 μM , respectively) were included.

Following a 24 h incubation (5% CO_2 ; 37 $^\circ\text{C}$), the cells were trypsinized and transferred to Eppendorf tubes and centrifuged (10 min, 1400 rpm, 4 $^\circ\text{C}$). The obtained pellet was resuspended in 100 μL of fresh PBS, mixed with 0.75% LMP agarose dissolved in PBS, and embedded onto microscope slides, previously precoated with 0.5% NMP agarose. The Trypan Blue dye exclusion test was used to determine the number of viable cells present in a cell suspension. Cell viability did not fall below the required 80%. The slides after agarose solidification were placed in a fresh, cold lysis buffer (pH 10, 1% Triton X-100, 2.5 M NaCl, 100 mM EDTA, 10 mM Tris) for 1 h (4 $^\circ\text{C}$, in dark), which subsequently was replaced by electrophoretic solution (1 mM EDTA, 300 mM NaOH, pH > 13) for another 40 min. Afterward, electrophoresis was performed (25 min, 0.73 V/cm, 300 mA, 4 $^\circ\text{C}$, in dark). Subsequently, the slides were neutralized with 0.4 M Tris, pH 7.5 (20 min, 4 $^\circ\text{C}$, in dark) and washed $3 \times$ in distilled water. Eventually, slides were drained, stained with DAPI (1 $\mu\text{g}/\text{mL}$) for at least 1 h (4 $^\circ\text{C}$), and analyzed with fluorescence microscope (Olympus, Tokyo, Japan).

The neutral version of the comet assay was conducted according to the same procedure as the alkaline counterpart with a few exceptions, including different electrophoretic buffer (100 mM Tris HCL, 300 mM sodium acetate, pH adjusted to 9.0 by glacial acetic acid), as well as different electrophoresis conditions (60 min; 4 $^\circ\text{C}$; in dark; electric field strength of 0.41 V/cm (50 mA)).

A total number of 50 randomly selected images were analyzed in the commercially available software CaspLab. Two parallel experiments with aliquots of the same sample of cells were performed for a total of 100 cells. From the available parameters, the percentage of DNA in comet tail was selected as the most appropriate as being negatively associated with the level of DNA cross-links, as well as positively correlated with alkali-labile sites and the amount of DNA single-strand breaks (SSBs) and double-strand breaks (DSBs) (alkaline version of the comet assay). The same parameter was used as the measure of DSBs present in the neutral version of the comet assay [63–65].

4.5.2. Immunocytochemical Detection of γ -H2AX

Immunocytochemical detection of the phosphorylated form of the histone protein component H2AX (γ -H2AX) is a well-known approach to estimate DNA DSB levels in both in vitro [47,53,66] and in vivo [67,68] studies. HCT 116 cells were grown on coverslips in 12-well plates at a density of 1.2×10^5 per well for 24 h (5% CO₂; 37 °C). Subsequently, the cells were exposed to investigated compounds in two different concentrations (IC₅₀ and $2 \times$ IC₅₀ values with respect to MTT results), by replacing the medium with an appropriate compound concentration. Negative control (cells treated only with DMSO at <0.5%) was also included.

The cells were fixed with 4% paraformaldehyde (10 min), washed twice with PBS, and permeabilized with 0.5% (*v/v*) Triton X-100/PBS solution (10 min). Afterward, the cells were incubated with a blocking solution containing 1.5% goat serum, and 0.1% Triton in PBS for 10 min and incubated with the primary antibody, anti-gamma-H2AX (phospho-Ser139) (Abcam, Cambridge, UK; 1:100) for 1 h. The cells were washed with PBS and were incubated for another 1 h with the secondary Goat anti-Mouse IgG Cross-adsorbed antibody, Alexa Fluor 488 (Invitrogen; Carlsbad, CA, USA, 1:500). Following incubation with a secondary antibody, the cells were additionally stained with DAPI (2 μ g/mL) in PBS (10 min). Finally, the cells were covered with slides in Fluoromount-G (Invitrogen, Carlsbad, CA, USA) mounting medium.

The slides were examined using a fluorescence microscope (Olympus) at 40 \times magnification. The commercially available software ImageJ was used to analyze the mean number of γ -H2AX foci per nucleus in each sample. A total number of 150 randomly selected cells from digital images per sample were measured. The data were exported and analyzed in GraphPad Prism 8.0 software system (GraphPad Prism Software Inc., San Diego, CA, USA).

4.6. Statistical Analysis

All data are presented as mean \pm 95% confidence intervals (MTT assay) or median with interquartile range and minimal and maximal values (comet assay and immunocytochemical detection of γ -H2AX). The results were obtained from three independent experiments. Statistical significance between the results was evaluated in GraphPad Prism 8.0 software system (GraphPad Prism Software Inc., San Diego, CA, USA), by using the Kruskal–Wallis test with Dunn’s test (multiple comparisons in distributions departing from normality). A *p*-value of < 0.05 was considered to be significant.

5. Conclusions

The current study shows for the first time the diverse, cell-line-dependent cytotoxicity and genotoxicity of **MM129**, **MM130** and **MM131** on HeLa, PC-3, HCT 116, and BxPC-3 cell lines. The MTT assay and the comet assay used in the alkaline and neutral versions, as well as immunocytochemical detection of γ -H2AX, proved high anticancer properties of **MM129**, **MM130** and **MM131** in vitro. Among all the examined MM compounds, **MM131** exhibited the strongest cytotoxic and genotoxic properties. Further investigations of biological activities of tested compounds, including their ability to induce oxidative stress and apoptosis, as well as their implications in the cell cycle progression, are currently being investigated. Nevertheless, our present results constitute a foundation for further in vivo studies, which may lead to the selection of the most efficient compounds among the group of de novo synthesized pyrazolo[4,3-*e*]tetrazolo[1,5-*b*][1,2,4]triazine sulfonamides.

Supplementary Materials: The following supporting information can be downloaded at: <https://www.mdpi.com/article/10.3390/molecules27123761/s1>, Figure S1: 1H NMR in CDCl₃ for derivative **1**; Figure S2: 1H NMR in CDCl₃ for derivative **2a**; Figure S3: 1H NMR in acetone for derivative **2a**; Figure S4: 13C NMR in acetone for derivative **2a**; Figure S5: HRMS for derivative **2a**; Figure S6: 1H-NMR in DMSO for derivative **2b**; Figure S7: 1H-NMR for derivative **2b** in DMSO with one drop of D₂O; Figure S8: 13C-NMR for derivative **2b**; Figure S9: HRMS for **2b**; Figure S10: 1H-NMR for derivative **2c**; Figure S11: 13C-NMR for derivative **2c**; Figure S12: HRMS for **2c**; Figure S13:

¹H NMR in MeOH-d₄ for derivative **MM129**; Figure S14: ¹³C NMR in MeOH-d₄ for derivative **MM129**; Figure S15: ¹H NMR in CDCl₃ for derivative **MM129**; Figure S16: ¹H-NMR in MeOH-d₄ for derivative **MM130**; Figure S17: ¹³C NMR in MeOH-d₄ for derivative **MM130**; Figure S18: ¹H-NMR in MeOH-d₄ for derivative **MM131**; Figure S19: ¹³C-NMR in MeOH-d₄ for derivative **MM131**.

Author Contributions: Conceptualization, K.B. and R.K.; methodology, K.B., B.M. and M.M.; investigation, K.B.; supervision of the synthesis: M.M.; writing—original draft preparation, K.B.; writing—review and editing, B.M., R.K., M.K. and M.M.; visualization, K.B.; supervision, R.K.; project administration, R.K. All authors have read and agreed to the published version of the manuscript.

Funding: This research received no external funding.

Institutional Review Board Statement: The study was conducted according to the guidelines of the Declaration of Helsinki and approved by the Bioethics Committee for Scientific Investigation, University of Lodz (agreement no. 8/KBBN-UŁ/1//2019).

Informed Consent Statement: The leukocyte-platelets buffy coat also containing erythrocytes was purchased from Blood Bank in Lodz, Poland. All procedures related to blood donation were executed at the Regional Centre of Blood Donation and Blood Treatment in Lodz, Poland. The blood donor recruitment was at the Centre, according to national legal procedures and European Union regulations (incl. the regulation (EU) 2016/679 OF THE EUROPEAN PARLIAMENT AND OF THE COUNCIL of 27 April 2016 on the protection of natural persons regarding the processing of personal data and the free movement of such data).

Data Availability Statement: Not applicable.

Conflicts of Interest: The authors declare no conflict of interest.

Sample Availability: Samples of the compounds **MM129**, **MM130** and **MM131** available from the authors.

References

1. Ferlay, J.; Colombet, M.; Soerjomataram, I.; Parkin, D.M.; Piñeros, M.; Znaor, A.; Bray, F. Cancer Statistics for the Year 2020: An Overview. *Int. J. Cancer* **2021**, *149*, 778–789. [CrossRef]
2. World Health Organization. Cancer. Available online: <https://www.who.int/news-room/fact-sheets/detail/cancer> (accessed on 3 February 2022).
3. Wang, X.; Zhang, H.; Chen, X. Drug Resistance and Combating Drug Resistance in Cancer. *CDR* **2019**, *2*, 141–160. [CrossRef] [PubMed]
4. Majidinia, M.; Mirza-Aghazadeh-Attari, M.; Rahimi, M.; Mihanfar, A.; Karimian, A.; Safa, A.; Yousefi, B. Overcoming Multidrug Resistance in Cancer: Recent Progress in Nanotechnology and New Horizons. *IUBMB Life* **2020**, *72*, 855–871. [CrossRef] [PubMed]
5. Nussinov, R.; Tsai, C.-J.; Jang, H. Anticancer Drug Resistance: An Update and Perspective. *Drug Resist. Updates* **2021**, *59*, 100796. [CrossRef]
6. Bhimani, J.; Philipps, L.; Simpson, L.; Lythgoe, M.; Soutati, A.; Webb, A.; Savage, P. The Impact of New Cancer Drug Therapies on Site Specialised Cancer Treatment Activity in a UK Cancer Network 2014–2018. *J. Oncol. Pharm. Pract.* **2020**, *26*, 93–98. [CrossRef] [PubMed]
7. Cross, D.; Burmester, J.K. Gene Therapy for Cancer Treatment: Past, Present and Future. *Clin. Med. Res.* **2006**, *4*, 218–227. [CrossRef]
8. Montaña-Samaniego, M.; Bravo-Estupiñan, D.M.; Méndez-Guerrero, O.; Alarcón-Hernández, E.; Ibáñez-Hernández, M. Strategies for Targeting Gene Therapy in Cancer Cells With Tumor-Specific Promoters. *Front. Oncol.* **2020**, *10*, 605380. [CrossRef]
9. Nussbaumer, S.; Bonnabry, P.; Veuthey, J.-L.; Fleury-Souverain, S. Analysis of Anticancer Drugs: A Review. *Talanta* **2011**, *85*, 2265–2289. [CrossRef]
10. Marchi, E.; O'Connor, O.A. Safety and Efficacy of Pralatrexate in the Treatment of Patients with Relapsed or Refractory Peripheral T-Cell Lymphoma. *Ther. Adv. Hematol.* **2012**, *3*, 227–235. [CrossRef]
11. Kabbaj, Y.; Lazrek, H.B.; Barascut, J.L.; Imbach, J.L. Synthesis and Biological Activity of Some Unsaturated 6-Azauracil Acyclonucleosides. *Nucleosides Nucleotides Nucleic Acids* **2005**, *24*, 161–172. [CrossRef]
12. Saad, H.; Moustafa, A. Synthesis and Anticancer Activity of Some New S-Glycosyl and S-Alkyl 1,2,4-Triazinone Derivatives. *Molecules* **2011**, *16*, 5682–5700. [CrossRef] [PubMed]
13. Kumar, R.; Sirohi, T.S.; Singh, H.; Yadav, R.; Roy, R.K.; Chaudhary, A.; Pandeya, S.N. 1,2,4-Triazine Analogs as Novel Class of Therapeutic Agents. *MRMC* **2014**, *14*, 168–207. [CrossRef] [PubMed]
14. Cascioferro, S.; Parrino, B.; Spanò, V.; Carbone, A.; Montalbano, A.; Barraja, P.; Diana, P.; Cirrincione, G. An Overview on the Recent Developments of 1,2,4-Triazine Derivatives as Anticancer Compounds. *Eur. J. Med. Chem.* **2017**, *142*, 328–375. [CrossRef] [PubMed]

15. Mojzych, M.; Rykowski, A.; Wierzchowski, J. Pyrazolo[4,3-*e*][1,2,4]Triazines: Purine Analogues with Electronic Absorption in the Visible Region. *Molecules* **2005**, *10*, 1298–1306. [[CrossRef](#)]
16. Lindner, H.J.; Schaden, G. Pyrazolo[4.3-*e*]As-triazin, Ein Neues Heterocyclisches System Aus *Pseudomonas Fluorescens* Var. *Pseudoidiodinum*. *Chem. Ber.* **1972**, *105*, 1949–1955. [[CrossRef](#)]
17. Smirnov, V.V.; Kiprianova, E.A.; Garagulya, A.D.; Esipov, S.E.; Dovjenko, S.A. Fluviols, Bicyclic Nitrogen-Rich Antibiotics Produced by *Pseudomonas Fluorescens*. *FEMS Microbiol. Lett.* **1997**, *153*, 357–361. [[CrossRef](#)]
18. Hirata, K.; Nakagami, H.; Takashina, J.; Mahmud, T.; Kobayashi, M.; In, Y.; Ishida, T.; Miyamoto, K. ChemInform Abstract: Novel Violet Pigment, Nostocine A, an Extracellular Metabolite from Cyanobacterium *Nostoc Spongiaeforme*. *ChemInform* **2010**, *27*, 1513–1519. [[CrossRef](#)]
19. Mojzych, M.; Tarasiuk, P.; Kotwica-Mojzych, K.; Rafiq, M.; Seo, S.-Y.; Nicewicz, M.; Fornal, E. Synthesis of Chiral Pyrazolo[4,3-*e*][1,2,4]Triazine Sulfonamides with Tyrosinase and Urease Inhibitory Activity. *J. Enzym. Inhib. Med. Chem.* **2017**, *32*, 99–105. [[CrossRef](#)]
20. Mojzych, M.; Bielawska, A.; Bielawski, K.; Ceruso, M.; Supuran, C.T. Pyrazolo[4,3-*e*][1,2,4]Triazine Sulfonamides as Carbonic Anhydrase Inhibitors with Antitumor Activity. *Bioorg. Med. Chem.* **2014**, *22*, 2643–2647. [[CrossRef](#)]
21. Mojzych, M.; Ceruso, M.; Bielawska, A.; Bielawski, K.; Fornal, E.; Supuran, C.T. New Pyrazolo[4,3-*e*][1,2,4]Triazine Sulfonamides as Carbonic Anhydrase Inhibitors. *Bioorg. Med. Chem.* **2015**, *23*, 3674–3680. [[CrossRef](#)]
22. Mojzych, M.; Šubertová, V.; Bielawska, A.; Bielawski, K.; Bazgier, V.; Berka, K.; Gucký, T.; Fornal, E.; Kryštof, V. Synthesis and Kinase Inhibitory Activity of New Sulfonamide Derivatives of Pyrazolo[4,3-*e*][1,2,4]Triazines. *Eur. J. Med. Chem.* **2014**, *78*, 217–224. [[CrossRef](#)]
23. Manning, G.; Whyte, D.B.; Martinez, R.; Hunter, T.; Sudarsanam, S. The Protein Kinase Complement of the Human Genome. *Science* **2002**, *298*, 1912–1934. [[CrossRef](#)] [[PubMed](#)]
24. Fabbro, D.; Cowan-Jacob, S.W.; Moebitz, H. Ten Things You Should Know about Protein Kinases: IUPHAR Review 14: Ten Things You Should Know about Protein Kinases. *Br. J. Pharmacol.* **2015**, *172*, 2675–2700. [[CrossRef](#)] [[PubMed](#)]
25. Krystof, V.; Uldrijan, S. Cyclin-Dependent Kinase Inhibitors as Anticancer Drugs. *CDT* **2010**, *11*, 291–302. [[CrossRef](#)] [[PubMed](#)]
26. Ades, F.; Metzger-Filho, O. Targeting the Cellular Signaling: BRAF Inhibition and Beyond for the Treatment of Metastatic Malignant Melanoma. *Dermatol. Res. Pract.* **2012**, *2012*, 259170. [[CrossRef](#)]
27. Bedi, A.; Zehnauer, B.; Barber, J.; Sharkis, S.; Jones, R. Inhibition of Apoptosis by BCR-ABL in Chronic Myeloid Leukemia. *Blood* **1994**, *83*, 2038–2044. [[CrossRef](#)]
28. Bazzoni, G.; Carlesso, N.; Griffin, J.D.; Hemler, M.E. Bcr/Abl Expression Stimulates Integrin Function in Hematopoietic Cell Lines. *J. Clin. Investig.* **1996**, *98*, 521–528. [[CrossRef](#)]
29. Cortez, D.; Stoica, G.; Pierce, J.H.; Pendergast, A.M. The BCR-ABL Tyrosine Kinase Inhibits Apoptosis by Activating a Ras-Dependent Signaling Pathway. *Oncogene* **1996**, *13*, 2589–2594.
30. Cambier, N.; Chopra, R.; Strasser, A.; Metcalf, D.; Elefanty, A.G. BCR-ABL Activates Pathways Mediating Cytokine Independence and Protection against Apoptosis in Murine Hematopoietic Cells in a Dose-Dependent Manner. *Oncogene* **1998**, *16*, 335–348. [[CrossRef](#)]
31. Carter, B.Z.; Mak, P.Y.; Mu, H.; Wang, X.; Tao, W.; Mak, D.H.; Dettman, E.J.; Cardone, M.; Zernovak, O.; Seki, T.; et al. Combined Inhibition of MDM2 and BCR-ABL1 Tyrosine Kinase Targets Chronic Myeloid Leukemia Stem/Progenitor Cells in a Murine Model. *Haematologica* **2020**, *105*, 1274–1284. [[CrossRef](#)]
32. Bernat, Z.; Szymanowska, A.; Kciuk, M.; Kotwica-Mojzych, K.; Mojzych, M. Review of the Synthesis and Anticancer Properties of Pyrazolo[4,3-*e*][1,2,4]Triazine Derivatives. *Molecules* **2020**, *25*, 3948. [[CrossRef](#)] [[PubMed](#)]
33. Ghorab, M.M.; Alsaid, M.S.; Abdullah-al-Dhfyhan, A.; Arafa, R.K. Cytotoxic Activity of Some Novel Sulfonamide Derivatives. *Acta Pol. Pharm.* **2015**, *72*, 79–87. [[PubMed](#)]
34. Gornowicz, A.; Szymanowska, A.; Mojzych, M.; Bielawski, K.; Bielawska, A. The Effect of Novel 7-Methyl-5-Phenyl-Pyrazolo[4,3-*e*]Tetrazolo[4,5-*b*][1,2,4]Triazine Sulfonamide Derivatives on Apoptosis and Autophagy in DLD-1 and HT-29 Colon Cancer Cells. *IJMS* **2020**, *21*, 5221. [[CrossRef](#)] [[PubMed](#)]
35. Hermanowicz, J.M.; Szymanowska, A.; Sieklucka, B.; Czarnomysy, R.; Pawlak, K.; Bielawska, A.; Bielawski, K.; Kalafut, J.; Przybyszewska, A.; Surazynski, A.; et al. Exploration of Novel Heterofused 1,2,4-Triazine Derivative in Colorectal Cancer. *J. Enzym. Inhib. Med. Chem.* **2021**, *36*, 535–548. [[CrossRef](#)] [[PubMed](#)]
36. Hermanowicz, J.M.; Pawlak, K.; Sieklucka, B.; Czarnomysy, R.; Kwiatkowska, I.; Kazberuk, A.; Surazynski, A.; Mojzych, M.; Pawlak, D. MM-129 as a Novel Inhibitor Targeting PI3K/AKT/MTOR and PD-L1 in Colorectal Cancer. *Cancers* **2021**, *13*, 3203. [[CrossRef](#)]
37. Gornowicz, A.; Szymanowska, A.; Mojzych, M.; Czarnomysy, R.; Bielawski, K.; Bielawska, A. The Anticancer Action of a Novel 1,2,4-Triazine Sulfonamide Derivative in Colon Cancer Cells. *Molecules* **2021**, *26*, 2045. [[CrossRef](#)]
38. Adisty Ridha Damasuri; Eti Nurwening Sholikhah; Mustofa Cytotoxicity of ((E)-1-(4-Aminophenyl)-3-Phenylprop-2-En-1-One)) on HeLa Cell Line. *Indones. J. Pharmacol. Ther.* **2020**, *1*, 1–6. [[CrossRef](#)]
39. Huanwen, W.; Zhiyong, L.; Xiaohua, S.; Xinyu, R.; Kai, W.; Tonghua, L. Intrinsic Chemoresistance to Gemcitabine Is Associated with Constitutive and Laminin-Induced Phosphorylation of FAK in Pancreatic Cancer Cell Lines. *Mol. Cancer* **2009**, *8*, 125. [[CrossRef](#)]

40. Ikehata, M.; Ogawa, M.; Yamada, Y.; Tanaka, S.; Ueda, K.; Iwakawa, S. Different Effects of Epigenetic Modifiers on the Cytotoxicity Induced by 5-Fluorouracil, Irinotecan or Oxaliplatin in Colon Cancer Cells. *Biol. Pharm. Bull.* **2014**, *37*, 67–73. [[CrossRef](#)]
41. Becit, M.; Aydın Dilsiz, S.; Başaran, N. Interaction of Curcumin on Cisplatin Cytotoxicity in HeLa and HepG2 Carcinoma Cells. *Istanbul J. Pharm.* **2020**, *50*, 202–210. [[CrossRef](#)]
42. Barbanente, A.; Iacobazzi, R.M.; Azzariti, A.; Hoeschele, J.D.; Denora, N.; Papadia, P.; Pacifico, C.; Natile, G.; Margiotta, N. New Oxaliplatin-Pyrophosphato Analogs with Improved In Vitro Cytotoxicity. *Molecules* **2021**, *26*, 3417. [[CrossRef](#)] [[PubMed](#)]
43. Aras, B.; Yerlikaya, A. Bortezomib and Etoposide Combinations Exert Synergistic Effects on the Human Prostate Cancer Cell Line PC-3. *Oncol. Lett.* **2016**, *11*, 3179–3184. [[CrossRef](#)] [[PubMed](#)]
44. Fong, C.W. Platinum Anti-Cancer Drugs: Free Radical Mechanism of Pt-DNA Adduct Formation and Anti-Neoplastic Effect. *Free Radic. Biol. Med.* **2016**, *95*, 216–229. [[CrossRef](#)] [[PubMed](#)]
45. Gajek, A.; Denel-Bobrowska, M.; Rogalska, A.; Bukowska, B.; Maszewski, J.; Marczak, A. Early Activation of Apoptosis and Caspase-Independent Cell Death Plays an Important Role in Mediating the Cytotoxic and Genotoxic Effects of WP 631 in Ovarian Cancer Cells. *Asian Pac. J. Cancer Prev.* **2016**, *16*, 8503–8512. [[CrossRef](#)]
46. Stornetta, A.; Zimmermann, M.; Cimino, G.D.; Henderson, P.T.; Sturla, S.J. DNA Adducts from Anticancer Drugs as Candidate Predictive Markers for Precision Medicine. *Chem. Res. Toxicol.* **2017**, *30*, 388–409. [[CrossRef](#)]
47. Burma, S.; Chen, B.P.; Murphy, M.; Kurimasa, A.; Chen, D.J. ATM Phosphorylates Histone H2AX in Response to DNA Double-Strand Breaks. *J. Biol. Chem.* **2001**, *276*, 42462–42467. [[CrossRef](#)]
48. Rogakou, E.P.; Pilch, D.R.; Orr, A.H.; Ivanova, V.S.; Bonner, W.M. DNA Double-Stranded Breaks Induce Histone H2AX Phosphorylation on Serine 139. *J. Biol. Chem.* **1998**, *273*, 5858–5868. [[CrossRef](#)]
49. Rogakou, E.P.; Boon, C.; Redon, C.; Bonner, W.M. Megabase Chromatin Domains Involved in DNA Double-Strand Breaks in Vivo. *J. Cell Biol.* **1999**, *146*, 905–916. [[CrossRef](#)]
50. Rothkamm, K.; Lobrich, M. Evidence for a Lack of DNA Double-Strand Break Repair in Human Cells Exposed to Very Low x-Ray Doses. *Proc. Natl. Acad. Sci. USA* **2003**, *100*, 5057–5062. [[CrossRef](#)]
51. Rothkamm, K.; Horn, S.; Scherthan, H.; Rößler, U.; De Amicis, A.; Barnard, S.; Kulka, U.; Lista, F.; Meineke, V.; Braselmann, H.; et al. Laboratory Intercomparison on the γ -H2AX Foci Assay. *Radiat. Res.* **2013**, *180*, 149. [[CrossRef](#)]
52. Meyer, B.; Voss, K.-O.; Tobias, F.; Jakob, B.; Durante, M.; Taucher-Scholz, G. Clustered DNA Damage Induces Pan-Nuclear H2AX Phosphorylation Mediated by ATM and DNA-PK. *Nucleic Acids Res.* **2013**, *41*, 6109–6118. [[CrossRef](#)] [[PubMed](#)]
53. Noubissi, F.K.; McBride, A.A.; Leppert, H.G.; Millet, L.J.; Wang, X.; Davern, S.M. Detection and Quantification of γ -H2AX Using a Dissociation Enhanced Lanthanide Fluorescence Immunoassay. *Sci. Rep.* **2021**, *11*, 8945. [[CrossRef](#)] [[PubMed](#)]
54. de Lapuente, J.; Lourenço, J.; Mendo, S.A.; Borràs, M.; Martins, M.G.; Costa, P.M.; Pacheco, M. The Comet Assay and Its Applications in the Field of Ecotoxicology: A Mature Tool That Continues to Expand Its Perspectives. *Front. Genet.* **2015**, *6*, 180. [[CrossRef](#)] [[PubMed](#)]
55. Chhabra, N.; Aseri, M.L.; Padmanabhan, D. A Review of Drug Isomerism and Its Significance. *Int. J. Appl. Basic Med. Res.* **2013**, *3*, 16–18. [[CrossRef](#)]
56. ISO-10993-5-2009; Biological Evaluation of Medical Devices—Part 5: Tests for In Vitro Cytotoxicity. International Organization for Standardization: Geneva, Switzerland, 2009. Available online: <https://nhs.uk/iso-10993-5-2009.pdf> (accessed on 25 March 2022).
57. Stockert, J.C.; Horobin, R.W.; Colombo, L.L.; Blázquez-Castro, A. Tetrazolium Salts and Formazan Products in Cell Biology: Viability Assessment, Fluorescence Imaging, and Labeling Perspectives. *Acta Histochem.* **2018**, *120*, 159–167. [[CrossRef](#)]
58. Da Violante, G.; Zerrouk, N.; Richard, I.; Provot, G.; Chaumeil, J.C.; Arnaud, P. Evaluation of the Cytotoxicity Effect of Dimethyl Sulfoxide (DMSO) on Caco2/TC7 Colon Tumor Cell Cultures. *Biol. Pharm. Bull.* **2002**, *25*, 1600–1603. [[CrossRef](#)]
59. de Abreu Costa, L.; Henrique Fernandes Ottoni, M.; dos Santos, M.; Meireles, A.; Gomes de Almeida, V.; de Fátima Pereira, W.; Alves de Avelar-Freitas, B.; Eustáquio Alvim Brito-Melo, G. Dimethyl Sulfoxide (DMSO) Decreases Cell Proliferation and TNF- α , IFN- γ , and IL-2 Cytokines Production in Cultures of Peripheral Blood Lymphocytes. *Molecules* **2017**, *22*, 1789. [[CrossRef](#)]
60. Singh, N.P.; McCoy, M.T.; Tice, R.R.; Schneider, E.L. A Simple Technique for Quantitation of Low Levels of DNA Damage in Individual Cells. *Exp. Cell Res.* **1988**, *175*, 184–191. [[CrossRef](#)]
61. Singh, N.P.; Stephens, R.E. Microgel Electrophoresis: Sensitivity, Mechanisms, and DNA Electrostretching. *Mutat. Res./DNA Repair* **1997**, *383*, 167–175. [[CrossRef](#)]
62. Lu, Y.; Liu, Y.; Yang, C. Evaluating In Vitro DNA Damage Using Comet Assay. *J. Vis. Exp.* **2017**, *128*, e56450. [[CrossRef](#)]
63. Hartmann, A. Recommendations for Conducting the in Vivo Alkaline Comet Assay. *Mutagenesis* **2003**, *18*, 45–51. [[CrossRef](#)]
64. Liao, W.; McNutt, M.A.; Zhu, W.-G. The Comet Assay: A Sensitive Method for Detecting DNA Damage in Individual Cells. *Methods* **2009**, *48*, 46–53. [[CrossRef](#)] [[PubMed](#)]
65. Gyori, B.M.; Venkatachalam, G.; Thiagarajan, P.S.; Hsu, D.; Clement, M.-V. OpenComet: An Automated Tool for Comet Assay Image Analysis. *Redox Biol.* **2014**, *2*, 457–465. [[CrossRef](#)] [[PubMed](#)]
66. Mosieniak, G.; Sliwinska, M.A.; Przybylska, D.; Grabowska, W.; Sunderland, P.; Bielak-Zmijewska, A.; Sikora, E. Curcumin-Treated Cancer Cells Show Mitotic Disturbances Leading to Growth Arrest and Induction of Senescence Phenotype. *Int. J. Biochem. Cell Biol.* **2016**, *74*, 33–43. [[CrossRef](#)]

67. Lassmann, M.; Hänscheid, H.; Gassen, D.; Biko, J.; Meineke, V.; Reiners, C.; Scherthan, H. In Vivo Formation of γ -H2AX and 53BP1 DNA Repair Foci in Blood Cells After Radioiodine Therapy of Differentiated Thyroid Cancer. *J. Nucl. Med.* **2010**, *51*, 1318–1325. [[CrossRef](#)] [[PubMed](#)]
68. Plappert-Helbig, U.; Libertini, S.; Frieauff, W.; Theil, D.; Martus, H.-J. Gamma-H2AX Immunofluorescence for the Detection of Tissue-Specific Genotoxicity in vivo: Gamma-H2AX Tissue-Specific Genotoxicity. *Environ. Mol. Mutagen.* **2019**, *60*, 4–16. [[CrossRef](#)] [[PubMed](#)]

Supplementary Materials

Pyrazolo[4,3-*e*]tetrazolo[1,5-*b*][1,2,4]triazine Sulfonamides as Novel Potential Anticancer Agents: Cytotoxic and Genotoxic Activities In Vitro

Karol Bukowski ^{1,*}, Beata Marciniak ¹, Mateusz Kciuk ^{1,2}, Mariusz Mojzych ³ and Renata Kontek ¹

¹ Department of Molecular Biotechnology and Genetics, Faculty of Biology and Environmental Protection, University of Lodz, 12/16 Banacha St., 90-237 Lodz, Poland; beata.marciniak@biol.uni.lodz.pl (B.M.); mateusz.kciuk@edu.uni.lodz.pl (M.K.); renata.kontek@biol.uni.lodz.pl (R.K.)

² Doctoral School of Exact and Natural Sciences, University of Lodz, 12/16 Banacha St., 90-237 Lodz, Poland

³ Department of Chemistry, Siedlce University of Natural Sciences and Humanities, 3 Maja 54, 08-110 Siedlce, Poland; mariusz.mojzych@uph.edu.pl

* Correspondence: karol.bukowski@edu.uni.lodz.pl

Figure S1: $^1\text{H-NMR}$ in CDCl_3 for derivative 1

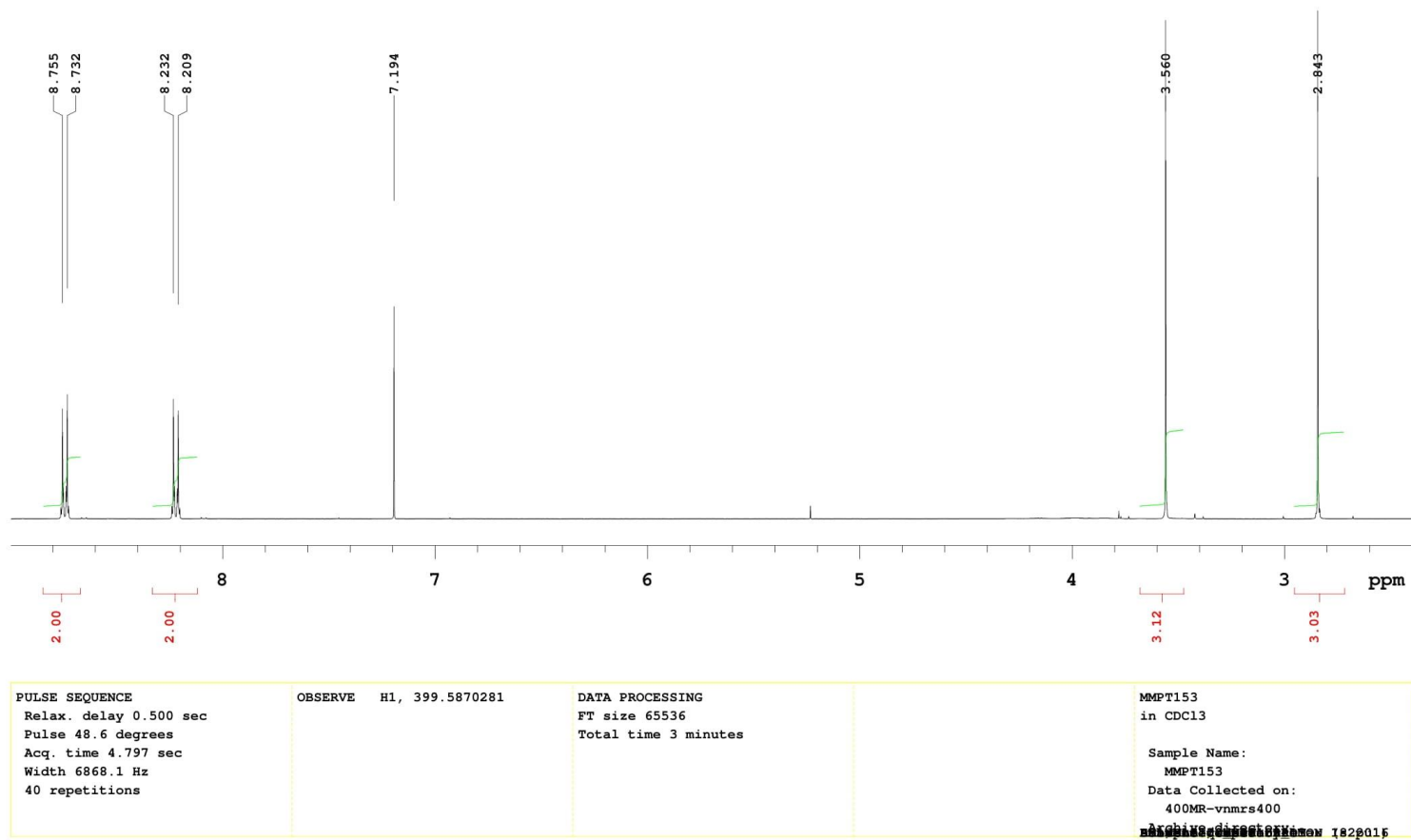
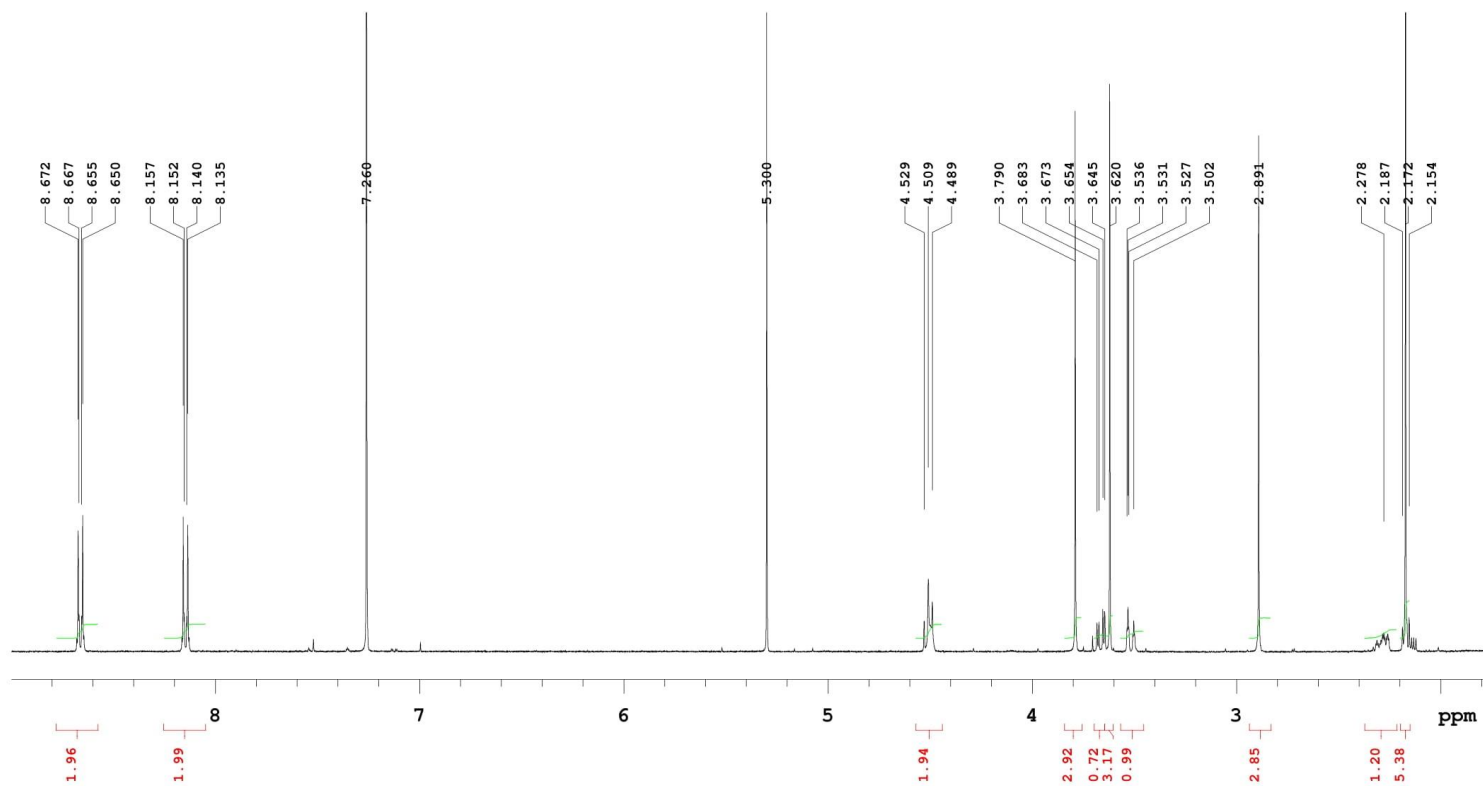


Figure S2: ¹H-NMR in CDCl₃ for derivative 2a



<p>PULSE SEQUENCE</p> <p>Relax. delay 0.500 sec</p> <p>Pulse 48.6 degrees</p> <p>Acq. time 4.797 sec</p> <p>Width 6793.5 Hz</p> <p>40 repetitions</p>	<p>OBSERVE H1, 399.5428928</p>	<p>DATA PROCESSING</p> <p>FT size 65536</p> <p>Total time 3 minutes</p>	<p>MMPT223</p> <p>in CDCl3</p> <p>Sample Name:</p> <p>MMPT223</p> <p>Data Collected on:</p> <p>400MR-vnmrs400</p> <p>MMPT223</p>
---	--------------------------------	---	--

Figure S3: ¹H-NMR in acetone for derivative 2a

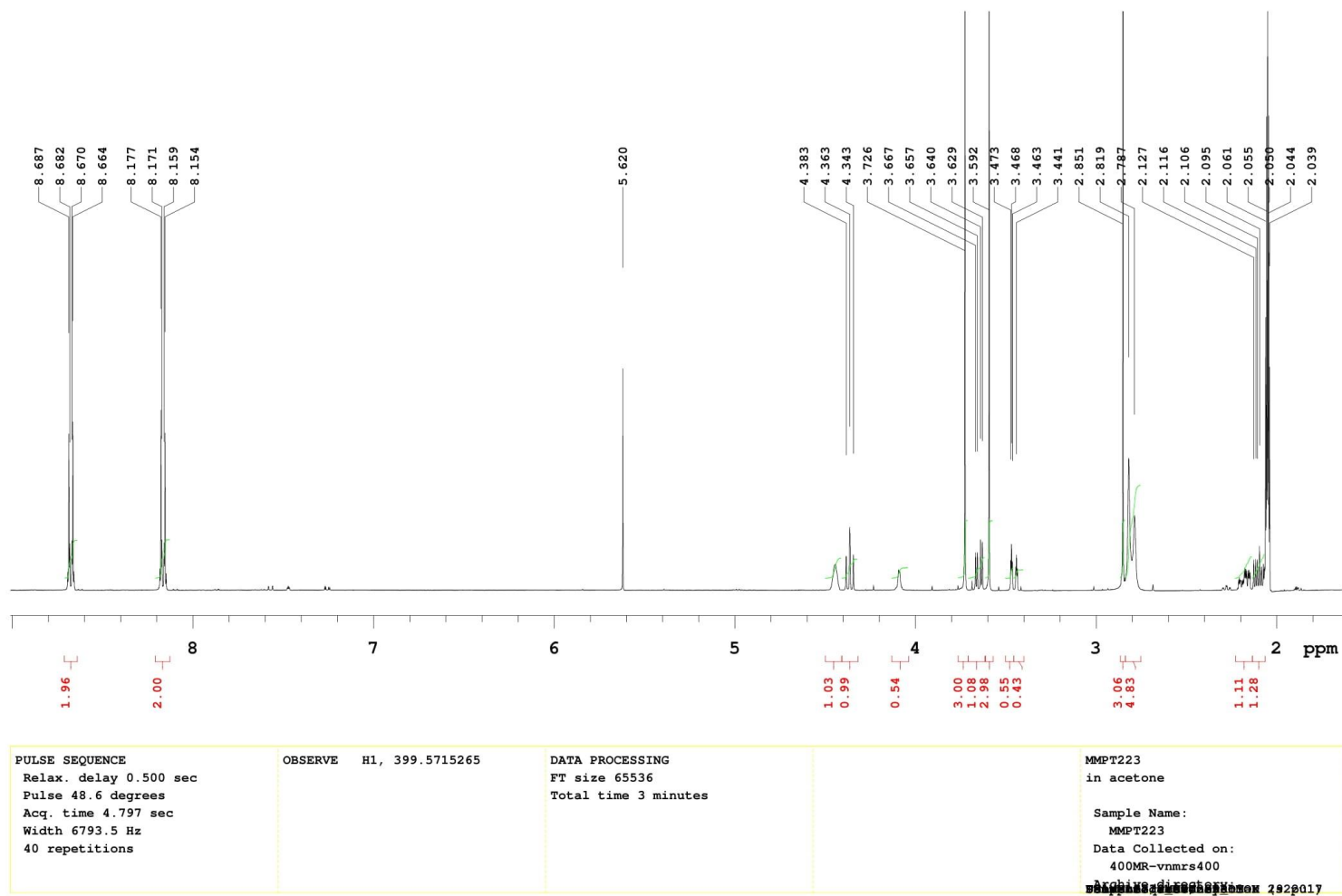
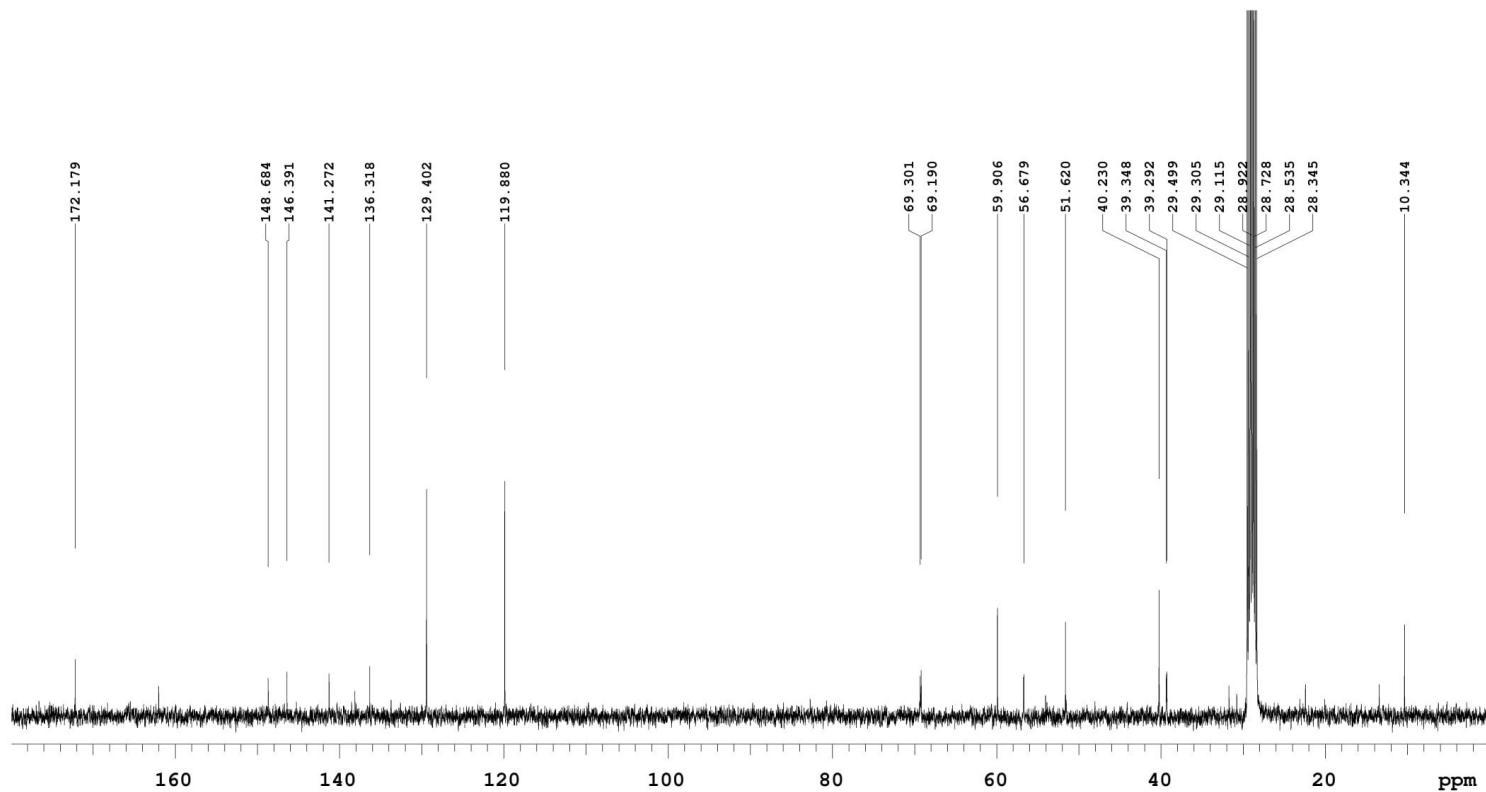
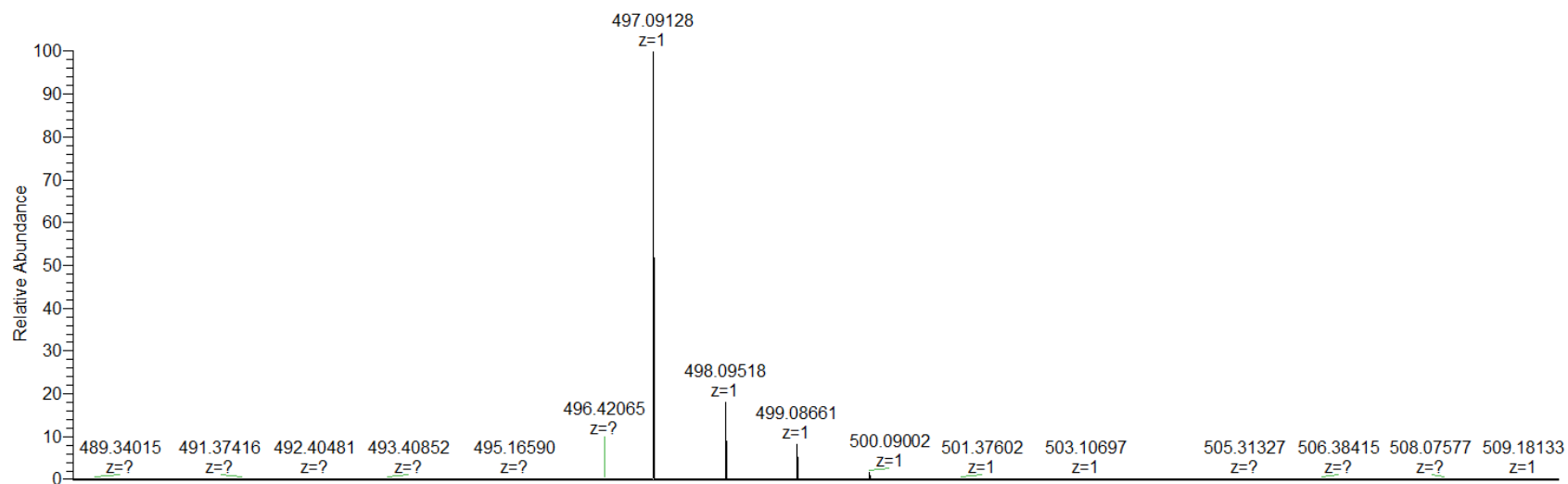


Figure S4: ¹³C-NMR in acetone for derivative 2a

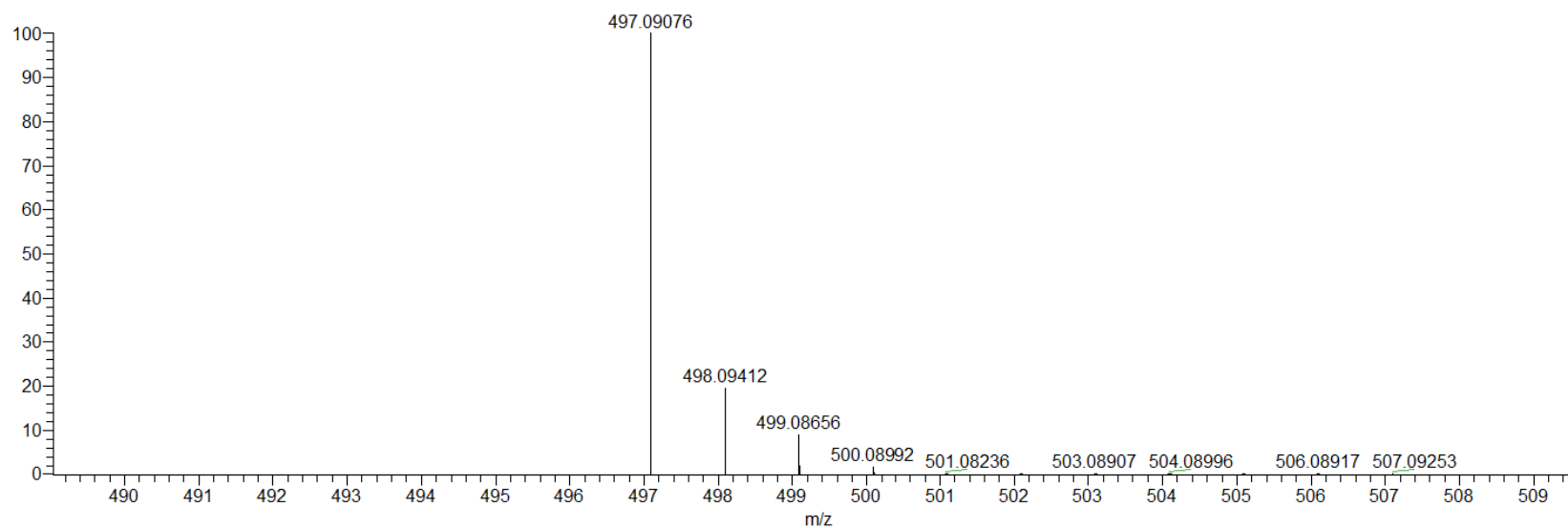


<p>PULSE SEQUENCE</p> <p>Relax. delay 1.500 sec</p> <p>Pulse 38.5 degrees</p> <p>Acq. time 2.674 sec</p> <p>Width 24509.8 Hz</p> <p>2944 repetitions</p>	<p>OBSERVE C13, 100.4723409</p> <p>DECOUPLE H1, 399.5735270</p> <p>Power 37 dB</p> <p>continuously on</p> <p>WALTZ-16 modulated</p>	<p>DATA PROCESSING</p> <p>Line broadening 1.5 Hz</p> <p>FT size 131072</p> <p>Total time 3.4 hours</p>	<p>MMPT223</p> <p>in acetone</p> <p>Sample Name:</p> <p>MMPT223</p> <p>Data Collected on:</p> <p>20140928 11:20:00 AM</p>
--	---	--	--

Figure S5: HRMS for derivative 2a

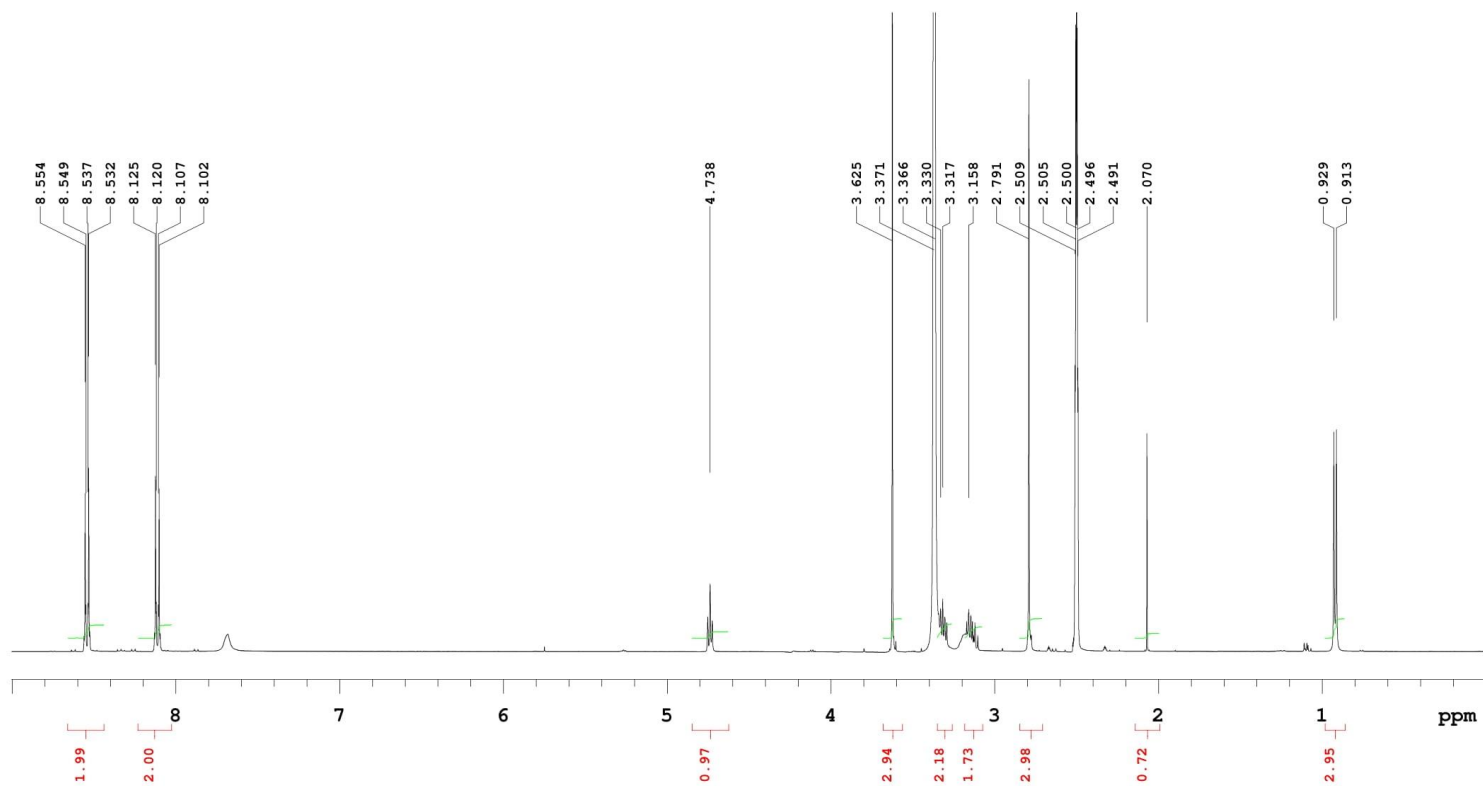


NL:
2.06E8
201214_MM_ASz_R_4
4#37-80 RT: 0.35-0.76
AV: 44 T: FTMS + p ESI
Full ms
[150.0000-2000.0000]



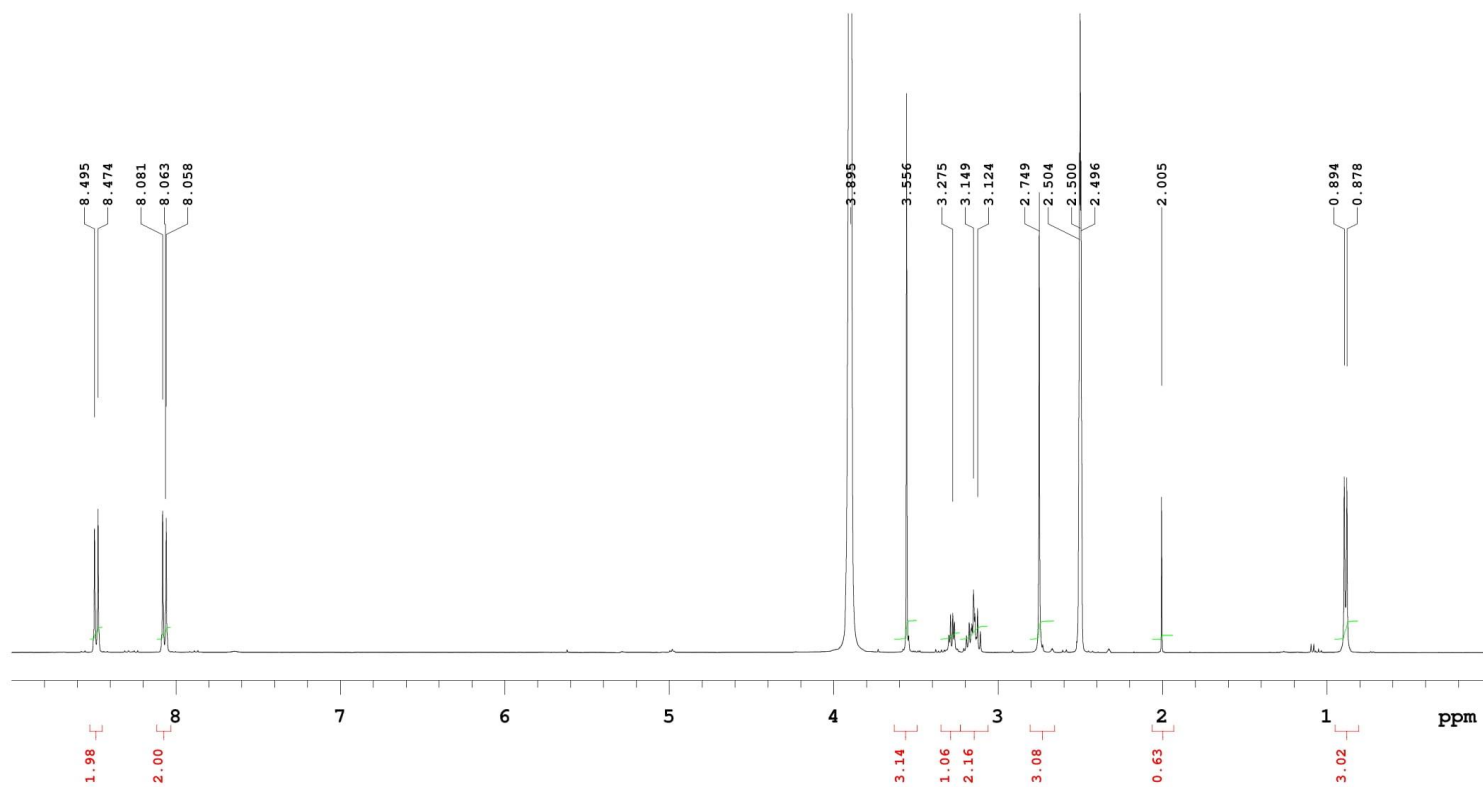
NL:
7.12E5
C₁₈H₂₀N₆O₇S₂+H:
C₁₈H₂₁N₆O₇S₂
pa Chrg 1

Figure S6: ¹H-NMR in DMSO for derivative 2b



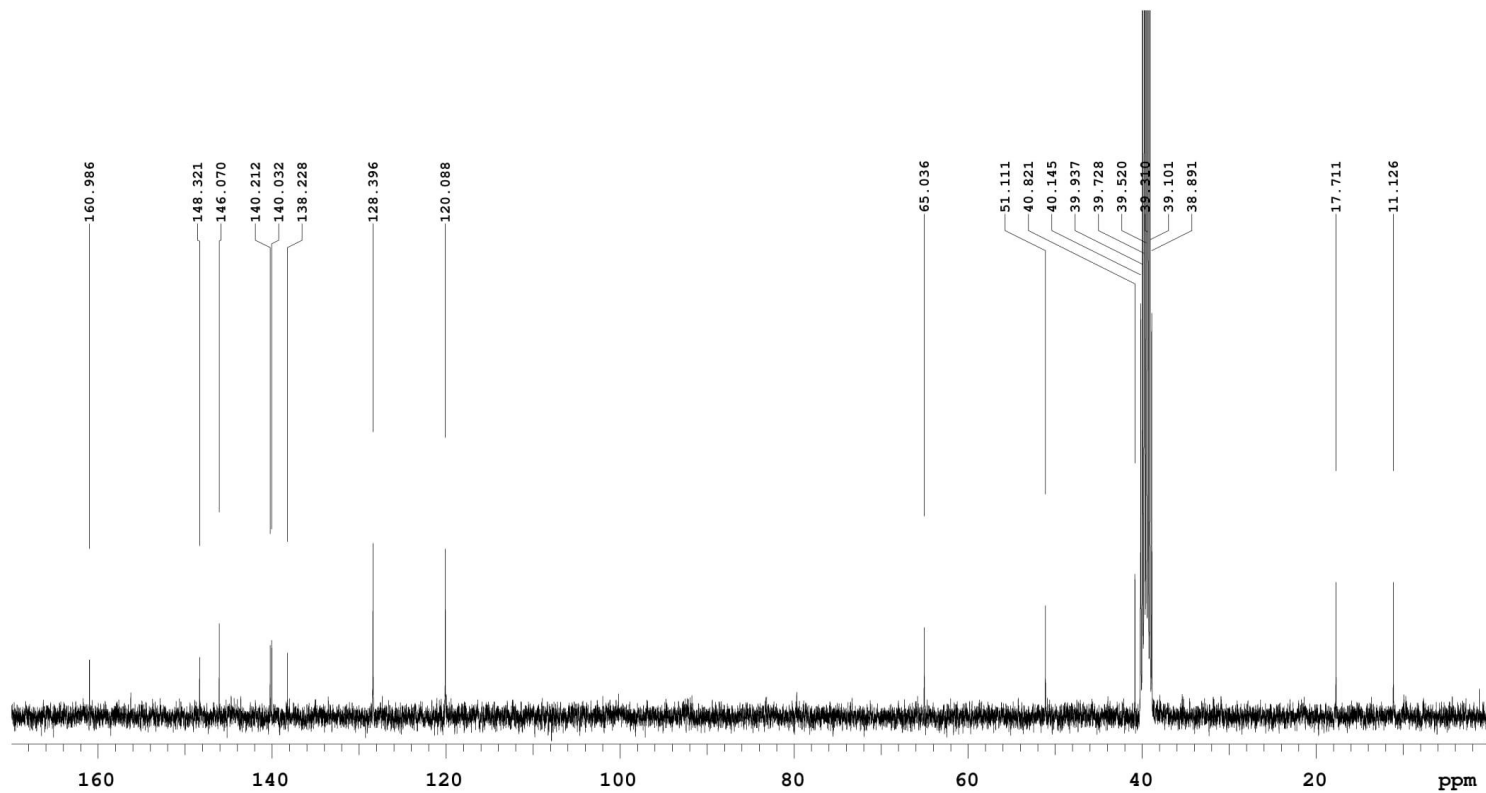
<p>PULSE SEQUENCE</p> <p>Relax. delay 0.500 sec</p> <p>Pulse 48.6 degrees</p> <p>Acq. time 4.797 sec</p> <p>Width 7225.4 Hz</p> <p>40 repetitions</p>	<p>OBSERVE H1, 399.5130588</p>	<p>DATA PROCESSING</p> <p>FT size 65536</p> <p>Total time 3 minutes</p>	<p>MMASz30</p> <p>in DMSO</p> <p>Sample Name:</p> <p>MMASz30</p> <p>Data Collected on:</p> <p>400MR-vnmrs400</p> <p>MMASz30</p>
---	--------------------------------	---	---

Figure S7: $^1\text{H-NMR}$ for derivative **2b** in DMSO with one drop of D_2O



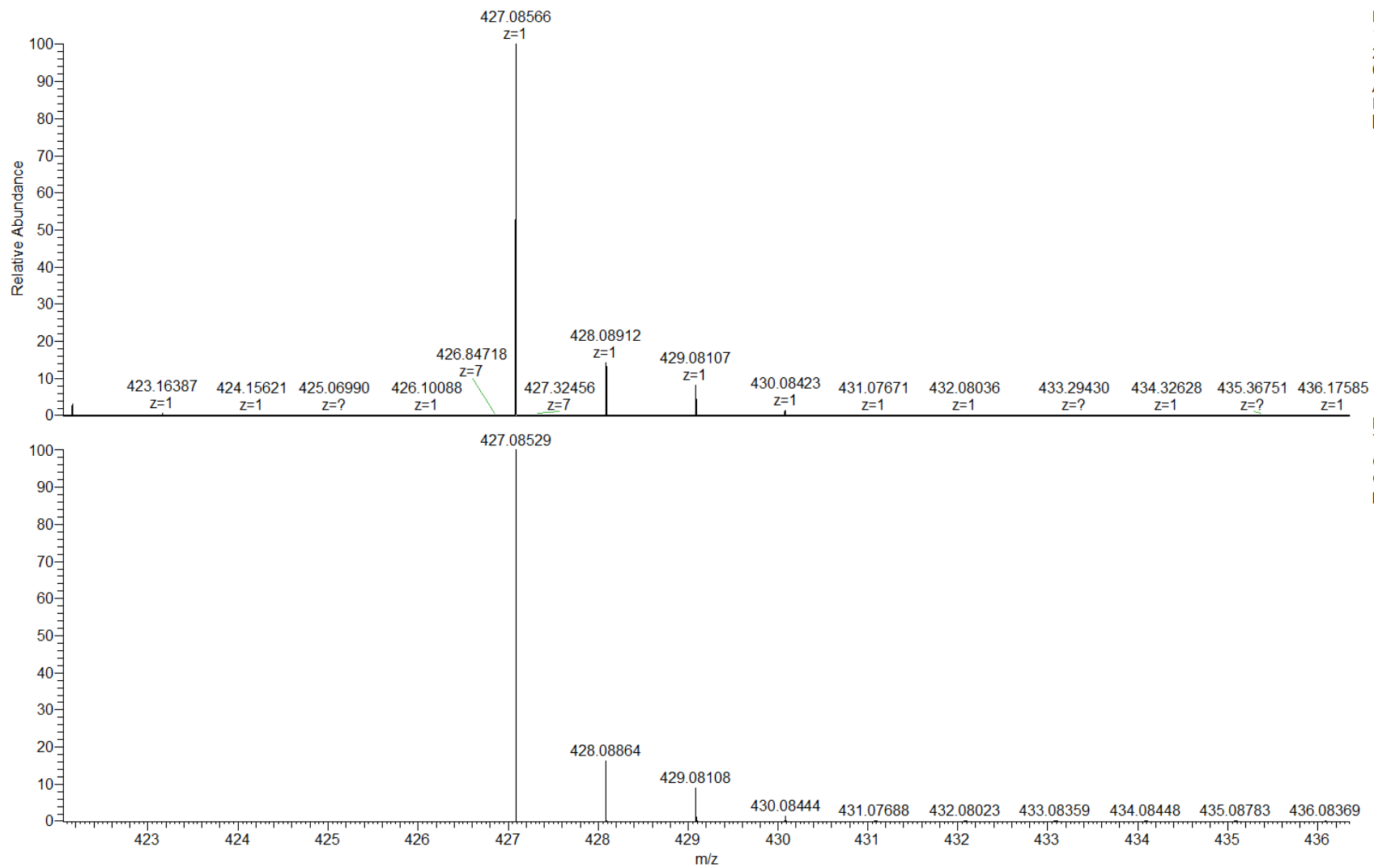
<p>PULSE SEQUENCE</p> <p>Relax. delay 0.500 sec</p> <p>Pulse 48.6 degrees</p> <p>Acq. time 4.797 sec</p> <p>Width 7225.4 Hz</p> <p>40 repetitions</p>	<p>OBSERVE H1, 399.5130595</p>	<p>DATA PROCESSING</p> <p>FT size 65536</p> <p>Total time 3 minutes</p>	<p>MMASz30_d2o</p> <p>in DMSO</p> <p>Sample Name:</p> <p>MMASz30_d2o</p> <p>Data Collected on:</p> <p>400MR-vnmrs400</p> <p>20100504132002</p>
---	--------------------------------	---	--

Figure S8: ¹³C-NMR for derivative 2b



<p>PULSE SEQUENCE</p> <p>Relax. delay 1.500 sec</p> <p>Pulse 38.5 degrees</p> <p>Acq. time 2.674 sec</p> <p>Width 24509.8 Hz</p> <p>1344 repetitions</p>	<p>OBSERVE C13, 100.4576802</p> <p>DECOUPLE H1, 399.5150667</p> <p>Power 37 dB</p> <p>continuously on</p> <p>WALTZ-16 modulated</p>	<p>DATA PROCESSING</p> <p>Line broadening 1.0 Hz</p> <p>FT size 262144</p> <p>Total time 93 minutes</p>	<p>MMASz30</p> <p>in DMSO</p> <p>Sample Name:</p> <p>MMASz30</p> <p>Data Collected on:</p> <p>400MR-vnmrs400</p> <p>1328020</p>
--	---	---	---

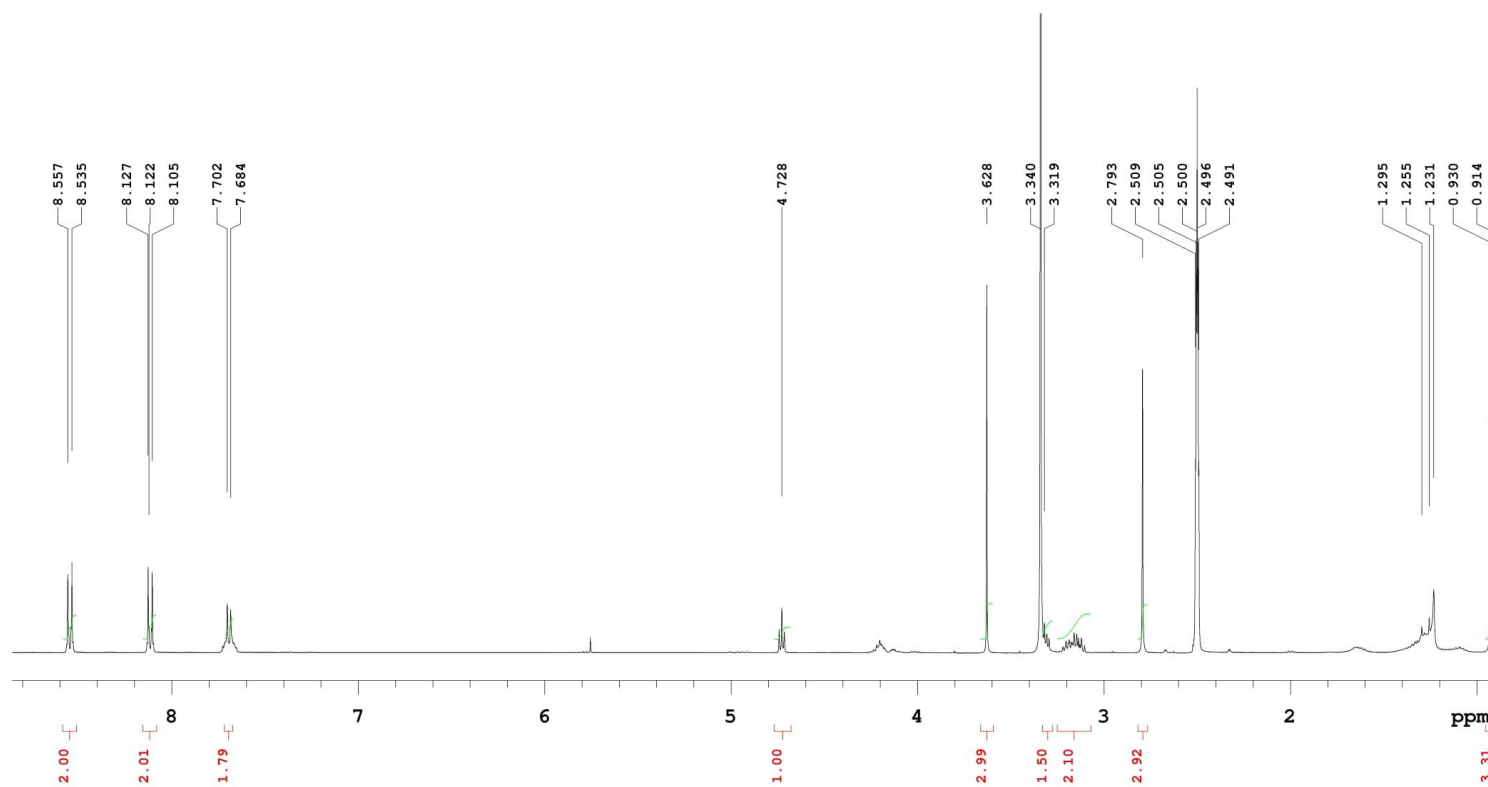
Figure S9: HRMS for 2b



NL:
1.33E8
201214_MM_ASz_R_3
0#12-49 RT: 0.11-0.47
AV: 38 T: FTMS + p ESI
Full ms
[150.0000-2000.0000]

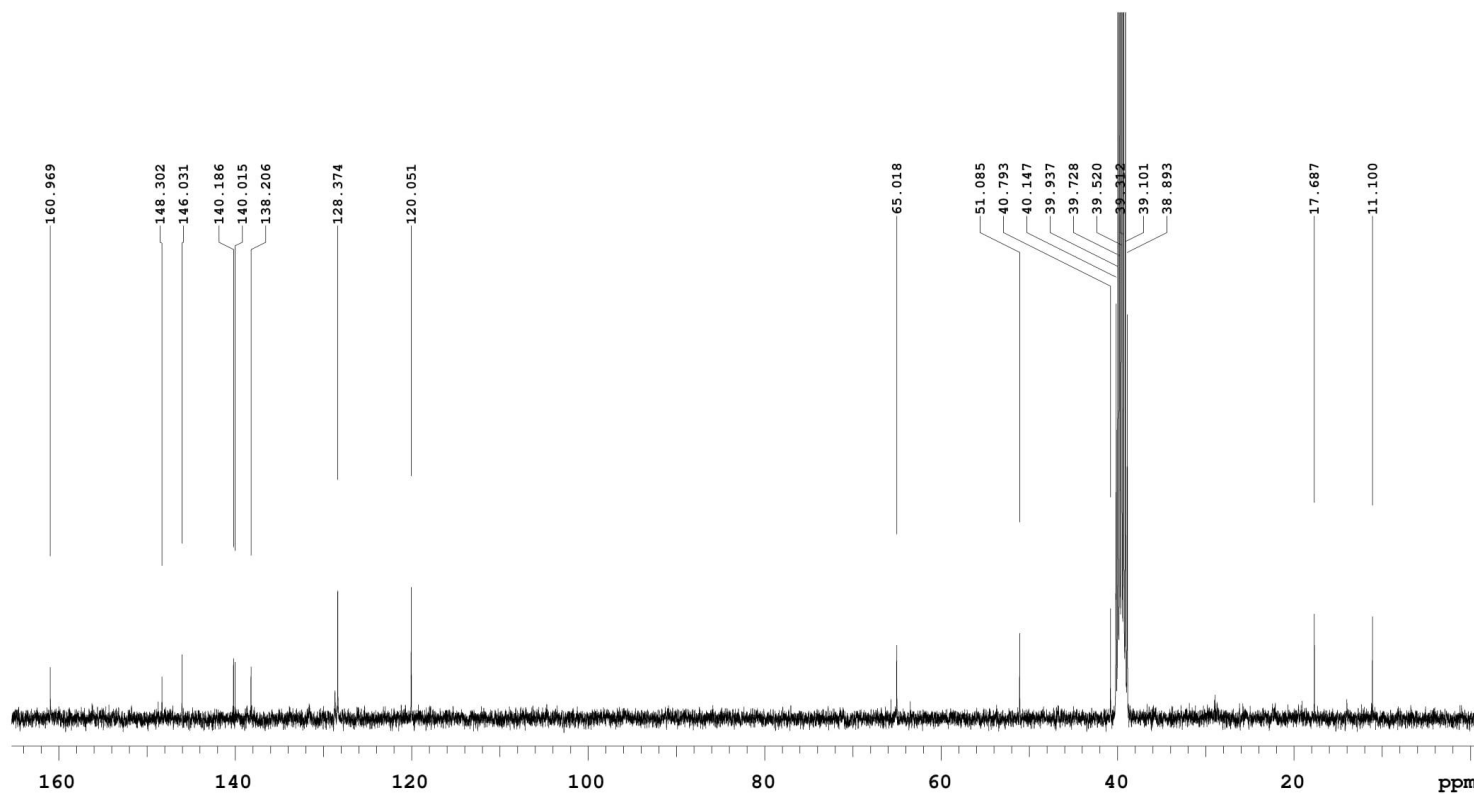
NL:
7.39E5
C15H18N6O5S2 +H
C15H19N6O5S2
pa Chrg 1

Figure S10: ¹H-NMR for derivative 2c



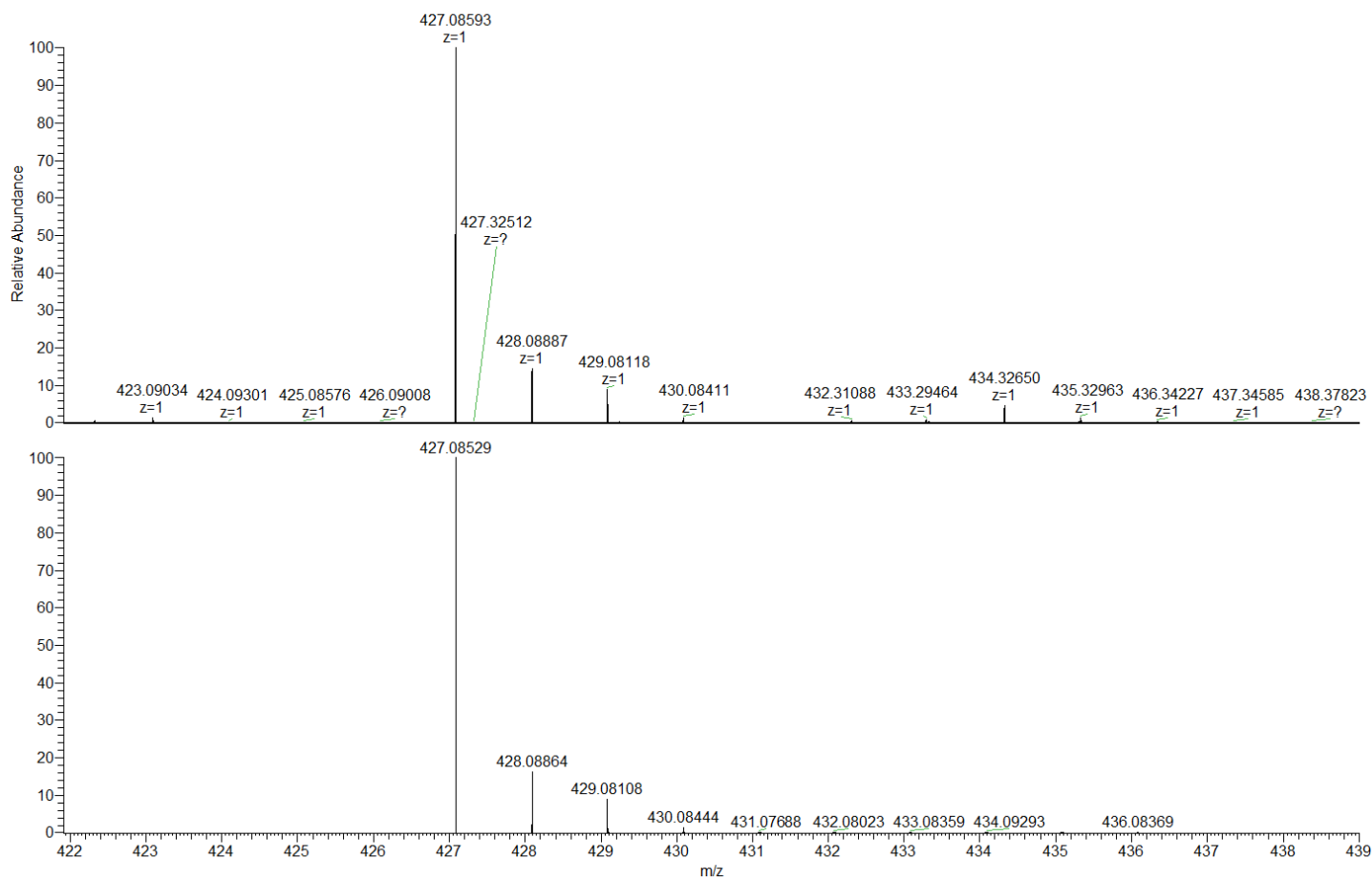
<p>PULSE SEQUENCE Relax. delay 0.500 sec Pulse 48.6 degrees Acq. time 4.797 sec Width 7225.4 Hz 40 repetitions</p>	<p>OBSERVE H1, 399.5130588</p>	<p>DATA PROCESSING FT size 65536 Total time 3 minutes</p>	<p>MMAZ29 in DMSO Sample Name: MMAZ29 Data Collected on: 400MR-vnmrs400 20231128 09:00:00 AM (428020)</p>
---	--------------------------------	---	---

Figure S11: ¹³C-NMR for derivative 2c



<p>PULSE SEQUENCE</p> <p>Relax. delay 1.500 sec</p> <p>Pulse 38.5 degrees</p> <p>Acq. time 2.674 sec</p> <p>Width 24509.8 Hz</p> <p>2416 repetitions</p>	<p>OBSERVE C13, 100.4576830</p> <p>DECOUPLE H1, 399.5150667</p> <p>Power 37 dB</p> <p>continuously on</p> <p>WALTZ-16 modulated</p>	<p>DATA PROCESSING</p> <p>Line broadening 1.0 Hz</p> <p>FT size 262144</p> <p>Total time 2.8 hours</p>	<p>MMASz29</p> <p>in DMSO</p> <p>Sample Name:</p> <p>MMASz29</p> <p>Data Collected on:</p> <p>400MR-vnmrs400</p> <p>DATE/TIME: 20180808 10:08:00 (428020)</p>
--	---	--	---

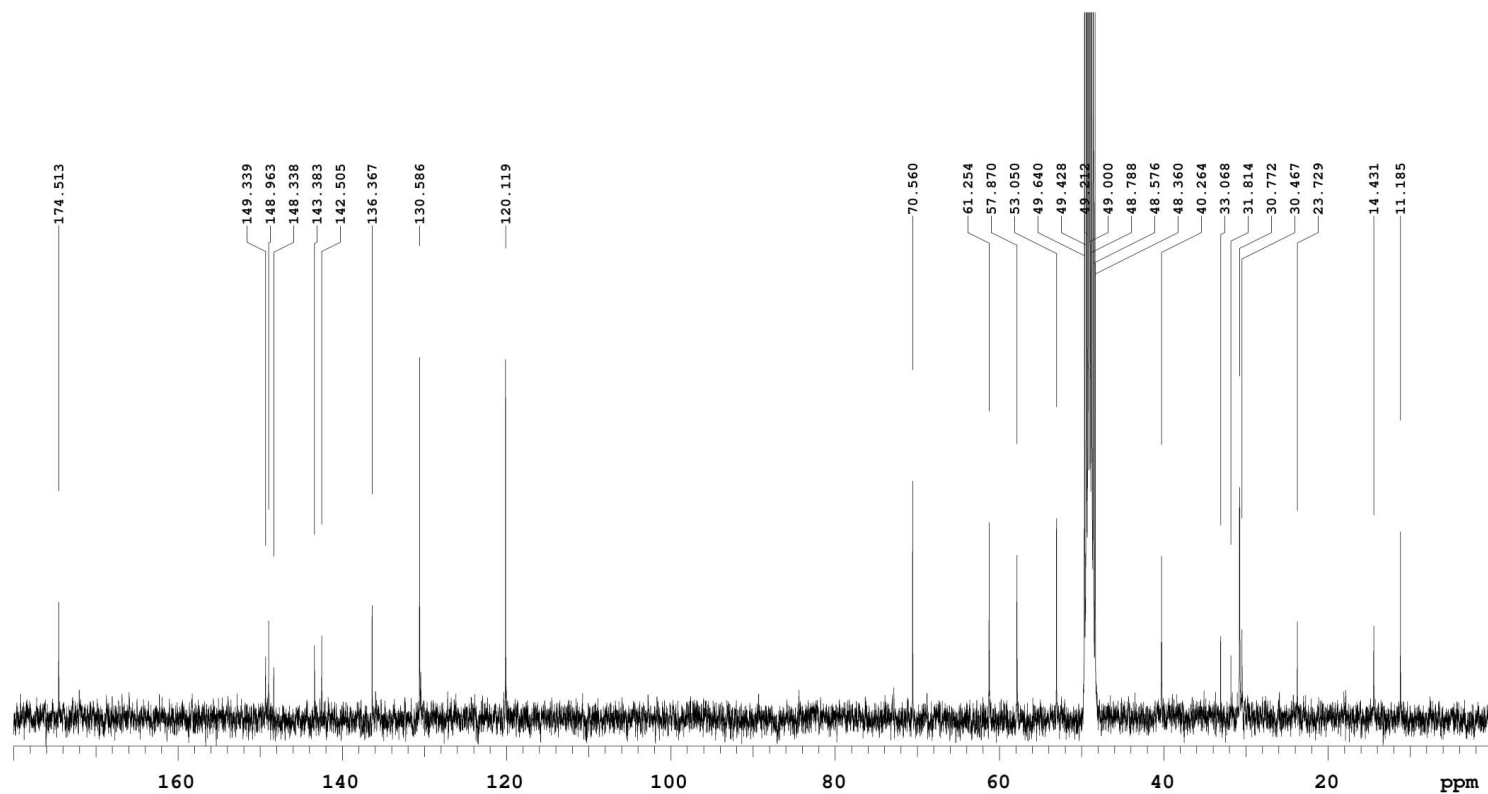
Figure S12: HRMS for 2c



NL:
1.37E8
201214_MM_ASz_R_29
#101-152 RT: 0.96-1.44
AV: 52 T: FTMS + p ESI
Full ms
[150.0000-2000.0000]

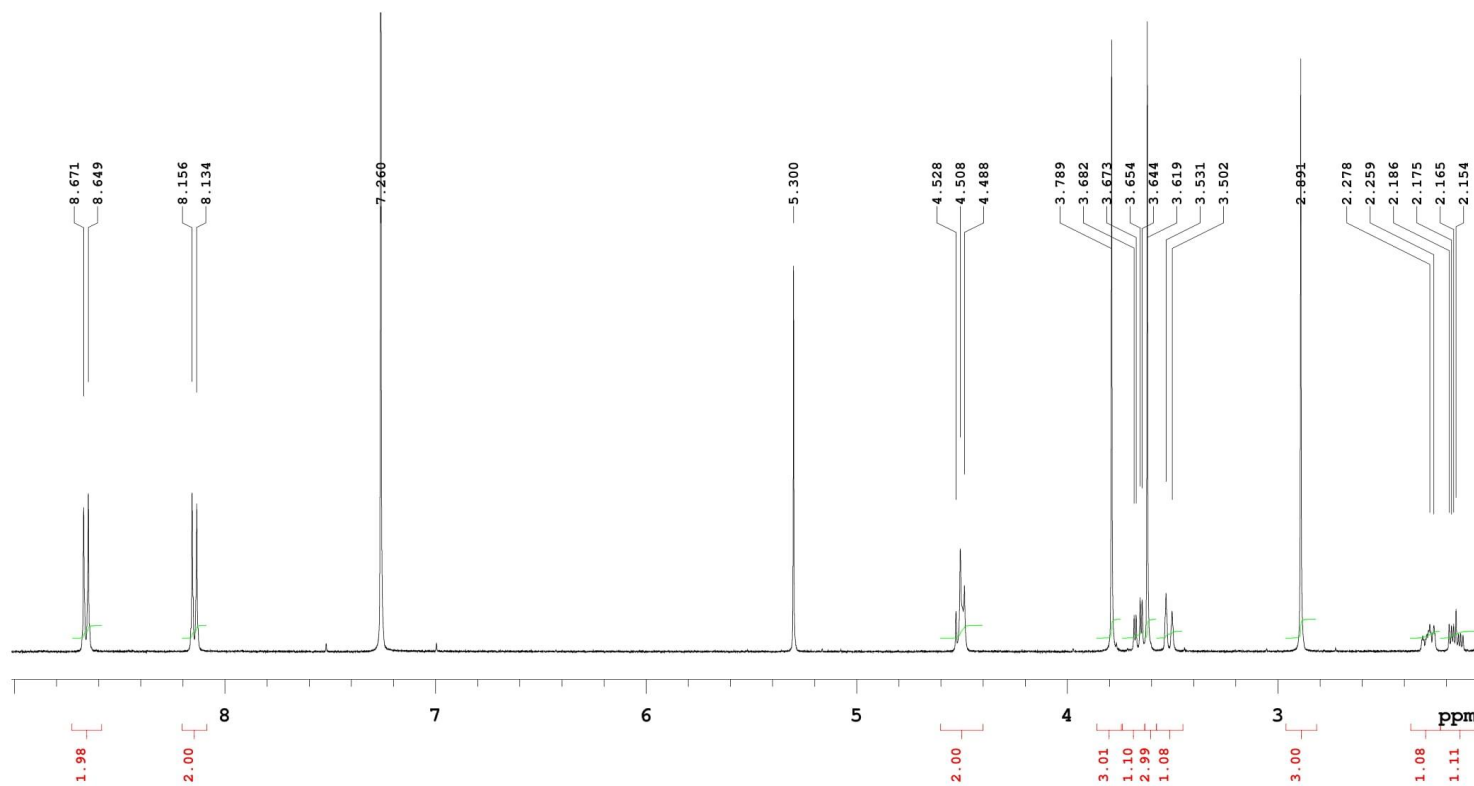
NL:
7.39E5
C₁₅H₁₈N₆O₅S₂+H:
C₁₅H₁₉N₆O₅S₂
pa Chrg 1

Figure S14: ¹³C-NMR in MeOH-d₄ for derivative MM129



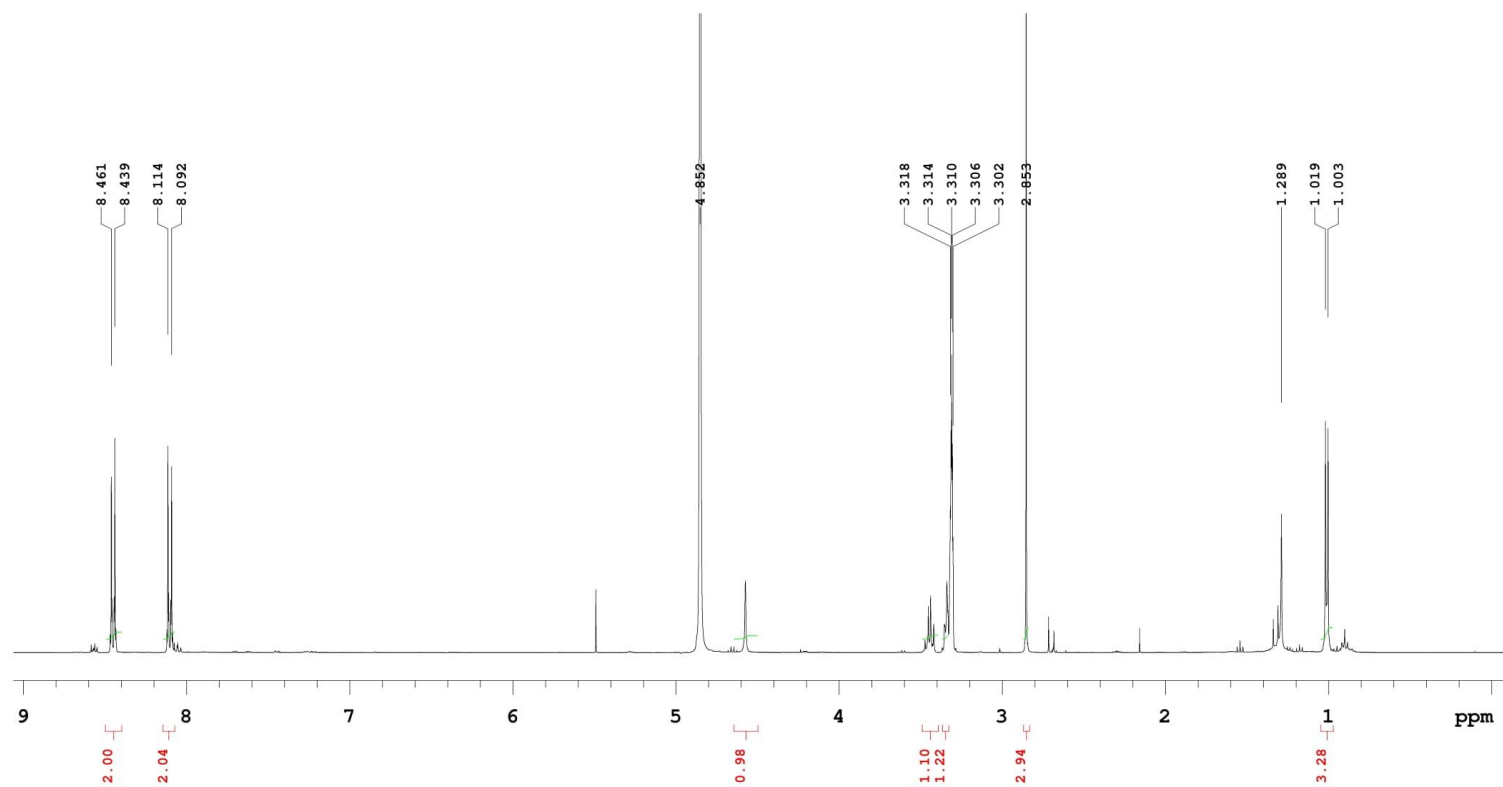
<p>PULSE SEQUENCE</p> <p>Relax. delay 1.500 sec</p> <p>Pulse 38.5 degrees</p> <p>Acq. time 2.674 sec</p> <p>Width 24509.8 Hz</p> <p>4800 repetitions</p>	<p>OBSERVE C13, 100.4720713</p> <p>DECOUPLE H1, 399.5730276</p> <p>Power 37 dB</p> <p>continuously on</p> <p>WALTZ-16 modulated</p>	<p>DATA PROCESSING</p> <p>Line broadening 1.5 Hz</p> <p>FT size 131072</p> <p>Total time 5.6 hours</p>	<p>MMPT235</p> <p>in methanol</p> <p>Sample Name:</p> <p>MMPT235</p> <p>Data Collected on:</p> <p>400MR-vnmrs400</p> <p>20230808 14:28:01</p>
--	---	--	---

Figure S15: ¹H-NMR in CDCl₃ for derivative MM129



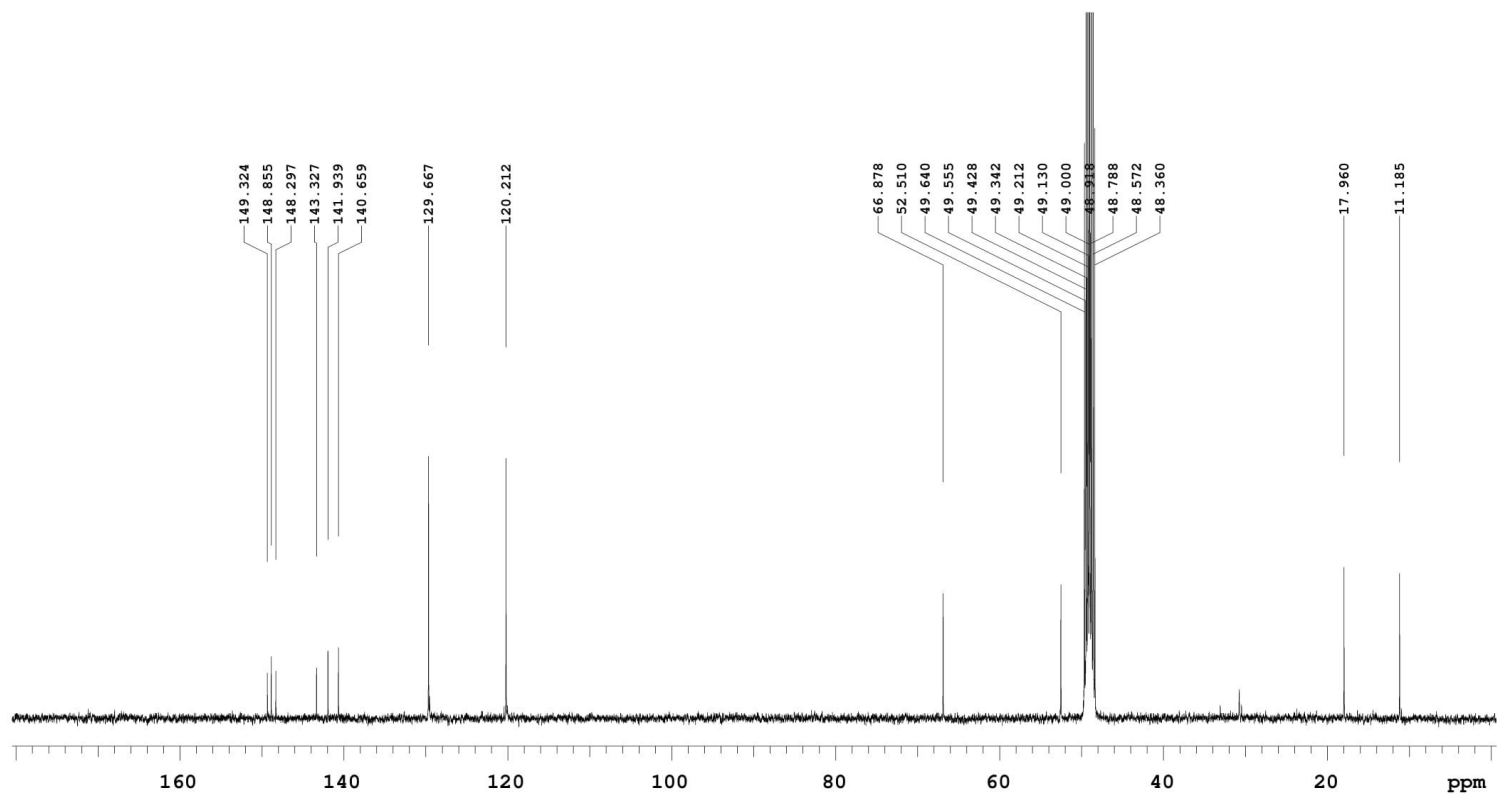
<p>PULSE SEQUENCE</p> <p>Relax. delay 0.500 sec</p> <p>Pulse 48.6 degrees</p> <p>Acq. time 4.797 sec</p> <p>Width 6793.5 Hz</p> <p>32 repetitions</p>	<p>OBSERVE H1, 399.5428928</p>	<p>DATA PROCESSING</p> <p>FT size 65536</p> <p>Total time 2 minutes</p>	<p>MMPT288</p> <p>in CDCl₃</p> <p>Sample Name:</p> <p>MMPT288</p> <p>Data Collected on:</p> <p>400MR-vnmrs400</p> <p>DATE_ TIME_ INSTRUM_ I328019</p>
---	--------------------------------	---	--

Figure S16: ¹H-NMR in MeOH-d₄ for derivative MM130



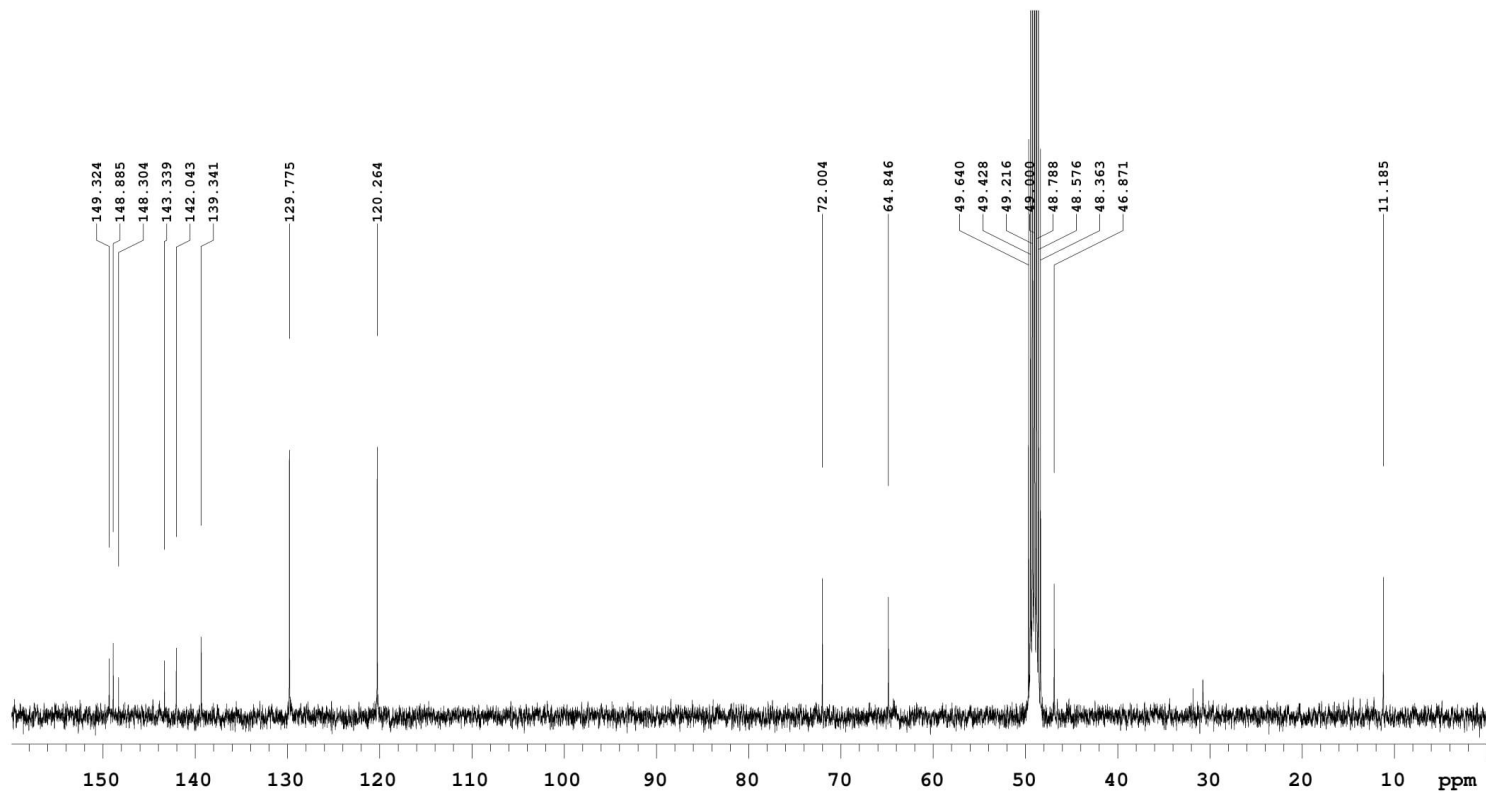
<p>PULSE SEQUENCE</p> <p>Relax. delay 0.500 sec</p> <p>Pulse 48.6 degrees</p> <p>Acq. time 4.797 sec</p> <p>Width 6793.5 Hz</p> <p>32 repetitions</p>	<p>OBSERVE H1, 399.5710239</p>	<p>DATA PROCESSING</p> <p>FT size 65536</p> <p>Total time 2 minutes</p>	<p>MMPT241</p> <p>in CD30D</p> <p>Sample Name:</p> <p>MMPT241</p> <p>Data Collected on:</p> <p>400MR-vnmrs400</p> <p>20170808 10:00:00 AM (120017)</p>
---	--------------------------------	---	--

Figure S17: ¹³C-NMR in MeOH-d₄ for derivative MM130



<p>PULSE SEQUENCE</p> <p>Relax. delay 1.500 sec</p> <p>Pulse 38.5 degrees</p> <p>Acq. time 2.674 sec</p> <p>Width 24509.8 Hz</p> <p>8000 repetitions</p>	<p>OBSERVE C13, 100.4720717</p> <p>DECOUPLE H1, 399.5730276</p> <p>Power 37 dB</p> <p>continuously on</p> <p>WALTZ-16 modulated</p>	<p>DATA PROCESSING</p> <p>Line broadening 1.5 Hz</p> <p>FT size 131072</p> <p>Total time 9.3 hours</p>	<p>MMPT241</p> <p>in methanol</p> <p>Sample Name:</p> <p>MMPT236</p> <p>Data Collected on:</p> <p>400MR-vnmrs400</p> <p>DATE: 20180808 10:00:00 (s2p017)</p>
--	---	--	--

Figure S19: ^{13}C -NMR in $\text{MeOH-}d_4$ for derivative MM131



<p>PULSE SEQUENCE</p> <p>Relax. delay 1.500 sec</p> <p>Pulse 38.5 degrees</p> <p>Acq. time 2.674 sec</p> <p>Width 24509.8 Hz</p> <p>1328 repetitions</p>	<p>OBSERVE C13, 100.4720717</p> <p>DECOUPLE H1, 399.5730276</p> <p>Power 37 dB</p> <p>continuously on</p> <p>WALTZ-16 modulated</p>	<p>DATA PROCESSING</p> <p>Line broadening 1.5 Hz</p> <p>FT size 131072</p> <p>Total time 92 minutes</p>	<p>MMPT233</p> <p>in methanol</p> <p>Sample Name:</p> <p>MMPT233</p> <p>Data Collected on:</p> <p>400MR-vnmrs400</p> <p>20180808 1428017</p>
--	---	---	--



Article

Pyrazolo[4,3-*e*]tetrazolo[1,5-*b*][1,2,4]triazine Sulfonamides as Novel Potential Anticancer Agents: Apoptosis, Oxidative Stress, and Cell Cycle Analysis

Karol Bukowski ¹, Beata Marciniak ¹, Mateusz Kciuk ^{1,2}, Somdutt Mujwar ³, Mariusz Mojzych ⁴
and Renata Kontek ^{1,*}

¹ Department of Molecular Biotechnology and Genetics, University of Lodz, 90-237 Lodz, Poland; karol.bukowski@edu.uni.lodz.pl (K.B.); beata.marciniak@biol.uni.lodz.pl (B.M.); mateusz.kciuk@edu.uni.lodz.pl (M.K.)

² Doctoral School of Exact and Natural Sciences, University of Lodz, 90-237 Lodz, Poland

³ Chitkara College of Pharmacy, Chitkara University, Rajpura 140401, Punjab, India; somduttmujwar@gmail.com

⁴ Department of Chemistry, Siedlce University of Natural Sciences and Humanities, 08-110 Siedlce, Poland; mariusz.mojzych@uph.edu.pl

* Correspondence: renata.kontek@biol.uni.lodz.pl

Abstract: The current study continues the evaluation of the anticancer potential of three de novo synthesized pyrazolo[4,3-*e*]tetrazolo[1,5-*b*][1,2,4]triazine sulfonamides—**MM129**, **MM130**, and **MM131**—against human cancer cells of HeLa, HCT 116, PC-3, and BxPC-3 lines. The pro-apoptotic activity of the investigated sulfonamides was shown by observations of changes in the mitochondrial transmembrane potential of the tested cells, externalization of phosphatidylserine on the cellular membrane surface, and cell morphology in microscopic imaging. The computational studies have shown that **MM129** exhibited the lowest binding energy values when docked against CDK enzymes. In addition, the highest stability was shown for complexes formed between **MM129** and CDK5/8 enzymes. All examined compounds induced cell cycle arrest in the G₀/G₁ phase in the BxPC-3 and PC-3 cells and simultaneously caused the accumulation of cells in the S phase in the HCT 116 cells. In addition, the increase in the subG₁ fraction was observed in PC-3 and HeLa cells. The application of a fluorescent H₂DCFDA probe revealed the high pro-oxidative properties of the tested triazine derivatives, especially **MM131**. In conclusion, the obtained results suggest that **MM129**, **MM130**, and **MM131** exhibited strong pro-apoptotic properties towards investigated cells, mainly against the HeLa and HCT 116 cell lines, and high pro-oxidative potential as well. Moreover, it is suggested that the anticancer activity of the tested compounds may be associated with their ability to inhibit CDK enzymes activities.

Keywords: pyrazolo[4,3-*e*]tetrazolo[1,5-*b*][1,2,4]triazine; sulfonamides; MM compounds; anticancer agents; cancer cells; cell cycle; apoptosis; oxidative stress; ROS; CDKs



Citation: Bukowski, K.; Marciniak, B.; Kciuk, M.; Mujwar, S.; Mojzych, M.; Kontek, R. Pyrazolo[4,3-*e*]tetrazolo[1,5-*b*][1,2,4]triazine Sulfonamides as Novel Potential Anticancer Agents: Apoptosis, Oxidative Stress, and Cell Cycle Analysis. *Int. J. Mol. Sci.* **2023**, *24*, 8504. <https://doi.org/10.3390/ijms24108504>

Academic Editors: Andrea Spallarossa and Chiara Brullo

Received: 7 April 2023

Revised: 3 May 2023

Accepted: 8 May 2023

Published: 9 May 2023



Copyright: © 2023 by the authors. Licensee MDPI, Basel, Switzerland. This article is an open access article distributed under the terms and conditions of the Creative Commons Attribution (CC BY) license (<https://creativecommons.org/licenses/by/4.0/>).

1. Introduction

Nowadays, cancer is among the leading causes of death worldwide. Therefore, searching for new effective strategies for cancer treatment is among the most challenging tasks in medicine [1–4]. The evaluation of the pro-apoptotic properties of novel potential antineoplastic agents, as well as their impact on cell cycle phase distribution, seems to be crucial in modern drug design. Apoptosis is a highly regulated process that plays a fundamental role in eliminating unwanted or unnecessary cells. Apoptosis dysregulation is connected with autoimmune disorders, neurological diseases, and many types of cancer. Because apoptosis evasion is a hallmark of all types of cancer, inducing apoptosis in cells to limit their uncontrolled proliferation appears to be a feasible and highly successful strategy to combat many types of cancer [5,6].

Apoptosis is linked to morphological changes in cells. The progressive process involves changes in the orientation of membrane phospholipids, which culminates in the externalization of phosphatidylserine (PS) onto the surface of cellular membranes [7–9]. Another characteristic feature of apoptotic cells is the increased permeability of the mitochondrial membrane and the simultaneous decrease in mitochondrial transmembrane potential ($\Delta\Psi_m$). At the end of the apoptosis process, cell shrinkage and nuclear chromatin condensation and fragmentation are observed [10–12].

Reactive oxygen species (ROS) play an important role in the pathophysiology of cancer. The excessive intracellular levels of ROS stimulate the growth factor-dependent pathways, increase oncogene activity, and oxidize enzymes, inducing genetic instability [13,14]. Additionally, high levels of ROS can generate DNA, protein, and lipid damage. The induction of excessive ROS in cells is the primary mechanism of the cytotoxic activity of many commonly used anticancer agents, including bleomycin or doxorubicin [15]. Therefore, the pro-oxidative activity of various antineoplastic agents may affect their genotoxicity, enhance their pro-apoptotic properties, and indirectly modulate the cell cycle progression [16].

The role of cell cycle checkpoints is to protect the DNA from the accumulation and propagation of genetic errors during cell division. A checkpoint can pause the cell cycle or induce programmed cell death (PCD) when there is a threat to genetic integrity, such as irreversible DNA damage [17]. Those checkpoints are primarily regulated by cyclin-dependent kinase inhibitors (CKIs), cyclin-dependent kinases (CDKs), and cyclins [18]. In response to environmental stressors that prevent the cell from dividing or when the G0 phase lasts too long, the G1/S checkpoint causes cell cycle arrest, allowing the cell to repair damaged DNA. In contrast, the activation of the G2/M restriction point is regulated by the TP53 and occurs in response to DNA damage leading to the elimination of any damaged and inaccurately duplicated cells. The last restriction point is the spindle checkpoint that occurs in the M phase and delays cell division to guarantee precise chromosome segregation [19,20]. Therefore, targeting cell cycle checkpoints seems to be a promising strategy for cancer treatment [21].

CDKs are involved in the control of transcription, cell growth, proliferation, and in the regulation of the cell cycle. Furthermore, they play a crucial role in the pathogenesis of cancers [22,23]. CDK1 interacts with cyclin B1, allowing the progression of the cell cycle through the G2 phase, while CDK2 is responsible for G1/S and S/G2 transition [23–28]. Moreover, CDK2 is involved in controlling proliferation, cell differentiation, adaptive immune response, and apoptosis. It also, together with CDK3, mediates either senescence or quiescence [22,29–32]. Overexpression of CDK1 and cyclin B, as well as CDK2 binding partner cyclins E and A, is frequently observed in many types of cancer, including lung, breast, prostate, and colorectal carcinomas [33–40]. The inhibition of the cyclin D-CDK4/6 dimer leads to cell cycle arrest in the G1 phase [23,41]. Interestingly, colorectal cancer pathogenesis is often associated with the amplification of genes encoding CDK4/6, CDK5, CDK8, or CDK9 or their increased activity [42–50]. CDK7 participates in the DNA repair process, allows S phase entry by phosphorylation of CDK2/cyclin E complex, and helps to activate CDK1/cyclin B complex, allowing cell cycle progression from the G2 to M phase [51]. Numerous studies have revealed that CDK8 is involved in the regulation of transcription and frequently participates in the development of cancer. Furthermore, it regulates the cancer cell stress response to chemotherapy and radiotherapy and promotes tumor cell invasion, metastasis, and drug resistance [52–56]. Additionally, CDK8 plays an essential role during TP53-dependent p21 transcriptional activation, required for cell cycle arrest as the response to DNA damage [57,58]. Silencing CDK genes in various types of cancer downregulates their proliferation and leads to cell death. Therefore, CDKs are an attractive target for the relatively new class of antineoplastic agents called CDK inhibitors [22,23].

Currently, several novel pyrazolo[4,3-*e*]tetrazolo[4,5-*b*][1,2,4]triazine derivatives are at different stages of the *in vitro* and *in vivo* investigations. In this paper, we present the anticancer properties of **MM129**, **MM130**, and **MM131** belonging to this group of structurally related compounds (Figure 1). Recent studies have shown that **MM129** may inhibit

CDK2, AKT serine/threonine-protein kinase, PD-1/PD-L1, Bruton's tyrosine kinase (BTK), phosphoinositide-3-kinase (PI3K) and mammalian target of rapamycin (mTOR) [59,60]. Furthermore, some studies suggest that the **MM129** may be a potentially safe and well-tolerated chemotherapeutic agent in colon cancer treatment [61]. Interestingly, **MM129** is characterized by a similar chemical structure compared to seliciclib (roscovitine). This antineoplastic agent is the first selective oral CDK inhibitor that entered clinical trials [62].

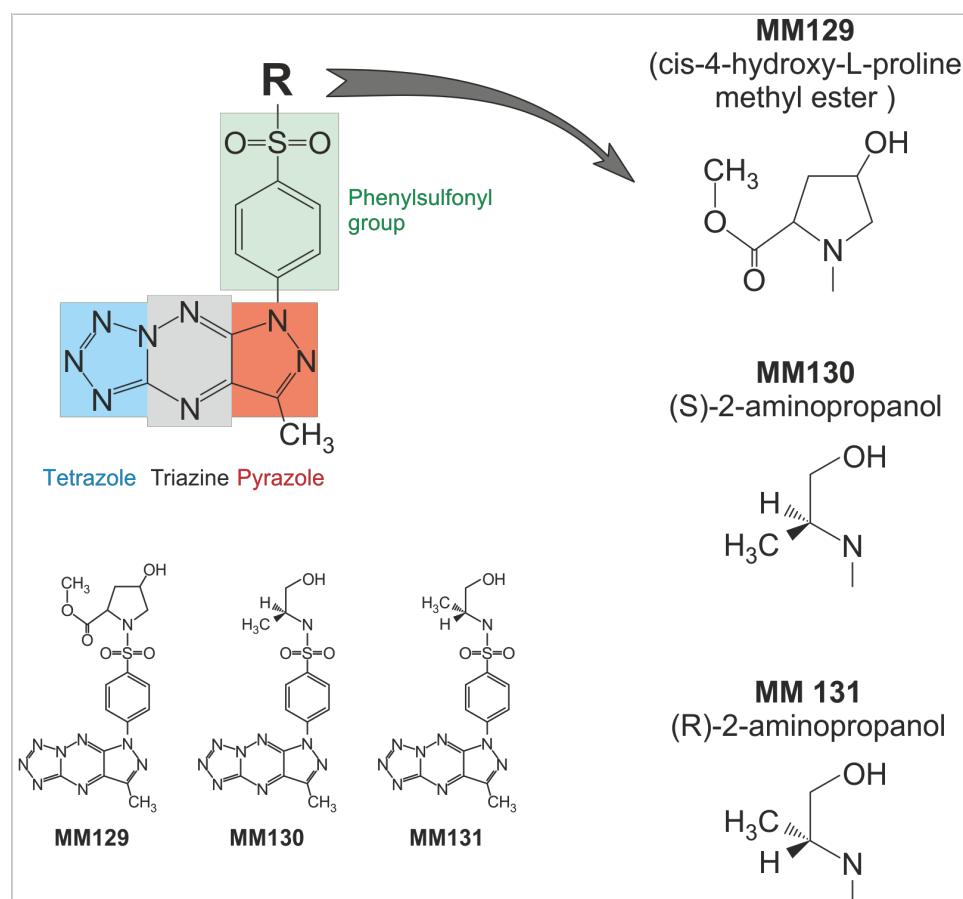


Figure 1. Chemical structure of the three investigated sulfonamides—**MM129**, **MM130**, and **MM131**.

Our previous paper described the synthesis of **MM129**, **MM130**, and **MM131** compounds. Furthermore, the high cyto- and genotoxic properties of the investigated triazine derivatives against the HeLa, HCT 116, PC-3, and BxPC-3 cancer cell lines have been demonstrated. Importantly, the investigated compounds were noticeably less cytotoxic toward normal cells—human foreskin fibroblast (Hs27) and human peripheral blood mononuclear cells (PBMCs). The IC_{50} values obtained in the MTT assay were shown in the Supplementary Material (Table S1) [63]. Therefore, we decided to investigate the pro-oxidative and pro-apoptotic properties of three novel derivatives of pyrazolo-triazine sulfonamides **MM129**, **MM130**, **MM131** against four adherent human cancer cell lines—HeLa, HCT 116, PC-3, and BxPC-3. The assessment of the effect of these compounds on the cell cycle phase distribution was also evaluated. Moreover, we conducted computational studies (molecular docking and molecular dynamics techniques) to confirm our results from the cell cycle analysis with the potential ability of examined sulfonamides to inhibit CDKs.

2. Results

2.1. Flow Cytometry Assessment of Annexin V Binding

Figure 2 shows the apoptosis induction in cancer cells following their 24 h, 48 h, and 72 h incubation with **MM129**, **MM130**, and **MM131** compounds. Studied pyrazole-triazine

derivatives induced time and concentration-dependent increase in the fraction of apoptotic cells. Among the examined cell lines, HeLa cells showed the highest sensitivity for the pro-apoptotic activity of MM compounds, even after the 24 h incubation, where the apoptosis induction for the IC_{50} and $2 \times IC_{50}$ compounds was significantly higher compared to the untreated cells (6.73% for the control group vs. 15.5–73.47% for experimental samples). Moreover, an increase in the percentage of apoptotic HCT 116 cells after their 24 h exposure to sulfonamides at the IC_{50} and $2 \times IC_{50}$ was noticed (6.92% for the untreated samples vs. 14.33–20.67% for experimental groups).

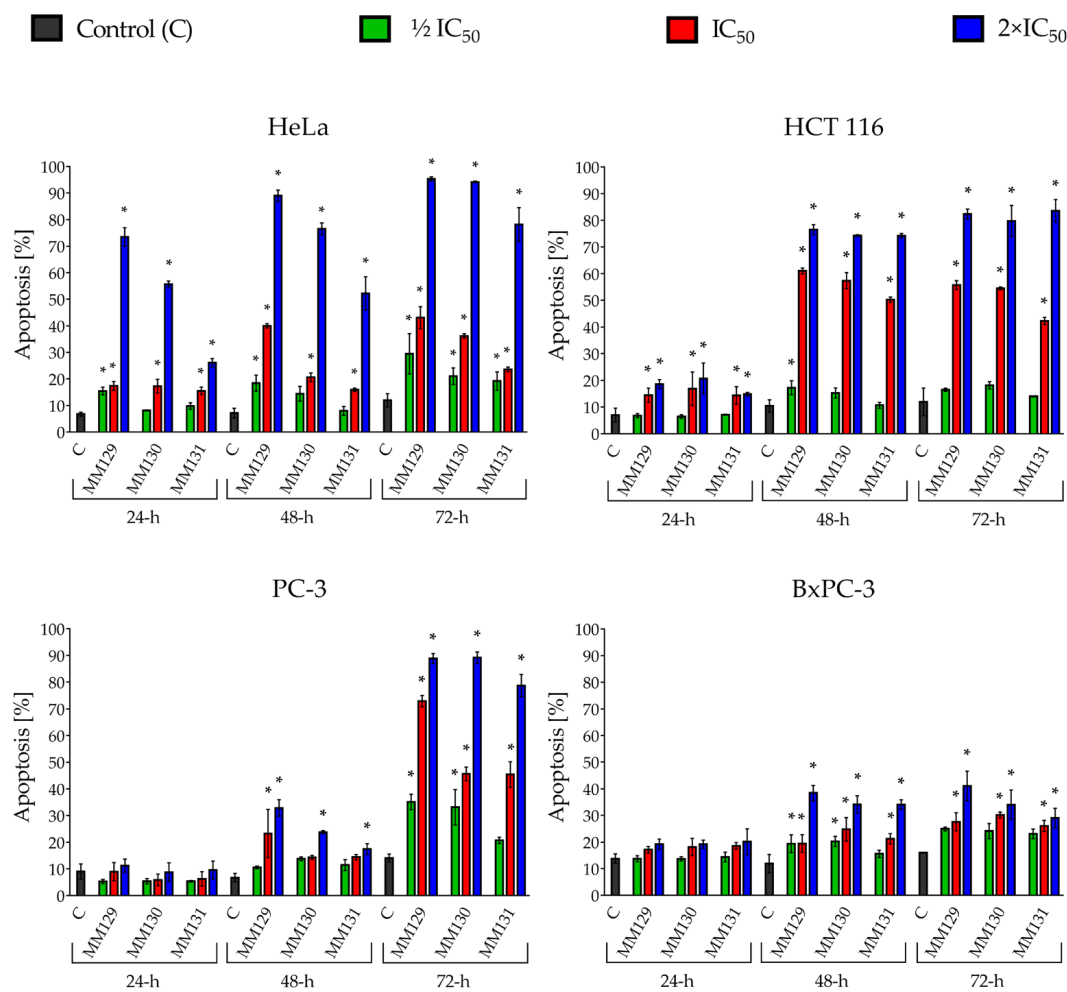


Figure 2. Percentage of apoptotic cells in the examined human cancer cell lines (HeLa, HCT 116, PC-3, and BxPC-3) following 24 h, 48 h, and 72 h treatment with **MM129**, **MM130**, and **MM131** used at $1/2 IC_{50}$, IC_{50} , and $2 \times IC_{50}$ and determined using FITC Annexin V Apoptosis Detection Kit I. Data are shown as the mean \pm SD. * $p < 0.05$ indicates a statistically significant difference compared to the negative control. $N = 1 \times 10^4$.

All triazine derivatives investigated at $2 \times IC_{50}$ induced apoptosis of cancer cells after the 48 h incubation (HeLa = 52.23–88.97%; HCT 116 = 74.23–76.47%; BxPC-3 = 34.05–38.4%; PC-3 = 17.43–32.83%). The most profound proapoptotic effect was noticed after the 72 h treatment of cells with sulfonamides. MM compounds at the IC_{50} and $2 \times IC_{50}$ induced significant pro-apoptotic activity in all tested cancer cell types (23.6–95.3% of apoptotic cells following treatment).

Among the investigated compounds, **MM129** exhibited the highest pro-apoptotic activity. **MM129** at $1/2 IC_{50}$ was the only one that induced apoptosis in HeLa cells following the 24 h of incubation. In addition, it was also the most effective toward PC-3 cells, where

significant changes in the apoptotic cell fraction after the 48 h of exposure were observed even at the IC_{50} .

The representative flow cytometry dot-plots for all cancer cell lines were demonstrated in Supplementary Materials (Figures S1–S12). The fraction of necrotic cells in all experimental series has not exceeded 15%, even after 72 h exposure of cells to the tested compounds in their highest concentrations ($2 \times IC_{50}$).

2.2. Dual Acridine Orange/Ethidium Bromide (AO/EB) Fluorescent Staining

Figure 3 represents apoptosis induction in cancer cells (HeLa, HCT 116, PC-3, and BxPC-3 cell lines) following their 48 h of exposure to MM compounds estimated by AO/EB double staining. The obtained results showed that the percentage of apoptotic cells increased in a concentration-dependent manner in all examined cancer cell types. Significant differences ($p < 0.05$) compared with vehicle control were observed for all examined compounds at $2 \times IC_{50}$ in all cancer cells. Moreover, all the investigated triazine derivatives induced apoptosis at the IC_{50} in HeLa, HCT 116, and BxPC-3 cells. MM129 at $2 \times IC_{50}$ presented the strongest pro-apoptotic effect compared to other MM compounds in the HeLa cell line ($73.7 \pm 5.86\%$ for MM129 vs. $38.67 \pm 4.73\%$ and $32.67 \pm 6.43\%$ for MM130 and MM131, respectively).

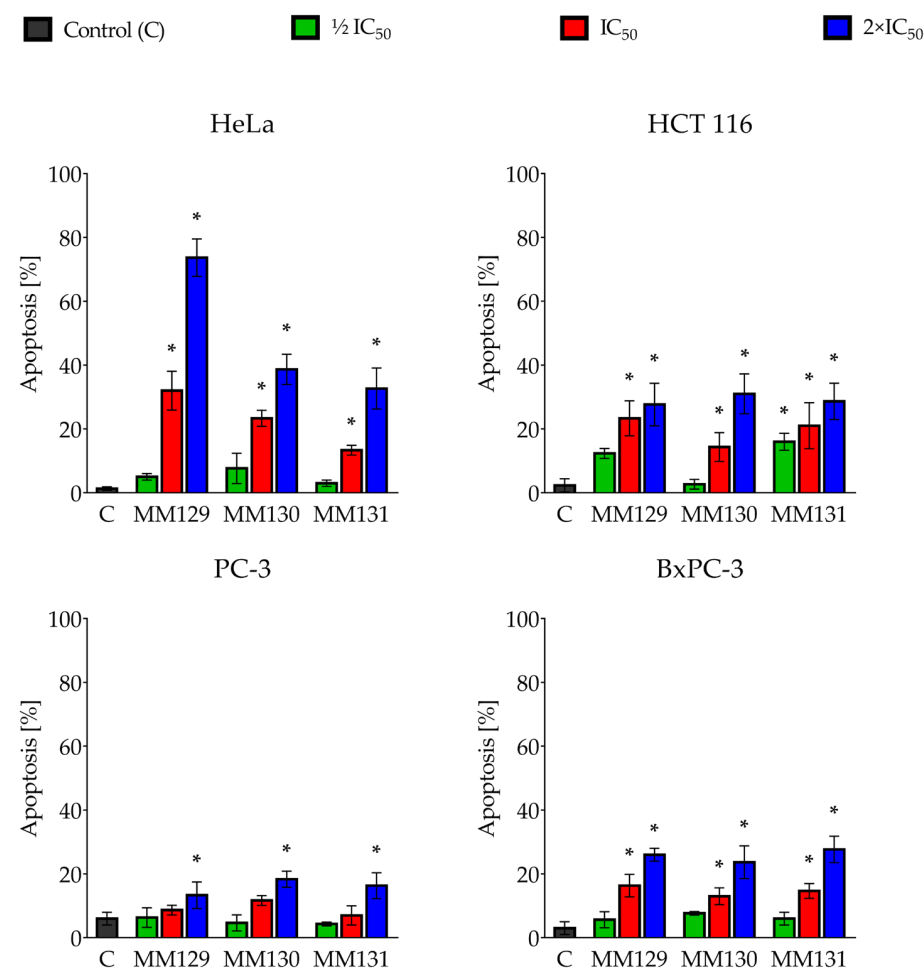


Figure 3. Apoptosis induction in human cancer lines (Hela, HCT 116, PC-3, and BxPC-3) treated for 48 h with MM129, MM130, and MM131 at $\frac{1}{2} IC_{50}$, IC_{50} , and $2 \times IC_{50}$ (obtained in the MTT assay). The results were based on AO/EB double staining, which allowed the distinguishing of viable, apoptotic, and necrotic cells. Data are shown as the mean percentage of apoptotic cells \pm SD values. Significant differences ($p < 0.05$) compared to the negative control (*). $N = 200$.

The results obtained in OA/EB staining confirmed the presence of morphological changes characteristic of apoptotic cells, such as shrinking and condensation of chromatin after exposure to the tested sulfonamides. Figure 4 shows the exemplary images from this experiment.

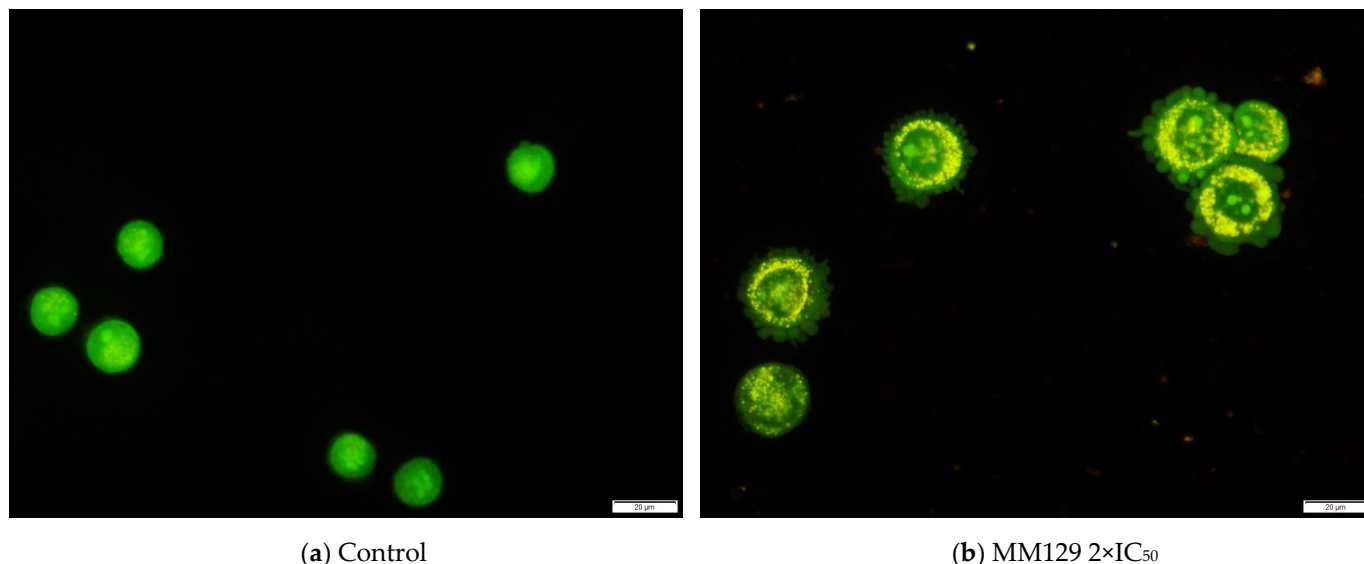


Figure 4. Representative images of HeLa cells obtained after AO/EB double staining following their 48 h incubation with **MM129** at $2\times IC_{50}$. (a) Negative control group (control cells)—rounded cells with a uniformly distributed green-fluorescent nucleus; (b) experimental group (apoptotic cells)—yellow-orange fluorescence and characteristic cells' membrane blebbing (apoptotic bodies formation). The scale bar is 20 μm . Magnification 40 \times .

2.3. Mitochondrial Membrane Potential ($\Delta\Psi_m$)

Figure 5 presents changes in the $\Delta\Psi_m$ induced by **MM129**, **MM130**, and **MM131** following 24 h and 48 h incubation time. Exposure to the investigated sulfonamides resulted in concentration-dependent depolarization of the inner mitochondrial membrane in cells from all tested cancer lines.

After 48 h of exposure to the studied sulfonamides at their highest applied concentration ($2\times IC_{50}$), significant alterations in $\Delta\Psi_m$ were observed in all tested types of cancer cells. Following the 24 h of incubation time, a significant disturbance of $\Delta\Psi_m$ was noticed only in HeLa and HCT 116 cells. The most profound decrease in the $\Delta\Psi_m$ was observed in the HeLa cell line after 48 h exposure to **MM129** ($67.53 \pm 7.94\%$ of control value).

2.4. Determination of Intracellular ROS Level Using H_2DCFDA

Figure 6 presents the changes in ROS level observed after 2 h exposure of the tested cells to MM compounds. Examined sulfonamides induced concentration-dependent increase in ROS level in all tested cancer cell types. All studied compounds caused significant changes in HCT 116 and BxPC-3 cancer cells when compared to the negative control, even at the lowest concentrations applied. The same results were obtained for HeLa and PC-3 cells except for **MM129**, which significantly increased intracellular ROS level only in its higher concentrations (IC_{50} and $2\times IC_{50}$ for the HeLa cell line and $2\times IC_{50}$ for the PC-3 cell line). The administration of **MM131** resulted in the most significant elevation of reactive oxygen species (ROS) levels across all the tested cancer cell lines, with an observed increase ranging from 206.3% to 316.3% compared to control conditions.

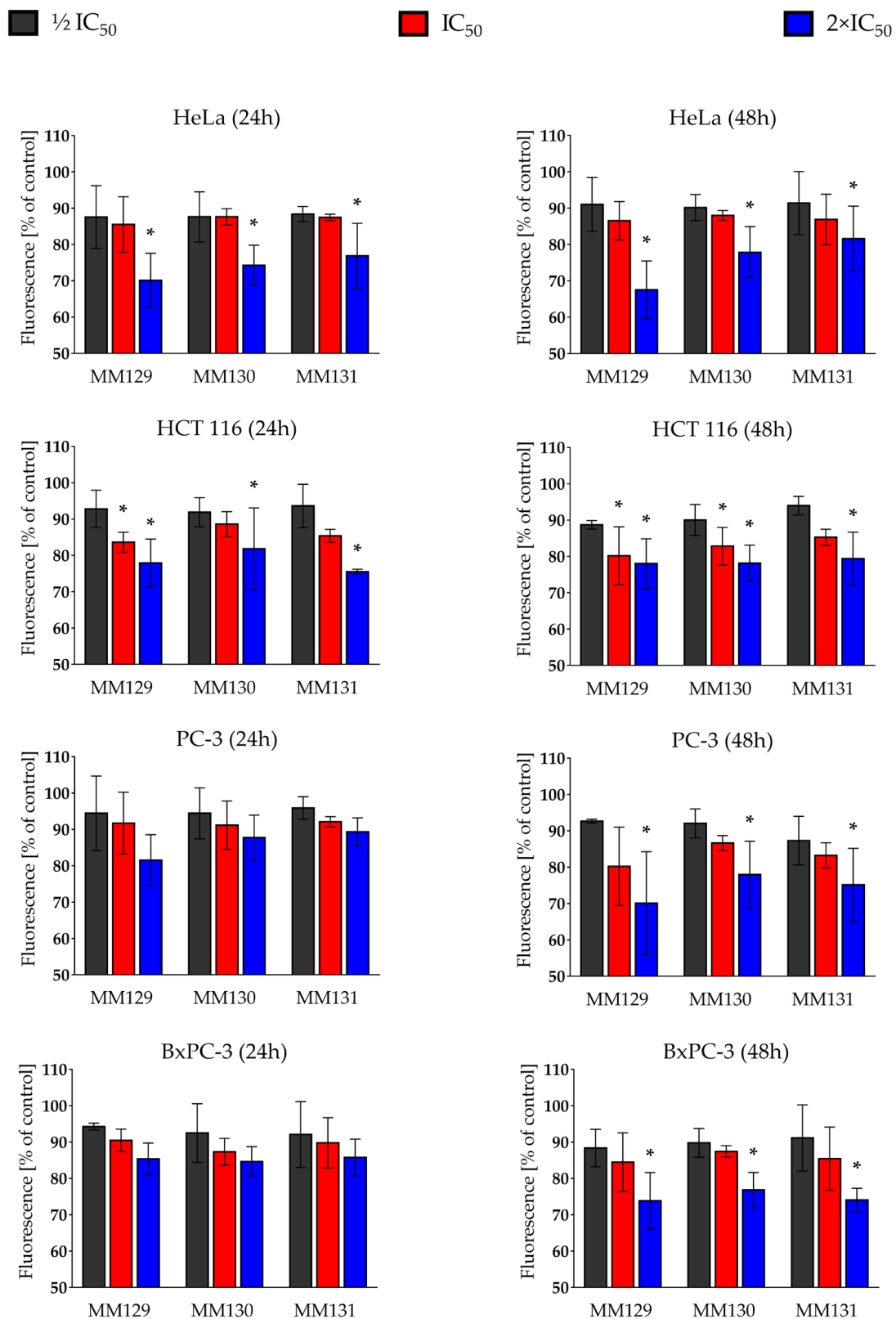


Figure 5. Changes in mitochondrial membrane potential ($\Delta\Psi_m$) in human cancer lines (Hela, HCT 116, PC-3, and BxPC-3) after 24 h and 48 h exposure to **MM129**, **MM130**, and **MM131** at $\frac{1}{2} IC_{50}$, IC_{50} , and $2 \times IC_{50}$ (obtained in the MTT assay) using MitoTracker Red CMXRos. Data are presented as the mean \pm SD relative to the control group normalized to 100%. * $p < 0.05$ indicates a statistically significant difference compared to the negative control.

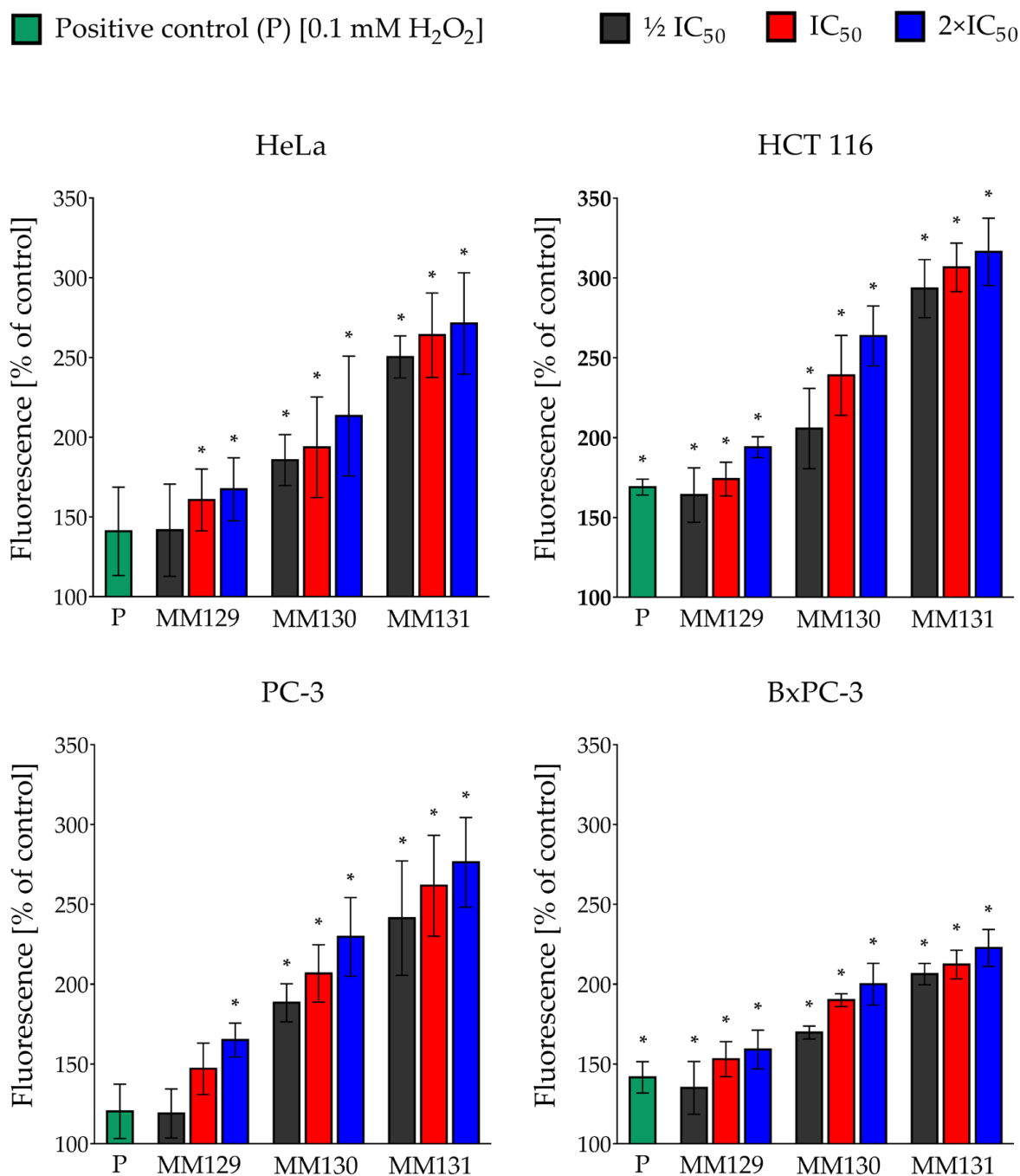


Figure 6. Changes in intracellular ROS level in the human cancer cell lines (HeLa, HCT 116, PC-3, and BxPC-3) following their 2 h treatment with MM129, MM130, and MM131 at $\frac{1}{2}$ IC₅₀, IC₅₀, and 2×IC₅₀ (values obtained in the MTT assay). ROS level is expressed as the mean percentage of fluorescence intensity of H₂DCFDA relative to control ± SD. Significant differences ($p < 0.05$) compared with negative control (*).

2.5. Cell Cycle Analysis

Figure 7 demonstrates the cell cycle phase distribution of tested cancer cells after 24 h exposure to MM compounds. Of the sulfonamides tested, only MM129 at the IC₅₀ concentration significantly affected cell cycle progression in HeLa cells. The incubation of the tested cells with MM129 caused an increase in the percentage (%) of cells in the subG1 phase, and simultaneous decrease in the number of cells (%) in the G0/G1 phase. In the case of HCT 116 cells, an accumulation of cells in the S phase and a reduction in

the proportion of cells in the G2/M phase after treatment with triazine derivatives at the IC₅₀ was observed. The cell cycle distribution of PC-3 cells showed that all tested MM compounds increased the number of cells (%) in the G0/G1 and subG1 phases and caused a decrease in the % of cells in the S phase. In contrast, an increase in the number of cells in the G0/G1 phase and a reduction in cells in the G2/M phase was observed following the exposure of BxPC-3 cells to examined sulfonamides at the IC₅₀. The representative flow cytometry histograms for the tested cell lines were demonstrated in Supplementary Materials (Figure S13).

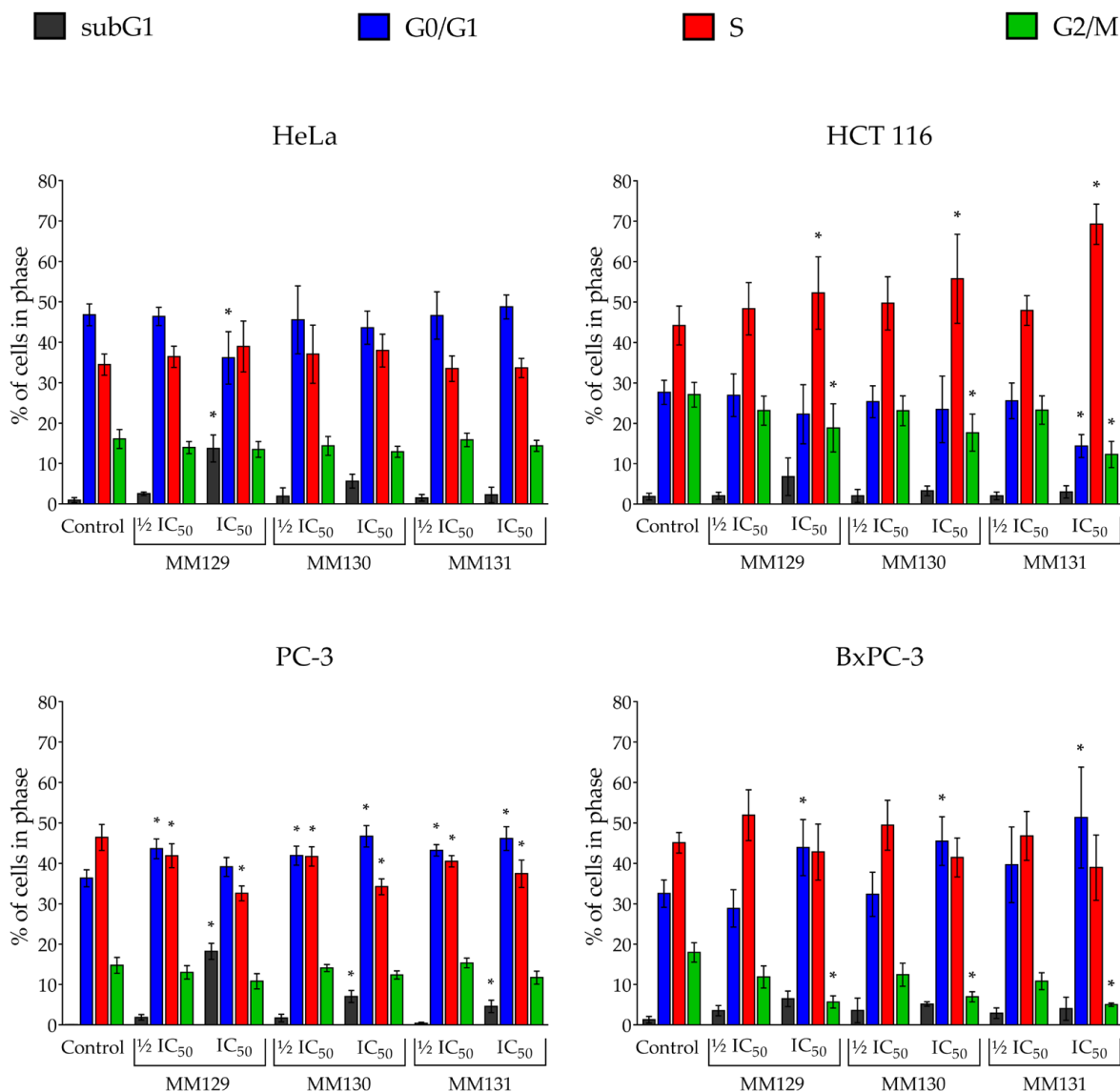


Figure 7. Cell cycle phase distribution of HeLa, HCT 116, PC-3, and BxPC-3 cancer cells after 24 h incubation with MM129, MM130, and MM131 at $\frac{1}{2}$ IC₅₀ and IC₅₀ are shown as the mean percentage of cells of a particular cell cycle phase \pm SD. Significant differences ($p < 0.05$) compared with control (*). $N = 1 \times 10^4$.

2.6. Molecular Docking

MM compounds/CDK complexes were analyzed according to their binding energy (kcal/mol) obtained during the molecular docking procedure as presented in Table 1.

Table 1. Molecular docking results of MM compounds and CDK enzymes.

Target	PDB Code	MM129	MM130	MM131	Reference Ligand
CDK1	6gu6	−8.85	−8.06	−8.72	−8.11
CDK2	3bhu	−9.19	−8.01	−8.73	−4.63
CDK4	2w9z	−9.48	−8.03	−8.25	−7.69
CDK5	1unh	−8.78	−7.14	−7.98	−6.65
CDK6	6oqo	−8.73	−8.0	−8.91	−8.35
CDK7	1ua2	−9.84	−8.71	−9.42	−7.81
CDK8	6t41	−8.69	−7.03	−8.28	−8.01
CDK9	3blq	−8.08	−6.86	−7.0	−8.2

MM129 exhibited the lowest binding energy values when docked against CDK enzymes. Therefore, it showed the best binding potential among the MM compounds (except for the docking of **MM131** with CDK6). **MM129** showed more profound binding potential compared with reference ligands of CDK enzymes (except for CDK9). The highest binding affinities were observed for CDK4 and CDK7 (binding energy of −9.48 and −9.84, respectively). However, we have decided to assess the molecular stability of **MM129** with all the investigated CDK enzymes.

2.7. Molecular Dynamics Simulations

Sufficient stability of the **MM129**/CKDs complexes was observed during molecular dynamics simulation. The highest stability based on the observed parameters such as root mean square deviation (RMSD), root mean square fluctuation (RMSF), protein–ligand contacts, and conserved secondary structure were shown for complexes formed between **MM129** and CDK5/8 enzymes. Thus, it has been supposed that **MM129** executes the anticancer effect via synergistic targeting of both CDK5 and CDK8 enzymes.

The target enzyme CDK5 has 276 residues distributed in a macromolecular chain consisting of 2225 heavy atoms out of a total of 4505 atoms. The macromolecular target has 35% of secondary structures in the form of 27% of alpha helices and 8% of beta-strands, which were found to be conserved during the simulation process. **MM129** possesses 32 heavy atoms out of a total of 51 atoms. Dynamic simulation of the macromolecular complex of **MM129** against the CDK5 target has clearly shown that the RMSD for the fluctuation of the protein backbone was in-between 1.2–2.0 Å, which is well within the acceptable range. Similarly, the ligand **MM129** showed some initial adjustment up to 5 ns within the active site to achieve the stable conformation followed by its stabilized vibrations within the range of 3.6–4.8 Å. Afterward, the complexed ligand attained the most stable conformation and remained stable throughout the simulation process. The RMSF of the macromolecular backbone was found to be well within the range of 0.4–2.0 Å throughout the simulation process. Macromolecular residues such as Ile10, Tyr15, Gly16, Val18, Cys83, Asp86, Lys128, Gln130, Asn131, Leu133, and Asn144 of CDK5 were found to interact with the ligand **MM129** throughout the simulation process.

The target enzyme CDK8 has 346 residues distributed in a macromolecular chain consisting of 2855 heavy atoms out of a total of 5716 atoms. The macromolecular target has 35% of secondary structures in the form of 25% of alpha helices and 10% of beta-strands, which were found to be conserved during the simulation process. Dynamic simulation of the macromolecular complex of **MM129** against the CDK8 target clearly showed that the RMSD for the fluctuation of the protein backbone was in-between 2.5–4.0 Å, which is well within the acceptable range. Similarly, the ligand **MM129** showed stable conformation within the range of 3.0–4.2 Å and remained stable throughout the simulation process. The RMSF of the macromolecular backbone was found to be well within the range of 0.6–2.4 Å except for some terminal residues throughout the simulation process. Macromolecular residues, such as Val27, Arg29, Thr31, Lys52, Phe97, Asp98, Ala100, Asp103, Trp105, Lys153, Ala155, Leu158, and Asp173 of CDK8 were found to interact with the ligand **MM129** throughout the simulation

process. The RMSD of the macromolecular complex of **MM129** against CDK5 and CDK8 observed during the 100 ns of the MD simulation is displayed in Figure 8.

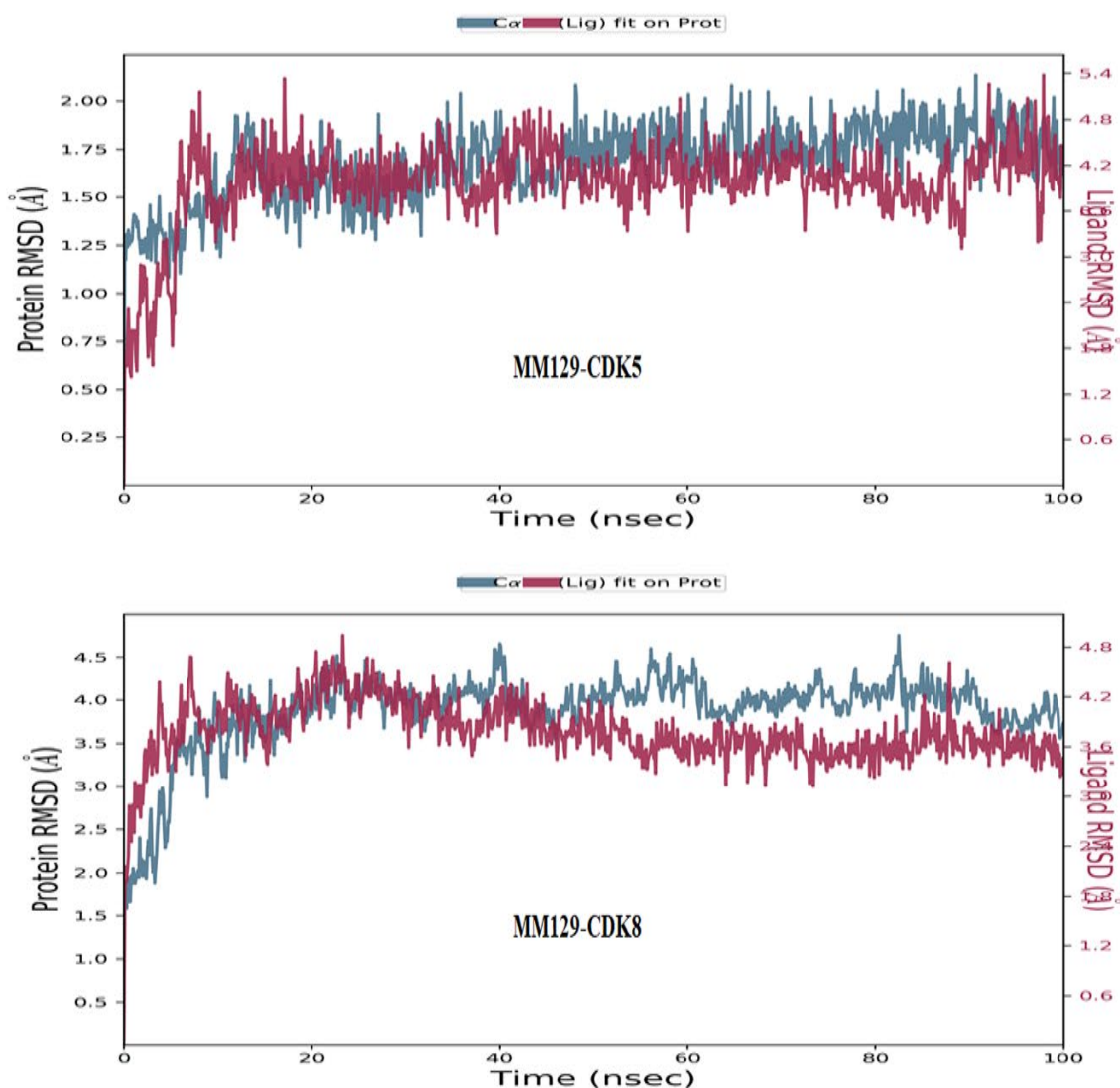


Figure 8. RMSD of the C α backbone of human CDK5-**MM129** and CDK8-**MM129** receptor–ligand complex observed during the 100 ns of MD simulation.

3. Discussion

In the current study, we have demonstrated the pro-apoptotic and pro-oxidative activity of **MM129**, **MM130**, and **MM131** towards HeLa, HCT 116, PC-3, and BxPC-3 cancer cells. Furthermore, our research included computational studies and analysis of cell cycle distribution in the tested cells after 24 h exposure to **MM129**, **MM130**, and **MM131**.

The obtained results of the Annexin V binding assay showed the pro-apoptotic activity of examined sulfonamides towards the HeLa, HCT 116, PC-3, and BxPC-3 cancer cell lines (Figure 2). Only the HeLa and HCT 116 cell lines showed significant changes in the apoptosis prevalence following 24 h exposure to the investigated compounds. A high number of apoptotic cells was detected following the treatment of the HeLa cells with **MM129** and **MM130** ($73.47 \pm 3.48\%$ and $55.63 \pm 1.27\%$ of apoptotic cells at $2 \times IC_{50}$, respectively). Following 48 h incubation, all MM compounds demonstrated an enhancement in apoptotic rates across all the cancer cell lines when administered at their highest concentration ($2 \times IC_{50}$). However, the most noticeable effect was observed for the HCT 116 and HeLa cells. The highest apoptotic response to the investigated triazine derivatives was

observed after 72 h incubation of the tested cancer cell lines. The high apoptotic properties of **MM129** and **MM131** towards other cancer cells (HT-29 and DLD-1) were confirmed by other researchers [60,64].

During microscopic analysis typical morphological features of apoptosis, including chromatin condensation, cell shrinkage, nuclear fragmentation, and membrane blebbing, were noticed following the treatment of cells with MM compounds (Figure 4). Furthermore, a quantitative analysis of the AO/EB double-stained cells confirmed the pro-apoptotic potential of examined sulfonamides observed in the Annexin V binding assay (Figure 3). A significant increase in the number of apoptotic cells in all the cancer cell lines was noticed after 48 h incubation with investigated compounds at their highest concentration. Similarly to the Annexin V assay, the results of AO/EB revealed that HeLa was the most sensitive cell line to the pro-apoptotic activity of the compounds. In addition, the results of the AO/EB dual staining confirmed the pro-apoptotic activity of **MM131** towards DLD-1 and HT-29 cancer cells [60]. Furthermore, a similar pattern was observed in the case of other triazine derivatives against several cancer cell lines.

In the present work, all studied sulfonamides depleted $\Delta\Psi_m$ in all the evaluated cell lines following 48 h of treatment. Additionally, a decrease in $\Delta\Psi_m$ was observed in the HeLa and HCT 116 cells after 24 h exposure to MM compounds in their highest concentration (Figure 5). The results of Hermanowicz et al. [64] also showed the ability of **MM129** to decrease the $\Delta\Psi_m$ in the DLD-1 and HT-29 cells. Moreover, the literature data have shown a similar activity of other MM compounds towards the different cancer cell lines [65,66]. According to the study of Ly et al. [67], loss of $\Delta\Psi_m$ may be an early event of the apoptotic-signaling pathway. However, $\Delta\Psi_m$ reduction may also be a consequence of apoptosis when it is triggered by the opening of the mitochondrial permeability transition pore (PTP) [67]. As mentioned above, the studies have indicated that the reduction of $\Delta\Psi_m$ is the effect of the opening of PTP. In contrast, other research works have suggested the opposite process—the loss of $\Delta\Psi_m$ is responsible for the opening of PTP [68]. Undoubtedly, loss of the $\Delta\Psi_m$ and opening of the PTP are associated with the release of pro-apoptotic proteins, such as cytochrome c, apoptosis-inducing factor (AIF), and procaspase-9. As a consequence, this leads to a circle of self-perpetuating apoptotic changes [67,69,70].

Moreover, the assessment of the pro-oxidative properties of examined compounds was conducted. All the investigated sulfonamides induced a concentration-dependent increase in ROS formation in all investigated cancer cell types following 2 h exposure (Figure 6). ROS accumulation may cause DNA strand break formation, mitochondrial DNA lesions, and degradation of mitochondrial DNA [16]. The high pro-oxidative activity of tested triazine derivatives is consistent with the data obtained from our previous studies, where examined compounds exhibited high genotoxicity against the same cancer cell lines. Similarly to the genotoxicity studies, **MM131** showed the most potent pro-oxidative potential among the tested compounds [63]. Furthermore, research has shown that the accumulation of ROS-related damages in lipids, proteins, and DNA may be responsible for the suppression of tumor cell proliferation and growth via cell cycle arrest and apoptosis. [71,72]. Literature data have suggested that raised cytosolic calcium ion levels and increased formation of ROS cause a decrease in electrolyte transport across the mitochondrial membrane, leading to the opening of PTP and collapse of $\Delta\Psi_m$ [68,73–75]. As a consequence, various pro-apoptotic molecules are released, activating the mitochondrial apoptosis pathway [15,73,76–86]. In addition, ROS can also enhance the death receptor-mediated apoptosis pathway by downregulation the FLICE-inhibitory protein (c-FLIP) half-life [87]. Moreover, ROS may bind to death receptors containing the death domain (DD), and thus initiate the extrinsic pathway of apoptosis through interaction with other adaptor proteins with DDs [88,89]. In addition, the activation of apoptosis by ROS is the result of mitochondrial damage and activation of poly(ADP-ribose) polymerase (PARP) and apoptosis signal-regulating kinase 1 (ASK1) [90]. Therefore, we conclude that the ROS formation observed in the tested cancer cells after the incubation with examined compounds may be the cause for the further loss of $\Delta\Psi_m$.

The cell cycle distribution of PC-3 cells showed a significant increase in the proportion of the cells in the G0/G1 phase and a reduction in the number of cells (%) in the S phase after the incubation with MM compounds. Similar results were obtained by Hermanowicz et al. [59] who treated the HT-29 and DLD-1 cells with **MM129**. A different response was observed in the BxPC-3 cell line. The incubation with triazine derivatives at the IC₅₀ concentration caused an accumulation of cells in the G0/G1 phase and a decrease in the proportion of the cells in the G2/M phase. A similar reduction in the number [%] of cells in the G2/M phase was observed following treatment of HCT 116 cells with the investigated sulfonamides at the IC₅₀. However, after incubation with the investigated compounds, HCT 116 cells showed an opposing trend in the distribution of cells in the S phase compared to PC-3 cells. All the tested compounds in at the IC₅₀ increased the percentage of the cells in the S phase. Gornowicz et al. [60] observed a similar activity of **MM131** in other colorectal cancer cell lines (HT-29 and DLD-1 cells), where this compound also increased the proportion of the cells in the S phase. The highest pro-apoptotic activity measured as a proportion of the cells in the subG1 phase in HeLa and PC-3 cells was noticed for **MM129** compound (Figure 7). Interestingly, the varied activity of the same antineoplastic drug against a diversity of cancer cell lines is consistent with earlier research findings. As an example, 5-fluorouracil (5-FU) increased the accumulation of cells in the G0/G1 phase in gastric cancer cells AGS and some colorectal cancer (CRC) cell lines, such as HT-29 and DLD-1 while also arresting oral cancer cells HSC-4 and colon cancer cells SW620 in the S phase [60,91–93]. Our previous research has shown that all examined triazine derivatives are highly genotoxic toward the tested cell lines [63]. Interestingly, the most noticeable increase in the number of cells in the S phase in HCT 116 cells was observed in the case of **MM131**. This is consistent with our previous results, where **MM131** induced the highest levels of DNA damage among the tested sulfonamides [63]. In turn, the elongated G0/G1 phase also provides the cell more time to repair DNA damage, preventing the it from entering the S phase. The genotoxic study of the investigated triazine derivatives has presented their high genotoxic activity not only against HCT 116 but also towards PC-3 and BxPC-3 cells [63]. Thus, the cell cycle arrest in the G0/G1 phase in PC-3 and BxPC-3 cells after the incubation with MM compounds may also be the effect of the accumulation of DNA damage.

Finally, our results of molecular docking have shown the high potential of **MM129**, as well as **MM130**, and **MM131** to bind with CDK enzymes. **MM129** exhibited the lowest binding energy values among examined sulfonamides, especially for CDK4 and CDK7 (Table 1). The results of molecular dynamics simulations confirmed sufficient stability of the **MM129**/CKDs complexes. The highest stability was observed for the associations of **MM129** with CDK5 and CDK8 enzymes. In the study of Hermanowicz et al. [59], an upregulation of TP53 and simultaneous downregulation of CDK2 was observed after the exposure of the HT-29 and DLD-1 cell lines to **MM129**. The cell cycle arrest in the G0/G1 phase was noticed in both CRC lines after the incubation with **MM129**. Thus, the change that was seen in those cells was most likely induced by an increase in TP53 expression in conjunction with a downregulation of CDK2 activity [59]. Therefore, we conclude that the interaction of investigated compounds with CDKs may be among the potential causes of observed disturbances in the cell cycle distribution in the tested cells.

4. Materials and Methods

4.1. Cell Culture and Chemicals

All the examined adherent human cancer cell lines, including HeLa (cervical cancer), HCT 116 (colorectal carcinoma), PC-3 (prostate cancer), and BxPC-3 (pancreatic adenocarcinoma), were purchased from American Type Culture Collection (ATCC[®], Rockville, MD, USA). HCT 116 and BxPC-3 cells were cultivated in RPMI 1640 medium, while IMDM and DMEM-F12 media were used for the cultivation of the HeLa and PC-3 cell lines, respectively. Media and Trypsin/EDTA used for cell culture were supplied by Biowest (CytoGen, Zgierz, Poland). All media were supplemented with 1% (*v/v*) penicillin-

streptomycin solution and 10% (*v/v*) fetal bovine serum (FBS) (Merck/Sigma Aldrich Chemical Co, Burlington, MA, USA). FITC Annexin V Apoptosis Detection Kit I was obtained from B.D. Biosciences (Franklin Lakes, NJ, USA). MitoTracker CMXRos was supplied by Invitrogen (Waltham, MA, USA). Buffered saline (PBS), ethanol, dimethyl sulfoxide (DMSO), acridine orange/ethidium bromide (AO/BE), 2',7'-dichlorodihydrofluorescein diacetate (H₂DCFDA), RNase A Solution, and propidium iodide (PI) were purchased from Merck/Sigma Aldrich Chemical Co (Burlington, MA, USA).

Cancer cells were maintained in a humidified incubator at 37 °C in a 5% CO₂ atmosphere and were systematically scanned for mycoplasma contamination. The proper number of cultivated cells was managed by their regular passaging at 90% confluence twice weekly using 0.025% trypsin/EDTA. Additionally, to maintain stable growth conditions for cell culture, the medium was replaced every 48 h. Each experiment was performed on cells from three independent passages and included a negative control (cells treated with DMSO at <0.5%). The concentrations for all experiments were based on the values obtained in the MTT assay after 72 h of cell incubation with examined compounds ($\frac{1}{2}$ IC₅₀, IC₅₀, and 2×IC₅₀) [63].

4.2. Flow Cytometry Assessment of Annexin V Binding

Evaluation of the induction of apoptosis in the HeLa, HCT 116, PC-3, and BxPC-3 cell lines was performed using the FITC Annexin V Apoptosis Detection Kit I via flow cytometry analysis. The translocation of the PS on the outer side of the cell membrane was associated with PCD. Annexin V conjugated with fluorescein isothiocyanate (FITC) binds to PS, which allows the identification of apoptotic cells, while not membrane-permeable PI binds to the DNA of necrotic cells. Double staining identifies independently early and late apoptosis (cells stained only with FITC or with both dyes, respectively) [94].

Cancer cells were cultured for 24 h in controlled conditions (5% CO₂; 37 °C) on 6-well plates, and then exposed to MM compounds in different concentrations ($\frac{1}{2}$ IC₅₀, IC₅₀, and 2×IC₅₀) for 24 h, 48 h, or 72 h. After incubation, the cells were trypsinized and transferred to conical tubes, then washed twice with cold PBS. Following centrifuging (10 min, 4 °C, 1400 rpm), the cells were suspended in Annexin V-binding buffer and stained with PI and FITC-labelled Annexin V for 15 min at room temperature in the dark. Additional controls were used to set up compensation and quadrants were included (unstained cells and cells dyed only with FITC Annexin V or PI). Measurements were performed using a flow cytometer (LSR II, Becton Dickinson, San Jose, CA, USA) at the wavelength of 530 nm. The obtained data (10,000 events per sample) were analyzed in FlowJo 10.8.1 software.

4.3. Dual Acridine Orange/Ethidium Bromide (AO/EB) Fluorescent Staining

Acridine orange (AO) intercalates into the DNA of living cells after penetration of their cell membrane and accumulates in lysosomes, emitting green and red fluorescence, respectively. In contrast, ethidium bromide (EB) interacts only with the DNA and RNA of membrane-damaged cells, emitting red fluorescence. This method allows the observation of the development of apoptotic bodies and detects nuclear alterations, which are both associated with apoptosis. The morphological changes in chromatin condensation in the dyed nucleus, combined with different uptake of AO and EB, allows for distinguishing three categories of cells as follows: viable (green-stained nucleus uniformly distributed in the center of the cell), apoptotic (orange-stained cell nuclei with condensation and chromatin clumping; the presence of cell membrane blebbing indicating the apoptotic bodies formation) and necrotic (increased cell's volume; uneven orange-red fluorescence without a sharp outline; cell near disintegration) [95,96].

The cells were seeded for 24 h in controlled conditions (5% CO₂; 37 °C) on 12-well plates, and then were incubated with MM compounds in different concentrations ($\frac{1}{2}$ IC₅₀, IC₅₀, and 2×IC₅₀) for 48 h. After being cultured, the cells were trypsinized, transferred to conical tubes, and then centrifuged (10 min, 4 °C, 1400 rpm). Afterward, the supernatant was removed, and the precipitate was diluted in 25 µL of PBS and transferred to the

Eppendorf tube. The suspension was mixed with dual fluorescent staining solution (1 μ L) containing 100 μ g/mL AO and 100 μ g/mL EB, transferred to glass slides, and then covered with a coverslip. The morphology of the cells was conducted, and 200 cells were counted within 10 min using a fluorescent microscope (Olympus BX60 F5, Olympus Optical Co., Ltd., Nagano, Japan) at 360 nm.

4.4. Mitochondrial Membrane Potential ($\Delta\Psi_m$)

Disruption of mitochondrial membrane potential is among the earliest changes associated with the induction of apoptosis [10]. As a result of the increased permeability of the internal and external mitochondrial membrane, the mitochondrial proteins, such as apoptosis-inducing factor (AIF) and cytochrome c migrate into the cytosol leading to the activation of the intrinsic apoptosis pathway. MitoTracker CMXRos, which contains thiol-reactive chloromethyl moiety passively diffuses across the plasma membrane. Accumulation of fluorescence probe in active mitochondria allows the measurement of changes in the $\Delta\Psi_m$ of the tested cells [67,97]

Cancer cells were seeded for 24 h in controlled conditions (5% CO₂; 37 °C) on 96-well plates and then were treated with investigated compounds in different concentrations ($\frac{1}{2}$ IC₅₀, IC₅₀, and 2 \times IC₅₀) for 24 h or 48 h. Following incubation, the cells were washed with PBS and stained with the probe at the final concentration of 0.1 μ M for 40 min at 37 °C in the dark. The transmembrane mitochondrial potential was measured using a microplate reader at the wavelength of 579/599 nm.

4.5. Determination of Intracellular ROS Level by H₂DCFDA

ROS are associated with the regulation of apoptosis pathways mediated via endoplasmic reticulum (ER), death receptors, and mitochondria [69]. Accordingly to the protocol described previously by Ruiz-Leal and George [98], H₂DCFDA was used to determine the level of intracellular ROS formation. H₂DCFDA is a cell-permeable stain widely used for the quick and effective detection of total intracellular oxidants. The probe can diffuse across an intact cellular membrane and then is hydrolyzed to 2',7'-dichlorodihydrofluorescein (H₂DCF) by intracellular esterases active in living cells. Finally, ROS oxidate dichlorodihydrofluorescein to a highly fluorescent 2',7'-dichlorofluorescein (DCF).

Cancer cells were cultured for 24 h in controlled conditions (5% CO₂; 37 °C) on black 96-well plates. Afterward, the culture medium was replaced by H₂DCFDA dissolved in PBS (final concentration was 20 mM), and the cells were incubated for 20 min in the dark. Following incubation, cell lines were exposed to examined sulfonamides in different concentrations ($\frac{1}{2}$ IC₅₀, IC₅₀, and 2 \times IC₅₀). After 120 min of incubation, the fluorescence was measured using a microplate reader at the wavelength of 485/535 nm using the SpectraMax[®] i3xMulti-Mode Detection Platform.

4.6. Cell Cycle

The effect of MM compounds on the cell cycle was determined by flow cytometry. The cell cycle distribution of a sample was estimated by staining the DNA with a fluorescent dye, such as PI, which binds to the DNA stoichiometrically. The analysis of the cellular DNA content frequency histograms reveals the differentiation of cells in the G₀/G₁, S, and G₂/M phases. Furthermore, this approach allows the identification of aneuploid populations, as well as apoptotic cells with fractional DNA content (subG₁) [99].

The cells were seeded for 24 h in controlled conditions (5% CO₂; 37 °C) on 6-well plates, and then were incubated with MM compounds at $\frac{1}{2}$ IC₅₀ and IC₅₀ for 24 h. After incubation, the cells were trypsinized and transferred to conical tubes, then washed with PBS. Following centrifuging (10 min, 4 °C, 1400 rpm), the cells were fixed with cold ethanol (70%), then washed with PBS. Afterward, the cells were treated with 10 μ g/mL of RNase A solution and stained with 5 μ g/mL of PI for 30 min at 37 °C in the dark. The measurements were performed using a flow cytometer (LSR II, Becton Dickinson) at the wavelength of 530 nm. The obtained data (10,000 events per sample) were analyzed in FlowJo 10.8.1 software.

4.7. Molecular Docking

In an attempt to explore the potential inhibitory effects of **MM129**, **MM130**, and **MM131** on CDK enzymes, we have performed molecular docking. MM compounds were sketched in ChemDraw 8.0 software and their three-dimensional structure was obtained following energy minimization using an MM2 force field. To get the ligands ready for molecular docking simulation, we used AutoDock Tools (The Scripps Research Institute, La Jolla, CA, USA) to find aromatic carbons and rotatable bonds, configure the automated torsion number, margin non-polar hydrogens, and add Gasteiger charges.

Three-dimensional structures of CDK enzymes (CDK1 (PDB ID: 6gu6), CDK2 (PDB ID: 3bhu), CDK4 (PDB ID: 2w9z), CDK5 (PDB ID: 1unh), CDK6 (PDB ID: 6oqo), CDK7 (PDB ID: 1ua2), CDK8 (PDB ID: 6t41), and CDK9 (PDB ID: 3blq) were obtained from Protein Data Bank (PDB) <https://www.rcsb.org/> (accessed on 1 January 2023). Using AutoDockTools, the macromolecules were assigned autodock atom type (AD4), and the Gasteiger charge was added and distributed along the macromolecule. The structures were saved in PDBQT file format.

The grid box values were adjusted following the docking of reference ligands already complexed in the PDB structure after throughout observation of the drug's conformational poses. The grid parameters for each CDK enzyme were saved in a grid parameter file (GPF). The Autogrid utility from the Autodock suite was used to create the additional map files required for running the molecular docking simulations (Table 2).

Table 2. The coordinates of the grid boxes used in the docking studies of MM compounds to currently investigated CDK enzymes.

Target	PDB Code	x-D	y-D	z-D	Spacing (Å)	X-Center	Y-Center	Z-Center
CDK1	6gu6	60	60	60	0.503	241.389	216.129	209.535
CDK2	3bhu	40	40	40	0.375	−7.638	20.962	−21.4
CDK4	2w9z	50	50	50	0.453	20.281	25.506	8.713
CDK5	1unh	40	40	40	0.469	39.357	16.375	31.45
CDK6	6oqo	40	40	40	0.469	21.984	38.012	−9.828
CDK7	1ua2	40	40	40	0.375	41.304	−4.892	23.033
CDK8	6t41	40	40	40	0.469	−3.707	−10.927	9.279
CDK9	3blq	40	40	40	0.469	50.291	−18.937	−11.183

4.8. Molecular Dynamics Simulations

To validate the obtained docking outcome for the thermodynamic stability of the macromolecular drug-receptor complex concerning time, a molecular dynamics (MD) simulation for 100 ns for the macromolecular complex of ligand **MM129** with all the CDKs considered in the current research paradigm was executed. MD simulation was performed at the molecular level at a constant temperature of 300 K and constant pressure conditions. Schrödinger-Desmond (version 2019.4) module of Maestro software was used to perform dynamics simulation by using OPLS3e force field and solvating it in an explicit water box of size 10. The single point charge (SPC) model was used to infer the water molecules [100]. The usage of the OPLS3e force field and the SPC water model for macromolecular complexes with small ligands were previously described to yield the optimum reproducible results [101]. The complex was neutralized by adding the contrary-charged ions followed by their energy minimization [102]. The long-range electrostatic connections between the macromolecule and the complexed ligand were computed by applying the particle-mesh Ewald (PME) method with 0.8 grid spacing and a cutoff radius of 9.0 for Coulomb interactions after the NPT ensemble, MD simulation was run.

4.9. Statistical Analysis

All data are presented as the mean values with standard deviations (SD) obtained from three independent experiments. The statistical analysis was evaluated with GraphPad

Prism 8.0 software system (GraphPad Prism Software Inc., San Diego, CA, USA), by using one-way ANOVA with Tukey's test (post hoc multiple comparisons in distributions not departing from normality). A p -value of <0.05 was considered significant.

5. Conclusions

The presented research demonstrates the diverse, cell-line-dependent pro-oxidative and pro-apoptotic activity of novel pyrazolo[4,3-*e*]tetrazolo[1,5-*b*][1,2,4]triazine sulfonamides, such as **MM129**, **MM130**, and **MM131**, on HeLa, PC-3, HCT 116, and BxPC-3 cells. The results from the H₂DCFDA and apoptotic assays (Annexin V binding assay, MitoTracker assay, and AO/EB) proved the high pro-oxidative and pro-apoptotic activity of **MM129**, **MM130**, and **MM131** in vitro. All investigated compounds also affected the cell cycle distribution inducing the cell-line-dependent cycle arrest in the G₀/G₁ or S phase. Our previous data have shown the high genotoxic potential of examined compounds toward tested cancer cells [63]. Therefore, we consider that the increase in apoptosis and the changes in the cell cycle distribution result from the strong genotoxicity of **MM129**, **MM130**, and **MM131**. Furthermore, based on computational studies, we conclude that the ability of the investigated sulfonamides to change the distribution of the cell cycle may result from their potential for CDKs inhibition. Moreover, we suggest that a high level of ROS may enhance the genotoxic and pro-apoptotic properties of the investigated triazine derivatives (Figure 9).

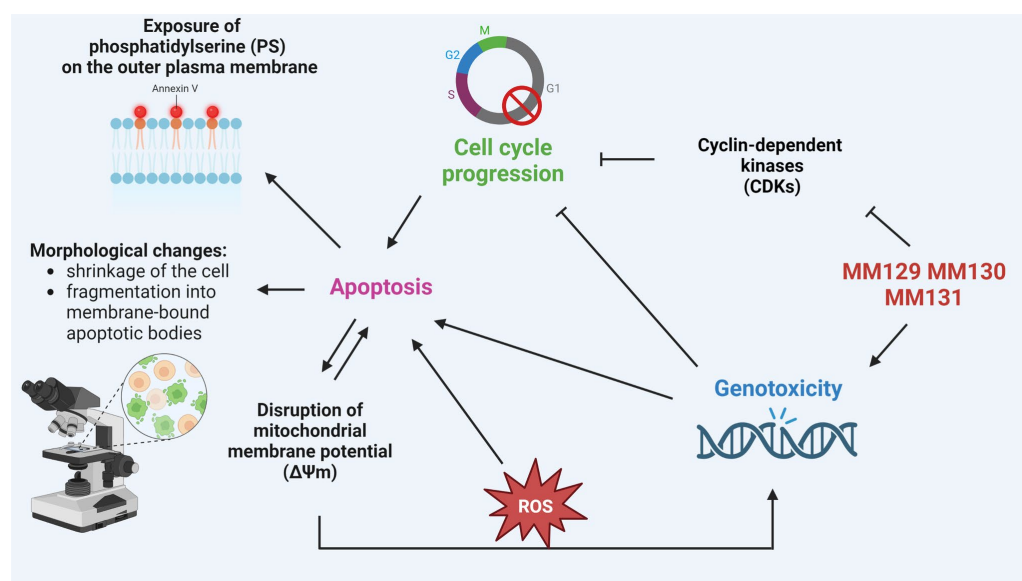


Figure 9. The potential mechanism of action of **MM129**, **MM130**, and **MM131**. Investigated sulfonamides cause DNA single-strand and double-strand breaks and simultaneously inhibit CDKs. High levels of DNA damage and inhibition of CDKs lead to cell cycle arrest. As the effect of high genotoxic stress and the action of the G₁/S cell cycle checkpoint, the cell is directed to the apoptosis pathway. The consequences of apoptosis include cell morphological changes and the exposition of PS on the outer plasma membrane. Furthermore, apoptotic changes cause loss of $\Delta\Psi_m$ and lead to the opening of PTP, which results in ROS formation. The continuous accumulation of ROS may enhance genotoxic stress and apoptosis, leading to a self-perpetuating cycle of changes.

In conclusion, the obtained data combined with the results from our previous study [63] provide important information on the biological response of the tested cancer cell lines to **MM129**, **MM130**, and **MM131**. Moreover, our results expand the general knowledge about the antineoplastic activity of a group of MM compounds. Interestingly, among examined sulfonamides, **MM129** at the IC₅₀ exhibited the highest apoptotic properties in the Annexin V binding assay against HeLa cells following the 48 h incubation period (Figure 2). Moreover, the same dose of **MM129** induced the highest accumulation of cells in the subG₁

phase in the case of HeLa and PC-3 cells after the 24 h of compound exposure, compared to other triazine derivatives (Figure 7). In addition, **MM129** has presented the lowest binding energy values when docked against CDK enzymes, compared to **MM130** and **MM131** (Table 1). In contrast, **MM131** at the IC₅₀ has revealed the highest pro-oxidative activity among examined sulfonamides towards all types of cancer cells following the 2 h of incubation time (Figure 6). However, our results suggest that, except for those differences, the anticancer activity of tested MM compounds seems to be relatively similar. The general comparison of the anticancer activity of the tested sulfonamides based on the IC₅₀ and 24 h and 48 h incubation times is demonstrated in the Supplementary Material (Table S2). Undoubtedly, all the investigated triazine derivatives exhibit high antineoplastic properties. Nevertheless, despite the solid base, further investigations of the chemotherapeutic potential of **MM129**, **MM130**, and **MM131** towards cervical cancer, colorectal carcinoma, prostate cancer, and pancreatic adenocarcinoma, especially on in vivo material, are required.

Supplementary Materials: The following supporting information can be downloaded at: <https://www.mdpi.com/article/10.3390/ijms24108504/s1>.

Author Contributions: Conceptualization, K.B., B.M., M.K. and R.K.; methodology, K.B., S.M., B.M. and R.K.; investigation, K.B. and S.M.; writing—original draft preparation, K.B., S.M. and M.K.; writing—review and editing, B.M., M.K., S.M., R.K. and M.M.; supervision, B.M. and R.K.; project administration, B.M. and R.K. All authors have read and agreed to the published version of the manuscript.

Funding: This research received no external funding.

Institutional Review Board Statement: This study was conducted according to the guidelines of the Declaration of Helsinki and approved by the Bioethics Committee for Scientific Investigation, University of Lodz (agreement no. 8/KBBN-UL/1//2019).

Informed Consent Statement: Not applicable.

Data Availability Statement: The data presented in this study are available in the main text of this article/supplementary materials of this article or on request from the corresponding author.

Conflicts of Interest: The authors declare no conflict of interest.

Sample Availability: Samples of the compounds **MM129**, **MM130**, and **MM131** available from the authors.

Abbreviations

5-FU	5-fluorouracil
AIF	apoptosis-inducing factor
AKT	Protein kinase B
AO/BE	acridine orange/ethidium bromide
ASK1	apoptosis signal-regulating kinase 1
BTK	Bruton's tyrosine kinase
CDKs	cyclin-dependent kinases
c-FLIP	FLICE-inhibitory protein
CKIs	cyclin-dependent kinase inhibitors
CRC	colorectal cancer
DCF	fluorescent 2',7'-dichlorofluorescein
DD	death domain
EB	ethidium bromide
ER	endoplasmic reticulum
FITC	fluorescein isothiocyanate
H ₂ DCF	2',7'-dichlorodihydrofluorescein
H ₂ DCFDA	2,7-dichlorodihydrofluorescein diacetate
mTOR	mammalian target of rapamycin
MTT	3-(4,5-Dimethylthiazol-2-yl)-2,5-diphenyltetrazolium bromide

PARP	poly(ADP-ribose) polymerase
PCD	programmed cell death
PD-1	programmed cell death protein 1
PD-L1	programmed death ligand-1
PI	propidium iodide
PI3K	phosphoinositide-3-kinase
PS	phosphatidylserine
PME	particle-mesh Ewald
PTP	permeability transition pore
RMSD	root mean square deviation
RMSF	root mean square fluctuation
ROS	reactive oxygen species
SPC	single point charge
TP53	cellular tumor antigen p53
$\Delta\Psi_m$	mitochondrial membrane potential

References

- Lang, D.K.; Kaur, R.; Arora, R.; Saini, B.; Arora, S. Nitrogen-Containing Heterocycles as Anticancer Agents: An Overview. *Anti Cancer Agents Med. Chem.* **2020**, *20*, 2150–2168. [[CrossRef](#)]
- Mukhtar, M.; Bilal, M.; Rahdar, A.; Barani, M.; Arshad, R.; Behl, T.; Brisc, C.; Banica, F.; Bungau, S. Nanomaterials for Diagnosis and Treatment of Brain Cancer: Recent Updates. *Chemosensors* **2020**, *8*, 117. [[CrossRef](#)]
- Ferlay, J.; Colombet, M.; Soerjomataram, I.; Parkin, D.M.; Piñeros, M.; Znaor, A.; Bray, F. Cancer Statistics for the Year 2020: An Overview. *Int. J. Cancer* **2021**, *149*, 778–789. [[CrossRef](#)]
- Ros, J.; Balconi, F.; Baraibar, I.; Saoudi Gonzalez, N.; Salva, F.; Tabernero, J.; Elez, E. Advances in Immune Checkpoint Inhibitor Combination Strategies for Microsatellite Stable Colorectal Cancer. *Front. Oncol.* **2023**, *13*, 1112276. [[CrossRef](#)]
- Brunelle, J.K.; Zhang, B. Apoptosis Assays for Quantifying the Bioactivity of Anticancer Drug Products. *Drug Resist. Updates* **2010**, *13*, 172–179. [[CrossRef](#)]
- D’Arcy, M.S. Cell Death: A Review of the Major Forms of Apoptosis, Necrosis and Autophagy. *Cell Biol. Int.* **2019**, *43*, 582–592. [[CrossRef](#)]
- Vermes, I.; Haanen, C.; Steffens-Nakken, H.; Reutellingsperger, C. A Novel Assay for Apoptosis Flow Cytometric Detection of Phosphatidylserine Expression on Early Apoptotic Cells Using Fluorescein Labelled Annexin V. *J. Immunol. Methods* **1995**, *184*, 39–51. [[CrossRef](#)]
- Fadok, V.A.; Bratton, D.L.; Frasch, S.C.; Warner, M.L.; Henson, P.M. The Role of Phosphatidylserine in Recognition of Apoptotic Cells by Phagocytes. *Cell Death Differ.* **1998**, *5*, 551–562. [[CrossRef](#)]
- Crowley, L.C.; Marfell, B.J.; Scott, A.P.; Waterhouse, N.J. Quantitation of Apoptosis and Necrosis by Annexin V Binding, Propidium Iodide Uptake, and Flow Cytometry. *Cold Spring Harb. Protoc.* **2016**, *2016*, pdb.prot087288. [[CrossRef](#)]
- Gornowicz, A.; Kałuża, Z.; Bielawska, A.; Gabryel-Porowska, H.; Czarnomysy, R.; Bielawski, K. Cytotoxic Efficacy of a Novel Dinuclear Platinum(II) Complex Used with Anti-MUC1 in Human Breast Cancer Cells. *Mol. Cell Biochem.* **2014**, *392*, 161–174. [[CrossRef](#)]
- Ricci, J.-E.; Muñoz-Pinedo, C.; Fitzgerald, P.; Bailly-Maitre, B.; Perkins, G.A.; Yadava, N.; Scheffler, I.E.; Ellisman, M.H.; Green, D.R. Disruption of Mitochondrial Function during Apoptosis Is Mediated by Caspase Cleavage of the P75 Subunit of Complex I of the Electron Transport Chain. *Cell* **2004**, *117*, 773–786. [[CrossRef](#)]
- Krysko, D.V.; Roels, F.; Leybaert, L.; D’Herde, K. Mitochondrial Transmembrane Potential Changes Support the Concept of Mitochondrial Heterogeneity During Apoptosis. *J. Histochem. Cytochem.* **2001**, *49*, 1277–1284. [[CrossRef](#)]
- Vander Heiden, M.G.; Cantley, L.C.; Thompson, C.B. Understanding the Warburg Effect: The Metabolic Requirements of Cell Proliferation. *Science* **2009**, *324*, 1029–1033. [[CrossRef](#)]
- Finkel, T. Signal Transduction by Reactive Oxygen Species. *J. Cell Biol.* **2011**, *194*, 7–15. [[CrossRef](#)]
- Perillo, B.; Di Donato, M.; Pezone, A.; Di Zazzo, E.; Giovannelli, P.; Galasso, G.; Castoria, G.; Migliaccio, A. ROS in Cancer Therapy: The Bright Side of the Moon. *Exp. Mol. Med.* **2020**, *52*, 192–203. [[CrossRef](#)]
- Srinivas, U.S.; Tan, B.W.Q.; Vellayappan, B.A.; Jeyasekharan, A.D. ROS and the DNA Damage Response in Cancer. *Redox Biol.* **2019**, *25*, 101084. [[CrossRef](#)]
- Ferrari, S. Protein Kinases Controlling the Onset of Mitosis. *Cell Mol. Life Sci.* **2006**, *63*, 781–795. [[CrossRef](#)]
- Morgan, D.O. Cyclin-Dependent Kinases: Engines, Clocks, and Microprocessors. *Annu. Rev. Cell Dev. Biol.* **1997**, *13*, 261–291. [[CrossRef](#)]
- Łukasiak, P.; Załuski, M.; Gutowska, I. Cyclin-Dependent Kinases (CDK) and Their Role in Diseases Development—Review. *Int. J. Mol. Sci.* **2021**, *22*, 2935. [[CrossRef](#)]

20. Vermeulen, K.; Van Bockstaele, D.R.; Berneman, Z.N. The Cell Cycle: A Review of Regulation, Deregulation and Therapeutic Targets in Cancer. *Cell Cycle Regul. Deregul. Cell Prolif.* **2003**, *36*, 131–149. [[CrossRef](#)]
21. Alimbetov, D.; Askarova, S.; Umbayev, B.; Davis, T.; Kipling, D. Pharmacological Targeting of Cell Cycle, Apoptotic and Cell Adhesion Signaling Pathways Implicated in Chemoresistance of Cancer Cells. *Int. J. Mol. Sci.* **2018**, *19*, 1690. [[CrossRef](#)]
22. Thoma, O.-M.; Neurath, M.F.; Waldner, M.J. Cyclin-Dependent Kinase Inhibitors and Their Therapeutic Potential in Colorectal Cancer Treatment. *Front. Pharmacol.* **2021**, *12*, 757120. [[CrossRef](#)]
23. Cicenias, J.; Kalyan, K.; Sorokinas, A.; Stankunas, E.; Levy, J.; Meskinyte, I.; Stankevicius, V.; Kaupinis, A.; Valius, M. Roscovitine in Cancer and Other Diseases. *Ann. Transl. Med.* **2015**, *3*, 135.
24. Bertoli, C.; Skotheim, J.M.; de Bruin, R.A.M. Control of Cell Cycle Transcription during G1 and S Phases. *Nat. Rev. Mol. Cell Biol.* **2013**, *14*, 518–528. [[CrossRef](#)]
25. Peng, C.; Zeng, W.; Su, J.; Kuang, Y.; He, Y.; Zhao, S.; Zhang, J.; Ma, W.; Bode, A.M.; Dong, Z.; et al. Cyclin-Dependent Kinase 2 (CDK2) Is a Key Mediator for EGF-Induced Cell Transformation Mediated through the ELK4/c-Fos Signaling Pathway. *Oncogene* **2016**, *35*, 1170–1179. [[CrossRef](#)]
26. Liu, H.; Li, Z.; Huo, S.; Wei, Q.; Ge, L. Induction of G0/G1 phase Arrest and Apoptosis by CRISPR/Cas9-mediated Knockout of CDK2 in A375 Melanocytes. *Mol. Clin. Oncol.* **2019**, *12*, 9–14. [[CrossRef](#)]
27. Malumbres, M. Cyclin-Dependent Kinases. *Genome Biol.* **2014**, *15*, 122. [[CrossRef](#)]
28. Narasimha, A.M.; Kaulich, M.; Shapiro, G.S.; Choi, Y.J.; Sicinski, P.; Dowdy, S.F. Cyclin D Activates the Rb Tumor Suppressor by Mono-Phosphorylation. *eLife* **2014**, *3*, e02872. [[CrossRef](#)]
29. Ying, M.; Shao, X.; Jing, H.; Liu, Y.; Qi, X.; Cao, J.; Chen, Y.; Xiang, S.; Song, H.; Hu, R.; et al. Ubiquitin-Dependent Degradation of CDK2 Drives the Therapeutic Differentiation of AML by Targeting PRDX2. *Blood* **2018**, *131*, 2698–2711. [[CrossRef](#)]
30. Grishina, I.; Lattes, B. A Novel Cdk2 Interactor Is Phosphorylated by Cdc7 and Associates with Components of the Replication Complexes. *Cell. Cycle* **2005**, *4*, 4120–4126. [[CrossRef](#)]
31. Saurus, P.; Kuusela, S.; Dumont, V.; Lehtonen, E.; Fogarty, C.L.; Lassenius, M.I.; Forsblom, C.; Lehto, M.; Saleem, M.A.; Groop, P.-H.; et al. Cyclin-Dependent Kinase 2 Protects Podocytes from Apoptosis. *Sci. Rep.* **2016**, *6*, 21664. [[CrossRef](#)]
32. Chunder, N.; Wang, L.; Chen, C.; Hancock, W.W.; Wells, A.D. Cyclin-Dependent Kinase 2 Controls Peripheral Immune Tolerance. *J. Immunol.* **2012**, *189*, 5659–5666. [[CrossRef](#)]
33. Perez de Castro, I.; de Carcer, G.; Malumbres, M. A Census of Mitotic Cancer Genes: New Insights into Tumor Cell Biology and Cancer Therapy. *Carcinogenesis* **2006**, *28*, 899–912. [[CrossRef](#)]
34. Sherr, C.J. Cancer Cell Cycles. *Science* **1996**, *274*, 1672–1677. [[CrossRef](#)]
35. Keyomarsi, K.; O’Leary, N.; Molnar, G.; Lees, E.; Fingert, H.J.; Pardee, A.B. Cyclin E, a Potential Prognostic Marker for Breast Cancer. *Cancer Res.* **1994**, *54*, 380–385.
36. Keyomarsi, K.; Tucker, S.L.; Buchholz, T.A.; Callister, M.; Ding, Y.; Hortobagyi, G.N.; Bedrosian, I.; Knickerbocker, C.; Toyofuku, W.; Lowe, M.; et al. Cyclin E and Survival in Patients with Breast Cancer. *N. Engl. J. Med.* **2002**, *347*, 1566–1575. [[CrossRef](#)]
37. Yang, L.; Fang, D.; Chen, H.; Lu, Y.; Dong, Z.; Ding, H.-F.; Jing, Q.; Su, S.-B.; Huang, S. Cyclin-Dependent Kinase 2 Is an Ideal Target for Ovary Tumors with Elevated Cyclin E1 Expression. *Oncotarget* **2015**, *6*, 20801–20812. [[CrossRef](#)]
38. Zhao, Z.; Fan, X.; Yang, L.; Song, J.; Fang, S.; Tu, J.; Chen, M.; Zheng, L.; Wu, F.; Zhang, D.; et al. The Identification of a Common Different Gene Expression Signature in Patients with Colorectal Cancer. *Math. Biosci. Eng.* **2019**, *16*, 2942–2958. [[CrossRef](#)]
39. Ding, L.; Cao, J.; Lin, W.; Chen, H.; Xiong, X.; Ao, H.; Yu, M.; Lin, J.; Cui, Q. The Roles of Cyclin-Dependent Kinases in Cell-Cycle Progression and Therapeutic Strategies in Human Breast Cancer. *Int. J. Mol. Sci.* **2020**, *21*, 1960. [[CrossRef](#)]
40. Li, J.; Wang, Y.; Wang, X.; Yang, Q. CDK1 and CDC20 Overexpression in Patients with Colorectal Cancer Are Associated with Poor Prognosis: Evidence from Integrated Bioinformatics Analysis. *World J. Surg. Oncol.* **2020**, *18*, 50. [[CrossRef](#)]
41. Malumbres, M.; Barbacid, M. Cell Cycle, CDKs and Cancer: A Changing Paradigm. *Nat. Rev. Cancer* **2009**, *9*, 153–166. [[CrossRef](#)]
42. Mastrogamvraki, N.; Zaravinos, A. Signatures of Co-Deregulated Genes and Their Transcriptional Regulators in Colorectal Cancer. *Npj Syst. Biol. Appl.* **2020**, *6*, 23. [[CrossRef](#)]
43. Jardim, D.L.; Millis, S.Z.; Ross, J.S.; Woo, M.S.-A.; Ali, S.M.; Kurzrock, R. Cyclin Pathway Genomic Alterations Across 190,247 Solid Tumors: Leveraging Large-Scale Data to Inform Therapeutic Directions. *Oncologist* **2021**, *26*, e78–e89. [[CrossRef](#)]
44. Zhuang, K.; Zhang, J.; Xiong, M.; Wang, X.; Luo, X.; Han, L.; Meng, Y.; Zhang, Y.; Liao, W.; Liu, S. CDK5 Functions as a Tumor Promoter in Human Colorectal Cancer via Modulating the ERK5–AP-1 Axis. *Cell Death Dis.* **2016**, *7*, e2415. [[CrossRef](#)]
45. Ruiz de Porras, V.; Bystrup, S.; Cabrero-de las Heras, S.; Musulén, E.; Palomero, L.; Alonso, M.H.; Nieto, R.; Arango, D.; Moreno, V.; Queralt, C.; et al. Tumor Expression of Cyclin-Dependent Kinase 5 (Cdk5) Is a Prognostic Biomarker and Predicts Outcome of Oxaliplatin-Treated Metastatic Colorectal Cancer Patients. *Cancers* **2019**, *11*, 1540. [[CrossRef](#)]
46. Huang, P.-H.; Chen, M.-C.; Peng, Y.-T.; Kao, W.-H.; Chang, C.-H.; Wang, Y.-C.; Lai, C.-H.; Hsieh, J.-T.; Wang, J.-H.; Lee, Y.-T.; et al. Cdk5 Directly Targets Nuclear P21CIP1 and Promotes Cancer Cell Growth. *Cancer Res.* **2016**, *76*, 6888–6900. [[CrossRef](#)]
47. Firestein, R.; Bass, A.J.; Kim, S.Y.; Dunn, I.F.; Silver, S.J.; Guney, I.; Freed, E.; Ligon, A.H.; Vena, N.; Ogino, S.; et al. CDK8 Is a Colorectal Cancer Oncogene That Regulates β -Catenin Activity. *Nature* **2008**, *455*, 547–551. [[CrossRef](#)]
48. Firestein, R.; Shima, K.; Noshio, K.; Irahara, N.; Baba, Y.; Bojarski, E.; Giovannucci, E.L.; Hahn, W.C.; Fuchs, C.S.; Ogino, S. CDK8 Expression in 470 Colorectal Cancers in Relation to β -Catenin Activation, Other Molecular Alterations and Patient Survival. *Int. J. Cancer* **2010**, *126*, 2863–2873. [[CrossRef](#)]

49. Kim, H.-E.; Kim, D.-G.; Lee, K.J.; Son, J.G.; Song, M.-Y.; Park, Y.-M.; Kim, J.-J.; Cho, S.-W.; Chi, S.-G.; Cheong, H.S.; et al. Frequent Amplification of CENPF, GMNN and CDK13 Genes in Hepatocellular Carcinomas. *PLoS ONE* **2012**, *7*, e43223. [[CrossRef](#)]
50. Wang, J.; Liu, J.; Tian, F.; Zhan, Y.; Kong, D. Cyclin-dependent Kinase 9 Expression and Its Association with CD8+ T Cell Infiltration in Microsatellite-stable Colorectal Cancer. *Oncol. Lett.* **2019**, *18*, 6046–6056. [[CrossRef](#)]
51. Lu, H.; Fisher, R.P.; Bailey, P.; Levine, A.J. The CDK7-CycH-P36 Complex of Transcription Factor IIH Phosphorylates P53, Enhancing Its Sequence-Specific DNA Binding Activity in Vitro. *Mol. Cell Biol.* **1997**, *17*, 5923–5934. [[CrossRef](#)]
52. Jo, Y.S.; Kim, M.S.; Lee, S.H.; Yoo, N.J. Mutational Heterogeneity of MED23 Gene in Colorectal Cancers. *Pathol. Oncol. Res.* **2015**, *21*, 1281–1282. [[CrossRef](#)]
53. Calon, A.; Espinet, E.; Palomo-Ponce, S.; Tauriello, D.V.F.; Iglesias, M.; Céspedes, M.V.; Sevillano, M.; Nadal, C.; Jung, P.; Zhang, X.H.-F.; et al. Dependency of Colorectal Cancer on a TGF- β -Driven Program in Stromal Cells for Metastasis Initiation. *Cancer Cell* **2012**, *22*, 571–584. [[CrossRef](#)]
54. Broude, E.; Györffy, B.; Chumanevich, A.; Chen, M.; McDermott, M.; Shtutman, M.; Catroppo, J.; Roninson, I. Expression of CDK8 and CDK8-Interacting Genes as Potential Biomarkers in Breast Cancer. *Curr. Cancer Drug Targets* **2015**, *15*, 739–749. [[CrossRef](#)]
55. Roninson, I.B.; Györffy, B.; Mack, Z.T.; Shtil, A.A.; Shtutman, M.S.; Chen, M.; Broude, E.V. Identifying Cancers Impacted by CDK8/19. *Cells* **2019**, *8*, 821. [[CrossRef](#)]
56. Wu, D.; Zhang, Z.; Chen, X.; Yan, Y.; Liu, X. Angel or Devil?—CDK8 as the New Drug Target. *Eur. J. Med. Chem.* **2021**, *213*, 113043. [[CrossRef](#)]
57. Donner, A.J.; Szostek, S.; Hoover, J.M.; Espinosa, J.M. CDK8 Is a Stimulus-Specific Positive Coregulator of P53 Target Genes. *Mol. Cell.* **2007**, *27*, 121–133. [[CrossRef](#)]
58. Audetat, K.A.; Galbraith, M.D.; Odell, A.T.; Lee, T.; Pandey, A.; Espinosa, J.M.; Dowell, R.D.; Taatjes, D.J. A Kinase-Independent Role for Cyclin-Dependent Kinase 19 in P53 Response. *Mol. Cell Biol.* **2017**, *37*, e00626-16. [[CrossRef](#)]
59. Hermanowicz, J.M.; Pawlak, K.; Sieklucka, B.; Czarnomysy, R.; Kwiatkowska, I.; Kazberuk, A.; Surazynski, A.; Mojzych, M.; Pawlak, D. MM-129 as a Novel Inhibitor Targeting PI3K/AKT/MTOR and PD-L1 in Colorectal Cancer. *Cancers* **2021**, *13*, 3203. [[CrossRef](#)]
60. Gornowicz, A.; Szymanowska, A.; Mojzych, M.; Czarnomysy, R.; Bielawski, K.; Bielawska, A. The Anticancer Action of a Novel 1,2,4-Triazine Sulfonamide Derivative in Colon Cancer Cells. *Molecules* **2021**, *26*, 2045. [[CrossRef](#)]
61. Hermanowicz, J.M.; Kalaska, B.; Pawlak, K.; Sieklucka, B.; Miklosz, J.; Mojzych, M.; Pawlak, D. Preclinical Toxicity and Safety of MM-129—First-in-Class BTK/PD-L1 Inhibitor as a Potential Candidate against Colon Cancer. *Pharmaceutics* **2021**, *13*, 1222. [[CrossRef](#)]
62. Benson, C.; White, J.; Bono, J.D.; O'Donnell, A.; Raynaud, F.; Cruickshank, C.; McGrath, H.; Walton, M.; Workman, P.; Kaye, S.; et al. A Phase I Trial of the Selective Oral Cyclin-Dependent Kinase Inhibitor Seliciclib (CYC202; R-Roscovitine), Administered Twice Daily for 7 Days Every 21 Days. *Br. J. Cancer* **2007**, *96*, 29–37. [[CrossRef](#)]
63. Bukowski, K.; Marciniak, B.; Kciuk, M.; Mojzych, M.; Kontek, R. Pyrazolo[4,3-e]Tetrazolo[1,5-b][1,2,4]Triazine Sulfonamides as Novel Potential Anticancer Agents: Cytotoxic and Genotoxic Activities In Vitro. *Molecules* **2022**, *27*, 3761. [[CrossRef](#)]
64. Hermanowicz, J.M.; Szymanowska, A.; Sieklucka, B.; Czarnomysy, R.; Pawlak, K.; Bielawska, A.; Bielawski, K.; Kalafut, J.; Przybyszewska, A.; Surazynski, A.; et al. Exploration of Novel Heterofused 1,2,4-Triazine Derivative in Colorectal Cancer. *J. Enzym. Inhib. Med. Chem.* **2021**, *36*, 535–548. [[CrossRef](#)]
65. Gornowicz, A.; Szymanowska, A.; Mojzych, M.; Bielawski, K.; Bielawska, A. The Effect of Novel 7-Methyl-5-Phenyl-Pyrazolo[4,3-e]Tetrazolo[4,5-b][1,2,4]Triazine Sulfonamide Derivatives on Apoptosis and Autophagy in DLD-1 and HT-29 Colon Cancer Cells. *Int. J. Mol. Sci.* **2020**, *21*, 5221. [[CrossRef](#)]
66. Kciuk, M.; Mujwar, S.; Szymanowska, A.; Marciniak, B.; Bukowski, K.; Mojzych, M.; Kontek, R. Preparation of Novel Pyrazolo[4,3-e]Tetrazolo[1,5-b][1,2,4]Triazine Sulfonamides and Their Experimental and Computational Biological Studies. *Int. J. Mol. Sci.* **2022**, *23*, 5892. [[CrossRef](#)]
67. Ly, J.D.; Grubb, D.R.; Lawen, A. The Mitochondrial Membrane Potential ($\Delta\psi(m)$) in Apoptosis; an Update. *Apoptosis* **2003**, *8*, 115–128. [[CrossRef](#)]
68. Wacquier, B.; Combettes, L.; Dupont, G. Dual Dynamics of Mitochondrial Permeability Transition Pore Opening. *Sci. Rep.* **2020**, *10*, 3924. [[CrossRef](#)]
69. Redza-Dutordoir, M.; Averill-Bates, D.A. Activation of Apoptosis Signalling Pathways by Reactive Oxygen Species. *Biochim. Biophys. Acta (BBA) Mol. Cell Res.* **2016**, *1863*, 2977–2992. [[CrossRef](#)]
70. Gottlieb, E.; Armour, S.M.; Harris, M.H.; Thompson, C.B. Mitochondrial Membrane Potential Regulates Matrix Configuration and Cytochrome c Release during Apoptosis. *Cell Death Differ.* **2003**, *10*, 709–717. [[CrossRef](#)]
71. Suski, J.; Lebiecinska, M.; Bonora, M.; Pinton, P.; Duszynski, J.; Wieckowski, M.R. Relation Between Mitochondrial Membrane Potential and ROS Formation. In *Mitochondrial Bioenergetics*; Palmeira, C.M., Moreno, A.J., Eds.; Methods in Molecular Biology; Springer New York: New York, NY, USA, 2018; Volume 1782, pp. 357–381, ISBN 978-1-4939-7830-4.
72. Sahoo, B.M.; Banik, B.K.; Borah, P.; Jain, A. Reactive Oxygen Species (ROS): Key Components in Cancer Therapies. *Anti Cancer Agents Med. Chem.* **2022**, *22*, 215–222. [[CrossRef](#)]
73. Pallardy, M.; Biola, A.; Lebrec, H.; Bréard, J. Assessment of Apoptosis in Xenobiotic-Induced Immunotoxicity. *Methods* **1999**, *19*, 36–47. [[CrossRef](#)]

74. Qi, H.; Xu, G.; Peng, X.-L.; Li, X.; Shuai, J.; Xu, R. Roles of Four Feedback Loops in Mitochondrial Permeability Transition Pore Opening Induced by Ca^{2+} and Reactive Oxygen Species. *Phys. Rev. E* **2020**, *102*, 062422. [[CrossRef](#)]
75. Vrabec, J.P.; Lieven, C.J.; Levin, L.A. Cell-Type-Specific Opening of the Retinal Ganglion Cell Mitochondrial Permeability Transition Pore. *Investig. Ophthalmol. Vis. Sci.* **2003**, *44*, 2774. [[CrossRef](#)]
76. Mounjaroen, J.; Nimmannit, U.; Callery, P.S.; Wang, L.; Azad, N.; Lipipun, V.; Chanvorachote, P.; Rojanasakul, Y. Reactive Oxygen Species Mediate Caspase Activation and Apoptosis Induced by Lipoic Acid in Human Lung Epithelial Cancer Cells through Bcl-2 Down-Regulation. *J. Pharmacol. Exp. Ther.* **2006**, *319*, 1062–1069. [[CrossRef](#)]
77. Kim, S.J.; Kim, H.S.; Seo, Y.R. Understanding of ROS-Inducing Strategy in Anticancer Therapy. *Oxidative Med. Cell. Longev.* **2019**, *2019*, 5381692. [[CrossRef](#)]
78. Khan, A.Q.; Rashid, K.; AlAmodi, A.A.; Agha, M.V.; Akhtar, S.; Hakeem, I.; Raza, S.S.; Uddin, S. Reactive Oxygen Species (ROS) in Cancer Pathogenesis and Therapy: An Update on the Role of ROS in Anticancer Action of Benzophenanthridine Alkaloids. *Biomed. Pharmacother.* **2021**, *143*, 112142. [[CrossRef](#)]
79. Shen, B.; He, P.-J.; Shao, C.-L. Norcantharidin Induced DU145 Cell Apoptosis through ROS-Mediated Mitochondrial Dysfunction and Energy Depletion. *PLoS ONE* **2013**, *8*, e84610. [[CrossRef](#)]
80. Brenneisen, P.; Reichert, A. Nanotherapy and Reactive Oxygen Species (ROS) in Cancer: A Novel Perspective. *Antioxidants* **2018**, *7*, 31. [[CrossRef](#)]
81. Qu, W.; Zhao, Z.; Chen, S.; Zhang, L.; Wu, D.; Chen, Z. Bisphenol A Suppresses Proliferation and Induces Apoptosis in Colonic Epithelial Cells through Mitochondrial and MAPK/AKT Pathways. *Life Sci.* **2018**, *208*, 167–174. [[CrossRef](#)]
82. Oliveira, M.d.S.; Barbosa, M.I.F.; de Souza, T.B.; Moreira, D.R.M.; Martins, F.T.; Villarreal, W.; Machado, R.P.; Doriguetto, A.C.; Soares, M.B.P.; Bezerra, D.P. A Novel Platinum Complex Containing a Piplartine Derivative Exhibits Enhanced Cytotoxicity, Causes Oxidative Stress and Triggers Apoptotic Cell Death by ERK/P38 Pathway in Human Acute Promyelocytic Leukemia HL-60 Cells. *Redox Biol.* **2019**, *20*, 182–194. [[CrossRef](#)]
83. Stennicke, H.R.; Deveraux, Q.L.; Humke, E.W.; Reed, J.C.; Dixit, V.M.; Salvesen, G.S. Caspase-9 Can Be Activated without Proteolytic Processing. *J. Biol. Chem.* **1999**, *274*, 8359–8362. [[CrossRef](#)]
84. Kaufmann, S.H.; Earnshaw, W.C. Induction of Apoptosis by Cancer Chemotherapy. *Exp. Cell Res.* **2000**, *256*, 42–49. [[CrossRef](#)]
85. Kagan, V.E.; Tyurin, V.A.; Jiang, J.; Tyurina, Y.Y.; Ritov, V.B.; Amoscato, A.A.; Osipov, A.N.; Belikova, N.A.; Kapralov, A.A.; Kini, V.; et al. Cytochrome c Acts as a Cardiolipin Oxygenase Required for Release of Proapoptotic Factors. *Nat. Chem. Biol.* **2005**, *1*, 223–232. [[CrossRef](#)]
86. Zuo, Y.; Xiang, B.; Yang, J.; Sun, X.; Wang, Y.; Cang, H.; Yi, J. Oxidative Modification of Caspase-9 Facilitates Its Activation via Disulfide-Mediated Interaction with Apaf-1. *Cell Res.* **2009**, *19*, 449–457. [[CrossRef](#)]
87. Wilkie-Grantham, R.P.; Matsuzawa, S.-I.; Reed, J.C. Novel Phosphorylation and Ubiquitination Sites Regulate Reactive Oxygen Species-Dependent Degradation of Anti-Apoptotic c-FLIP Protein. *J. Biol. Chem.* **2013**, *288*, 12777–12790. [[CrossRef](#)]
88. Zhang, N.; Hartig, H.; Dzhagalov, I.; Draper, D.; He, Y.W. The Role of Apoptosis in the Development and Function of T Lymphocytes. *Cell. Res.* **2005**, *15*, 749–769. [[CrossRef](#)]
89. Kavurma, M.M.; Tan, N.Y.; Bennett, M.R. Death Receptors and Their Ligands in Atherosclerosis. *Arterioscler. Thromb. Vasc. Biol.* **2008**, *28*, 1694–1702. [[CrossRef](#)]
90. Villalpando-Rodriguez, G.E.; Gibson, S.B. Reactive Oxygen Species (ROS) Regulates Different Types of Cell Death by Acting as a Rheostat. *Oxidative Med. Cell. Longev.* **2021**, *2021*, 9912436. [[CrossRef](#)]
91. Gao, K.; Liang, Q.; Zhao, Z.-H.; Li, Y.-F.; Wang, S.-F. Synergistic Anticancer Properties of Docosahexaenoic Acid and 5-Fluorouracil through Interference with Energy Metabolism and Cell Cycle Arrest in Human Gastric Cancer Cell Line AGS Cells. *World J. Gastroenterol.* **2016**, *22*, 2971. [[CrossRef](#)]
92. Li, M.-H.; Ito, D.; Sanada, M.; Odani, T.; Hatori, M.; Iwase, M.; Nagumo, M. Effect of 5-Fluorouracil on G1 Phase Cell Cycle Regulation in Oral Cancer Cell Lines. *Oral. Oncol.* **2004**, *40*, 63–70. [[CrossRef](#)]
93. Gao, L.; Shen, L.; Yu, M.; Ni, J.; Dong, X.; Zhou, Y.; Wu, S. Colon Cancer Cells Treated with 5-Fluorouracil Exhibit Changes in Polylactosamine-Type N-Glycans. *Mol. Med. Rep.* **2014**, *9*, 1697–1702. [[CrossRef](#)]
94. Wlodkowic, D.; Skommer, J.; Darzynkiewicz, Z. Flow Cytometry-Based Apoptosis Detection. In *Apoptosis*; Erhardt, P., Toth, A., Eds.; Methods in Molecular Biology; Humana Press: Totowa, NJ, USA, 2009; Volume 559, pp. 19–32, ISBN 978-1-60327-016-8.
95. Kasibhatla, S.; Amarante-Mendes, G.P.; Finucane, D.; Brunner, T.; Bossy-Wetzell, E.; Green, D.R. Acridine Orange/Ethidium Bromide (AO/EB) Staining to Detect Apoptosis. *Cold Spring Harb. Protoc.* **2006**, *2006*, pdb.prot4493. [[CrossRef](#)]
96. Wu, X. Dual AO/EB Staining to Detect Apoptosis in Osteosarcoma Cells Compared with Flow Cytometry. *Med. Sci. Monit. Basic Res.* **2015**, *21*, 15–20. [[CrossRef](#)]
97. Xiao, B.; Deng, X.; Zhou, W.; Tan, E.-K. Flow Cytometry-Based Assessment of Mitophagy Using MitoTracker. *Front. Cell. Neurosci.* **2016**, *10*, 76. [[CrossRef](#)]
98. Ruiz-Leal, M.; George, S. An in Vitro Procedure for Evaluation of Early Stage Oxidative Stress in an Established Fish Cell Line Applied to Investigation of PHAH and Pesticide Toxicity. *Mar. Environ. Res.* **2004**, *58*, 631–635. [[CrossRef](#)]
99. Pozarowski, P.; Darzynkiewicz, Z. Analysis of Cell Cycle by Flow Cytometry. In *Checkpoint Controls and Cancer*; Humana Press: New Jersey, USA, 2004; Volume 281, pp. 301–312, ISBN 978-1-59259-811-3.
100. Toukan, K.; Rahman, A. Molecular-Dynamics Study of Atomic Motions in Water. *Phys. Rev. B* **1985**, *31*, 2643–2648. [[CrossRef](#)]

101. Gahtori, J.; Pant, S.; Srivastava, H.K. Modeling Antimalarial and Antihuman African Trypanosomiasis Compounds: A Ligand- and Structure-Based Approaches. *Mol. Divers.* **2020**, *24*, 1107–1124. [[CrossRef](#)]
102. Posch, H.A.; Hoover, W.G.; Vesely, F.J. Canonical Dynamics of the Nosé Oscillator: Stability, Order, and Chaos. *Phys. Rev. A* **1986**, *33*, 4253–4265. [[CrossRef](#)]

Disclaimer/Publisher's Note: The statements, opinions and data contained in all publications are solely those of the individual author(s) and contributor(s) and not of MDPI and/or the editor(s). MDPI and/or the editor(s) disclaim responsibility for any injury to people or property resulting from any ideas, methods, instructions or products referred to in the content.

Table S1. Cytotoxic properties of **MM129**, **MM130**, and **MM131** presented as IC_{50} . Mean values and 95% confidence intervals (parentheses) are given in μM [1].

Cell type	MM129	MM130	MM131
PBMCs	1.11 (0.98–1.26)	0.77 (0.71–0.84)	0.62 (0.52–0.72)
Hs27	1.15 (0.95–1.37)	0.81 (0.64–0.99)	0.62 (0.43–0.82)
HeLa	0.9 (0.73–1.06)	0.59 (0.51–0.67)	0.41 (0.28–0.54)
HCT 116	0.6 (0.58–0.62)	0.44 (0.43–0.45)	0.39 (0.37–0.41)
PC-3	0.36 (0.32–0.4)	0.22 (0.18–0.28)	0.17 (0.16–0.17)
BxPC-3	0.26 (0.2–0.32)	0.17 (0.13–0.21)	0.13 (0.11–0.15)

1. Flow Cytometry Assessment of Annexin V Binding

Figures S1-S12 show the exemplary flow cytometry (Annexin V-FITC/PI assay) dot-plots for depicting apoptotic and necrotic changes in examined cancer cell lines (Hela, HCT 116, PC-3, and BxPC-3) exposed to **MM129**, **MM130**, and **MM131** in concentrations of $\frac{1}{2} IC_{50}$, IC_{50} , and $2 \times IC_{50}$ for 24-h, 48-h, and 72-h. Q1 (upper left quadrant) – necrotic cells (Annexin V-, PI+); Q2 (upper right quadrant) – late apoptotic cells (Annexin V+, PI+); Q3 (lower right quadrant) – early apoptotic cells (Annexin V+, PI-); Q4 (lower left quadrant) – live cells (Annexin V-, PI-).

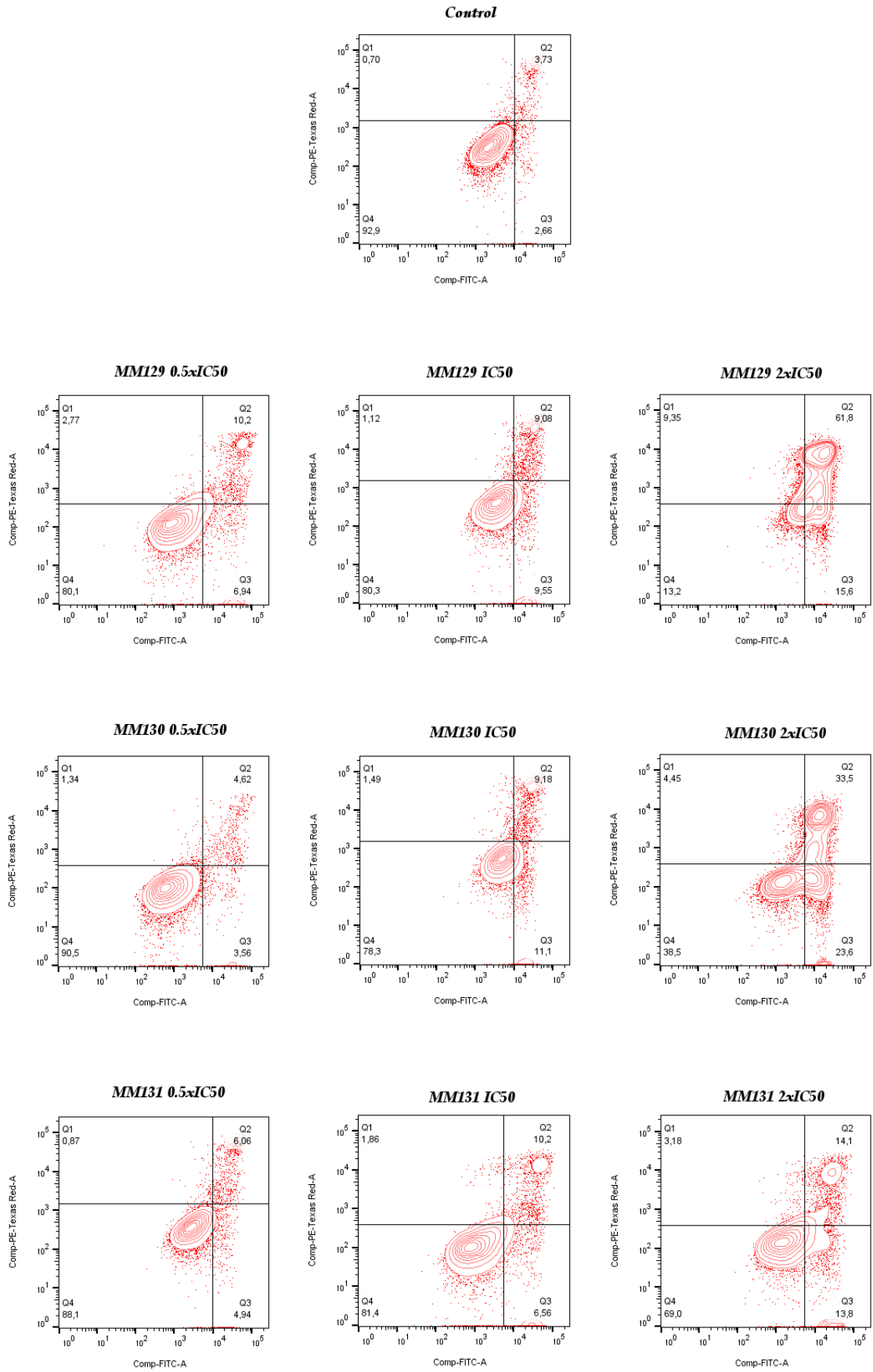


Figure S1. Hela cells after 24-h of exposure to MM-compounds.

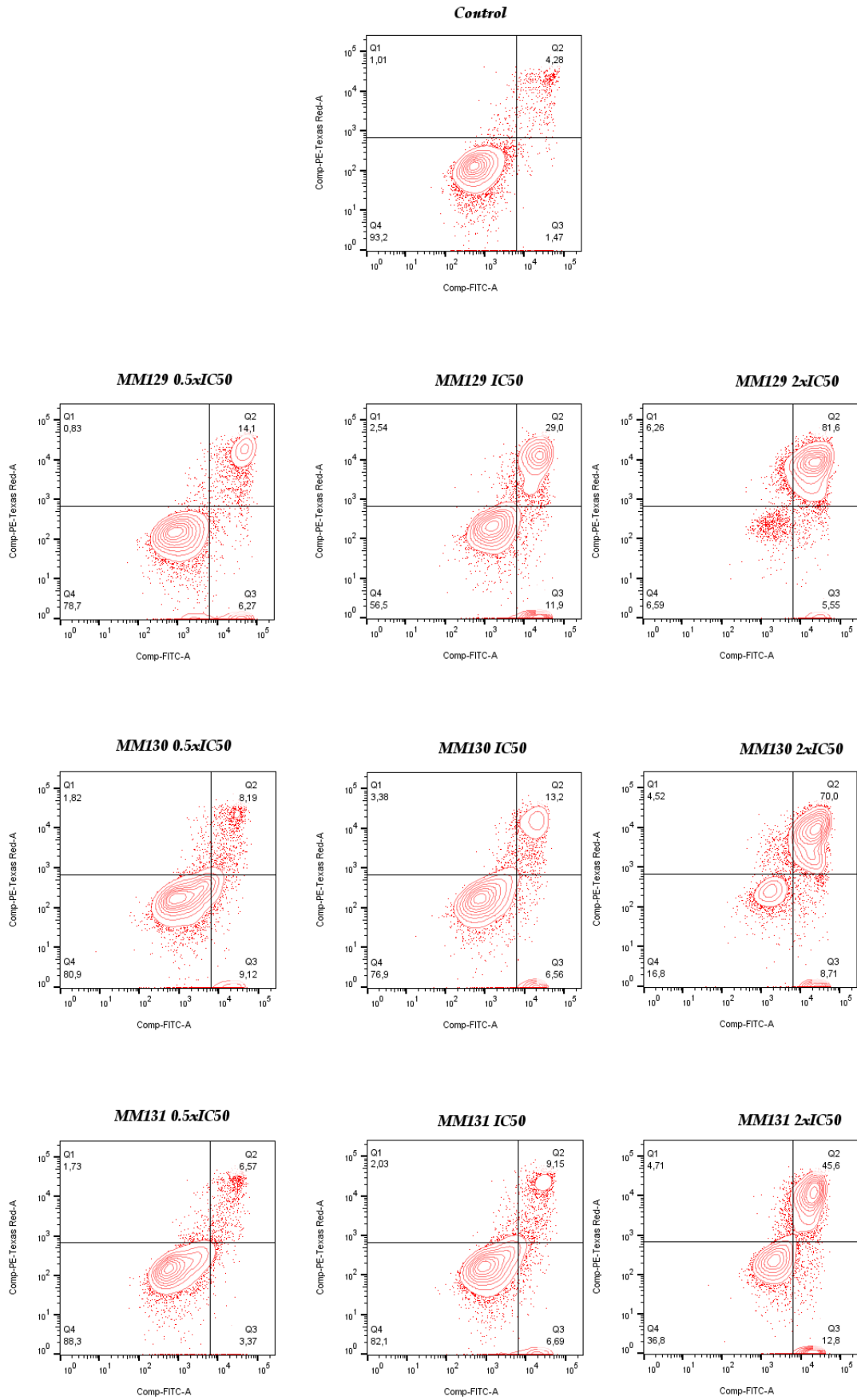


Figure S2. Hela cells after 48-h of exposure to MM-compounds.

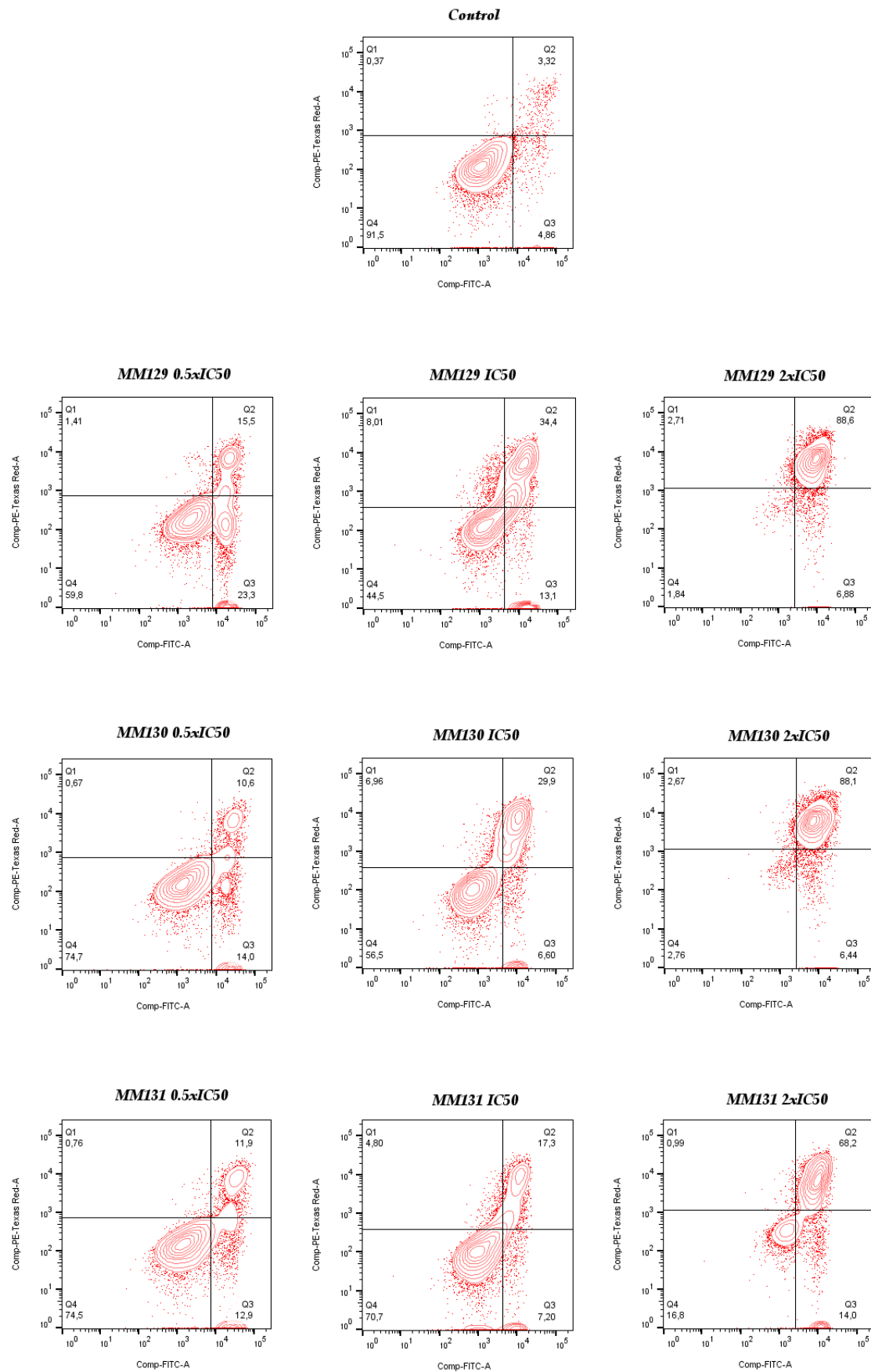


Figure S3. HeLa cells after 72-h of exposure to MM-compounds.

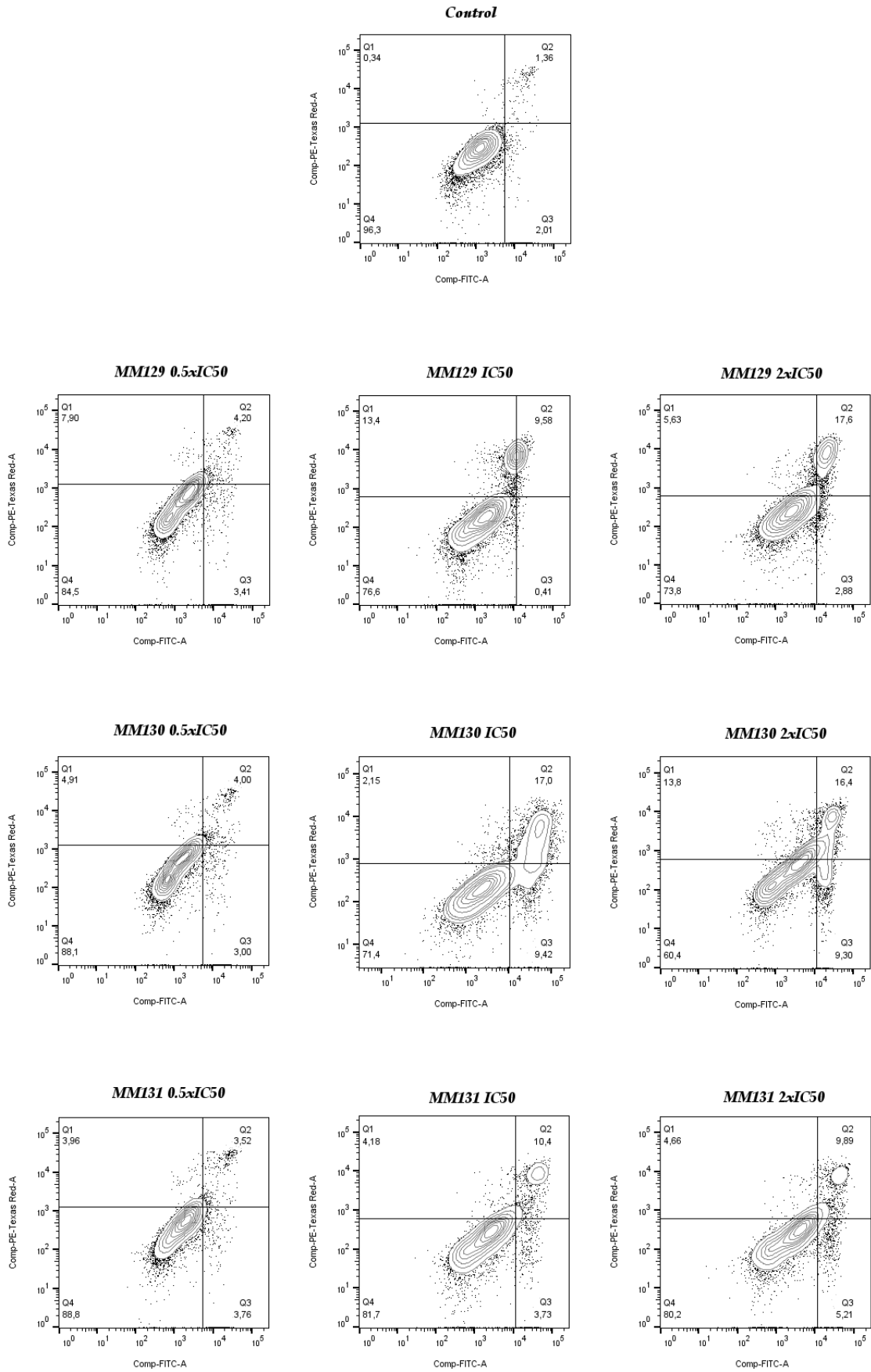


Figure S4. HCT 116 cells after 24-h of exposure to MM-compounds.

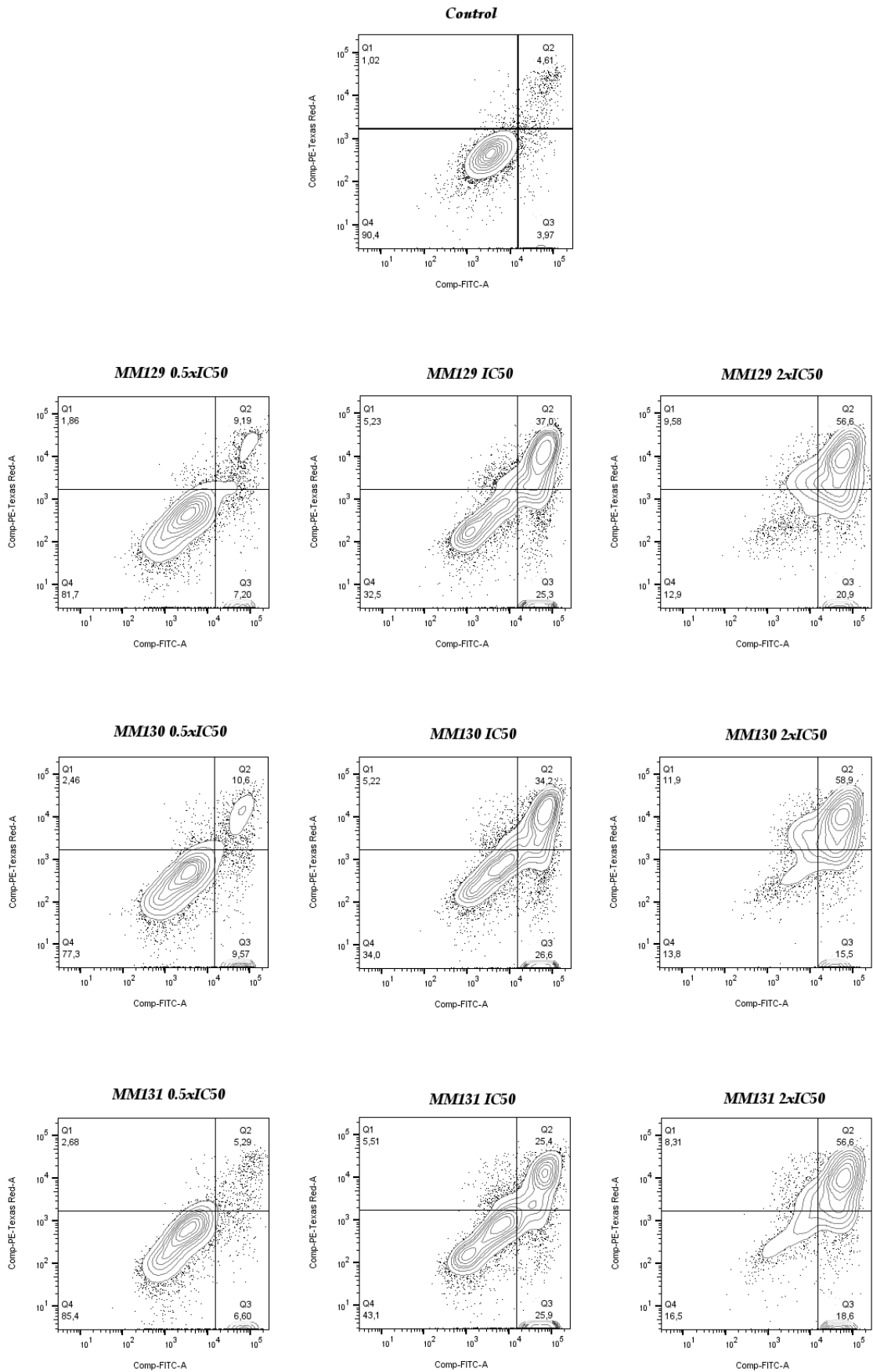


Figure S5. HCT 116 cells after 48-h of exposure to MM-compounds.

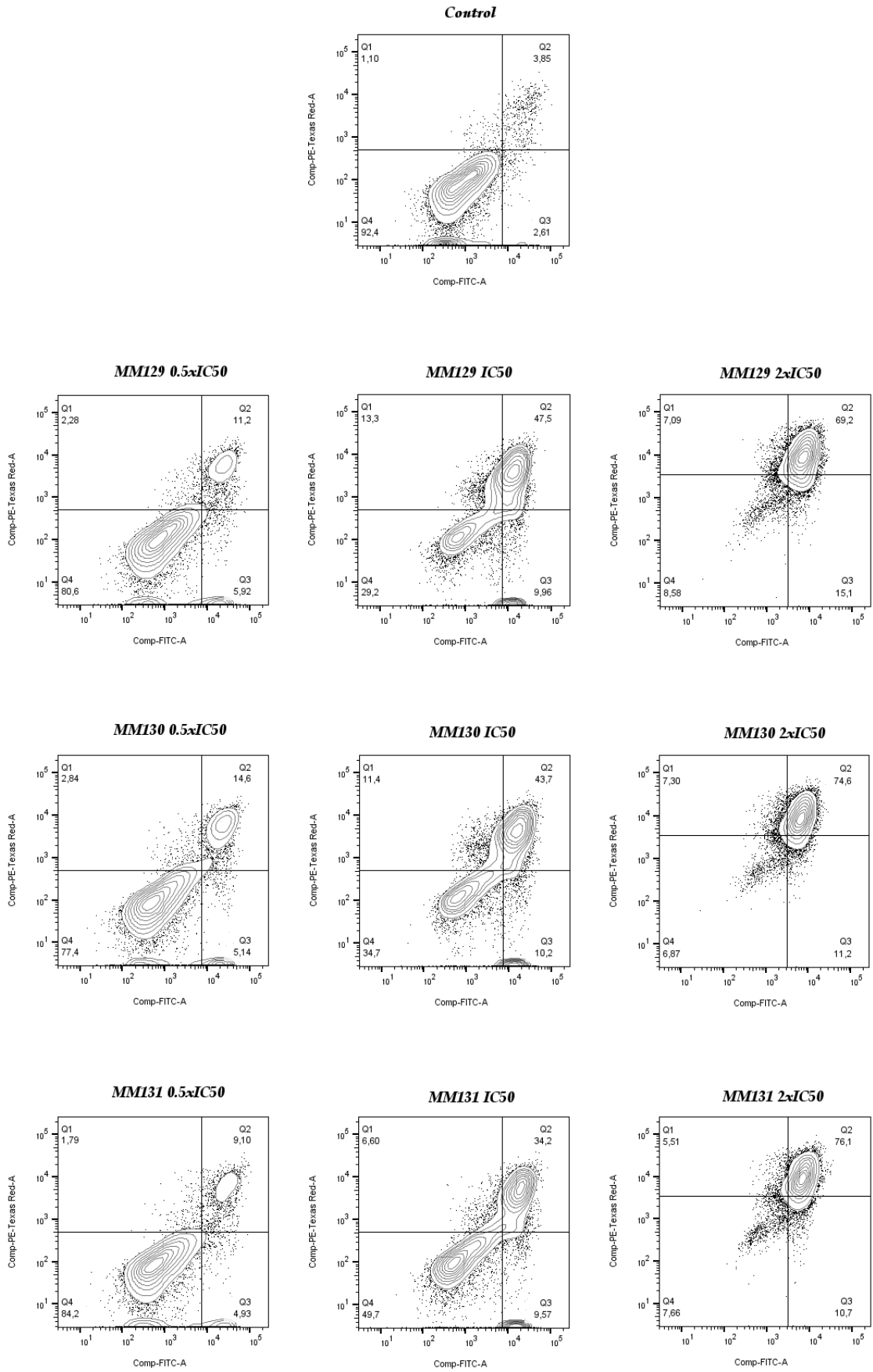


Figure S6. HCT 116 cells after 72-h of exposure to MM-compounds.

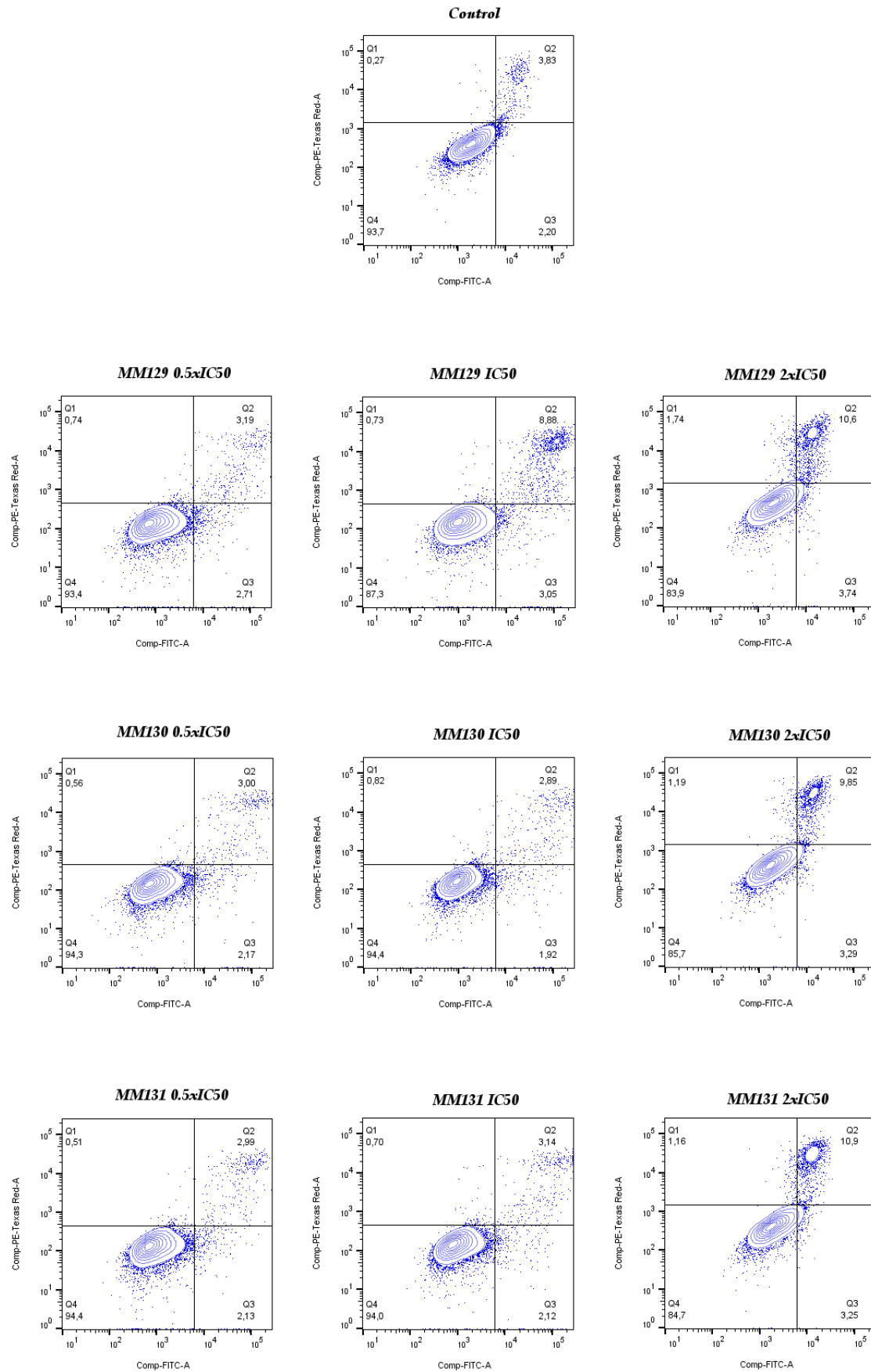


Figure S7. PC-3 cells after 24-h of exposure to MM-compounds.

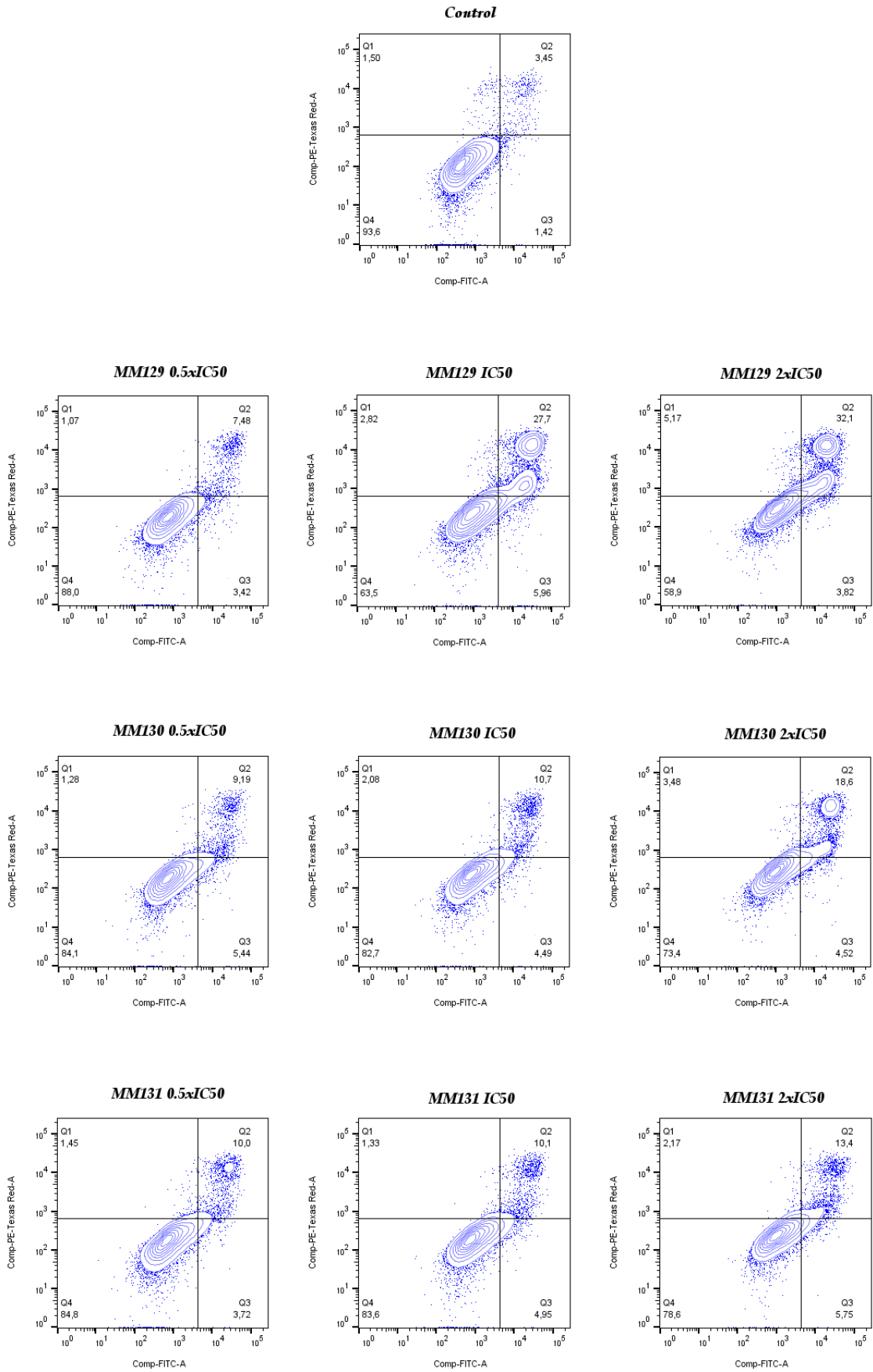


Figure S8. PC-3 cells after 48-h of exposure to MM-compounds.

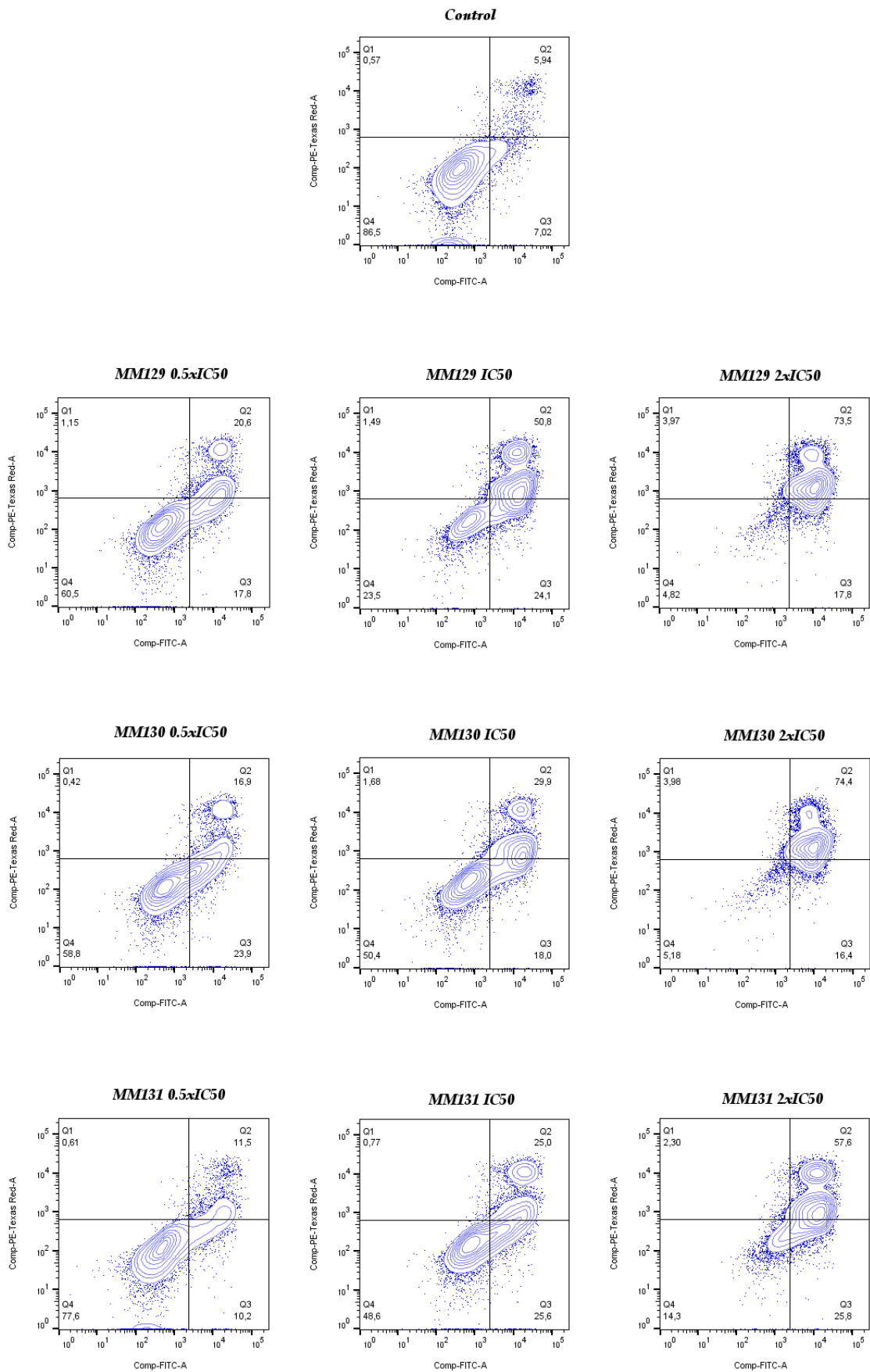


Figure S9. PC-3 cells after 72-h of exposure to MM-compounds.

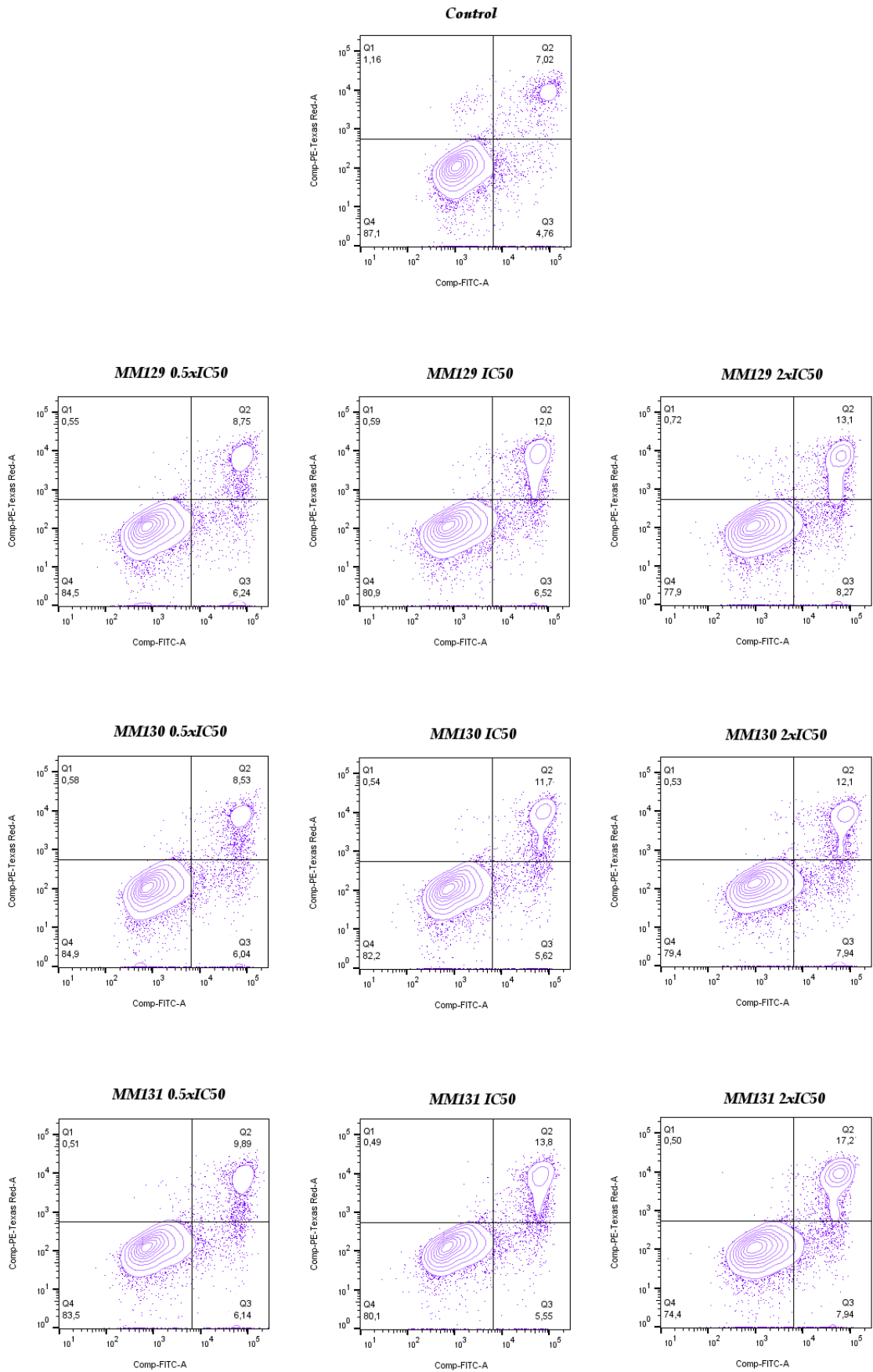


Figure S10. BxPC-3 cells after 24-h of exposure to MM-compounds.

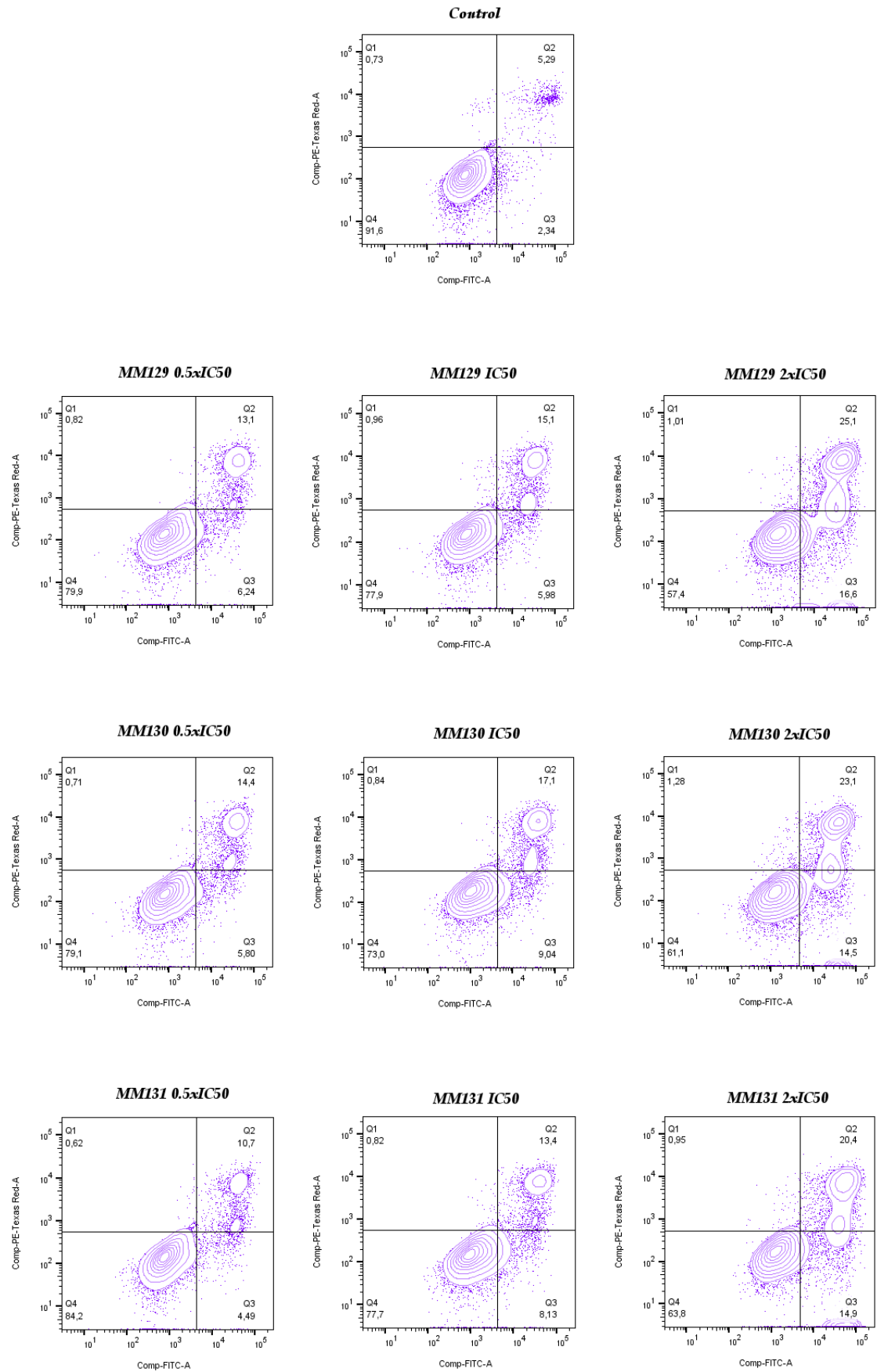


Figure S11. BxPC-3 cells after 48-h of exposure to MM-compounds.

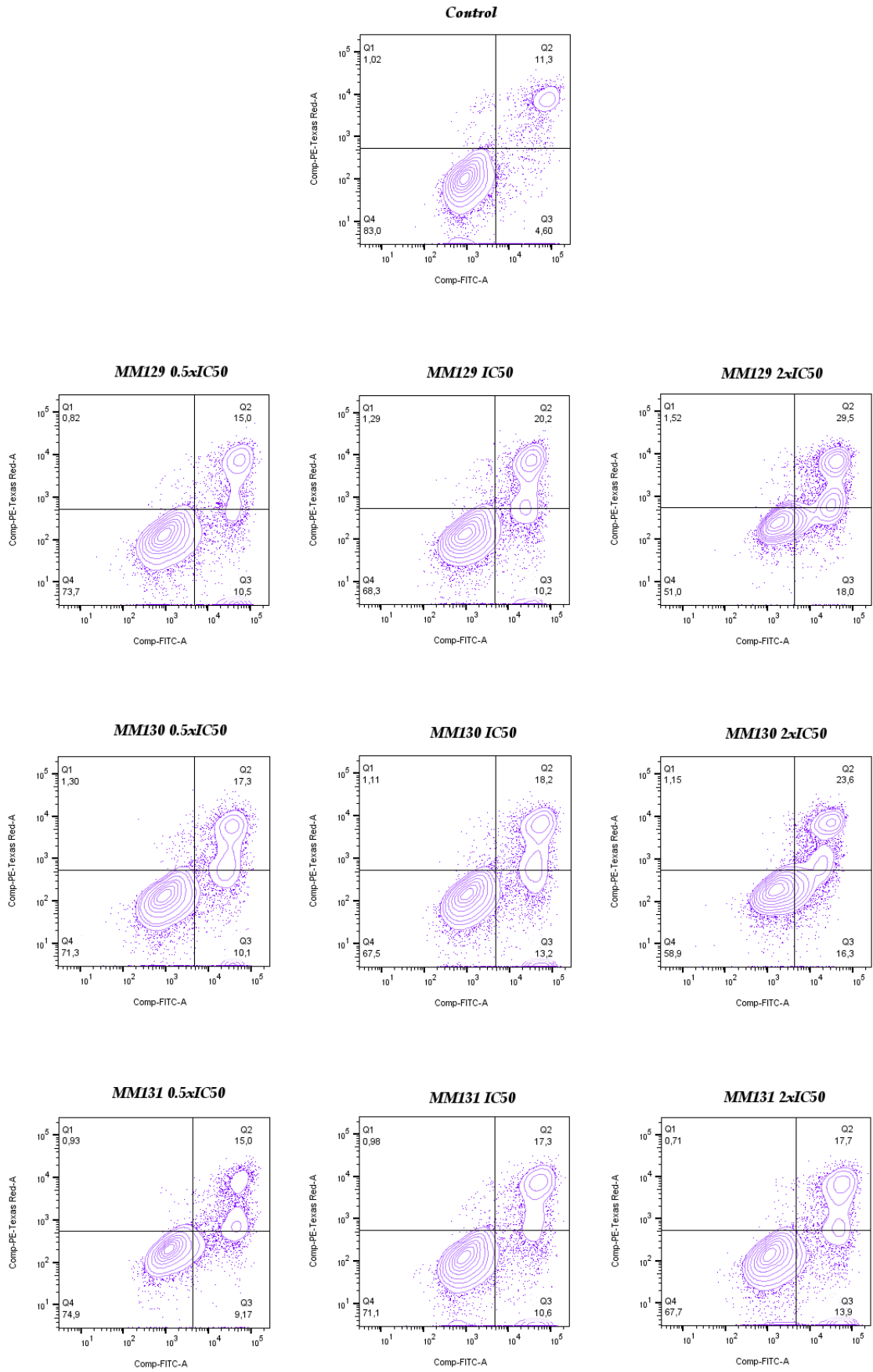


Figure S12. BxPC-3 cells after 72-h of exposure to MM-compounds.

2. Cell cycle analysis

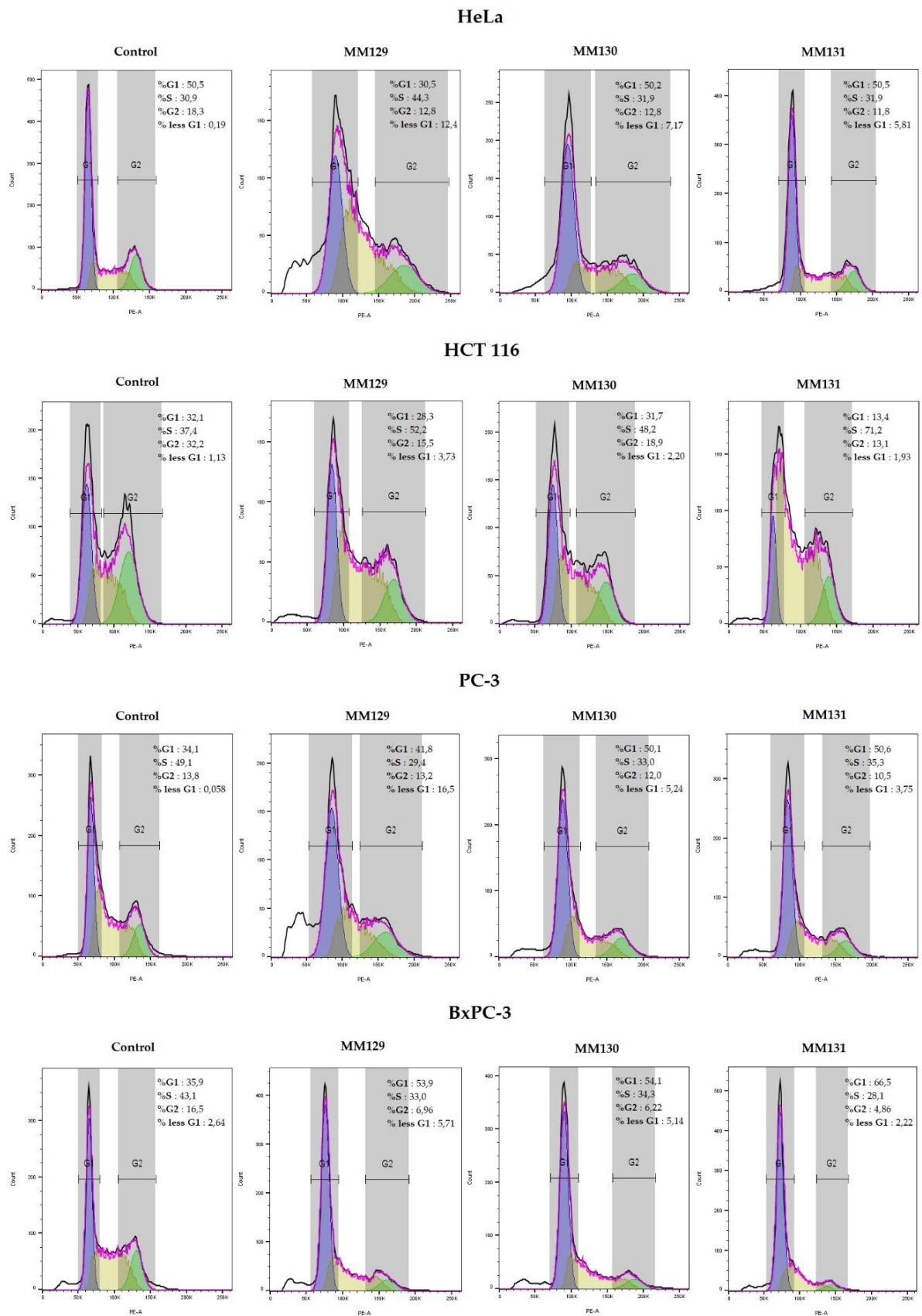


Figure S13. Representative dot-plots presenting the cell cycle distribution of HeLa, HCT 116, PC-3 and BxPC-3 cell lines after their 24-h incubation with MM129, MM130, and MM131 in the concentration of IC₅₀.

Table S2. Comparison of anticancer activity of **MM129**, **MM130**, and **MM131** in the concentration of IC_{50} toward HeLa, HCT 116, PC-3, and BxPC-3 cancer cells following 24-h and/or 48-h treatment. Significant differences ($p < 0.05$) compared with control (bold and *). MM compound that exhibited the highest activity (significant differences $p < 0.05$) among investigated sulfonamides in the given assay is blue color-coded.

Method	Exposure time	Cell line	Control	MM129	MM130	MM131
Annexin V binding ¹	24-h	HeLa	6.7 ± 0.7	17.4 ± 1.7 *	17.3 ± 2.6 *	15.5 ± 1.4 *
		HCT 116	6.9 ± 2.6	14.4 ± 2.7 *	16.8 ± 6.3 *	14.3 ± 3.3 *
		PC-3	9 ± 2.8	9 ± 3.4	5.9 ± 2.2	6.2 ± 2.7
		BxPC-3	13.8 ± 1.8	17.1 ± 1.2	18.1 ± 3.2	18.5 ± 1.3
	48-h	HeLa	7.1 ± 1.8	40 ± 0.82 *	20.6 ± 1.7 *	15.9 ± 0.66 *
		HCT 116	10.4 ± 2.3	61 ± 1.1 *	57.3 ± 3 *	50.2 ± 1 *
		PC-3	6.7 ± 1.6	23.3 ± 9 *	14.3 ± 0.8	14.4 ± 1
		BxPC-3	12 ± 3.4	19.4 ± 3.3 *	24.8 ± 4.4 *	21.2 ± 1.9 *
MitoTracker Red CMXRos ²	24-h	HeLa		85.5 ± 7.6	87.6 ± 2.2	87.5 ± 0.9
		HCT 116		83.6 ± 2.8 *	88.6 ± 3.5	85.4 ± 1.8
		PC-3		91.7 ± 8.5	91.2 ± 6.7	92.1 ± 1.4
		BxPC-3		90.5 ± 3.1	87.3 ± 3.7	89.8 ± 7
	48-h	HeLa		86.5 ± 5.3	88 ± 1.3	86.9 ± 6.9
		HCT 116		80.2 ± 7.9 *	82.8 ± 5.2 *	85.3 ± 2.3
		PC-3		80.2 ± 10.8	86.6 ± 2.1	83.2 ± 3.5
		BxPC-3		84.5 ± 8.1	87.4 ± 1.6	85.4 ± 8.7
AO/EB dual staining ¹	48-h	HeLa	1.3 ± 0.6	32 ± 6.1 *	23.3 ± 2.5 *	13.3 ± 1.5 *
		HCT 116	2.3 ± 2.1	23.3 ± 5.5 *	14.3 ± 4.5 *	21 ± 7.2 *
		PC-3	6 ± 2	8.7 ± 1.5	11.7 ± 1.5	7 ± 3
		BxPC-3	3 ± 2	16.3 ± 3.5 *	13 ± 2.6 *	14.7 ± 2.3 *
Cell cycle ³	24-h	HeLa		↑ subG1; ↓ G0/G1	—	—
		HCT 116		↑ S; ↓ G2/M	↑ S; ↓ G2/M	↑ S; ↓ G2/M; ↓ G0/G1
		PC-3		↑ subG1; ↓ S;	↑ subG1; ↓ S; ↑ G0/G1	↑ subG1; ↓ S; ↑ G0/G1
		BxPC-3		↑ G0/G1; ↓ G2/M	↑ G0/G1; ↓ G2/M	↑ G0/G1; ↓ G2/M

¹ Percentage of apoptotic cells shown as the mean ± SD.

² Changes in $\Delta\Psi_m$ presented as a mean ± SD relative to the control group normalized to 100%.

³ A significant ($p < 0.05$) increase (↑) or decrease (↓) in the percentage of cells in a particular cell cycle phase.

References:

- Bukowski, K.; Marciniak, B.; Kciuk, M.; Mojzych, M.; Kontek, R. Pyrazolo[4,3-e]Tetrazolo[1,5-b][1,2,4]Triazine Sulfonamides as Novel Potential Anticancer Agents: Cytotoxic and Genotoxic Activities In Vitro. *Molecules* **2022**, *27*, 3761, doi:10.3390/molecules27123761.

Oświadczenia współautorów publikacji

Łódź dn.31.05.2023

Mgr Karol Bukowski

Katedra Biotechnologii Molekularnej i Genetyki

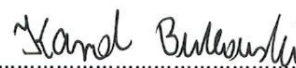
Uniwersytet Łódzki

Oświadczenie współautora

Dotyczy publikacji

Bukowski, K.; Kciuk, M.; Kontek, R. Mechanisms of Multidrug Resistance in Cancer Chemotherapy. Int. J. Mol. Sci. 2020, 21, 3233. <https://doi.org/10.3390/ijms21093233> (MEiN= 140 pkt, IF = 5,923).

Oświadczam, że mój udział w publikacji polegał na opracowaniu koncepcji pracy, zebraniu odnośników literaturowych, wykonaniu grafik, napisaniu pracy i korekty po jej recenzji. Mój udział oceniam na 80%.



Mgr Karol Bukowski

Łódź dn.31.05.2023

Mgr Mateusz Kciuk

Katedra Biotechnologii Molekularnej i Genetyki

Uniwersytet Łódzki

Oświadczenie współautora

Dotyczy publikacji

Bukowski, K.; Kciuk, M.; Kontek, R. Mechanisms of Multidrug Resistance in Cancer Chemotherapy. Int. J. Mol. Sci. 2020, 21, 3233. <https://doi.org/10.3390/ijms21093233> (MEiN= 140 pkt, IF = 5,923).

Oświadczam, że mój udział w publikacji polegał na zebraniu odnośników literaturowych i współudziale w napisaniu rozdziału „*Increased DNA Repair Capacity*” w pracy. Mój udział oceniam na 5%.

Mateusz Kciuk

Mgr Mateusz Kciuk

Łódź dn.31.05.2023

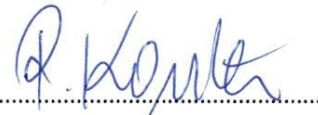
dr hab. Renata Kontek, prof. UŁ
Katedra Biotechnologii Molekularnej i Genetyki
Uniwersytet Łódzki

Oświadczenie współautora

Dotyczy publikacji

Bukowski, K.; Kciuk, M.; Kontek, R. Mechanisms of Multidrug Resistance in Cancer Chemotherapy. Int. J. Mol. Sci. 2020, 21, 3233. <https://doi.org/10.3390/ijms21093233> (MEiN = 140 pkt, IF = 5,923).

Oświadczam, że mój udział w publikacji polegał na współudziale w powstaniu koncepcji pracy, ocenie merytorycznej pracy oraz korekcje manuskryptu. Mój udział oceniam na 15%.



dr hab. Renata Kontek

Łódź dn.31.05.2023

Mgr Karol Bukowski

Katedra Biotechnologii Molekularnej i Genetyki

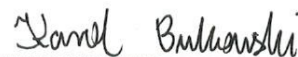
Uniwersytet Łódzki

Oświadczenie współautora

Dotyczy publikacji

Bukowski K., Marciniak, B.; Kciuk, M.; Mojzych, M.; Kontek, R. Pyrazolo[4,3-e]tetrazolo[1,5-b][1,2,4]triazine Sulfonamides as Novel Potential Anticancer Agents: Cytotoxic and Genotoxic Activities In Vitro. *Molecules* **2022**, 27, 3761. <https://doi.org/10.3390/molecules27123761>. (MEiN= 140 pkt, IF = 4,927).

Oświadczam, że mój udział w publikacji polegał na współudziale w powstaniu koncepcji pracy, zaplanowaniu doświadczeń oraz ich wykonaniu. Przeprowadziłem wszystkie eksperymenty dotyczące oceny właściwości cytotoksycznych i genotoksycznych badanych związków MM (analiza uszkodzeń jedno- i dwuniciowych DNA metodą kometową, zarówno w wersji alkalicznej, jak i neutralnej, a także immunocytochemiczne barwienie histonu H2AX). Dokonałem interpretacji i analizy statystycznej wyników oraz opracowałem manuskrypt publikacji. Mój udział oceniam na 70%.



Mgr Karol Bukowski

Łódź dn.31.05.2023

dr Beata Marciniak

Katedra Biotechnologii Molekularnej i Genetyki

Uniwersytet Łódzki

Oświadczenie współautora

Dotyczy publikacji

Bukowski K., Marciniak, B.; Kciuk, M.; Mojzych, M.; Kontek, R. Pyrazolo[4,3-e]tetrazolo[1,5-b][1,2,4]triazine Sulfonamides as Novel Potential Anticancer Agents: Cytotoxic and Genotoxic Activities In Vitro. *Molecules* **2022**, 27, 3761. <https://doi.org/10.3390/molecules27123761>. (MEIN = 140 pkt, IF = 4,927).

Oświadczam, że mój udział w publikacji polegał na nadzorze merytorycznym nad prowadzonymi doświadczeniami oraz na korekcie napisanego manuskryptu. Mój udział oceniam na 10%.



dr Beata Marciniak

Łódź dn.20.05.2023

Mgr Mateusz Kciuk

Katedra Biotechnologii Molekularnej i Genetyki

Uniwersytet Łódzki

Oświadczenie współautora

Dotyczy publikacji

Bukowski K., Marciniak, B.; Kciuk, M.; Mojzych, M.; Kontek, R. Pyrazolo[4,3-e]tetrazolo[1,5-b][1,2,4]triazine Sulfonamides as Novel Potential Anticancer Agents: Cytotoxic and Genotoxic Activities In Vitro. *Molecules* **2022**, 27, 3761. <https://doi.org/10.3390/molecules27123761>. (MEiN= 140 pkt, IF= 4,927).

Oświadczam, że mój udział w publikacji polegał na pomocy w ustawieniu metody dotyczącej immunocytochemicznego barwienia histonu H2AX. Mój udział oceniam na 5%.

Mateusz Kciuk

Mgr Mateusz Kciuk

Siedlce, 17.05.2023 r.

Oświadczenie współautora

Dotyczy publikacji:

Bukowski K., Marciniak, B.; Kciuk, M.; Mojzych, M.; Kontek, R. *Pyrazolo[4,3-e]tetrazolo[1,5-b][1,2,4]triazine Sulfonamides as Novel Potential Anticancer Agents: Cytotoxic and Genotoxic Activities In Vitro. Molecules* **2022**, *27*, 3761. <https://doi.org/10.3390/molecules27123761>. (MEiN= 140 pkt, IF = 4,927).

Oświadczam, że mój udział w publikacji polegał na wykonaniu syntezy analizowanych związków, przygotowaniu materiałów z zakresu biosyntezy do Suplementary Materials oraz udziale w pisaniu i w korekcie manuskryptu. Mój udział oceniam na 5%.



Mariusz Mojzych

Łódź dn.31.05.2023

dr hab. Renata Kontek, prof. UŁ

Katedra Biotechnologii Molekularnej i Genetyki

Uniwersytet Łódzki

Oświadczenie współautora

Dotyczy publikacji

Bukowski K., Marciniak, B.; Kciuk, M.; Mojzych, M.; Kontek, R. Pyrazolo[4,3-e]tetrazolo[1,5-b][1,2,4]triazine Sulfonamides as Novel Potential Anticancer Agents: Cytotoxic and Genotoxic Activities In Vitro. *Molecules* **2022**, 27, 3761. <https://doi.org/10.3390/molecules27123761>. (MEiN = 140 pkt, IF = 4,927).

Oświadczam, że mój udział w publikacji polegał na współudziale w powstaniu koncepcji pracy, nadzorze merytorycznym, a także korekcie manuskryptu. Mój udział oceniam na 10%.



dr hab. Renata Kontek

Łódź dn.31.05.2023

Mgr Karol Bukowski

Katedra Biotechnologii Molekularnej i Genetyki

Uniwersytet Łódzki

Oświadczenie współautora

Dotyczy publikacji

Bukowski K., Marciniak, B.; Kciuk, M.; Mujwar, S.; Mojzych, M.; Kontek, R. Pyrazolo[4,3-e]tetrazolo[1,5-b][1,2,4]triazine Sulfonamides as Novel Potential Anticancer Agents: Apoptosis, Oxidative Stress, and Cell Cycle Analysis. *Int. J. Mol. Sci.* **2023**, 24, 8504. <https://doi.org/10.3390/ijms24108504> (MEiN= 140 pkt, IF = 6,208).

Oświadczam, że mój udział w publikacji polegał na współudziale w powstaniu koncepcji pracy, zaplanowaniu eksperymentów oraz ich wykonaniu. Przeprowadziłem analizę wpływu związków MM na poziom stresu oksydacyjnego oraz na przebieg cyklu komórkowego i jego poszczególnych faz. Wykonałem wszystkie doświadczenia związane z oceną potencjału proapoptotycznego badanych pochodnych pirazolo-triazyny (test z Aneyksyną V przy wykorzystaniu cytometrii przepływowowej; określenie zmian potencjału mitochondrialnego; ocena zmian morfologicznych komórek przy pomocy podwójnego barwienia z wykorzystaniem oranżu akrydyny i bromku etydyny). Dokonałem interpretacji graficznej otrzymanych wyników, przeprowadziłem ich analizę statystyczną oraz opracowałem manuskrypt publikacji. Mój udział oceniam na 60%.


.....

Mgr Karol Bukowski

Łódź dn.31.05.2023

dr Beata Marciniak

Katedra Biotechnologii Molekularnej i Genetyki

Uniwersytet Łódzki

Oświadczenie współautora

Dotyczy publikacji

Bukowski K., Marciniak, B.; Kciuk, M.; Mujwar, S.; Mojzych, M.; Kontek, R. Pyrazolo[4,3-e]tetrazolo[1,5-b][1,2,4]triazine Sulfonamides as Novel Potential Anticancer Agents: Apoptosis, Oxidative Stress, and Cell Cycle Analysis. *Int. J. Mol. Sci.* **2023**, 24, 8504. <https://doi.org/10.3390/ijms24108504> (MEiN = 140 pkt, IF = 6,208).

Oświadczam, że mój udział w publikacji polegał na nadzorze merytorycznym nad prowadzonymi doświadczeniami oraz na korekcie napisanego manuskryptu. Mój udział oceniam na 10%.



dr Beata Marciniak

Łódź dn.20.05.2023

Mgr Mateusz Kciuk

Katedra Biotechnologii Molekularnej i Genetyki

Uniwersytet Łódzki

Oświadczenie współautora

Dotyczy publikacji

Bukowski K., Marciniak, B.; Kciuk, M.; Mujwar, S.; Mojzych, M.; Kontek, R. Pyrazolo[4,3-e]tetrazolo[1,5-b][1,2,4]triazine Sulfonamides as Novel Potential Anticancer Agents: Apoptosis, Oxidative Stress, and Cell Cycle Analysis. *Int. J. Mol. Sci.* **2023**, 24, 8504. <https://doi.org/10.3390/ijms24108504> (MEiN= 140 pkt, IF = 6,208).

Oświadczam, że mój udział w publikacji polegał na współudziale graficznej części publikacji. Mój udział oceniam na 5%.

Mateusz Kciuk

Mgr Mateusz Kciuk

Lodz, 31.05.2023

dr Somdutt Mujwar

Chitkara College of Pharmacy,

Chitkara University

Contributor's Statement

Publication:

Bukowski K., Marciniak, B.; Kciuk, M.; Mujwar, S.; Mojzych, M.; Kontek, R. Pyrazolo[4,3-e]tetrazolo[1,5-b][1,2,4]triazine Sulfonamides as Novel Potential Anticancer Agents: Apoptosis, Oxidative Stress, and Cell Cycle Analysis. *Int. J. Mol. Sci.* **2023**, 24, 8504. <https://doi.org/10.3390/ijms24108504> (MEiN = 140 pkt, IF = 6,208).

I declare that my participation in the publication was associated with *in silico* studies (molecular docking and molecular dynamics simulations). In addition, I participated in editing and proofreading the manuscript. I rate my participation as 10%.



.....
dr Somdutt Mujwar

Siedlce dn. 17.05.2023

Oświadczenie współautora

Dotyczy publikacji:

Bukowski K., Marciniak, B.; Kciuk, M.; Mujwar, S.; Mojzych, M.; Kontek, R. *Pyrazolo[4,3-e]tetrazolo[1,5-b][1,2,4]triazine Sulfonamides as Novel Potential Anticancer Agents: Apoptosis, Oxidative Stress, and Cell Cycle Analysis*. *Int. J. Mol. Sci.* **2023**, 24, 8504. <https://doi.org/10.3390/ijms24108504> (MEiN= 140 pkt, IF = 6,208).

Oświadczam, że mój udział w publikacji polegał na korekcie manuskryptu. Mój udział oceniam na 5%.



Mariusz Mojzych

Łódź dn.31.05.2023

dr hab. Renata Kontek, prof. UŁ

Katedra Biotechnologii Molekularnej i Genetyki

Uniwersytet Łódzki

Oświadczenie współautora

Dotyczy publikacji

Bukowski K., Marciniak, B.; Kciuk, M.; Mujwar, S.; Mojzych, M.; Kontek, R. Pyrazolo[4,3-e]tetrazolo[1,5-b][1,2,4]triazine Sulfonamides as Novel Potential Anticancer Agents: Apoptosis, Oxidative Stress, and Cell Cycle Analysis. *Int. J. Mol. Sci.* **2023**, 24, 8504. <https://doi.org/10.3390/ijms24108504> (MEiN = 140 pkt, IF = 6,208).

Oświadczam, że mój udział w publikacji polegał na współudziale w powstaniu koncepcji pracy, nadzorze merytorycznym, a także na korekcie manuskryptu. Mój udział oceniam na 10%.



dr hab. Renata Kontek